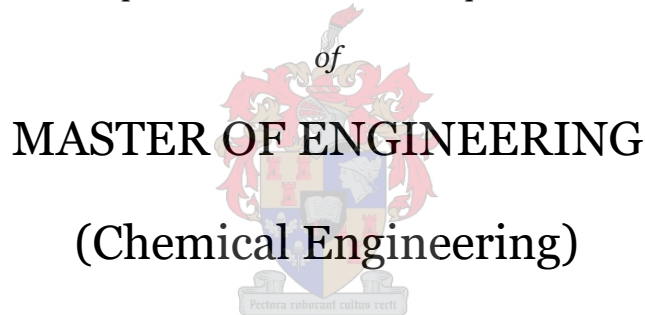# Solute transport in a submerged forward osmosis membrane system

by

Linda Alida van Wyk

Thesis presented in partial fulfilment of the requirements for the degree

of

MASTER OF ENGINEERING

(Chemical Engineering)

in the Faculty of Engineering
at Stellenbosch University

Supervisor

Prof. A.J. Burger

December 2019

Declaration

By submitting this thesis electronically, I declare that the entirety of the work contained therein is my own, original work, that I am the sole author thereof (save to the extent explicitly otherwise stated), that reproduction and publication thereof by Stellenbosch University will not infringe any third party rights and that I have not previously in its entirety or in part submitted it for obtaining any qualification.

Date: December 2019

i

Plagiarism declaration

1. Plagiarism is the use of ideas, material and other intellectual property of another's work and to present it as my own.

2. I agree that plagiarism is a punishable offence because it constitutes theft.

3. I also understand that direct translations are plagiarism.

4. Accordingly, all quotations and contributions from any source whatsoever (including the internet) have been cited fully. I understand that the reproduction of text without quotation marks (even when the source is cited) is plagiarism.

5. I declare that the work contained in this assignment, except where otherwise stated, is my original work and that I have not previously (in its entirety or in part) submitted it for grading in this module/assignment or another module/assignment.

Student number:

Initials and surname: L.A. van Wyk

Signature:

Date: December 2019

Abstract

Wastewater treatment with forward osmosis (FO), an osmotically driven membrane process, has been investigated for the osmotic dilution of seawater prior to desalination in an attempt to lower the energy consumption of seawater reverse osmosis (RO). This hybrid FO-RO process provides a dual-barrier for the effective rejection of wastewater contaminants, thereby potentially producing a high quality permeate. Due to the higher rejection capacity of FO membranes compared to ultrafiltration membranes, the FO process can advance wastewater treatment in submerged membrane bioreactors.

The aim of this study was to investigate the transport and rejection of selected weakly-rejected solutes in a submerged FO system with a commercially available FO membrane. The benefit of the dual-barrier rejection mechanism of the FO-RO hybrid could then be investigated by simulation of its final permeate quality with the experimentally determined rejections of the selected model solutes. To this end, a bench-scale FO setup was designed and constructed. The baseline performance of the FO membrane was firstly evaluated by considering the effects of the membrane orientation, hydrodynamic conditions and osmotic pressure gradient on the water flux and reverse draw solute flux. Phenol, as an organic water contaminant, and boron and lithium, as inorganic water contaminants, all with different physicochemical properties and potentially weak membrane rejections, were used to study the solute transport and rejection.

With a draw solution of seawater quality, water fluxes of 20 $L·m^{-2}·h^{-1}$ and 32 $L·m^{-2}·h^{-1}$ were obtained when the active layer of the membrane was in contact with the feed solution (AL-FS orientation) and draw solution (AL-DS orientation), respectively. The AL-FS orientation exhibited exceptional flux stability at the expense of dilutive internal concentration polarisation.

With no hydrodynamic conditions at the submerged membrane surface, concentrative external concentration polarisation (CECP) of the reverse diffused draw solute resulted in a significant water flux decline to below 8 $L·m^{-2}·h^{-1}$ in both membrane orientations. A Reynolds number of 1 100 at the submerged membrane surface was sufficient to mitigate CECP.

It was found that the solute rejection improved with an increasing osmotic pressure gradient. The rejection of the neutrally charged solutes, boron and phenol, was independent of their concentration gradients in both membrane orientations. An increase in the ionic strength and decrease in the pH of the feed solution with increasing concentrations of lithium chloride and boric acid increased the rejection of lithium, most likely due to its reduced electrostatic interactions with the negatively charged membrane surface.

As opposed to boron and phenol, the lithium rejection in the AL-DS orientation was higher than in the AL-FS orientation as the electrostatic attraction of lithium to the membrane in the AL-

iii

DS orientation was perceived to be insignificant. It is postulated that the electrostatic attraction of lithium to the negatively charged membrane surface significantly compromised its rejection, such that it was approximately 16% lower than that of phenol and boron in the AL-FS orientation at neutral pH conditions.

The respective experimental phenol, boron and lithium rejections of 91%, 93% and 81% were implemented in the simulation of the FO-RO hybrid process. By its dual-barrier and intermediate dilution effects, the FO-RO hybrid provided an improved permeate phenol concentration of 1.1 $\mu g \cdot L^{-1}$, compared to 9.0 $\mu g \cdot L^{-1}$ provided by a standalone wastewater RO process. The permeate quality of a standalone seawater RO unit could be improved from 315 $\mu g \cdot L^{-1}$ boron and 149 $\mu g \cdot L^{-1}$ lithium to 32 $\mu g \cdot L^{-1}$ boron and 25 $\mu g \cdot L^{-1}$ lithium with typical influent seawater concentrations.

Opsomming

Die behandeling van afvalwater met voorwaartse of direkte osmose (FO), wat 'n osmoties gedrewe membraanproses is, kan die osmotiese verdunning van seewater voor ontsouting fasiliteer ten einde die energieverbruik van seewater tru-osmose (RO) te verlaag. Hierdie gekoppelde FO-RO proses voorsien 'n dubbele versperring vir die effektiewe verwerping van kontaminerende komponente in afvalwater, met 'n hoë kwalitieit permeaat as produk. Met die hoër verwerpingskapasitieit van FO membrane in vergelyking met ultrafiltrasiemembrane, kan die FO proses die behandeling van afvalwater bevorder.

Hierdie projek het beoog om die oordrag en verwerping van sekere swak verwerpde komponente in 'n gedompelde FO sisteem te ondersoek met 'n kommersieël beskikbare FO membraan. Die voordeel van die dubbele verwerpingsmeganisme van die gekoppelde FO-RO proses kon vervolgens ondersoek word deur die simulasie van die finale permeaatkwaliteit met die eksperimenteel bepaalde verwerpings van geselekteerde modelkomponente. 'n Bank-skaal FO opstelling was ontwerp en opgerig. Die basislyn gedrag van die FO membraan was eerstens ge-evalueer deur die effekte van die membraanoriëntasie, hidrodinamiese kondisies en die osmotiese drukgradiënt op die watervloed en tru-soutvloed (RSF) te oorweeg. Fenol, as 'n organiese waterkomponent, en boor en litium, as anorganiese waterkomponente, al drie met verskillende fisies-chemiese eienskappe en potensiële swak membraanverwerpings, was gebruik om die oordrag en verwerping van opgeloste stowwe in FO te bestudeer.

In die teenwoordigheid van 'n trekoplossing van seewater kwaliteit was 'n watervloed van 20 L·m^{-2}·h^{-1} en 32 L·m^{-2}·h^{-1} gelewer deur die membraan met die aktiewe laag na die voeroplossing (AL-FS oriëntasie) en trekoplossing (AL-DS oriëntasie), onderskeidelik. 'n Merkwaardige vloed-stabiliteit was vertoon in die AL-FS oriëntasie ten koste van interne verdunning konsentrasie polarisasie (DICP).

Met geen hidrodinamiese kondisies by die gedompelde membraanoppervlak nie het eksterne konsentrerende konsentrasie polarisasie (CECP) van die tru-gediffundeerde trekoplosmiddel 'n afname in die water vloed tot onder 8 L·m^{-2}·h^{-1} veroorsaak in albei oriëntasies. 'n Reynoldsgetal van 1 100 by die gedompelde membraanoppervlak was voldoende om CECP teen te werk.

Dit was bevind dat die verwerping van waterkomponente in FO verbeter met 'n toenemende osmotiese drukgradiënt oor die membraan. Die verwerping van die ongelaaide komponente, boor en fenol, was onafhanklik van hul konsentrasiegradiënt in albei membraanoriëntasies. 'n Toename in die ioonkonsentrasie en afname in die pH van die voeroplossing met toenemende konsentrasies van litiumchloried en boorsuur het die verwerping van litium verbeter, heel

waarskynlik as gevolg van die verminderde elektrostatiese interaksies van litium met die elektronegatiewe membraan.

Kontrasterend teenoor boor en fenol was die verwerping van litium in die AL-DS oriëntasie hoër as in die AL-FS oriëntasie, aangesien die elektrostatiese aantrekking van litium na die membraan in die AL-DS oriëntasie moontlik gering was. Dit word gepostuleer dat die verwerping van litium noemenswaardig ly onder elektrostatiese aantrekkings na die elektronegatiewe membraanoppervlak tot so 'n mate dat eersgenoemde 16% laer was as die verwerping van fenol en boor in die AL-FS oriëntasie onder neutrale pH kondisies.

Die onderskeidelike eksperimenteel bepaalde fenol-, boor- en litiumverwerpings van 91%, 93% en 81% was geïmplementeer in die simulasie van die gekoppelde FO-RO proses. As gevolg van die dubbele versperring- en verdunningseffek, kon die proses 'n verbeterde permeaatkonsentrasie van 1.1 µg·L⁻¹ fenol lewer, in vergelyking met die alleenstaande afvalwater RO permeaatkonsentrasie van 9.0 µg·L⁻¹. Die permeaatkwaliteit van 'n alleenstaande seewater RO eenheid kon verbeter word van 315 µg·L⁻¹ boor en 149 µg·L⁻¹ litium na 32 µg·L⁻¹ boor en 25 µg·L⁻¹ litium met tipiese konsentrasies in die seewater en afvalwater voerstrome.

Acknowledgements

The following people are thanked for their contribution to the process and outcome of this project:

- Professor A.J Burger. I could always exit your office after our meetings with a better state of mind and perspective on my project, and on life in general.

- The Wilhelm Frank Trust. For the financial assistance throughout this project.

- The workshop staff at the Stellenbosch University Department of Process Engineering, Mr. Jos Weerdenburg, Mr. Anton Cordier and Mr. Bevan Koopman. Your assistance in the construction of my experimental setup is greatly appreciated.

- Mrs Hanlie Botha and Mr. Jaco van Rooyen from our analytical laboratory. For the analysis of my samples and advice on analytical procedures.

- The administrative staff, Mrs. Francis Layman and Mrs. Juliana Steyl. For the processing of orders for equipment and chemicals.

- My fellow postgraduate students. It was a pleasure to work alongside all of you.

- My parents, Clené and Heléne. My education would not have been possible without your hard work. Your support throughout this process was invaluable.

- My husband, Gareth. You undertook the whole of this rewarding, but challenging journey with me. A mere "thank you" does not suffice.

Dedicated to my late grandfather - H.J.M Smuts

Contents

Nomenclature

Abbreviations

Abbreviation	Description
AL	Active layer
AL-FS	Active layer facing the feed solution
AL-DS	Active layer facing the draw solution
CECP	Concentrative external concentration polarisation
CF	Concentration factor
CFV	Cross-flow velocity
CICP	Concentrative internal concentration polarisation
CP	Concentration polarisation
CTA	Cellulose triacetate
DECP	Dilutive external concentration polarisation
DI	Deionised
DICP	Dilutive internal concentration polarisation
DS	Draw solution
ECP	External concentration polarisation
EDC	Endocrine disrupting compound
FO	Forward osmosis
FS	Feed solution
ICP	Internal concentration polarisation
MF	Microfiltration
MBR	Membrane bioreactor
MW	Molecular weight
MWCO	Molecular weight cut-off
NF	Nanofiltration
ODMP	Osmotically driven membrane process
OMBR	Osmotic membrane bioreactor
PAO	Pressure-assisted osmosis
PFD	Process flow diagram
PhAC	Pharmaceutically active compound
PRO	Pressure retarded osmosis
PVC	Polyvinyl chloride
RDP	Relative difference percentage
RO	Reverse osmosis
RSD	Reverse solute diffusion
RSF	Reverse solute flux
SAD	Specific aeration demand
SEM	Scanning electron microscopy
SL	Support layer
SMBS	Sodium metabisulfite
TDS	Total dissolved solids
TFC	Thin-film composite
TrOC	Trace organic compound

Dimensionless numbers

Symbol	Name	Description
Re	Reynolds number	Ratio of inertial forces to viscous forces
Sc	Schmidt number	Ratio of momentum diffusivity to mass diffusivity
Sh	Sherwood number	Ratio of convective mass transfer to the rate of diffusive mass transport

Greek symbols

Symbol	Description
Δ	Gradient
κ	Conductivity
μ	Dynamic viscosity
π	Osmotic pressure
τ	Support layer tortuosity
ϕ	Porosity

Latin symbols

Symbol	Description	Symbol	Description
A	Water permeability coefficient	R	Rejection
A	Area	S	Membrane structural parameter
B	Solute permeability coefficient	t	Time
c/C	Concentration	T	Temperature
d	Diameter	v	Velocity
D	Diffusion coefficient	V	Volume
h	Height	w	Width
J	Flux	x	thickness
k	Mass transfer coefficient		
K	Solute resistivity		
K_{OW}	Octanol-water coefficient		
l	Length		
m	Mass		
n	Van't Hoff factor		
pK_a	Dissociation constant		
P	Pressure		
Q	Volumetric flowrate		
r	Recovery		
r	Solute radius		

xiii

Physical constants

Name	Description	Value
R_g	Universal gas constant	8.314 J·mol⁻¹·K⁻¹

Subscripts

Subscript	Description	Subscript	Description
b	Bulk	mix	Mixer
B	Boron	p	Permeate
c	Channel	$PhOH$	Phenol
c	Concentrate	R	Reference
D	Draw solution	RO	Reverse osmosis stage
dsw	Diluted seawater	S	Solute
f	Feed	s	Submerged
F	Feed solution	$spacer$	Spacer
FO	Forward osmosis stage	sl	Support layer
$FO - RO$	FO-RO hybrid	sw	Seawater
h	Hydraulic	t	Tube
i	AL-SL interface	T	Experimental temperature
Li	Lithium	W	Water
m	Make-up		
m	Membrane		

Chapter 1

Introduction

Wastewater reclamation and seawater desalination have been identified as alternative strategies to supply fresh water in higher quantities for the remediation of diminished water sources. Currently, membrane processes are the preferred separation technology in wastewater treatment and desalination (Wang, et al., 2014). Secondary municipal wastewater effluent, industrial wastewaters, brackish groundwater and seawater can be purified with reverse osmosis membranes for the production of ultra-pure water for potable, industrial and agricultural purposes (Fritzmann, et al., 2007). Engineered osmosis processes, such as forward osmosis, may further diversify the future of water supply through low-energy desalination and wastewater reuse.

1.1 Wastewater treatment

As an alternative method to seawater desalination by reverse osmosis, water reuse through wastewater treatment processes has been accepted as a sustainable option to supplement water supplies. However, the occurrence of a wide range of micropollutants in treated and untreated water sources contribute to the contamination of freshwater systems. This includes organic contaminants, such as endocrine disrupting compounds, and inorganic substances that commonly occur in reclaimed water, groundwater and surface water. Generally, these contaminants occur at low concentrations from $ng·L^{-1}$ to $\mu g·L^{-1}$ levels. Nevertheless, they raise considerable toxicological concern (Blandin, et al., 2016; Coday, et al., 2014; Bowen & Mukhtar, 1996).

It is well known that conventional water and wastewater treatment facilities, using either conventional activated sludge or membrane bioreactors, do not provide complete removal of many micropollutants (Schwarzenbach, et al., 2006; Ternes, et al., 2004). Nanofiltration (NF)

and reverse osmosis (RO) membrane processes have shown to provide a higher removal of organic compounds than these conventional processes (Snyder, et al., 2007; Yoon, et al., 2006). However, the rejection of contaminants of low molecular weight is particularly limited in NF (Nagy, 2012).

Forward osmosis (FO) has been investigated as an alternative membrane process in the treatment of wastewater (Lutchmiah, et al., 2014). Like NF and RO, the FO process involves a semi-permeable membrane, which provides a suitable barrier against contaminants in the feed water. However, FO does not require large additional hydraulic pressures to drive water permeation. It is emphasised that FO cannot replace RO, but that FO can provide a different mode of operation which is attractive for the treatment of complex wastewaters.

1.1.1 Forward osmosis

FO is an osmotically driven membrane process (ODMP) of which pressure-retarded osmosis (PRO), typically used for power generation, and pressure-assisted osmosis (PAO) are other variations (Cath, et al., 2006; Lee, et al., 2015). The difference between FO and pressure-driven membrane processes is the driving force for water permeation. As the name suggests, the driving force for water permeation in FO is the osmotic pressure difference between an impaired solution, called the feed solution (FS), and a more concentrated solution, called the draw solution (DS). The FS becomes concentrated, while the DS is diluted. In contrast, water permeation in pressure-driven membrane processes, such as RO, is induced when a hydraulic pressure is applied against the osmotic pressure gradient, whereby water is extracted from the brine. The differences between ODMPs and RO are visually described in Figure 1-1.
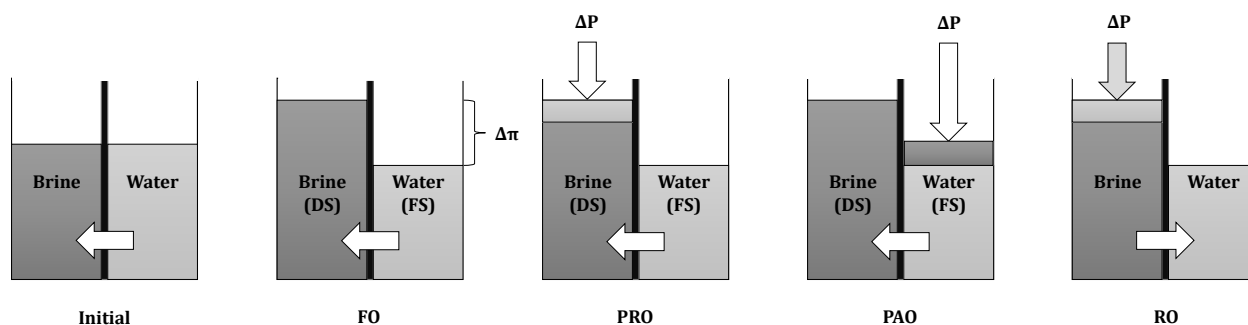
Figure 1-1: Illustration of the direction of water permeation in ODMPs (FO, PRO and PAO) and a pressure-driven membrane process (RO).

Ultimately, the speculated advantages of the FO process over current technologies have been the motivation for its application in the treatment of complex feeds such as activated sludge (Cornelissen, et al., 2008), municipal wastewater effluent (Lutchmiah, et al., 2011; Valladares Linares, et al., 2013), nutrient-rich liquid streams (centrate) (Holloway, et al., 2007) and

produced water from oil and gas extraction (Bell, et al., 2017; Maltos, et al., 2018). Studies have suggested that membrane fouling in FO is relatively low (Achilli, et al., 2009), more reversible (Mi & Elimelech, 2010a; Mi & Elimelech, 2010b) and can be mitigated by optimising the hydrodynamic conditions at the membrane surface (Lee, et al., 2010). Another advantage of the FO process, which is potentially the most attractive, is the low operational hydraulic pressure of the process, which could contribute to a lower energy consumption (Elimelech & Phillip, 2011; McGinnis & Elimelech, 2007).

The major pitfalls of the FO process are the limitations imposed on the water transport by the asymmetric structure and imperfect selectivity of the FO membrane. The theoretical water transport across the semi-permeable membrane in ODMPs is described by Equation 1-1, where J_W is the water flux, A is the water permeability coefficient and π_D and π_F are the osmotic pressures of the draw solution and feed solution, respectively (Cath, et al., 2013).

$$J_W = A(\pi_D - \pi_F) \qquad \qquad (1\text{-}1)$$

FO membranes have a thin selective layer that is cast on a thick, porous support layer. As water permeates from the feed solution, the rejected solutes accumulate on the feed side and the draw solution becomes diluted on the permeate side. A boundary layer is established on the surface of the membrane, which is called external concentration polarisation (ECP), as well as within the porous support layer, which is called internal concentration polarisation (ICP). The effective osmotic pressure gradient that generates the water flux is only established at the active-support layer interface. Hence, both ICP and ECP contribute to a reduction in the effective driving force for water permeation in FO (Cath, et al., 2013), which renders Equation 1-1 invalid.

McCutcheon & Elimelech (2006) developed an equation to account for both the ECP and ICP phenomena through the mass transfer coefficient on either side of the membrane (Equation 1-2).

$$J_W = A\left[\pi_{D,b}\exp\left(-\frac{J_W}{k_{D,eff}}\right) - \pi_{F,b}\exp\left(-\frac{J_W}{k_F}\right)\right] \qquad \qquad (1\text{-}2)$$

Here, $\pi_{D,b}$ and $\pi_{F,b}$ refer to the bulk DS and FS osmotic pressure, respectively, and $k_{D,eff}$ and k_F refer to the mass transfer coefficients on the respective sides of the active-support layer interface (Cath, et al., 2013). Equation 1-2 has been developed for the case where the membrane active layer is in contact with the feed solution (AL-FS orientation). FO can also be operated in the alternative orientation were the active layer is in contact with the draw solution (AL-DS orientation).

ICP and ECP can be aggravated by the reverse diffusion of the draw solute, a phenomena which is inevitable in FO due to the concentration difference between the draw solution and feed solution. Reverse diffused draw solutes accumulate within the membrane boundary layers, thereby decreasing the effective osmotic pressure gradient. The reverse solute flux, expressed as J_S in Equation 1-3, is dependent on the permeability of the solute through the membrane, which is quantified by the solute permeability coefficient (B). The symbols n, R_g and T refer to the number of dissociated species of the draw solute, the universal gas constant and temperature, respectively (Phillip, et al., 2010; Tang, et al., 2010).

$$\frac{J_S}{J_W} = \frac{A}{B} n R_g T \qquad (1\text{-}3)$$

1.1.1.1 *The osmotic membrane bioreactor*

The membrane bioreactor (MBR) is a well-known technology implemented for wastewater treatment and water reuse. The MBR combines conventional activated sludge (CAS) treatment and membrane separation, traditionally with ultrafiltration (UF) or microfiltration (MF) membranes (Holloway, et al., 2015a). The concept of combining CAS treatment with the younger FO process, as shown in Figure 1-2, has recently been investigated (Cornelissen, et al., 2008; Achilli, et al., 2009; Qin, et al., 2009). This is commonly referred to as the osmotic membrane bioreactor (OMBR).
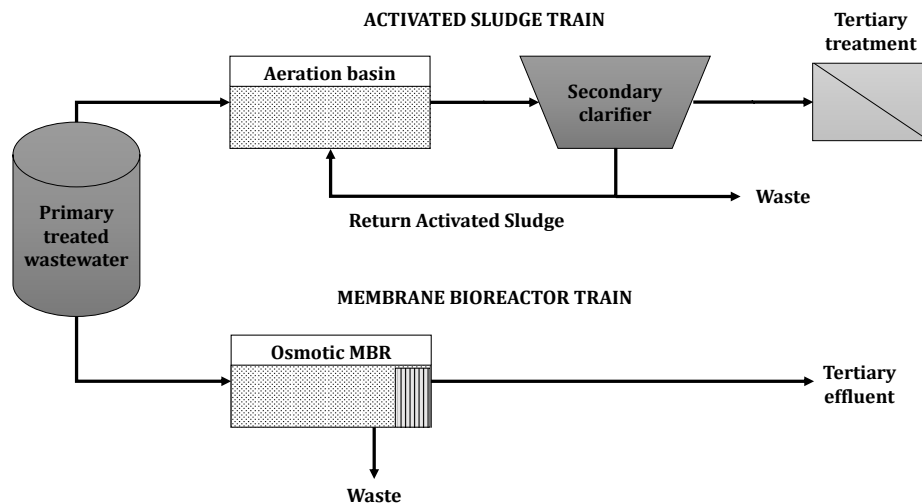

Figure 1-2: The conventional activated sludge and MBR process trains for wastewater treatment (Holloway, et al., 2015a).

4

The OMBR preserves the inherent advantages of both the FO and conventional MBR processes. Typically, a plate-and-frame FO membrane module is submerged in the aerated reactor and the draw solution is continuously circulated through the membrane cell to extract high quality water from the impaired feed (Holloway, et al., 2015a). This high quality effluent can be produced with a small physical footprint and low sludge production (Hai, et al., 2014).

1.1.1.2 Contaminant removal

Membrane separation is a popular method for wastewater treatment due to the high rejection capacity of membranes to a wide range of contaminants. The rejection capacity of FO membranes are comparable to that of RO membranes for the effective removal of water constituents that are smaller than 1 nm (Eyvaz, et al., 2018; Fang, et al., 2014). With their tight polymer matrices, FO membranes are capable of rejecting organic compounds, as well as dissolved ionic compounds, unlike conventional treatment technologies (Cath, et al., 2006; Ternes, et al., 2004).

Owing to this advantage, a number of research groups have studied the removal of trace organic and inorganic compounds with FO membranes (Coday, et al., 2014; Jin, et al., 2012b; Liu, et al., 2019). The rejection mechanisms of organic compounds in FO was first proposed and elucidated by Alturki, et al. (2013) in a study on 40 different solutes. It was found that the rejection of charged organic compounds was governed by both steric exclusion and electrostatic repulsion, while neutral compounds were rejected by steric exclusion only. Xie, et al. (2012a) reported that the rejection capacity of FO membranes is further enhanced by reverse draw solute diffusion.

The membrane orientation plays an important role in the rejection of solutes in FO processes (Jin, et al., 2011; Liu, et al., 2019). The AL-FS orientation is commonly preferred in operation to avoid significant flux declines resulting from membrane fouling within the support layer (She, et al., 2012). However, the AL-DS orientation can generate higher water fluxes than the AL-FS orientation for the same osmotic pressure gradient (Tang, et al., 2010). Jin, et al. (2011) showed by modelling and experiments that a higher boric acid rejection can be achieved in the AL-FS orientation relative to the AL-DS orientation. However, contrasting evidence was recently published by Liu, et al. (2019) for the rejection of caesium cations.

1.2 Simultaneous wastewater treatment & seawater desalination

Wastewater treatment has been studied with FO as a standalone process and as part of a hybrid system with seawater RO in an attempt to moderate the energy requirements of seawater desalination (Cath, et al., 2010; Hancock, et al., 2012). The relatively low salinity of impaired waters makes them ideal candidates to dilute the seawater prior to RO to decrease the osmotic

pressure of the seawater. However, the direct dilution or combination of the impaired stream with the highly saline stream may alter the chemistry of the RO feed stream and aggravate the fouling of RO membranes (Lew, et al., 2005; Chekli, et al., 2016).

The FO and RO processes have been coupled such that the seawater feed acts as the draw solution in the FO stage and the extracted water from the FO stage osmotically dilutes the seawater. The diluted seawater is then fed to the RO stage for the production of high quality product water. This process, as shown in Figure 1-3, is referred to as the FO-RO hybrid (Blandin, et al., 2016). This configuration, used for the osmotic dilution of seawater, is distinguished from other closed-loop configurations where draw solution regeneration is the primary purpose of the hybrid (Shaffer, et al., 2015; Park, et al., 2012; Tan & Ng, 2010; McCutcheon, et al., 2006).
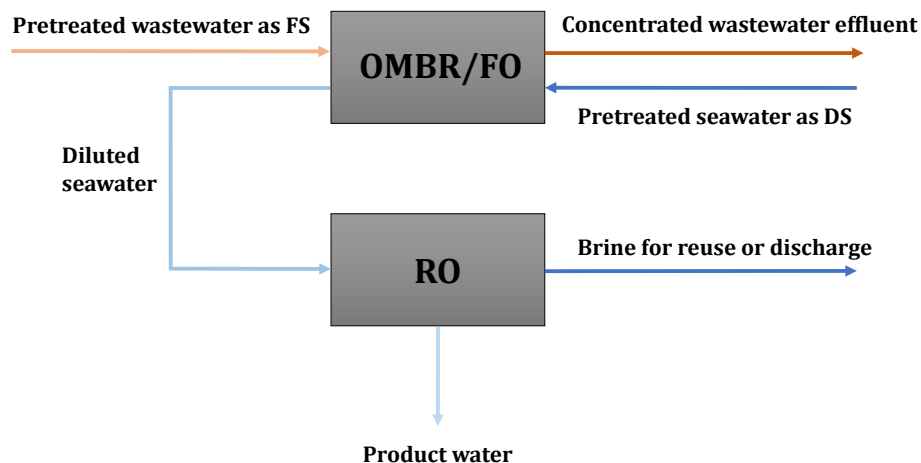
Figure 1-3: Schematic illustration of the FO-RO hybrid process used for the osmotic dilution of seawater prior to seawater desalination. The pre-treated seawater is used as the DS in the FO stage before desalination.

The economic sustainability of the FO-RO hybrid process still remains questionable as the integration of the two units requires additional investment costs (Wang, et al., 2018). There is also no clear advantage of the FO-RO hybrid compared to using two simpler, more established water treatment processes to perform the same task, i.e., seawater RO and wastewater treatment implemented individually (Blandin, et al., 2015). However, the hybrid process offers some advantages over the standalone processes with regards to the quality of the process streams. The fouling potential of the seawater feed stream to the RO process is lowered as a result of the dilution by the extracted water in the FO stage and the reduced operating pressures in the RO stage (Blandin, et al., 2016).

The most attractive advantage of the FO-RO hybrid is the dual-barrier rejection mechanism it provides for wastewater contaminants; the extracted water from the wastewater stream is treated

by two membranes (Cath, et al., 2010). Importantly, FO membranes are tighter than UF membranes. Therefore, the FO stage provides a superior removal of wastewater contaminants relative to a conventional UF MBR stage (Coday, et al., 2014; Eyvaz, et al., 2018). In the FO-RO hybrid process, all potential contaminants in the permeate from the FO stage and influent seawater are also diluted prior to the RO stage, thereby contributing to a high quality permeate. Furthermore, the osmotic agent of the draw solution is obtained from seawater, hence there is no chemical make-up required in the process. For these reasons, the FO-RO hybrid has attracted interest in the research fields of wastewater treatment and seawater desalination (Cath, et al., 2010; Blandin, et al., 2016; Chekli, et al., 2016).

1.3 Problem identification

1. Mass transfer limitations in submerged FO

Submerged FO is of interest in wastewater treatment with osmotic membrane bioreactors. Thus far, most research efforts have been directed towards the evaluation of scaling, fouling, compound removal and biological stability in osmotic membrane bioreactors (Luo, et al., 2017; Qiu, et al., 2016; Holloway, et al., 2015b; Zhang, et al., 2012). Insights into the mass-transfer and effects of hydrodynamic conditions in submerged modules have been limited, although the membrane performance in this configuration suffers remarkably from the mass transfer-limiting phenomena inherent to the FO process. More particularly, reverse solute diffusion increases the salinity of the FS in the submerged configuration, which can potentially aggravate external concentration polarisation when the hydrodynamic conditions at the submerged membrane surface are insufficient (Holloway, et al., 2015a).

2. Solute removal by FO and the FO-RO hybrid

Fresh water systems are contaminated by a wide range of organic and inorganic constituents that occur in water resources. FO membranes have the potential to provide superior solute rejection efficiencies relative to conventional water treatment methods. Like RO and NF, the solute rejection mechanisms in FO involve a complex combination of steric exclusion and electrostatic or hydrophobic interactions between the solutes and the membrane. Hence, the membrane rejection performance is highly dependent on the structural and physicochemical properties of both the solute and membrane, as well as the operating conditions and solution chemistry on both sides of the membrane (Coday, et al., 2014).

Thus far, the rejection of FO membranes has predominantly been investigated with interest in the removal of solutes which occur in the impaired feed solution only (Coday, et al., 2014; Xie, et al.,

2015; Sauchelli, et al., 2018). To the knowledge of the author, the solute transport behaviour in FO has not been evaluated with the particular solute of interest present in both the feed solution and draw solution. Such insight is particularly important in the FO-RO hybrid, where the seawater draw solution contains several inorganic constituents, although in minor or trace concentrations (<100 mg·L^{-1}), such as boron and lithium.

The FO-RO hybrid process provides an improved removal efficiency of wastewater contaminants relative to the respective standalone processes (Cath, et al., 2010). Still, the solutes that permeate across the FO membrane migrate to the RO permeate, thereby affecting its purity. Therefore, the quality of the permeate from the FO-RO hybrid process is dependent on both the FO and RO membrane rejections of a particular contaminant. Experimentally determined solute rejections can be implemented in a simple simulation approach to estimate the concentrations of the contaminants in the permeate of the dual-barrier FO-RO hybrid process.

From the above, a few research questions arise:

- What hydrodynamic conditions are sufficient to reduce the effects of external concentration polarisation in the submerged FO configuration?
- How does the FO membrane transport and rejection behaviour of solutes with different structural and physicochemical properties compare?
- How is the membrane rejection affected when the solute is present in both the feed solution and draw solution?
- How does the permeate quality of the FO-RO hybrid process compare to that of a standalone RO process?

1.4 Research objectives

The primary aim of this study was to evaluate the solute transport and rejection behaviour in a submerged FO system with a commercially available FO membrane for the purpose of investigating the advantage of the dual-barrier rejection mechanism of the FO-RO hybrid process. Solutes with potentially weak membrane rejections were considered in particular. To this end, the objectives listed below were pursued in this study:

1. Design and construct a bench-scale submerged FO system.
2. Establish the baseline performance of the submerged FO membrane in terms of the water flux and reverse draw solute flux, with consideration of the effects of the a) membrane orientation, b) hydrodynamic conditions at the submerged membrane surface and c) osmotic pressure gradient between the draw solution and feed solution.

3. Experimentally evaluate the transport and rejection of the selected solutes in FO with variation in the osmotic pressure and solute concentration gradients (with and without the solute in the draw solution) and relate the solute physicochemical properties and FO operating conditions to the rejection behaviour.

4. Simulate the FO-RO hybrid in the typical osmotic dilution configuration proposed in literature and apply the experimentally determined FO rejections to determine the quality of the final permeate.

1.5 Thesis overview

In Chapter 2 of this work, a literature review is presented. Firstly, the principles and mass transport phenomena of the FO process are discussed, followed by an overview of submerged FO, solute rejection by FO membranes and the FO-RO hybrid process. A summary of the literature is presented at the end of Chapter 2, together with the properties of the model solutes identified for the experimental study.

The design and characterisation of the laboratory-scale experimental setup is presented in detail in Chapter 3. An overview of the materials used and experimental plan and procedures followed during the experimental work is also provided. The results obtained in the experimental phase of this work are discussed in Chapter 4. In Chapter 5, the simulation of the FO-RO hybrid permeate quality is presented. The conclusions from this study are outlined in Chapter 6, together with suggestions of future directions in FO research.

Chapter 2

Literature review

In this literature review, the fundamental principles of FO is discussed, with particular attention to the mass transport phenomena inherent to the process. Considerations in the design and operation of submerged FO modules are also outlined. An in-depth discussion of feed solute transport in FO follows to explore the mechanisms by which solutes are rejected by membranes. A summary of the model solutes identified for this experimental study is provided at the end of this chapter.

2.1 Fundamental principles of FO

2.1.1 Osmosis and osmotic pressure

The driving force in FO is the difference in the water chemical potential between the two solutions separated by a semi-permeable membrane acting as a selective barrier. The semi-permeable membrane is selective to the water and obstructs the passage of the solute dissolved within it (Lachish, 2007). According to the Second Law of Thermodynamics, the system will spontaneously evolve towards a state of equilibrium where the entropy is maximised or solute concentration is minimised (Perry, 2013). Hence, pure water diffuses though the semi-permeable membrane from the solution of high water chemical potential, which is the feed solution (FS), to the solution of low water chemical potential, which is the draw solution (DS). As a result, the water chemical potential of the FS is reduced.

Osmotic flow is more often described in terms of the osmotic pressure rather than the chemical potential. Developed by van't Hoff (1888), the definition of the osmotic pressure of a solution, shown by Equation 2-1, is a direct consequence of the Second Law of Thermodynamics as it has been derived for a closed cycle reversible isothermal process. Hence, it bears similarity to the ideal gas formula.

$$\pi = nCR_gT \qquad\qquad (2\text{-}1)$$

where π = osmotic pressure (Pa)

        n = Van't Hoff factor

        C = concentration of the solute (mol·L⁻¹)

        R_g = universal gas constant (L·Pa·K⁻¹·mol⁻¹)

        T = absolute temperature (K)

Osmotic flow will cease when the osmotic pressure gradient between the FS and DS is zero. This state is called osmotic equilibrium. The implication of osmotic equilibrium in FO is that it is the fundamental thermodynamic constraint of the process. It limits the volume of water that is recovered from the FS and consequently the quality of the effluent streams (Benavides, et al., 2015).

The osmotic pressure differential in FO continuously changes. In conventional cross-flow (co-current and countercurrent) membrane modules, the influent DS and FS become more dilute and concentrated along their flow path over the membrane, respectively (Shaffer, et al., 2015). In the submerged configuration, the complete volume of FS being treated by the FO membrane becomes concentrated as the DS draws pure water from the solution (Chowdhury, et al., 2017; Blandin, et al., 2018). Thus, the osmotic pressure gradient as driving force in FO is a dynamic feature that is dependent on the module configuration, among other factors such as the hydrodynamic conditions and membrane area. However, the effluent FS will never have a higher osmotic pressure than the influent DS due to the thermodynamic limit of osmotic equilibrium.

2.1.2 Basic terms describing FO membrane performance

2.1.2.1 Water flux

The water transport in membrane processes is described by the water flux (Cath, et al., 2006). Simply stated, the water flux is a measure of the volumetric flowrate of water permeating through the semi-permeable membrane per unit area. The theoretical water flux in membrane processes can be determined with Equation 2-2 (Baker, 2012).

$$J_W = A(\Delta\pi - \Delta P) \qquad\qquad (2\text{-}2)$$

where J_W = water flux (L·m⁻²·h⁻¹)

        A = water permeability coefficient (L·m⁻²·h⁻¹·Pa⁻¹)

        $\Delta\pi$ = osmotic pressure gradient across the membrane (Pa)

        ΔP = hydraulic pressure gradient across the membrane (Pa)

For the FO process, the second term in Equation 2-2 is eliminated as ΔP is normally zero. The water flux is from the low salinity FS to the concentrated DS until osmotic equilibrium is established. In pressure retarded osmosis or PRO, an intermediate process between FO and RO, the water flux is still in the direction of the concentrated DS, but the volume expansion of the DS is restricted to increase the hydraulic pressure (ΔP) on the DS side (Straub & Elimelech, 2016). The pressurised DS is then driven through a hydro-turbine to generate power (Loeb, 1976).

According to Equation 2-2, the water flux in FO increases with the water permeability characteristic of the membrane. Since the introduction of the first commercial FO membrane by Hydration Technologies Inc., the research in FO has been directed towards to the advancement in the water permeability of membranes (Zhao, et al., 2012). With new approaches to FO membrane fabrication, thin film composite (TFC) membranes have been developed, which offer higher water permeability and reduced concentration polarisation compared to cellulose triacetate (CTA) membranes. The typical water flux of four commercially available TFC FO membranes reported in literature are provided Table 2-1.

Table 2-1: The water flux (J_W) generated by commercially available FO membranes, as reported in literature (Blandin, et al., 2016). All water fluxes indicated were evaluated with a deionised water FS and the active layer of the membrane facing the feed solution.

Company	Commercial name	Draw solution	J_W/ L·m⁻²·h⁻¹	Reference
HTI	TFC	1.0 M NaCl	10	Coday, et al. (2013)
Oasys	TFC	1.0 M NaCl	30	Coday, et al. (2013)
Woongjin Chemicals	TFC-1	1.0 M KCl	16	Fam, et al. (2013)
Woongjin Chemicals	TFC-2	1.0 M KCl	28	Phunthso, et al. (2013)
CSM Toray	FO8040	1.0 M NaCl	35	CSM Toray (2015)

2.1.2.2 Rejection

The rejection coefficient, R, has been defined for membrane processes to describe the ability of the membrane to separate the feed solute from the permeate (Baker, 2012). The analytical expression of the solute rejection in Equation 2-3 can be formulated from the assumption that the permeate and feed solution volume are equal. Hence, it describes an instantaneous rejection of a solute.

$$R = 1 - \frac{c_p}{c_{F,b}}$$
(2-3)

where R = solute rejection (-)

         c_p = concentration of the solute in the permeate (mg·L⁻¹)

         $c_{F,b}$ = concentration of the solute in the bulk feed solution (mg·L⁻¹)

For a membrane with perfect selectivity, the permeate concentration is zero and the rejection 100%. However, the membrane rejection is affected by the properties of the solute in addition to that of the membrane. This includes the ionic charge, degree of dissociation, molecular weight, polarity, degree of hydration and degree of molecular branching of the solute. In general, the membrane rejection is proportional to all of the properties named, except the polarity (Kucera, 2010).

Due to their mutually tight polymer matrices, FO membranes typically exhibit comparable rejections to nanofiltration and reverse osmosis membranes (Perry, 2013). The general rejection capabilities of polyamide TFC membranes, as summarised by Kucera (2010), are provided in Table 2-2. From the values indicated it is clear, for example, that the rejection of multi-valent ions are greater than that of mono-valent ions.

Table 2-2: The typical rejection capacity of polyamide TFC membranes (Kucera, 2010).

Species	Rejection / %
Sodium	92-98
Chloride	92-98
Hardness	93-99
Magnesium	93-98
Potassium	92-96
Ammonium[1]	80-90
Calcium	93-99+
Sulfate	96-99+
Phosphate	96-98

2.1.3 Mass transport

2.1.3.1 Transport models

Although membrane processes provide a simple method of separation, the mass transport through membranes is complex and dependent on many factors including the membrane structure, orientation, the temperature and composition of the draw and feed solution and hydraulics (Klaysom, et al., 2013). Fundamental models have been developed as tools to understand membrane transport (Wang, et al., 2014).

Transport models can either be 1) mechanistic or 2) phenomenological. Mechanistic models relate the membrane separation performance to the physical and chemical properties of the membrane materials and solute. Phenomenological models describe the membrane separation in terms of quantifiable parameters such as the water flux and solute passage, thereby treating the membrane

---

[1] Below pH 7.8

as a 'black box' (Wang, et al., 2014). Regardless of the model, two major assumptions are made in the definition of mass transport theory across membranes. Firstly, transport models assume that the fluids on both sides of the membrane are in equilibrium with the membrane at its interface. Thus, the chemical potential gradient across the membrane is continuous. Secondly, it is assumed that the pressure within the membrane is uniform and the chemical potential gradient across the membrane is only expressed as a concentration (Paul, 1974; Wijmans & Baker, 1995).

The solution diffusion or pore flow models are commonly used to describe mass transport through membranes (Baker, 2012; Wang, et al., 2014). Lonsdale, et al. (1965) proposed the use of the solution diffusion model for dense, non-porous membranes. This model is perhaps the most popular transport model adopted to describe the mass transport in FO. According to solution-diffusion theory, permeants diffuse along a concentration gradient through the membrane after dissolving at the membrane interface. Hence, the solvent and solute are separated based on their dissimilarities in solubility in the membrane material and rate of diffusion through the membrane (Baker, 2012).

The solution diffusion model has previously been derived in detail by Baker (2012) and Cussler (2007). The flux of the permeant is defined as being proportional to its concentration difference between the feed and permeate side of the membrane (Equation 2-4).

$$J = \frac{D}{l}(C_{10} - C_{1l}) \tag{2-4}$$

where J = flux of the permeating species (mol·m^{-2}·s^{-1})

       D = diffusion coefficient of the permeating species (m^{-2}·s^{-1})

       l = membrane thickness (m)

       C_{10} = concentration of permeant in the membrane on the feed side (mol·m^{-3})

       C_{1l} = concentration of permeant in the membrane on the permeate (DS) side (mol·m^{-3})

There are three important aspects concerning Equation 2-4 that are relevant to membrane separation (Cussler, 2007):

1) The separation of the solute and solvent by the membrane is dependent on their rates of transport. In other words, the degree of separation is dependent on diffusion.
2) The separation by the membrane is affected by the partition of the solute between the membrane and the adjacent solution. This implicates that the solute concentration within the membrane may be higher or lower than that in the solution.

14

3) The membrane itself acts as one of several resistances in series along the path of the permeant.

The majority of the semi-permeable membranes implemented in FO are either cellulose triacetate or thin film composite membranes with an asymmetric structure. A dense thin layer (0.1-1 μm) provides the majority of the selectivity of the membrane while a thick porous layer (100-200 μm) provides mechanical support to the fragile selective layer. Therefore, the structure and transport properties of the membrane vary across its thickness (Wang, et al., 2014). The effects of the matrix structure and chemical properties (charge and hydrophobicity) of the support layer have been the reason for the re-evaluation of the transport through osmotic membranes.

2.1.3.2 Diffusion coefficients

The diffusion coefficient of a permeating species, D, is a measure of the frequency and size of each movement of the solute. Hence, the magnitude of the diffusion coefficient is influenced by the restraining forces of the surrounding medium on the diffusing species (Baker, 2012). The diffusion coefficient of a solute in a liquid can be estimated with the Stokes-Einstein equation (Equation 2-5). However, it is highlighted that the estimation of diffusion coefficients in liquids is not always reliable (Cussler, 2007). Equation 2-5 provides an indication of the factors that influence the diffusion of species in liquids (Cussler, 2007; Baker, 2012)

$$D = \frac{k_B T}{\beta \pi \mu r} \tag{2-5}$$

where D = diffusion coefficient (m^{-2}·s^{-1})

k_B = Boltzmann's constant (kg·m^2·s^{-2}·K^{-1})

T = absolute temperature (K)

μ = dynamic viscosity of the solution (kg·m^{-1}·s^{-1})

r = solute radius (m)

The denominator in Equation 2-5 represents the friction coefficient of the solute. The diffusion coefficient is viscosity-dependent as the solution viscosity often depends on much longer range interactions than diffusion (Cussler, 2007). The value of the coefficient β depends on the solute radius and typically varies between 1 and 6 (Edward, 1970). The temperature dependence of the diffusion coefficient described in Equation 2-5 is accurate (Cussler, 2007).

To describe the diffusion of strong electrolytes, such as sodium chloride, it is appropriate to implement a single diffusion coefficient. This seems acceptable, as there is always referred to as

sodium chloride as if it does not ionise. However, sodium chloride completely ionises in water. Hence, sodium and chloride have presumably similar rates of diffusion. The reason for this is that the larger cation and smaller anion are electrostatically coupled for the sake of electroneutrality. The diffusion coefficients of a sodium cation and chloride anion are 1.33 and 2.03, respectively. Thus, the overall rate of diffusion will be dictated by the slower, larger sodium cation (Cussler, 2007).

Diffusion coefficients are complex quantities and are obtained through several experimental methods such as tracer diffusion determination. Diffusion coefficients of solutes can be found in literature and the values fall in the range of 10^{-9} m·s^{-1} (Cussler, 2007; Baker, 2012). The range of diffusion coefficients is small as the viscosity of simple liquids such as water does not vary significantly and the diffusion coefficient is a weak function of the size of the ion or molecule.

For electrolyte solutions, the measurement of the electrical conductivity, or reciprocal of the electrical resistance, can provide an accurate means of determining the ion concentration in solutions. Cussler (2007) formulated a conversion of the conductivity of a solution to the diffusion coefficient. Therefore, it was suggested that conductivity per se can be used as a measure of the ion transport through membranes.

The measurement of the electrical conductivity of a solution provides a significantly simpler method for the characterisation of ion transport through membranes. However, it is emphasised that the ion conductance indicates the arithmetic mean of the ion mobility and charge of the ions in solution. In contrast, the single diffusion coefficient representing the ions in solution is a harmonic average of their properties. Hence, electrical conductivity is dictated by the ion with larger mobility and diffusion is dominated by the ion with the lower mobility (Cussler, 2007).

2.1.3.3 Solute hydration

Ions combine with water to form a new species, which is effectively the species diffusing. The combination of the ion with the water is called hydration. The idea of hydration has been based on an alternative flux equation described by Cussler (2007). The equation was formulated on the assumption that the diffusion coefficient of the solute in a dilute solution is derived from the Stokes-Einstein equation.

When formulating the flux of a solute from its degree of hydration, the radius of the solute becomes that of its hydrated form, named the hydration radius (Cussler, 2007). Briefly, the hydrated radius is governed by the charge and true radius of the central ion (David, et al., 2001).

Typically, the hydration radius of cations decrease with increasing ionic radii. However, no correlation exists between the hydration radius and ionic radius of anions (Tansel, 2012).

As water molecules from a solution tend to permeate through the membrane, the crowding of ions at the membrane surface results in some ions being retained while others are allowed to diffuse across the membrane. Despite this solute-water interaction, the hydration radius of a species alone is not the determining factor for the permeation of cations across membranes (Tansel, 2012).

2.1.3.4 Solute-membrane interactions

When permeants diffuse across FO membranes, they proceed through two mediums, namely the 1) dense active layer and 2) porous support layer of the asymmetric membrane. Depending on the orientation of the membrane towards the feed solution, the one layer may proceed the other. When the membrane is operated such that the active layer faces the FS, the configuration is called the AL-FS orientation. Similarly, in the AL-DS orientation, the FS is in contact with the support layer. The mass transport through the FO membranes is influenced by the membrane orientation as a result of the difference in the structure and chemical properties of the active and support layers.

As mentioned in Section 2.1.3.1, the solution-diffusion model is sufficient for describing the mass transport across the *active layer* as this model has been developed for dense membranes (Kim, et al., 2017; Luo, et al., 2016). Furthermore, the active layer is selective to water, thereby retaining other solutes and pollutants. The FO water flux is therefore governed by the selectivity of the active layer to the water, with the latter quantified in terms of the water permeability coefficient:

$$J_W = A\Delta\pi \tag{2-6}$$

where J_W = water flux (L·m^{-2}·h^{-1})

A = water permeability coefficient (L·m^{-2}·h^{-1}·bar^{-1})

$\Delta\pi$ = osmotic pressure difference between the DS and FS (bar)

Theoretically, the water flux through the membrane increases proportionally with the water permeability of the membrane. The water permeability coefficient (A) is equal to the factor $\frac{D}{l}$ in Equation 2-4 (Section 2.1.3.1). In a similar fashion, the solute transport through the active layer can be evaluated from the solute permeability coefficient, B (Baker, 2012):

$$J_S = B\Delta C \tag{2-7}$$

where J_S = solute flux (g·m⁻²·h⁻¹)

          B = solute permeability coefficient (L·m⁻²·h⁻¹)

          ΔC = solute concentration difference between the FS and DS (g·L⁻¹)

Depending on its concentration gradient between the feed solution and draw solution, a solute can diffuse across the semi-permeable in the FO process from 1) the feed solution to the draw solution (forward diffusion) and 2) the draw solution to the feed solution (reverse diffusion). In both these cases, a low solute permeability coefficient is desired to facilitate 1) the rejection of feed solutes and 2) the prevention of draw solute leakage to the feed solution, respectively.

Solute transport in the *support layer* of the FO membrane is governed by diffusion and convection (Mehta & Loeb, 1978; Tang, et al., 2011). For the purpose of providing mechanical strength to the thin active layer, the support layer of the asymmetric FO membrane is remarkably thicker than the active layer. The flow paths of diffusing species are effectively lengthened by its porous and tortuous structure, which results in an increased hindrance to solute diffusion (Wang, et al., 2014). As a result of this hindered diffusion, solutes accumulate in the membrane support layer, a phenomenon which is called internal concentration polarisation (ICP).

The porous support layer is characterised by the structural parameter, S (Equation 2-8).Typically, a low value of S is preferred to reduce the severity of ICP (Manickam & McCutcheon, 2017). However, Mazlan (2016) highlighted that the structural parameter is not always a sufficient representation of ICP as it does not incorporate the dominance of one property (e.g. pore size) over another (e.g. support layer thickness).

$$S = \frac{\Delta x_{sl}\tau}{\phi_{sl}} = KD \tag{2-8}$$

where S = structural parameter of the support layer (m)

          Δx_{sl} = support layer thickness (m)

          τ = support layer tortuosity (-)

          ϕ_{sl} = support layer porosity (-)

          K = solute resistivity (s·m⁻¹)

          D = diffusion coefficient (m²·s⁻¹)

2.1.3.5 Mass transfer limitations

Reverse solute diffusion (RSD), concentration polarisation (CP) and membrane fouling are mass-transfer-limiting phenomena in the FO process that are closely interrelated with one another, as shown in Figure 2-1. In addition, concentration polarisation, reverse solute diffusion and membrane fouling are influenced by the membrane characteristics and draw solute properties. For the purpose of this study, RSD and CP will be discussed in further detail. Both these phenomena contribute to reduced driving forces for water flux in submerged FO modules (Holloway, et al., 2015a).
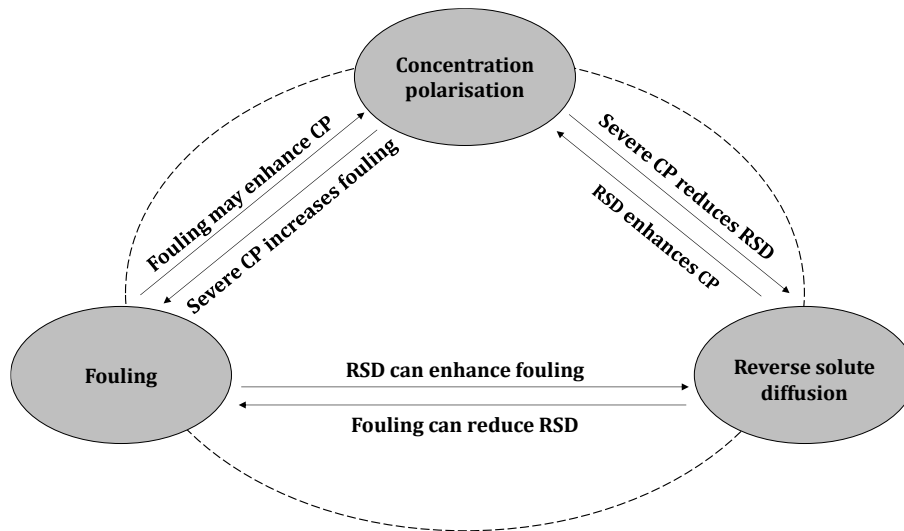
Figure 2-1: The interrelationships among concentration polarisation, reverse solute diffusion and membrane fouling (She, et al., 2016).

2.1.3.5.1   Reverse solute diffusion

In ODMPs, the reverse diffusion of the draw solute to the feed solution is inevitable. It is the result of the non-ideality of the membrane in conjunction with the tendency of the FO system to equilibrate the high osmotic pressure gradient across the membrane. The solute is transported across the porous support layer and boundary layers on the membrane surfaces by convection and diffusion, while the transport across the dense active layer is governed by diffusion only (Phillip, et al., 2010).

The reverse solute flux (RSF), for which a modelling equation has been developed by Phillip, et al., (2010), is a measure of the rate of reverse draw solute diffusion per unit membrane area. The reverse solute flux is influenced by a variety of factors including the DS concentration, type of counter ions, membrane properties and hydrodynamic conditions at the membrane surface (She, et al., 2012; Saren, et al., 2011; Tang, et al., 2010; Phillip, et al., 2010). Generally, a greater rate of RSD is observed with an increase in the DS concentration (Phillip, et al., 2010).

The *specific* reverse solute flux, which is the ratio of the reverse solute flux to the forward water flux, is a measure of the membrane selectivity (Hancock & Cath, 2009). A greater value of the specific reverse solute flux reflects a decrease in the selectivity of the membrane active layer to water, but it is independent of the DS concentration and the structure of the support layer (Phillip, et al., 2010). The ratio of the specific reverse solute flux to the concentration of the feed solution provides an indication of the relative importance of the RSD and convection of the feed solution in concentration polarisation (She, et al., 2016).

RSD is an undesirable mass transport phenomena in FO. It is responsible for the loss of the draw solute to the FS, thereby elevating the concentration of the feed solution. As a result, concentration polarisation near and within the membrane matrix is enhanced and the driving force for water permeation is reduced (Figure 2-1). A low reverse solute flux is desired in FO, especially in OMBR applications, as the reverse diffused solutes accumulate in the feed water, which subsequently compromises the stable FO performance and activity of the microbial community in the activated sludge (Holloway, et al., 2015a).

2.1.3.5.2 Concentration polarisation

CP is a common phenomenon in membrane processes, which occurs when the concentration of the solute near the surface of the membrane is different from that in the bulk solution. This arises from the formation of boundary layers at the selective interface of the membrane. CP in FO not only reduces the effective driving force for water permeation across the membrane, but the rejection of feed solutes by the membrane is also affected (Sauchelli, et al., 2018; Luo, et al., 2016).

With asymmetric FO membranes, mass transfer boundary layers are established on both sides of the active-support layer interface, with one of them embedded in the porous support layer (Manickam & McCutcheon, 2017). Thus, there are two variations of concentration polarisation in FO – external concentration polarisation (ECP) and internal concentration polarisation (ICP). ECP occurs outside of the membrane matrix in the vicinity of the membrane surface. Therefore, ECP can be alleviated with the optimisation of the hydrodynamic conditions at the membrane surface with cross-flow or agitation. ICP occurs within the porous support layer where solutes remain protected from any turbulent conditions, which hinders mass transfer (She, et al., 2016; McCutcheon & Elimelech, 2006).

In both cases of ECP and ICP, the effective solute concentration at the selective interface of the membrane is different from that in the bulk feed or draw solution. It is emphasised that CP in FO results from both solution convection and reverse solute diffusion (She, et al., 2013; Wei, et al., 2013; She, et al., 2012; Yip, et al., 2011)

Both ECP and ICP in the FO process are either concentrative or dilutive, depending on the membrane orientation. As water permeates from the FS of lower osmotic pressure to the DS of higher osmotic pressure, the FS becomes increasingly concentrated and the DS becomes diluted. Accordingly, concentrative CP occurs on the FS side and dilutive CP occurs on the DS side. Thus, four types of CP are encountered in FO processes, namely 1) concentrative ECP (CECP), 2) dilutive ECP (DECP), 3) concentrative ICP (CICP) and dilutive ICP (DICP). Figure 2-2 is provided to visibly distinguish the different types of CP exhibited by the asymmetric membrane in each membrane orientation, as well as the ideal case where the membrane is symmetric or dense.
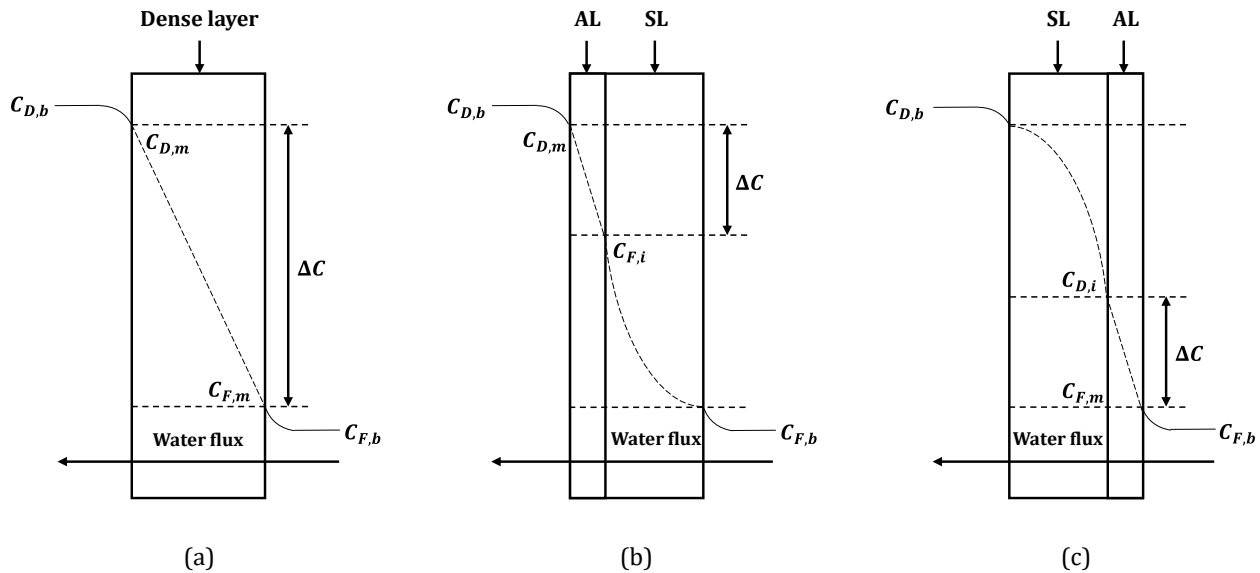
Figure 2-2: Schematic illustration of the concentration profiles across (a) a dense membrane and concentrative and dilutive CP of an asymmetric membrane in the (b) AL-DS orientation and (c) AL-FS orientation (McCutcheon & Elimelech, 2006). The symbols C_F and C_D refer to the concentrations of the solute in the feed and draw solution, respectively, and the subscripts b, i and m refer to the bulk, membrane interface and membrane surface conditions. The concentration profiles depict DECP and CICP in the AL-DS orientation and CECP and DICP in the AL-FS orientation for asymmetric membranes.

In the AL-FS orientation (Figure 2-2c), solutes build-up at the surface of the active layer as a result of the selectivity of the membrane to water. As the water permeates, the draw solution within the porous support layer becomes diluted. In the AL-DS orientation (Figure 2-2b), solutes in the feed are confined to the porous support layer by convective water flow and hindered diffusion. As a result, the solutes become concentrated in the support layer. Accordingly, CICP and DECP are coupled in the AL-DS orientation and DICP and CECP in the AL-FS orientation (Table 2-3).

Table 2-3: A summary of the types of concentration polarisation (CP) in FO (Lee, et al., 2010).

Variation of CP	Location	Type	Membrane orientation
External (ECP)	Surface of active layer	Concentrative (CECP)	AL-FS
		Dilutive (DECP)	AL-DS
Internal (ICP)	Within the support layer	Concentrative (CICP)	AL-FS
		Dilutive (DICP)	AL-DS

An exception is that ECP may occur at the support layer surface when the solute does not move freely in the external boundary layer at the support layer due the absence of turbulence (Kim, et al., 2015). In this case, an additional boundary layer to that on the membrane active layer and within the support layer is created (Manickam & McCutcheon, 2017). Such ECP at the support layer can only be neglected when the boundary layer thickness is significantly smaller than the structural parameter of the support layer (She, et al., 2016).

ECP has previously been modelled by McCutcheon & Elimelech (2006) with the use of boundary layer film theory. Accordingly, ECP moduli (Equations 2-9 and 2-10) that describe the degree of CECP or DECP were developed in terms of the mass transfer coefficient, k (Mulder, 1996; McCutcheon & Elimelech, 2006):

$$\frac{C_{F,m}}{C_{F,b}} = \exp\left(\frac{J_W}{k}\right) \quad \text{(CECP)} \tag{2-9}$$

$$\frac{C_{D,m}}{C_{D,b}} = \exp\left(-\frac{J_W}{k}\right) \quad \text{(DECP)} \tag{2-10}$$

where $C_{F,m}$ = solute concentration at the membrane surface in the feed solution (mol·m^{-3})

$C_{F,b}$ = concentration of the solute in the bulk FS (mol·m^{-3})

$C_{D,m}$ = solute concentration at the membrane surface in the draw solution (mol·m^{-3})

$C_{D,b}$ = concentration of the solute in the bulk DS (mol·m^{-3})

J_W = water flux (m^3·m^{-2}·s^{-1})

k = mass transfer coefficient (m·s^{-1})

The mass transfer coefficient is related to the Sherwood number (Sh), according to Equation 2-11, where D is the diffusion coefficient and d_h is the hydraulic diameter of the flow geometry. Empirically determined correlations of the Sherwood number for different flow geometries have previously been summarised by Wang, et al. (2014).

$$k = \frac{ShD}{d_h} \tag{2-11}$$

Classical diffusion-convection theory has been adopted to model the effect of ICP on the FO water flux (Lee, et al., 1981). Thus, the solute resistivity, K (Equation 2-8) is incorporated in the CICP and DICP moduli (Equations 2-12 and 2-13) to quantify the ratio of the solute concentration at the active-support layer interface to that of the bulk solution (McCutcheon & Elimelech, 2006).

$$\frac{C_{F,i}}{C_{F,b}} = \exp(J_W K) \quad \text{(CICP)} \tag{2-12}$$

$$\frac{C_{D,i}}{C_{D,b}} = \exp(-J_W K) \quad \text{(DICP)} \tag{2-13}$$

where $C_{F,i}$ = solute concentration at the membrane interface in the feed solution (mol·m⁻³)

   $C_{F,b}$ = concentration of the solute in the bulk FS (mol·m⁻³)

   $C_{D,i}$ = solute concentration at the membrane interface in the draw solution (mol·m⁻³)

   $C_{D,b}$ = concentration of the solute in the bulk DS (mol·m⁻³)

   J_W = water flux (m³·m⁻²·s⁻¹)

   K = solute resistivity (s·m⁻¹)

By combination of Equations 2-12 and 2-13, respectively, with the relationship of the solute resistivity to the structural parameter, S (Equation 2-8), it is evident that the characteristics of the membrane support layer determines the extent of ICP. A membrane with a thin, non-tortuous, hydrophilic, high-porosity support layer provides the lowest hindrance to diffusion (Widjojo, et al., 2011).

By their definitions, the CP moduli indicate the ratio of the solute concentration at the membrane surface or interface to that of the bulk solution. Hence, no CP occurs when the calculated modulus approximates unity. When CP prevails, be it ECP or ICP, the modulus will deviate from unity (Baker, 2012). The value of the concentrative modulus will be larger than unity as the solute becomes enriched within the laminar mass transfer boundary layer by water permeation. The value of the dilutive modulus will be smaller than unity as a result of the depletion of the solute within the mass transfer boundary layer as water permeates across the membrane.

With regards to the four types of CP mentioned above, the following points are highlighted:

1) Both ECP and ICP reduce the effective *osmotic pressure* gradient in FO processes as their concentrative effect increases the effective osmotic pressure of the FS and their dilutive effect decreases the effective osmotic pressure of the DS (Zhao, et al., 2012). In contrast,

significant ECP and ICP enhances the effective concentration gradient of a solute that has a higher concentration in the FS than in the DS.

2) A loss in driving force for water flux by CECP and CICP arises from the accumulation of draw solutes on the FS side by FS convection and RSD. The relative importance of FS convection and RSD in concentrative CP is dependent on the relative values of the FS solute concentration and the specific reverse solute flux (She, et al., 2016).

3) DECP and DICP is the result of the dilution of the DS from convective water flow as well as the loss of the draw solute by RSD (She, et al., 2016).

ICP has been recognised as the most important mass-transfer limiting phenomena in ODMPs. Several researchers have reported that the water flux decline in the FO process is predominantly the result of ICP (Mehta & Loeb, 1979; Mehta & Loeb, 1978; Gray, et al., 2006; McCutcheon & Elimelech, 2006). ICP remains an inevitable phenomena in FO as it cannot be mitigated by altering the hydrodynamic conditions such as increasing the turbulence or flow rate at the membrane surface (Zhao, et al., 2012). The experimental data of Gray, et al. (2006), illustrated in Figure 2-3, demonstrate the effects of ICP and coupled ECP and ICP on the water flux in the AL-FS and AL-DS orientations.
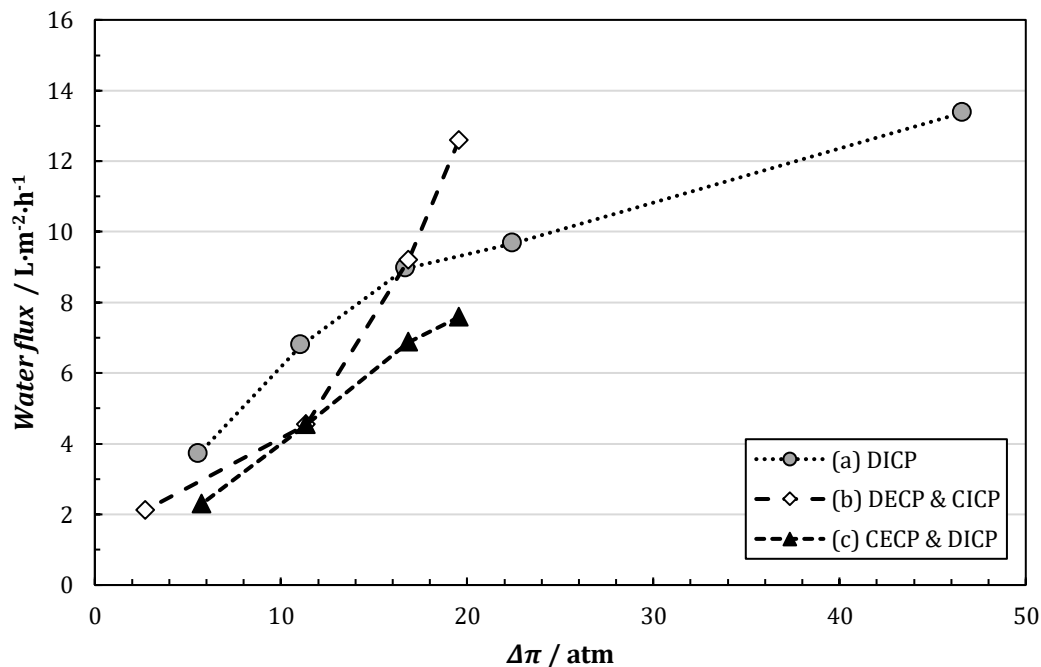

Figure 2-3: Experimental data measured by Gray, et al. (2006) with a) a DS varying between 0.125 M and 1.0 M NaCl and deionised water FS in the AL-FS orientation, b) a DS of 0.5 M NaCl and FS varying from 0.0625 M to 0.375 M NaCl in the AL-DS orientation and c) a DS of 0.5 M NaCl and FS varying from 0.0625 M to 0.375 M NaCl in the AL-FS orientation.

When the active layer faces a FS of deionised water (Figure 2-3a), ECP becomes insignificant (McCutcheon, et al., 2006; Gray, et al., 2006). Thus, DICP is responsible for a non-linear relationship between the osmotic pressure gradient and the water flux in the AL-FS orientation. When the DS osmotic pressure remains constant and the FS osmotic pressure is increased in the AL-FS orientation, the effect of CECP becomes clear (Figure 2-3c) and a linear relationship between the osmotic pressure gradient and water flux exists.

When the support layer faces a FS with a significant concentration of the draw solute (Figure 2-3b), CICP results from the convective flow of water concentrating the solute at the active-support layer interface. In this case, a non-linear relationship exists between the osmotic pressure gradient and the water flux. Note that at the highest osmotic pressure gradient of 19.5 atm in Figure 2-3b, the FS osmotic pressure is the lowest. Consequently, the extent of ICP is the smallest and the flux is the highest. When the FS osmotic pressure is increased, or the osmotic pressure gradient is decreased, the increase in CICP causes the water flux to reduce rapidly and nonlinearly.

In general, it is clear from Figure 2-3 that higher fluxes are obtained when the FS faces the support layer (AL-FS orientation). The reason for this is that the FS of a lower draw solute concentration causes less severe ICP than when the highly concentrated DS faces the support layer. Furthermore, the lower water fluxes observed from Figure 2-3c relative to Figure 2-3a confirm that DICP is more severe than CICP (Tang, et al., 2010; Gray, et al., 2006).

2.2 Submerged FO modules

FO membrane processes can be operated in the cross-flow or submerged configuration (Cath, et al., 2013; Blandin, et al., 2018). In cross-flow filtration, the feed solution and draw solution flow bilaterally over membrane surface to facilitate a continuous concentration of the feed solution across the membrane surface. In submerged FO modules, there is no continuous tangential flow of the feed solution over the membrane, but the membrane module is immersed in the feed solution. The draw solution is circulated externally on the opposite side of the submerged membrane surface (Holloway, et al., 2015a). Thus, submerged FO can be regarded as a hybrid configuration of dead-end and cross-flow filtration.

The submerged FO membrane configuration has primarily been implemented in the research of wastewater treatment with OMBRs, which is potentially a low fouling alternative to conventional MBRs with enhanced solute removal (Luo, et al., 2017; Alturki, et al., 2012). An illustration of the OMBR is provided in Figure 2-4 and a number of studies on submerged FO are summarised in Table 2-4.
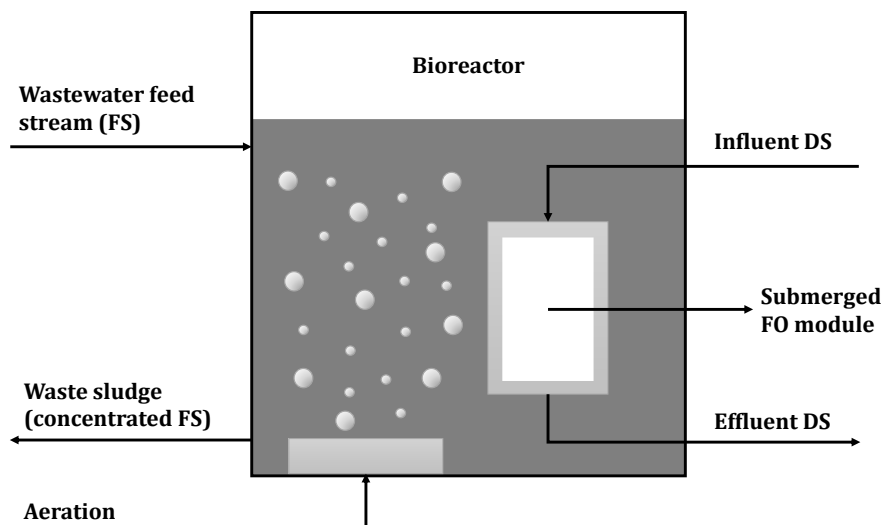
Figure 2-4: A simplified illustration of a submerged FO module operated in an OMBR. The FS may be continuously fed and the DS is circulated through the cross flow channels of the FO module. Aeration is supplied for agitation of the bioreactor.

There is little information known on the design and operation of the FS and DS channels of submerged FO units. It can also be observed from Table 2-4 that a wide range of operating conditions have been applied in the submerged FO configuration. Relevant design considerations for submerged FO modules surveyed from previous findings in literature are discussed in the following sub-sections.

2.2.1 Hydrodynamic conditions

The submerged membrane configuration facilitates the concentration of highly viscous feed waters, such as activated sludge, that cannot be easily circulated through cross-flow channels (Blandin, et al., 2018). However, a technical limitation in submerged membrane operation is the build-up of foulants and reverse diffused solutes in the feed water tank. To mitigate the coupled effects of CECP and fouling at the membrane surface, high turbulence is required.

Table 2-4: Summary of experimental studies in the submerged FO configuration.

Membrane	Orientation	FS hydrodynamic conditions	FS volume	DS	CFV / m·s⁻¹	Temperature	Operating time	J_W[2] / L·m⁻²·h⁻¹	Reference
CTA	AL-FS	Aeration	14 L	50 g·L⁻¹ NaCl	-	23.1 ± 1°C	8 hours	11	Achilli, et al. (2009)
TFC	AL-FS & AL-DS	Recirculation	-	0.5 M NaCl	-	20.2 ± 2°C	7-8 hours	5.5 (AL-FS) 6.5 (AL-DS)	Cornelissen, et al. (2008)
CTA (HTI)	AL-FS & AL-DS	Aeration	5 L	0.5 M NaCl	4	25.5 ± 1°C	160 minutes	5 (AL-FS) 7.5 (AL-DS)	Alturki, et al. (2012)
CTA (HTI)	AL-FS	Aeration	6 L	3.0 M NaCl	0.167	23.1 ± 1°C	220 minutes	25	Gu, et al. (2013)
CTA (HTI)	AL-FS & AL-DS	Aeration	4.85 L	38 g·L⁻¹ NaCl	-	23.2 ± 1°C	10 hours	6 (Al-FS) 8 (AL-DS)	Qiu & Ting (2014)
CTA (HTI)	AL-FS & AL-DS	Aeration	-	40.5 g·L⁻¹ TDS	-	20.0 ± 0.5°C	48 hours	5.5 (AL-FS) 8.5 (Al-DS)	Valladares Linares, et al. (2016)
CTA and TFC (HTI)	AL-FS	Stirring or recirculation	0.5 L	3.0 M NaCl	0.24	Ambient	10 hours	15 (CTA) 20 (TFC)	Chowdhury, et al. (2017)
TFC (CSM Toray)	AL-FS	Aeration or recirculation	25 L	35 g·L⁻¹ TDS	0.05-0.15	-	30 minutes	13	Blandin, et al. (2018)

---

[2] Initial pure water flux

In the context of OMBRs, submerged plate-and-frame or hollow fiber membrane modules have been investigated at bench- and pilot scale with air scouring used as a common strategy to mitigate CECP and fouling (Holloway, et al., 2015b; Qiu, et al., 2016; Zhang, et al., 2012; Lay, et al., 2011). The aeration intensity required to reduce fouling, known as the specific aeration demand (SAD) in conventional ultrafiltration and microfiltration MBRs have been well established (Cui, et al., 2003). However, this has not been thoroughly studied for submerged FO membranes in OMBRs (Holloway, et al., 2015a). Some studies have suggested that the aeration demand in an OMBR is typically smaller compared to that of a traditional MBR (Luo, et al., 2015; Holloway, et al., 2015b). In the study by Holloway, et al. (2015b), it was found that an OMBR can operate at an SAD as low as 1.5 $m^3 \cdot m^{-2} \cdot h^{-1}$, compared to 29 $m^3 \cdot m^{-2} \cdot h^{-1}$ typically required in UF and MF MBRs (Judd, 2008).

In the recent studies of Chowdhury & McCutcheon (2018) and Chowdhury, et al. (2017), submerged FO was operated with a hybrid dead-end/cross-flow FO system, a setup very similar to that constructed in this study. The feed solution was either agitated by an overhead mechanical mixer at 500 rpm or recirculated by an external gear pump at 1 $L \cdot min^{-1}$. The draw solution was circulated through the cross-flow cell opposite to the FS at a cross-flow velocity of 24 $cm \cdot s^{-1}$. It was visually presented in their first study (Chowdhury, et al., 2017) that overhead stirring created dead zones within the rectangular feed tank. It was emphasised that the modelling of the Reynolds number in the feed cell was problematic in the case where recirculation was implemented.

Blandin, et al. (2018) conducted the first study on mass transfer limitations particular to the submerged FO configuration with the same TFC membrane used in this work. This was done in an attempt to optimise the design and operation of submerged FO modules. In their study, turbulence was supplied to a 25 litre feed solution either by 1) aeration ranging from 0.67 to 3.33 $m^3 \cdot m^{-2} \cdot h^{-1}$ or 2) recirculation of the FS up to a maximum rate corresponding to a flow velocity of 9 $cm \cdot s^{-1}$ over the membrane surface. Aeration provided the most effective mitigation of the CECP on the feed side of the membrane, and consequently higher water fluxes. However, it was highlighted that aeration can decrease the surface area available for the contact of the water with the membrane. Under non-turbulent conditions, CECP resulting from RSD resulted in severe declines of the water flux from approximately 15 $L \cdot m^{-2} \cdot h^{-1}$ to 8 $L \cdot m^{-2} \cdot h^{-1}$ over 30 minutes of operation in the AL-FS orientation.

2.2.2 Membrane orientation

FO membranes operated with the active layer facing the FS (AL-FS orientation) can provide a stable water flux (Chun, et al., 2017; Tang, et al., 2010) and higher resistance to fouling compared to pressure driven membrane processes (Mi & Elimelech, 2010a). However, the severity of ICP

can be reduced by operating the membrane with the active layer orientated towards the DS (AL-DS orientation). In the AL-DS membrane orientation, CICP on the FS side of the membrane occurs rather than DICP on the DS side. As a result, higher water fluxes in the AL-DS orientation can be achieved (McCutcheon & Elimelech, 2006).

The major disadvantages of operating a submerged FO membrane in the AL-DS orientation are the higher rate of RSD (Zhao, et al., 2011) and higher membrane fouling potential (She, et al., 2016). Firstly, CICP is aggravated by severe RSD in the AL-DS orientation. Secondly, foulants in complex feed waters such as inorganic salts and organic solids become entrapped in the porous structure of the support layer. Both these occurrences result in an unstable behaviour in the water flux. However, due to the potential advantages of FO in the AL-DS orientation, both membrane orientations have been considered in the evaluation of OMBRs (Qiu & Ting, 2014; Alturki, et al., 2012; Zhang, et al., 2012; Cornelissen, et al., 2008).

2.3 Solute transport in FO

In this section, the concepts of forward solute flux and rejection are elaborated in the context of the solution-diffusion model introduced in Section 2.1.3.1. The mechanisms by which solutes are rejected by membranes are outlined, as well as a number of factors that affect the feed solute transport in FO. Lastly, an overview of organic and inorganic solute removal in membrane processes are provided.

2.3.1 Transport equations

The forward diffusion of a solute through a FO membrane and its retention by the membrane are expressed by the forward solute flux (J_S) and rejection (R_s) respectively (Schutte, 2003). When comparing the transport of various solutes through the FO membrane, the membrane rejection may provide an indication of the removal efficiency of the membrane. However, the difference in the transport behaviour of solutes cannot be understood without consideration of the forward solute flux (Schutte, 2003).

2.3.1.1 Forward solute flux

As mentioned in Section 2.1.3.5.2, the solute flux through the membrane can be derived from the solution-diffusion model for the active layer (Geise, et al., 2014) and the diffusion-convection transport for the support layer (Lee, et al., 1981). Schematics of the transport of solutes from the FS to the DS in the AL-FS and AL-DS orientations are provided in Figure 2-5. When no ECP prevails, Equations 2-14 and 2-15 are valid to express the forward solute flux (Luo, et al., 2016; Jin, et al., 2011).

$$J_S = B\left(c_{F,b} - c_{D,i}\right) \quad \text{(AL-FS)} \tag{2-14}$$

$$J_S = B\left(c_{F,i} - c_{D,b}\right) \quad \text{(AL-DS)} \tag{2-15}$$

where B = solute permeability coefficient (L·m⁻²·h⁻¹)

$c_{F,b}$ = concentration of the solute in the bulk FS (g·L⁻¹)

$c_{D,i}$ = concentration of the solute at the active-support layer interface on the DS side (g·L⁻¹)

$c_{F,i}$ = concentration of the solute at the active-support layer interface on the FS side (g·L⁻¹)

$c_{D,b}$ = concentration of the solute in the bulk DS (g·L⁻¹)
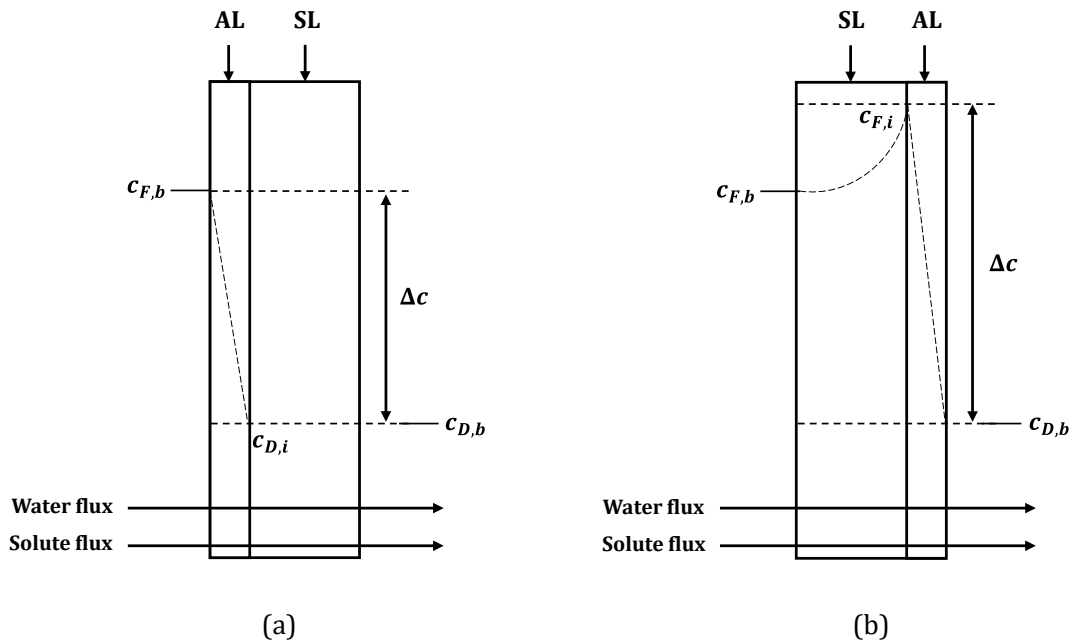
Figure 2-5: Schematic illustration of the forward transport of feed solutes from the FS to the DS in the a) AL-FS orientation and b) AL-DS orientation. The symbols c_F and c_D refer to the concentration of the solute in the feed and draw solution, respectively, and the subscripts b and i refer to the bulk and membrane interface conditions, respectively (McCutcheon, et al., 2006).

In the AL-FS orientation, once the solute permeates the active layer, it is carried away from the active-support layer interface through the support layer by convection. The solute concentration of the DS at the membrane interface ($c_{D,i}$) can therefore be related to the water flux with a boundary condition of $c_{D,b}$=0, as shown in Equation 2-16 (Jin, et al., 2011),

$$c_{D,i} = \frac{J_S}{J_W} \quad \text{(AL-FS)} \tag{2-16}$$

When the active layer is facing the DS, the feed solute freely enters the porous support layer by convective water flow and diffusion. The solute concentration at the active-support layer interface

($c_{F,i}$) is higher than that in the bulk feed solution ($c_{F,b}$) as a result of the solute retention by the selective active layer. Thus, ICP of the solute occurs in a similar way to the ICP of the draw solute. Equation 2-17 (Jin, et al., 2011), which can be derived from film theory (Elimelech & Bhattacharjee, 1998), relates the concentration of the solute at the membrane interface to the water flux.

$$\frac{c_{F,i}-c_{D,b}}{c_{F,b}-c_{D,b}} = \exp(J_W K) \quad \text{(AL-DS)} \tag{2-17}$$

By combination of Equations 2-14 and 2-16 for the AL-FS orientation and Equations 2-15 and 2-17 for the AL-DS orientation, analytical expressions are obtained that describe the forward solute flux in terms of the solute permeability coefficient, water flux and solute resistivity (Jin, et al., 2011). These expressions are listed in Table 2-5.

2.3.1.2 Feed solute rejection

Consistent with the definition of rejection given in Equation 2-3 (Section 2.1.2.2), the theoretical solute rejection by the membrane can be defined from the ratio of the solute flux to the permeate flux (Jin, et al., 2011):

$$R_S = 1 - \frac{c_p}{c_{F,b}} = 1 - \frac{J_S}{J_W c_{F.b}} \tag{2-18}$$

With its formulation from a mass balance on the membrane, Equation 2-18 is based on the assumption that the feed and permeate volumes are equal. By substitution of Equations 2-14 and 2-15 into Equation 2-18, expressions for the solute rejection by the membrane in the AL-FS and AL-DS orientation are obtained, as presented in Table 2-5.

Table 2-5: Analytical equations for the forward solute flux and rejection in FO (Luo, et al., 2017; Jin, et al., 2011), where B is the solute permeability coefficient, J_W is the water flux, $c_{F,b}$ is the solute concentration in the bulk FS and K the solute resistivity.

Membrane orientation	Solute flux (J_S)		Solute rejection (R_S)	
AL-FS	$\frac{B}{1+\frac{B}{J_W}}c_{F,b}$	(2-19)	$1-\frac{B}{B+J_W}$	(2-20)
AL-DS	$\frac{B\exp(J_W K)}{1+\frac{B\exp(J_W K)}{J_W}}c_{F,b}$	(2-21)	$1-\frac{B\exp(J_W K)}{B\exp(J_W K)+J_W}$	(2-22)

2.3.2 Solute rejection mechanisms

Convective and diffusive mechanisms govern the transport of solutes through membranes, but the solute rejection mechanisms of membranes involve a complex combination of 1) steric or size exclusion, 2) electrostatic repulsion and 3) hydrophobic interactions (Jang, et al., 2018; Coday, et al., 2014; Alturki, et al., 2013; Hancock & Cath, 2009). These three rejection mechanisms are illustrated in Figure 2-6. The extent to which these mechanisms as one or in combination govern the rejection of the solute is dependent on the physicochemical properties of the solute and membrane, which is further influenced by the solution chemistry (Nghiem, et al., 2010).
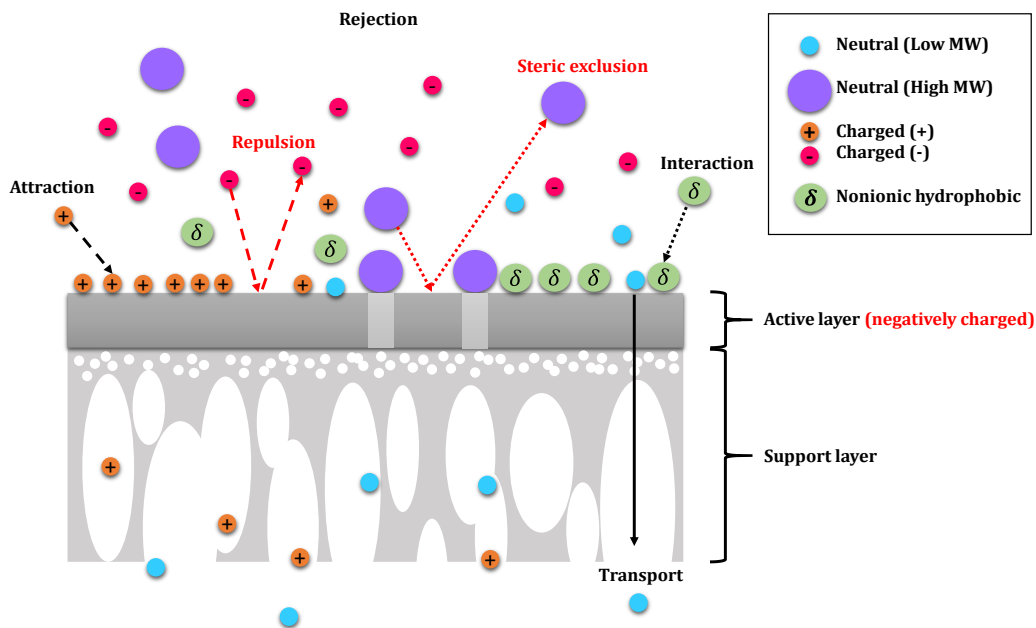
Figure 2-6: Schematic illustration of the possible solute rejection mechanisms in membrane processes (Jang, et al., 2018). The low and high molecular weight (MW) solutes, charged solutes and non-ionic hydrophobic solutes depict the mechanisms of steric exclusion, electrostatic repulsion and hydrophobic interactions, respectively.

Steric hindrance is solely responsible for the retention of neutral compounds and non-adsorptive solutes (Nghiem, et al., 2010). It is essentially a molecular sieving effect based on the mean effective pore size of the membrane in relation to the radius, or molecular weight (MW), of the solute. Typically, the pore size distribution of a particular membrane is determined by permeability experiments with solutes of different molecular weights. The molecular weight cut-off (MWCO) is defined as the molecular weight of the solute at which a 90% rejection is obtained. Alternatively, the mean effective pore size is quantified as the mean diameter of the solute at which a rejection of 50% is obtained (Cui, et al., 2016). Thus, solutes with a MW or hydrated radius smaller than the MWCO or mean effective pore size of the membrane will be rejected weaker than compounds with a higher MW or hydrated radius (Jang, et al., 2018).

Steric hindrance of solutes may also result from the reverse diffusion of draw solutes (Fam, et al., 2014; Hancock & Cath, 2009). When the hydrated radius of the draw solute is comparable to the mean effective pore size of the membrane, RSD is facilitated and the forward permeation of the feed solutes will be retarded. In previous studies, the higher solute rejection of FO membranes than RO membranes has been attributed to this hindered forward diffusion of solutes by severe RSD (Xie, et al., 2012a; Hancock & Cath, 2009).

Charged solutes can be attracted or repelled by electronegative TFC membranes. Thus, electrostatic interactions influence the rejection of charged solutes. Accordingly, it has been found that negatively charged compounds exhibit higher membrane rejections than positively charged or neutral compounds when the membrane surface is electronegative (Jang, et al., 2018; Coday, et al., 2014). However, steric exclusion cannot be completely excluded from the rejection mechanism of charged solutes. The effective membrane and solute charge is further affected by the feed solution chemistry such as the ionic strength and pH. Therefore, it has been found that the solute rejection by TFC FO membranes is heavily dependent on the concentration and pH of the feed (Jin, et al., 2012a).

The rejection of hydrophilic non-ionic solutes larger than the MWCO of the membrane is generally controlled by steric exclusion. However, hydrophobic neutral solutes may establish hydrophobic (Van der Waals) interactions with a hydrophobic membrane surface. The hydrophobicity of a solute is usually expressed as the logarithm of its octanol-water coefficient (log K_{OW}). The hydrophobicity of membrane surfaces is quantified by their contact angle (θ) with a water droplet. The initial adsorption of these hydrophobic solutes to the membrane surface is an important factor in their rejection (Coday, et al., 2014). In order to obtain an accurate indication of the membrane rejection, saturation of the membrane with the hydrophobic solute of interest must be achieved; the initial rejection of hydrophobic solutes appears high as a result of the adsorption to the membrane (Verliefde, 2008).

It has been shown that negatively charged solutes with higher values of log K_{OW} exhibit lower adsorption capacities to TFC membrane surfaces than neutral compounds. Negatively charged solutes are not easily attached to the membrane surface as a result of the electrostatic repulsion by the negatively charged membrane surface (Jang, et al., 2018; Coday, et al., 2014).

2.3.3 Factors affecting solute rejection

A number factors affect the rejection of solutes by FO membranes. This includes, but is not limited to, the membrane and DS properties, the FS chemistry and membrane orientation. The DS properties and membrane orientation are specific to ODMPs, while the other factors also

influence the transport in pressure-driven membrane processes (Xie, et al., 2015; Nghiem, et al., 2010; Wen, et al., 2006).

2.3.3.1 *Membrane properties*

The progress in the development of high performance TFC membranes as an alternative to CTA membranes has resulted in a surging number of studies comparing the rejection performance of the two types of membranes. Commercial asymmetric CTA membranes tailored for the FO process are only chemically stable within a limited pH range of 4 to 7. Such CTA membranes will hydrolyse when exposed to an alkaline draw solution such as ammonium bicarbonate (Xie, et al., 2015). Furthermore, CTA membranes deliver significantly lower fluxes than TFC FO membranes (Fam, et al., 2013; Jin, et al., 2012a).

The rejection performances of CTA and TFC membranes have previously been compared by Jin, et al. (2012a), Xie, et al. (2013b) and Xiao, et al. (2017). Due to the marginal negative charge of CTA membranes compared to TFC membranes, the contribution of electrostatic interactions to the rejection of charged compounds by CTA membranes is likely unimportant. With such membranes, the hydrophobicity of solutes strongly influence their rejection. Thus, hydrophobic interaction and steric exclusion are the dominant mechanisms of solute rejection by CTA membranes.

In general, TFC polyamide membranes exhibit higher rejections than CTA membranes (Xiao, et al., 2017; Jin, et al., 2012a). In the case of charged compounds, this can be attributed to their significant electrostatic interactions with the negatively charged active layer of the membrane. Furthermore, the steric exclusion effect is greater in the case of TFC membranes as a result of the lower ratio of the solute permeability coefficient to water permeability coefficient of TFC membranes compared to that of CTA membranes (Jin, et al., 2012a).

2.3.3.2 *Draw solution properties*

The chemistry of the draw solution is an important consideration in the FO process as it generates the driving force for water flux. The ideal draw solute in FO facilitates a high water flux and low reverse solute flux (Corzo, et al., 2017; Achilli, et al., 2010). For engineered draw solutions, it is favorable when the draw solute is inexpensive and easily separated from the product water.

The rejection of solutes is favoured by the ideal draw solute which generates a high water flux as the solute rejection improves with the water flux, or draw solute that generates a higher osmotic pressure (Jin, et al., 2011). Conversely, the rejection of feed solutes is improved when the reverse flux of the draw solute is significant, which is not desired in the normal operation of the FO

34

process. Hence, there exists a trade-off between the loss of the draw solute by reverse diffusion and the rejection of feed solutes (Xie, et al., 2015).

The reverse flux of the draw solute is related to the diffusivity of its ions. A draw solute with a low diffusivity exhibits a lower reverse solute flux than a draw solute with a high diffusivity. Typically, draw solutes of divalent ions, such as $MgSO_4$, have lower diffusivities than draw solutes of monovalent ions, such as NaCl (Holloway, et al., 2015). Accordingly, Achilli, et al. (2010) found that the reverse solute flux of $MgSO_4$ and Na_2SO_4 were lower than that of $MgCl_2$ and NaCl.

A number of studies have been conducted in order to understand the mechanism of retarded forward diffusion by reverse draw solute flux, as well as the bi-directional mass transfer across membranes (Xie, et al., 2012a; Yong, et al., 2012; Hancock & Cath, 2009). The reverse transport of the draw solute can influence the interaction of the feed solute with the membrane surface. Xie, et al. (2012a) observed that the adsorption of hydrophobic trace organic compounds in the feed were lower with a significant reverse salt flux, which effectively improved the rejection of the feed contaminants.

Kim, et al. (2012) examined the rejection of boron with draw solutes of different diffusivities. The boron rejection with a NaCl draw solution was double that observed with lanthanum (III) chloride as the draw solute, with the latter exhibiting a lower reverse flux due to its larger hydrated radius compared to NaCl. Thus, reverse solute flux enhances the molecular sieving effect of the membrane.

2.3.3.3 *Feed solution chemistry: pH and ionic strength*
Both the membrane charge and speciation of ionic solutes are influenced by the solution pH, thereby affecting the electrostatic interactions between the solutes and membrane. For instance, at neutral and acidic conditions, phenolic compounds are neutrally charged, whereas a TFC membrane typically has a negative charge at the same conditions. As such, electrostatic repulsion by the membrane is not significant at neutral and acidic conditions. At alkaline conditions, phenolic compounds become negatively charged, while the membrane surface charge is negative. Therefore, increased electrostatic repulsion between the compounds and membrane become significant and the phenolic compounds are rejected to a greater extent at alkaline conditions (Zhang, et al., 2017).

Research in RO and NF has shown that an increase in the local ionic strength of composite membranes 'shrinks' the membrane matrix. This reduces the permeability of neutral organic compounds in particular (Bellona, et al., 2004; Braghetta, et al., 1997). The local feed solution

ionic strength at the membrane surface further influences the electrostatic interactions of charged compounds with the negatively charged membrane surface (Liu, et al., 2019; Sauchelli, et al., 2018; Wen, et al., 2006). Sauchelli, et al. (2018) found that the rejection of positively charged compounds by a TFC membrane increased with the ionic strength of the FS as a result of the reduced electrostatic attraction of the solutes to the negatively charged membrane.

2.3.3.4 *Membrane orientation*

The physicochemical properties of the support layer of FO membranes can be significantly different to that of the active layer. In addition, the magnitude of the water flux and extent of CP encountered in the AL-FS and AL-DS orientations are not similar. As a result, the solute transport and rejection mechanisms of the two orientations are not the same. In the study by Alturki, et al. (2013), the rejection of charged and low molecular weight neutral organic compounds was lower in the AL-DS orientation. The same observation for inorganic contaminants including calcium, boron and arsenate was made in the study by Jin, et al. (2012b). This consistently lower rejection in the AL-DS orientation has been attributed to the CICP effect that increases the effective concentration gradient of the solute across the membrane. Thereby the solute flux is increased and rejection decreased (Xie, et al., 2015; Jin, et al., 2012b).

Contradicting observations of the caesium rejection by a TFC membrane were made by Liu, et al. (2019). The caesium rejection in the AL-FS orientation was lower than in the AL-DS orientation, but the difference became diminished as the FS ionic strength was increased. This result suggests that the electrostatic repulsion of positively charged solutes by a TFC membrane is more significant in the AL-FS orientation than in the AL-DS orientation.
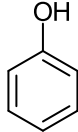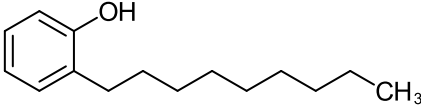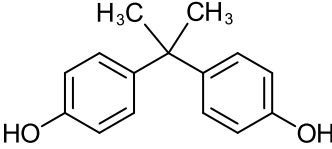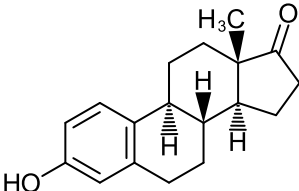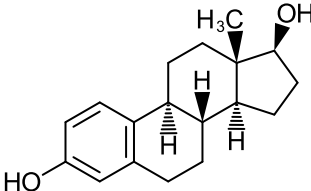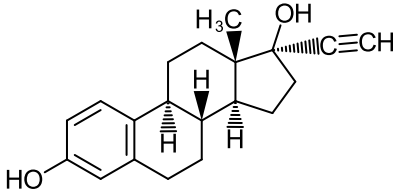
2.3.4 Organic contaminant rejection

Trace organic compounds (TrOCs) in reclaimed water, surface water and groundwater include a wide range of charged, hydrophobic nonionic and hydrophilic nonionic contaminants such as endocrine disrupting compounds (EDCs), pharmaceutically active compounds (PhACs) and disinfection byproducts (Coday, et al., 2014). These compounds are released into the environment from industrial, urban and rural sources. The reader is referred to the work of Chen, et al. (2006) and Coday, et al. (2014) for an extensive list of TrOCs occurring in wastewater and those already considered in the research of FO membrane rejection, respectively.

EDCs are typically phenolic compounds, such as nonylphenol, bisphenol A and the estrogens estrone, 17β-estradiol, 17α-ethinylestradiol and estriol (Alturki, et al., 2012; Alturki, et al., 2013; Hancock, et al., 2011; Valladares Linares, et al., 2011; Xie, et al., 2012a). The molecular structures of phenol and its derivatives are presented in Table 2-6. These compounds are nonionic and

moderately to highly hydrophobic as a result of the benzenoid ring in their structures (Pereira, et al., 2009).

Table 2-6: The molecular structures of common EDCs (Xie, et al., 2015).

Phenol	Nonylphenol	Bisphenol A
Estrone	17β-estradiol	17α-ethinylestradiol

In accordance with the solute rejection mechanisms discussed in Section 2.3.2, it has been shown that hydrophobic nonionic TrOCs are rejected less efficiently by FO membranes than negatively charged TrOCs (Coday, et al., 2014). Furthermore, the rejection of hydrophobic compounds decreases with decreasing hydrophobicity. However, it has been found that their rejection varies greatly with molecular weight (Jin, et al., 2012a).

2.3.4.1 Phenol

Phenol consists of a phenyl group (-C$_6$H$_5$OH) bonded to a hydroxyl group (-OH). It has a low hydrophobicity (log K_{OW}=1.46), and a low molecular weight (94.11 g·mol^{-1}) in comparison to the MWCO of typical TFC membranes (Cui, et al., 2016). Phenol has been listed as a toxic organic compound due to its bio-toxicity and unpleasant odor, despite occurring at low concentrations (Hill & Robinson, 2004; USEPA, 1979) in the environment. An extensive review on the chemistry and toxicology of phenol can be found in the publication of Anku, et al. (2017).

The application of pressure-driven membrane processes for the removal of phenol from wastewater has been reported. NF membranes typically show a lower phenol rejection than RO membranes as the latter have a 'tighter' membrane matrix. The phenol rejection by RO membranes can exceed 90% (Hidalgo, et al., 2011; Li, et al., 2010). Not many investigations have been made into the potentially low rejection of phenol by FO membranes, considering its low

molecular weight and the low operating pressures in the FO process, which facilitate the passage of this compound across the membrane.

The limited number of experimental studies on the removal of phenol by FO membranes are summarised in Table 2-7 at the end of this sub-section. It is clear that relatively similar experimental testing conditions have been applied in these investigations. However, the majority of the feed phenol concentrations considered were significantly higher than environmentally relevant levels (>1 mg·L^{-1}). The reason for this is that the adsorption of phenol to the system components influences the observed rejection of the compound at very low concentrations (Huang, et al., 2018). Cui, et al. (2016) and Huang, et al. (2018) evaluated the phenol transport and rejection at feed concentrations greater than 100 mg·L^{-1}. However, at these high concentrations of phenol, the water flux was affected as a result of the increased osmotic pressure of the FS.

Huang, et al. (2018), Cui, et al. (2016) and Xiao, et al. (2017) evaluated the effect of the water flux on the phenol rejection. Among all three studies, it was found that the phenol rejection was favoured by an increase in the water flux in the AL-FS membrane orientation (Section 2.3.3.2). However, the AL-DS orientation was not investigated. Furthermore, the pH dependence of the phenol rejection by TFC membranes above its dissociation constant was observed by Xiao, et al. (2017) and Huang, et al. (2018) with TFC membranes. At a water flux of approximately 10 L·m^{-2}·h^{-1}, an increase in the FS pH from 7 to 11 provided a 30% increase in the phenol rejection in the former study, but only a 10-12% improvement in rejection for the same change in FS pH was found by Huang, et al. (2018).

In general, the phenol rejection of sourced FO membranes used thus far by research groups are significantly low, between 20 and 60% (Heo, et al., 2013; Li, et al., 2017; Xiao, et al., 2017). The TFC membranes fabricated and tested by Cui, et al. (2016) and Huang, et al. (2018) provided phenol rejections higher than 70%. The active and support layer of these membranes were fabricated from polyamide and polysulfone, respectively, like those commercially available.

2.3.5 Inorganic contaminant rejection

The fate and occurrence of inorganic substances in untreated water sources is a crucial public and environmental concern. FO has been considered for the removal of heavy metals from a wide range of high strength wastewaters. Vital, et al. (2018) observed a near perfect rejection of heavy metal ions present in acid mine drainage with a TFC membrane. Of particular importance in groundwater treatment, Jin, et al. (2012b) showed that FO membranes can provide a 60-95% arsenic rejection.

Liu, et al. (2019) considered the removal of cobalt (Co), strontium (Sr) and caesium (Cs) from radioactive wastewater by CTA and TFC membranes. Both types of membranes showed high rejections of cobalt and strontium (90-100%). However, the TFC membrane was ineffective in rejecting caesium, such that the caesium removal was approximately 50% lower than that of the divalent cobalt and strontium ions.

The removal of boron and lithium is an important consideration in the treatment of produced water, salt lake brine, highly contaminated groundwater, as well as seawater (Bell, et al., 2017; Li, et al., 2018; Turek, et al., 2007). A brief background of the chemistry of these elements in water and research on their rejection by membranes follows below.

2.3.5.1 *Boron*

Boron is the only non-metallic element in group 13 and has a molecular weight of 10.8 g·mol^{-1}. Depending on its feed concentration and the pH of the local solution, boron may exist as various species in the aqueous environment. It has been shown that surface and ground water in industrial areas may contain up to 3.8 mg·L^{-1} and 140 mg·L^{-1} boron, respectively (Xu, et al., 2010). The average boron concentration in seawater is approximately 4.5 mg·L^{-1}, but in some seawaters this level can reach 15 mg·L^{-1}. At these levels, boron predominantly exists as the mononuclear species, boric acid and borate anions. The distribution of boron between these two species is further dependent on its pK$_a$ of 9.24 at 25°C. Thus, at neutral and low pH conditions, the dissociation of boron is low and boric acid is the dominant species (Sunbul, 2018). The reader is referred to the review on the chemistry of boron in water by Kochkodan, et al. (2015).

With the development of high rejection TFC RO membranes for seawater desalination, the boron rejection in a single-pass RO configuration is typically greater than 90% (Farhat, et al., 2013). The experimental testing conditions and results from previous studies on the boron rejection in FO are provided in Table 2-8. Despite the limited number of studies that have been published thus far, a wide range of testing conditions have been applied. In the majority of the studies summarised in Table 2-8, boron concentrations above seawater levels, up to 100 mg·L^{-1}, have been investigated. Typically, the accuracy of boron quantification was compromised at lower feed concentrations (Fam, et al., 2014). Most studies suggested that TFC FO membranes exhibit low boron rejections, between 20 and 50%, at practical DS osmotic pressures, such as that of seawater (Jin, et al., 2012b; Valladares Linares, et al., 2014; Jin, et al., 2011).

The effects of the feed water chemistry and operating conditions on the rejection of boron in FO have been investigated. It was generally found that the boron rejection is independent of its concentration in the feed water (Fam, et al., 2014; Kim, et al., 2012), but its rejection at higher

39

concentrations in the DS, which simulates a seawater draw solution, has not been evaluated. A key parameter in the transport and rejection of boron is the solution pH. The rejection of boron can be improved by an increase in the FS pH. Alkaline conditions facilitate the speciation of boron to borate anions, thereby allowing it to be readily rejected (Wang, et al., 2017; Fam, et al., 2014; Kim, et al., 2012)

2.3.5.2 Lithium

Lithium is the lightest metal element, with a MW almost half that of boron (6.9 g·mol^{-1}). Lithium is mainly sourced from salt lake brines with lithium concentrations ranging from 5×10^{-3} mg·L^{-1} to 2000 mg·L^{-1}. It is present in seawater at a concentration of approximately 0.17 mg·L^{-1}. The lithium concentration in some groundwater samples tested have ranged from <0.2 mg·L^{-1} to 0.24 mg·L^{-1} (Oram, 2014). The reader is referred to the work of Adams Kszos & Stewart (2003) for an extensive review on the occurrence and toxicity of lithium in the aqueous environment.

Lithium compounds, such as lithium chloride, are highly soluble and relatively chemically inert. Due to its coexistence with other minerals at a very low concentration, the extraction of lithium from its sources is a challenging task (Wen, et al., 2006). Currently, conventional methods such as precipitation (Jianfeng, et al., 2017), extraction (Liang, et al., 2009) and adsorption (Lee, 1980) are employed to remove lithium from the aqueous environment.

Lithium removal by membranes has only been evaluated recently, but more often for NF and RO membranes. NF membranes typically show a weaker rejection of lithium (<75%), while RO is capable of removing more than 80% of the lithium in the feed water (Bi, et al., 2014; Somrani, et al., 2013; Wen, et al., 2006). Furthermore, Wen, et al. (2006) observed that the lithium rejection in RO was heavily influenced by the ionic strength of the FS.

The first study on the lithium removal by FO membranes was published by Coday, et al. (2013). They observed a 78-88% lithium rejection with a TFC FO membrane (Oasys) operated in the AL-FS orientation with a 47 bar NaCl DS. Li, et al. (2018) evaluated the concentration of lithium from salt lake brines with a feed concentration of 0.78 mg·L^{-1}. However, the calculated lithium rejection was not reported in their work. To the author's knowledge, there is still limited research on the lithium transport in FO[3].

---

[3] Due to a shortage in literature, a table summarising the research on the lithium rejection by FO membranes is not included.

Table 2-7: Summary of the studies on the phenol rejection by FO membranes. The symbol c_F refers to the phenol concentration in the feed solution.

Membrane	Orientation	c_F / mg·L^{-1}	FS	DS	T	pH	J_W / L·m^{-2}·h^{-1}	Rejection	Reference
CTA (HTI)	AL-FS	0.5	DI water	1 M NaCl	20°C ± 1°C	7	10	20%	Heo, et al. (2013)
TFC (in-house fabricated)	AL-FS	500-2000	DI water	1 M NaCl	-	-	15-18	72-75%	Cui, et al. (2016)
TFC (Solvay)	AL-DS	500	10 mM Na$_2$SO$_4$	1 M Na$_2$SO$_4$	Ambient	-	12	±50%	Li, et al. (2017)
TFC (HTI)	AL-FS	100	DI water	-	25°C	2-11	9	-	Zhang, et al. (2017)
TFC (FTS)	AL-FS	100	1000 mg·L^{-1} NaCl	1-4 M NaCl	25°C ± 1°C	7	5-10	30-60%	Xiao, et al. (2017)
TFC (in-house fabricated)	AL-FS & AL-DS	100-500	DI water	1 M NaCl	-	7	7-8 (AL-FS) 7.5-12 (AL-DS)	85-89% (AL-FS) 82-83% (AL-DS)	Huang, et al. (2018)

Table 2-8: Summary of the studies on the boron rejection by FO membranes. The symbol c_F refers to the boron concentration in the feed solution and n indicates a neutral pH.

Membrane	Orientation	c_F / mg·L^{-1}	FS	DS	T	pH	J_W / L·m^{-2}·h^{-1}	Rejection	Reference
CTA (HTI)	AL-FS & AL-DS	5	DI water	0.1-5 M NaCl	24°C	5.9	3.6-25 (AL-FS) 3.6-38 (AL-DS)	20-60% (AL-FS) 10% (AL-DS)	Jin, et al. (2011)
CTA (HTI)	AL-FS & AL-DS	10	7 mM NaCl & 1 mM CaCl$_2$	0.5-5 M NaCl	24°C	6	7.2-25 (AL-FS & AL-DS)	30-65% (AL-FS) 10-20% (AL-DS)	Jin, et al. (2012b)
CTA (HTI)	AL-FS	20-80	10 mM NaCl	2 M NaCl	20°C	7	14.4	50%	Kim, et al. (2012)
TFC (Woongjin)	AL-FS	30-80	35 g·L^{-1} NaCl	2 M KCl	-	n	16	50%	Fam, et al. (2014)
TFC (HTI)	AL-FS & AL-DS	0.5	DI water	0.32 M NaCl	20°C	7.2	8.5	-	Valladares Linares, et al. (2014)
CTA (HTI)	AL-FS	5	DI water	32 g·L^{-1} NaCl	25°C	6-8	5.5	80-100%	Choi, et al. (2016)
TFC (in-house fabricated)	AL-FS & AL-DS	100	DI water	0.5-4 M NaCl	23°C	n	10-35 (AL-FS) 13-65 (AL-DS)	50-75% (AL-FS) 25-45% (AL-DS)	Luo, et al. (2016)
TFC (in-house fabricated)	AL-FS & AL-DS	10	DI water	0.75 M (AL-FS) 0.2 M (AL-DS) NaCl	-	7-10	9.5	48-86% (AL-FS) 18-52% (AL-DS)	Wang, et al. (2017)

2.4 FO-RO hybrid processes

2.4.1 Osmotic dilution of seawater

A number of reviews on the applications, challenges and future prospects of hybrid FO systems have been published (Awad, et al., 2019; Chekli, et al., 2016; Blandin, et al., 2016). FO-RO hybrids have been considered for regeneration of the DS, advanced desalination pretreatment, alternative desalination and wastewater treatment. Their application for simultaneous desalination and wastewater treatment, facilitating the intermediate osmotic dilution of seawater, is of importance to this study. The typical configuration of this process is illustrated in Figure 2-7.
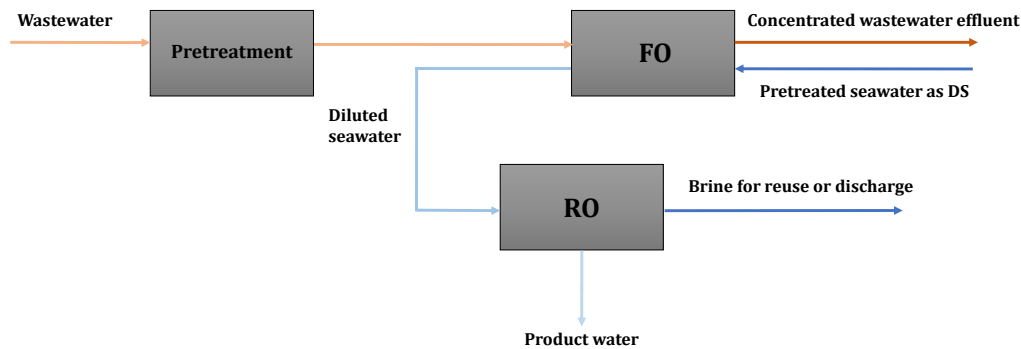

Figure 2-7: The FO-RO hybrid process used for osmotic dilution of seawater (Awad, et al., 2019; Blandin, et al., 2016).

The FO-RO hybrid process used for osmotic dilution has been installed on large-scale for research purposes on two occasions. These installations are summarised in Table 2-9. The FO-RO osmotic dilution process has been modelled by Jeon, et al. (2016), Choi, et al. (2015) and Altaee, et al. (2015) with interest in the analysis of the energy consumption of the process.

Table 2-9: Two large-scale installations of the FO-RO hybrid, used for the osmotic dilution of seawater prior to RO, as surveyed from literature.

Location	Feed	DS	FO membrane	RO membrane	Capacity / m³/day	Reference
Korea	Power-plant wastewater	Seawater	Flat sheet TFC (PFO-100, Porifera)	SW30 HR-380 (DOW)	21.8	Choi, et al. (2017)
USA	Secondary effluent & tertiary effluent	Seawater	Flat sheet CTA (HTI)	SW30-2540 (DOW)	-	Hancock, et al. (2011)/Cath, et al. (2010)

2.4.2 Contaminant removal

The rejection of TrOCs by the FO-RO hybrid process was experimentally investigated by Hancock, et al. (2011) and Cath, et al. (2010) at pilot-scale and by Valladares Linares, et al. (2011) at bench-scale. These studies are summarised in Table 2-10. The results from these studies were in

agreement, with conclusion that the FO-RO hybrid is capable of achieving a >99% rejection for strongly rejected compunds, with concentrations in the permeate below detection limits.

Table 2-10: Summary of studies on TrOC removal by FO-RO hybrids used for the osmotic dilution of seawater.

Membrane		Feed solution	Draw solution	No. of TrOCs	Rejection (min.,max.)	Reference
FO	RO					
CTA (HTI)	SW30-2540 (DOW)	Secondary effluent	Seawater	6	>72%, >99%	Cath, et al. (2010)
CTA (HTI)	SW30-2540 (DOW)	MBR permeate	Seawater	32	>96%, >99%	Hancock, et al. (2011)
CTA (HTI)	BW30	Secondary effluent	Seawater	13	>89%, >99%	Valladares Linares, et al. (2011)

2.5 Literature summary

The literature review was conducted to provide insight into the FO process with regards to the mass transport phenomena, the submerged FO configuration and the rejection of feed solutes. Essential considerations to systematically perform this experimental study on solute transport in FO were outlined. Furthermore, important equations to analyse the experimental results were highlighted. Although not exhaustive, several key points from the literature review are listed below:

1. FO principles and mass transport

i)   The osmotic pressure gradient between the FS and DS ($\Delta\pi$) is the driving force for the water flux (J_W) in FO. The osmotic pressure of a solution is directly affected by its solute concentration and temperature.

ii)   The diffusion of sodium chloride across membranes can be quantified from the conductivity of the adjacent solutions.

iii) The hydrated radius of a positively charged solute is not the determining factor of its transport across membranes.

iv)   RSD and CP are unavoidable mass transport phenomena in the FO process due to the 1) draw solute concentration difference across the membrane and 2) the formation of boundary layers on and within the membrane.

v)   ECP is mitigated by optimised hydrodynamic conditions at the membrane surface. ICP occurs within the membrane support layer. Thus, it cannot be mitigated by hydrodynamic conditions. Both these phenomena result in a loss of driving force for water permeation. The ECP and ICP moduli can be implemented to evaluate the significance of CP.

vi) The mass transport in FO is heavily dependent on whether the membrane active layer faces the FS (AL-FS orientation) or DS (AL-DS orientation).

2. Submerged FO

There is limited information on the design of submerged FO units. A survey of previous studies showed that the hydrodynamic conditions in submerged FO units is not standardised.

i) Agitation of the feed is required in the submerged FO configuration to mitigate ECP. This has previously been achieved with aeration, stirring or recirculation of the FS.

ii) RSD results in the alteration of the FS chemistry due the accumulation of the draw solute in the FS. This further aggravates CP.
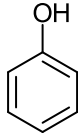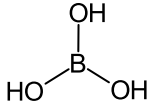
3. Trace solute removal by FO membranes

i) The solute rejection can be used to quantify and compare the removal of solutes by the FO membrane. The solute flux must be considered to understand the difference in the transport behaviour that influences the rejection.

ii) Solutes are transported across the FO membrane by diffusion and convection.

iii) The solute rejection mechanisms of membranes include steric exclusion, electrostatic repulsion/attraction and hydrophobic interaction. Steric exclusion is governed by the solute molecular weight or ionic/hydrated radius, electrostatic interaction by the charge of the solute and membrane and hydrophobic interactions by log K_{OW} of the solute.

iv) The forward diffusion of trace solutes may become hindered when the reverse diffusion of the draw solute to the FS is significant.

v) The rejection of both uncharged and charged feed solutes may be affected by the FS ionic strength and pH as a result of the constriction of the membrane matrix and shielded electronegativity of TFC membranes.

vi) The solute rejection is affected by the membrane orientation as a result of the difference in the transport mechanisms between the AL-FS and AL-DS orientations.

Phenol, boron and lithium were identified as model solutes for this study. With consideration of the abovementioned points, important properties of these feed solutes, as well as that of the NaCl draw solute, are summarised in Table 2-11

From the surveyed literature, it is evident that the rejection of phenol by TFC FO membranes can potentially range from ±50% to ±89%, depending on the process conditions. Boron rejections

ranging from ±50% to ±86% have previously been achieved with TFC membranes. There is a lack of concrete evidence of the lithium rejection of TFC membranes in FO.

Table 2-11: Summary of the properties of the model feed solutes (phenol, boron as boric acid and lithium) and the draw solute (sodium chloride) for this study. The molecules indicated are as the solutes of interest speciate in water.

Property	Phenol	Boric acid	Lithium	Sodium	Chloride
Aqueous species	(phenol structure, OH)	(boric acid structure, OH, HO, B, OH)	Li^+	Na^+	Cl^-
MW / g·mol^{-1}	94.11	61.83	6.94	22.99	35.45
pK$_a$ (25°C in water)	9.98[4]	9.24	-	-	-
log K$_{OW}$	1.46	0.175	-	-	-
Stokes radius / nm	-	0.155[5]	0.074[6]	0.183	0.120
Hydrated radius / nm	-	-	0.382[7]	0.358[7]	0.332[7]
D (x 10^9) / m^2.s^{-1}	1.025[8]	1.28[9]	1.03[10]	1.33[10]	2.03[10]

4. FO-RO hybrid processes

In support of simulating the permeate quality of the FO-RO hybrid at practical RO membrane rejections and operating conditions, important literature is provided in context in Chapter 5 . The reader is referred to the comprehensive reviews on FO-RO hybrid processes previously published by Awad, et al. (2019), Blandin, et al. (2016) and Chekli, et al. (2016).

[4] Gross & Seybold (2001)

[5] Tu, et al. (2013)

[6] Ionic radius

[7] Volkov, et al. (1997)

[8] Winkelmann (2017)

[9] Oren & Biesheuvel (2018)

[10] Cussler (2007)

Chapter 3

Experimental setup, materials and methods

3.1 Bench-scale experimental setup

A bench-scale membrane system was constructed to experimentally investigate the solute transport in submerged FO. According to the specific design problem, a number of design requirements were identified to facilitate the functionality and robustness of the system. A unique experimental method was developed for the constructed prototype, which was followed by the characterisation of the unit. The design process is detailed in the following sub-sections.

3.1.1 Design problem

The submerged OMBR module provides a compact water treatment technology for wastewater reuse applications. In contrast to bilateral cross-flow FO units, circulation of the FS is not required in the submerged configuration, which is advantageous in the treatment of wastewaters with high viscosities. It has also been highlighted in the literature study that sufficient turbulence is required in submerged FO configurations to mitigate ECP, which is normally achieved by tangential flow over the membrane in cross-flow units. Aeration by bubble-diffusers has most commonly been implemented in OMBR studies (Holloway, et al., 2015a).

Recently, Chowdhury, et al. (2017) and Blandin, et al. (2018) evaluated the submerged FO flux performance with stirring of the FS instead of aeration. Chowdhury, et al. (2017) observed from fouled membrane coupons that dead zones can exist in a system which implements an overhead mechanical stirrer at the membrane surface. It was also highlighted in the study of Blandin, et al.

(2018) that stirring might not be ideal for submerged FO due to the excessive shearing on the FO membrane surface.

3.1.2 Design requirements and specifications

With consideration of the principles and performance indicators of the FO process in conjunction with the inherent design and operation of submerged FO units, the most critical design requirements for this bench-scale setup are:

1. a feed reservoir that accommodates a submerged FO membrane,
2. a cross-flow channel for the circulation of the DS on the opposite side of the submerged membrane surface,
3. a functional agitation mechanism in the FS to maintain turbulence and reduce dead zones at the submerged membrane surface,
4. a means of maintaining a constant osmotic pressure with a recirculated DS,
5. a method of measurement of the FO water flux,
6. maintenance of an equal FS and DS temperature and
7. a method of measurement of DS flowrate to evaluate its cross-flow velocity in the cross-flow channel.

Several design specifications for submerged FO units, such as the appropriate DS cross-flow velocity and hydrodynamic conditions on the feed side of the submerged FO membrane, have not been stated in the public domain thus far. For the purpose of this design, these parameters were either extrapolated from existing standard methodology for cross-flow configurations (Cath, et al., 2013) or evaluated in preliminary experimentation. Each of the listed design requirements are addressed in the following discussions.

3.1.3 Proposed design

3.1.3.1 Overview

The proposed design of the FO system implemented a rectangular dead-end FS reactor vertically attached to an external cross-flow membrane cell. The DS would be circulated horizontally under the submerged membrane at the base of the reactor. A similar dead-end/cross flow unit has been used in the studies of Chowdhury & McCutcheon (2018) and Chowdhury, et al. (2017). In this work, turbulence was maintained in the reactor by means of the internal circulation of the feed solution by a prototype agitator constructed from a submersible pump and distribution plate. The distribution plate ensured that the flow pattern in the reactor would resemble that created by impellers in cylindrical vessels.

47

With the proposed design, the operation of the submerged FO unit could be significantly simplified by the direct attachment of the membrane cell to the base of the FS reactor. However, this design might not be completely practical in full-scale applications. Nevertheless, the agitation mechanism implemented in this work could avoid the establishment of dead-zones within the submerged space and membrane abrasion created by impellers. Furthermore, circulation may be an improvement on aeration as intense bubbling may reduce the contact time of the bulk FS with the membrane surface, which could result in a compromised water flux. As a result, a highly performant submerged FO system could be assembled.

3.1.3.2 Approach

The design of the FO system was based on the active membrane area and admissible water flux. With membrane dimensions of 180×94 mm and cross-flow channel width of 1.5 mm, a theoretical cross-flow velocity of 0.25 m·s^{-1} could be achieved with a DS flowrate of 1.8 L·min^{-1}. This cross-flow velocity has been regarded as standard methodology for cross-flow membrane configurations (Cath, et al., 2013). However, the operability of the FO system at this cross-flow velocity in the DS channel had to be confirmed.

The membrane active area of 169.2×10^{-4} m^2 with the dimensions mentioned above provided the base of the FS reactor. The complete volumetric capacity of the FS reactor was designed to minimise the increase in the FS osmotic pressure resulting from RSD at a design water flux of 20 L·m^{-2}·h^{-1} and specific reverse solute flux of 0.5 g·L^{-1}, as specified by the membrane supplier. As shown in Figure 3-1, a FS volume of approximately 6 litres would be sufficient to keep the change in the FS osmotic pressure below 0.1 bar over a permeation time of 4 hours. Herewith, the agitator could also be accommodated above the membrane, while a compact and simple design could be achieved.

In order to avoid the consumption of large amounts of water during experimental testing, a continuously recycled DS was implemented. The disadvantages of recycling the DS is that it becomes increasingly diluted by the FS permeate volume and contaminated with the FS solutes as the filtration time is increased. Hence, its osmotic pressure and purity is affected. A DS volume of 200 L was used in the design based on the findings presented in Figure 3-2. With this working volume, the relative change in the DS osmotic pressure resulting from dilution could be minimised to 0.7% with an initial osmotic pressure of 27 bar (osmotic pressure of seawater), admissible water flux of 20 L·m^{-2}·h^{-1} and maximum estimated test duration of 4 hours.
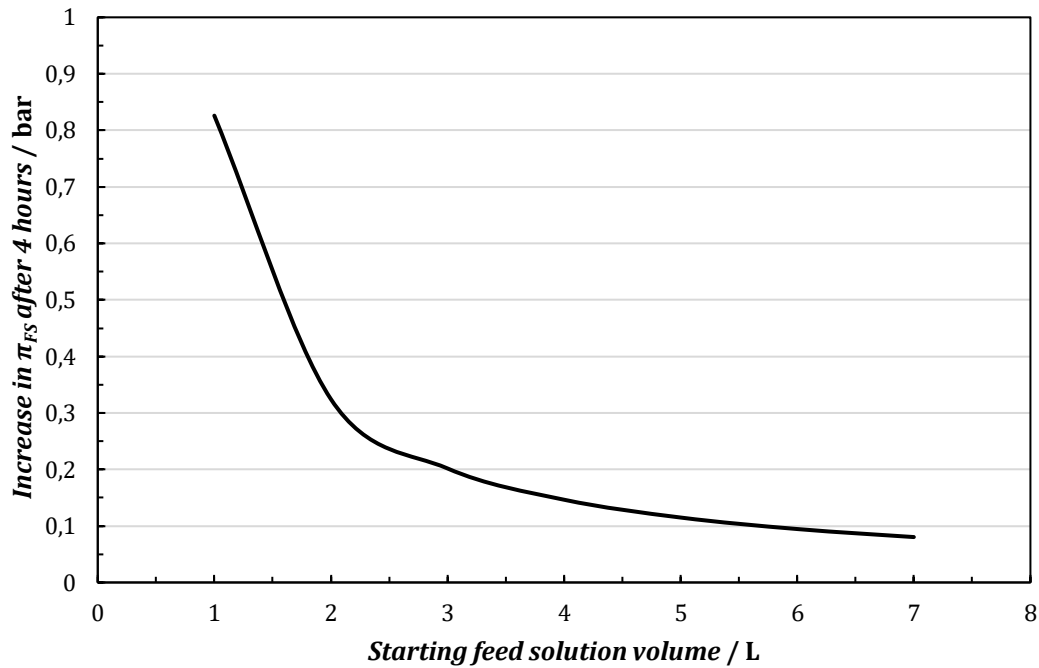
Figure 3-1: The calculated increase in the osmotic pressure of the FS (π_{FS}) after 4 hours of water permeation as a function of the initial FS volume. The basis for calculation was a specific reverse solute flux of 0.5 g·L^{-1}, an active membrane area of 169.2 × 10^{-4} m^{2} and the design water flux of 20 L·m^{-2}·h^{-1}.
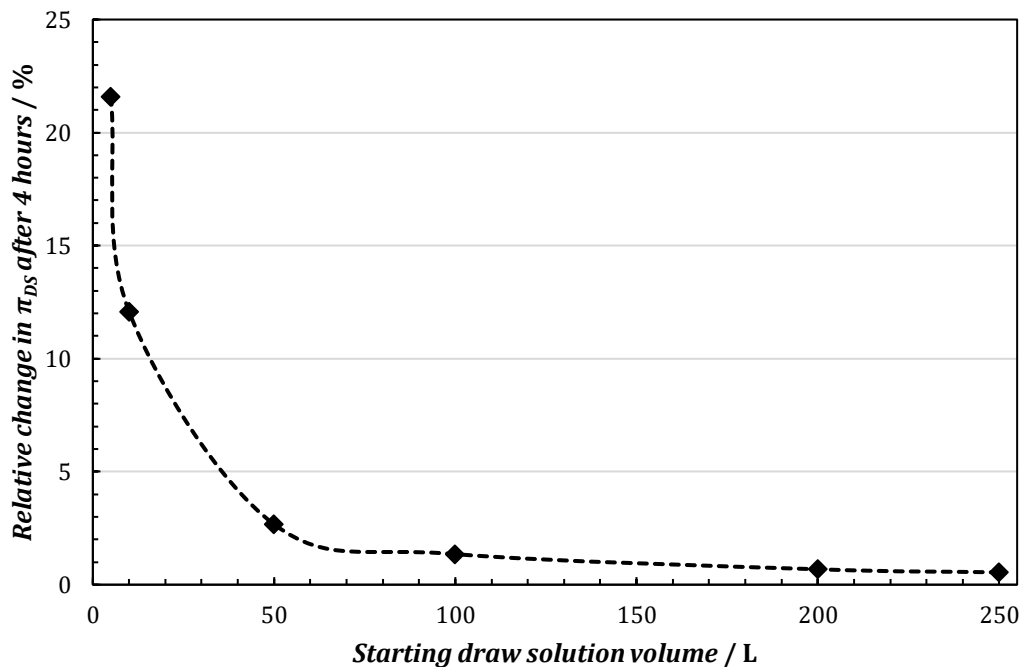

Figure 3-2: The calculated relative change in the osmotic pressure of the DS (π_{DS}) after 4 hours of dilution by the FO flux as a function of the initial DS volume (L). The basis for calculation was the active membrane area of 169.2 × 10^{-4} m^{2}, the design water flux of 20 L·m^{-2}·h^{-1} and a starting DS osmotic pressure of 27 bar (35 g·L^{-1} NaCl).

A critical consideration in this design was the method by which the FO permeate water flux would be measured. Quantifying the water flux in FO is more complex than in RO, as the permeate volume combines with the DS volume. A commonly used method is the measurement of the change in mass of the FS or DS over time with a balance (Cath, et al., 2013). In this design, determination of the water flux from the change in mass or volume of the DS could not be considered due to the high volume of the DS relative to that of the permeate. The desired accuracy in the FO water flux would not have been obtained by this method. For this reason, the water flux was quantified from the change in volume of the FS measured on a graduated cylinder integrated in the cover of the FS reactor.

3.1.4 Prototype

In this section, the designed and constructed submerged FO system is described in detail. Firstly, the process flow is detailed with a process-flow diagram (PFD). The various parts of the setup are also described with particular attention to the FS reactor, hydrodynamic agitation device and the outlet flowmeter.

3.1.4.1 *Process flow description*

A PFD of the FO system is provided in Figure 3-3. The DS with a NaCl concentration of preference is prepared in TK-101, which is equipped with a calibrated, externally fitted transparent tube to indicate the level of the DS within the tank. A tank heater, HX-101, with a thermostat can be switched on and submersed in the DS. Provision for the temporary shut-off of TK-101 is made with VA-101. TK-101 is drained through VA-102.

The preferred FS is loaded into TK-103, which is furnished with the prototype agitator consisting of a submersible fish tank pump, P-102, and distribution plate, DIS-101. The FS in TK-103 rests on top of the active area of the membrane cell, FO-101, as depicted in Figure A-1 in Appendix A. During operation, a peristaltic pump, P-101, pumps the DS in TK-101 through a strainer (FS-101) and cartridge filter (FF-101) to the cross-flow channel in the base of the membrane cell. By osmosis, the FS becomes concentrated and the DS diluted. The water flux is quantified from the reduction in the liquid level in TK-103, which is measured from the graduation on the cylindrical tube integrated its cover.

The diluted DS flows from the membrane cell through the in-line flowmeter, FM-101, which is used to measure the flowrate of the DS by the bucket-and-stopwatch principle. During normal operation when no flowrate measurement is taken, VA-104 is open to allow the diluted DS to collect in the DS reservoir, TK-102. A submersible pump in the reservoir, P-103, recycles the DS back to the feed DS tank (TK-101) when the level switch is triggered.

50

Figure 3-3: Process flow diagram of the bench-scale FO membrane system.
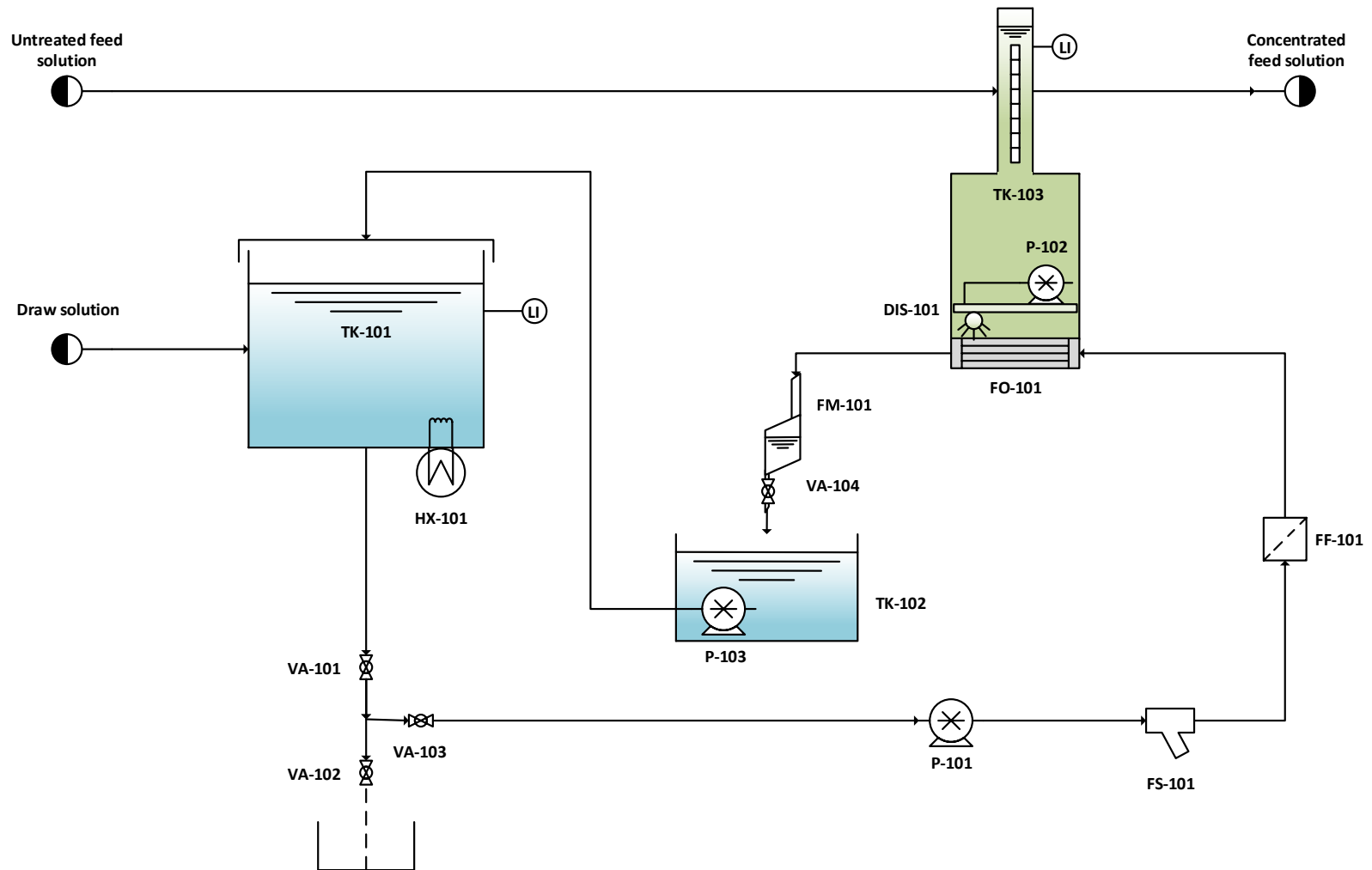
TK-101	HX-101	P-103	TK-102	FM-101	P-101	DIS-101	FO-101	P-102	TK-103	FS-101	FF-101
Feed DS tank	Submersible DS tank heater	Submersible DS recycle pump	Diluted DS reservoir	DS flowmeter	Feed DS peristaltic pump	FS flow distribution plate	FO membrane cell	Submerged FS circulation pump	FS reactor	Inlet DS strainer	Inlet DS cartridge filter

3.1.4.2 Equipment description

A list and brief description of all the components integrated in the bench-scale FO setup are provided in Table 3-1. Detailed descriptions of the submerged FO unit, the agitation device and outlet flowmeter follow.

Table 3-1: List and descriptions of equipment integrated in the bench-scale FO setup.

Component	Description	Operation
DS handling		
TK-101: Feed DS tank	Cylindrical plastic tank	Total volume of 200 litres
TK-102: Diluted DS reservoir	68 litre rectangular container	Collection of the diluted DS from FO-101 for recycling back to the feed DS tank (TK-101)
P-101: Feed DS peristaltic pump	Watson-Marlow 520 S peristaltic pump with thermoplastic Marprene® tubing (8.0 mm bore size/1.6 mm wall thickness)	Pump speed of 100 rpm for a DS flow rate of 1.2 L·min^{-1}
P-103: Submersible DS recycle pump	DAB® Nova Salt W M-A submersible pump for high salinity waters with level switch	Submersible pump in TK-102 for recycling of the diluted DS from low level to TK-101
HX-101: Submersible DS tank heater	300 W water heating element of explosion proof glass with thermostat	20-34°C operating temperature for 200 litres of liquid
FS-101: Inlet DS strainer	200 µm wire strainer	In-line removal of unwanted solids in the DS, periodically cleaned
FF-101: Inlet DS cartridge filter	1 µm polypropylene media filter cartridge in plastic housing	In-line removal of finer particles in the DS, periodically replaced
FM-101: DS flowmeter	In-house fabricated measuring cylinder (4.75 litre capacity) with shut-off valve (VA-104)	Measurement of the DS flowrate
Pipelines	Flexible hose	
FS handling		
TK-103: FS reactor	In-house fabricated rectangular Perspex® tank and cover with integrated measuring cylinder	Total volume of ~ 5.7 litres, P-102 and DIS-101 housed in cavity
FO-101: FO membrane cell	In-house fabricated PVC membrane block with external cross-flow channel	Housing of FO membrane coupon (180×94 mm active area)
P-102: Submerged FS circulation pump	B.I.C.I.S.A® 600 L·h^{-1} aquarium pump	Circulation of the FS within TK-103, connected to DIS-101
Flow distribution plate (DIS-101)	In-house fabricated PVC distribution plate	Plate fixed into FS reactor cavity by Grubbs screws, connected to outlet of P-102

3.1.4.2.1   Submerged FO unit

The submerged FO unit consists of the external cross-flow membrane cell (FO-101) and FS reactor (TK-103). PVC and clear Perspex® were used to fabricate the two components, respectively. Both these materials were chemically compatible with the chemistry of the FS and clear Perspex® could provide visibility of the contents of the reactor.

The external cross-flow membrane cell formed the base of the FO unit with dimensions of $260 \times 174 \times 30$ mm. This cell is essentially one half of a typical cross-flow membrane unit. The dead-end FS reactor, consisting of its flanged rectangular column and cover, represents the other half of the FO cell. The bottom and top flange of the column had the outer dimensions of the membrane cell and inner dimensions of the submerged membrane active area (180×94 mm) to create the cavity for the batch fed feed solution. The graduated cylinder, used for measuring the water flux, was integrated in the cover of the reactor. The FS reactor could accommodate a total volume of 5.7 litres, which includes the volume of the graduated cylinder of 0.74 litres. Detailed design drawings of the membrane cell and FS reactor are provided in Appendix A.2.1 and A.2.2, respectively.

The complete submerged FO unit was assembled as shown in Figure 3-4, with the membrane cell, FS reactor and its cover attached with 8 mm galvanised nuts and bolts. The membrane coupon was inserted over the DS channel between the membrane cell and reactor flange. A diamond-patterned spacer was included in the DS channel to enhance the turbulence of the cross-flow over the membrane surface (Siddiqui, et al., 2017). Tight sealing of the FO unit was critical to the accurate quantification of the water flux. For this reason, a 1.5 mm thick silicone rubber gasket was inserted in the assembly on both sides of the membrane and between the top reactor flange and cover. The assembly was fixed at the top and bottom flange at a predetermined torque of 1.5 N·m and 3.0 N·m, respectively, at which no FS leakage occurred, but damage to the membrane and Perspex® was still avoided.

3.1.4.2.2   Agitation device

The hydrodynamic agitator, consisting of a submersible fish tank pump (P-102) and distribution plate (DIS-101), was used to create turbulent conditions at the submerged membrane surface by recirculation of the FS within the reactor. The distribution plate was fabricated in-house with grey PVC and the submersible pump, with a pumping capacity of 600 L·h⁻¹, was modified to connect to the distribution plate. A detailed design drawing of the distribution plate is provided in Appendix A.2.3.
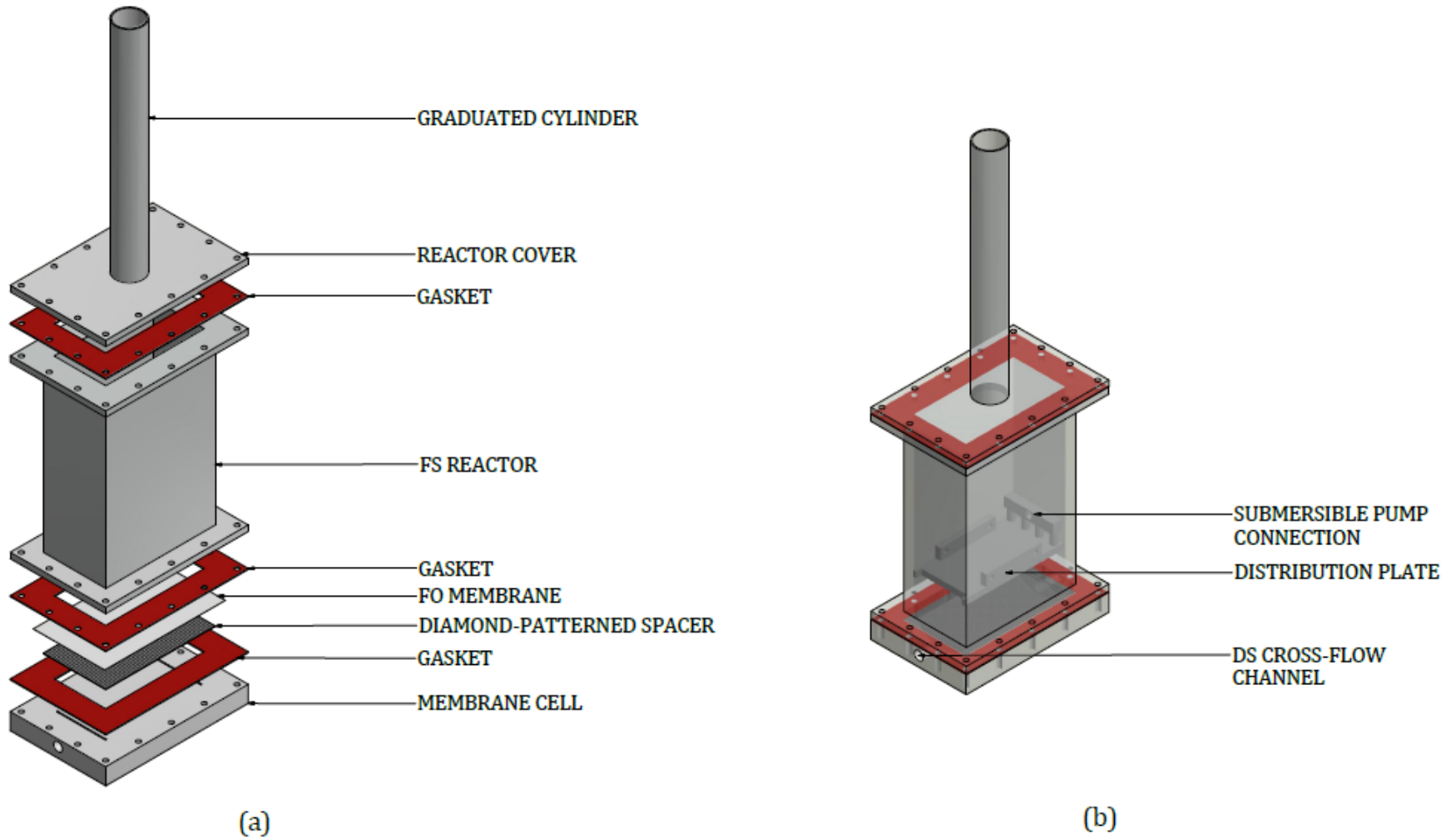
53

Figure 3-4: Illustration of the submerged FO unit consisting of the FS reactor and membrane cell. The unit was assembled as shown in (a). The completely assembled unit, with the distribution plate fixed in the FS reactor, is shown in (b) (Grubbs screws and submersible pump not illustrated).

The distribution plate, as shown in Figure 3-5, was designed with particular concern of the flow pattern that was desired at the submerged membrane surface. The circumference of the plate was equal to that of the cavity in the FS reactor, while small tolerances between the plate edge and reactor wall allowed the plate to move vertically within the cavity. Four Grubbs screws were used to secure the plate to the column walls. The outlet of the submersible pump was elongated to connect to the inlet channel of the distribution plate through a single hole. During operation, the pumped feed solution was ejected over the membrane surface from four 8 mm holes located on the bottom surface of the plate under the inlet channel.

The following considerations were made in the design of the distribution plate to maximise the flow pattern over the submerged membrane surface:

1. The flat surface of the plate, as large as the complete membrane area below, allowed the flow pattern to continue horizontally over the membrane surface from edge A to edge D (Figure 3-5b), while reduced tolerances between the column wall and plate edges minimised the vertical loss of flow at edges B and C.
2. The number of ejection holes were maximised along the width of the plate (Figure 3-5b) to provide the most uniform flow pattern over the complete width of the membrane.
3. A larger tolerance at the opposite end to the ejection point of the plate (edge D, Figure 3-5) provides a means for the circulated liquid to mix with the bulk solution above the plate for recirculation (Figure 3-5c).
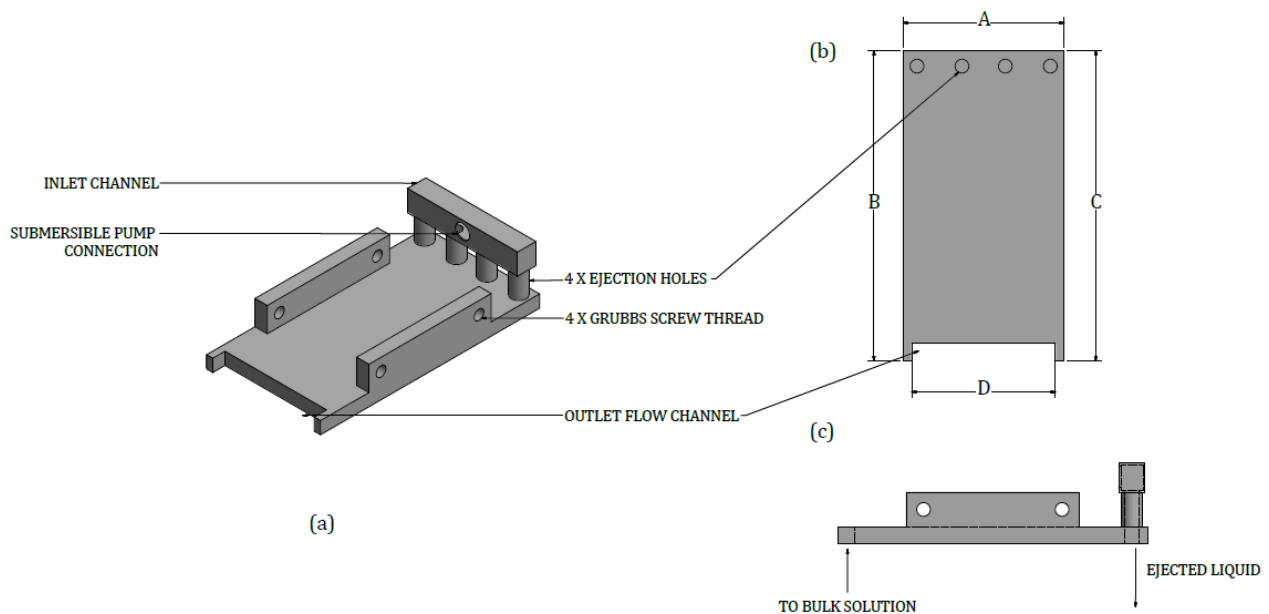

Figure 3-5: Illustration of the fabricated distribution plate with a (a) diagonal view, (b) bottom view and (c) side view.

3.1.4.2.3   Draw solution flowmeter

An in-line flowmeter, or measuring cylinder, was included in the FO setup for the measurement of the volumetric flowrate of the DS. The design of the flowmeter was adapted from Hurter (2019). A detailed design drawing is provided in Appendix A.2.4. As shown in Figure 3-6, the cylinder was equipped with a ball valve at its base and calibrated for a certain volume. While the DS is pumped through the FO system, the valve is closed and the time elapsed for the cylinder to be filled to the predetermined volume is recorded. This design provided a relatively accurate method for determining the DS flowrate without interruption of the process.
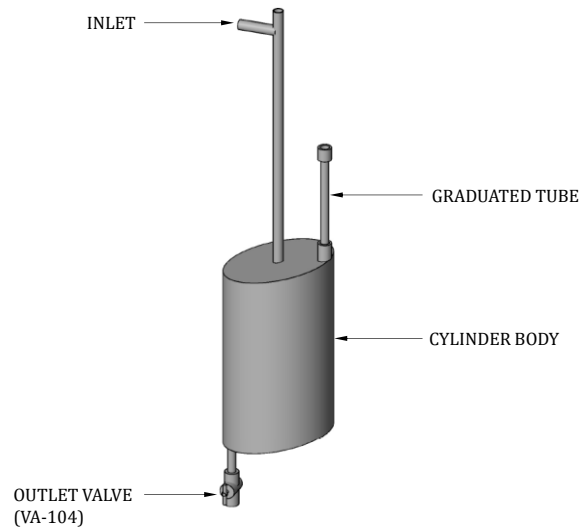
Figure 3-6: Illustration of the in-line flowmeter (FM-101) used to estimate the flowrate of the draw solution.

Several features where included in the design of the flowmeter to improve the accuracy of the flowrate measurement Firstly, the top and bottom surfaces of the cylinder were constructed with a 12° angle to prevent the entrapment of air and hold-up of liquid within the cylinder. The diluted DS pumped from the membrane cell was fed horizontally through a T-piece which was open to the atmosphere through its vertical port. This avoided back-pressure into the DS pipeline. Next to the inlet, a narrow (12 mm inner diameter) graduated tube was located on which the predetermined volume was calibrated in order to note the elapsed time precisely, while still avoiding a significant meniscus error. The cylinder had a large enough volume to prolong the duration of the measurement to above 1 minute.

The cylinder body was fabricated from clear PVC and the graduated tube from Perspex®. The calibrated volume of the cylinder was 4 750 ml, with an error of 0.589 ml and relative error of 1.24%.

3.1.5 Method development

An experimental method applicable to the unique design of this FO system was developed for the analysis of the membrane performance. This required the integration of the system geometry, operating conditions and measured variables by mathematical relationships. The diagram in Figure 3-7 depicts the interdependence among the parameters.
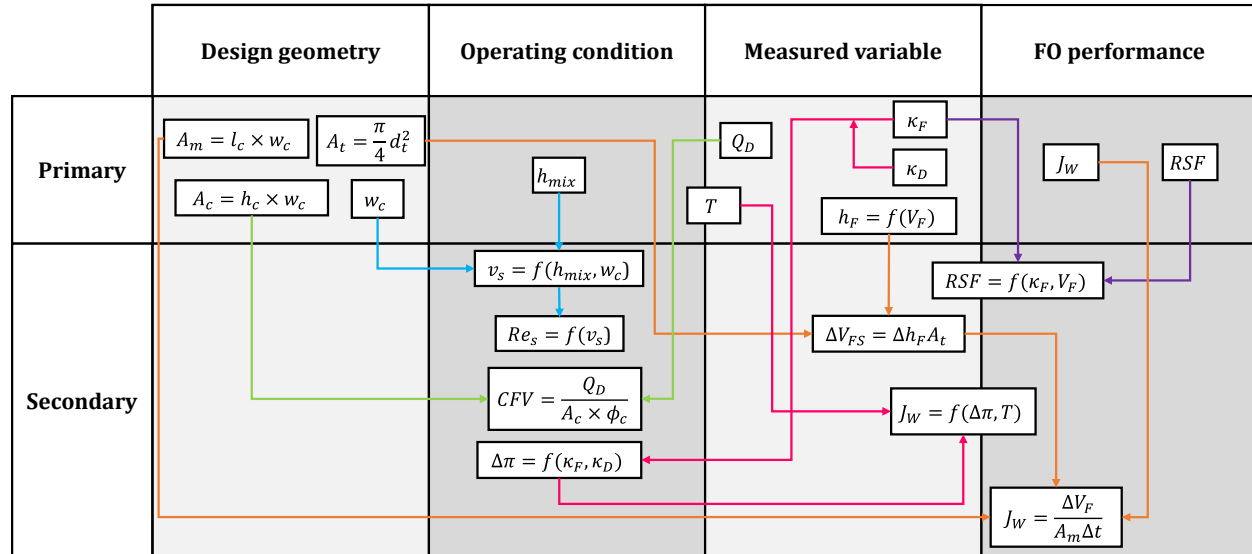

Figure 3-7: Diagram illustrating the interdependence of the design geometry, operating conditions, measured variables and FO performance in terms of parameters and relationships. A_m is the membrane area, l_c, w_c and h_c are the length, width and height of the DS channel, ϕ_c is the spacer porosity, A_c is the cross-sectional area of the channel, A_t and d_t are the cross-sectional area and diameter of the measuring tube, h_{mix} is the height of the distribution plate above the membrane surface, v_s is the velocity of the circulated liquid over the membrane surface, Re_s is the Reynolds number in the submerged space, CFV is the cross-flow velocity, Q_D is the DS flowrate, T is the solution temperature, κ_F and κ_D are the FS and DS conductivities, h_F is the height of the FS liquid level in the reactor, V_F is the volume of the FS, $\Delta\pi$ is the osmotic pressure gradient, Δt is the interval time, J_W is the water flux and RSF is the reverse solute flux.

The measured variables in Figure 3-7 represent the data collected during a specific experimental run. The measured variables were combined with the existing design geometries by the developed mathematical expressions in order to quantify the FO performance and operating conditions. The development of the methodology is detailed in the following sections.

3.1.5.1 Raw data

In fulfilment of the measured variables in Figure 3-7, the data listed below were required from the FO experiments to quantify the FO performance with the secondary variables:

1. interval time, Δt
2. the height of the liquid level in the FS reactor, h_F
3. the temperature, T, and conductivity of the FS, κ_F
4. the temperature, T, and conductivity of the inlet and outlet DS, κ_D

57

5. the flowrate of the DS, Q_D

3.1.5.2 Water flux

The change in the FS volume (ΔV_F) over time was quantified from the change in the FS liquid level (Δh_F), as measured from the graduated cylinder of the reactor. The water flux could then be evaluated from the mathematical expression in Equation 3-1.

$$J_{W_T} = \frac{\Delta V_F}{A_m \Delta t} = \frac{V_p}{A_m \Delta t} = \frac{\Delta h_F A_t}{A_m \Delta t} \tag{3-1}$$

where J_{W_T} = water flux at the experimental temperature T (L·m⁻²·h⁻¹ or m·h⁻¹)

V_F = FS volume (L)

A_m = membrane area (m²)

Δt = interval time (h)

V_p = permeate volume (L)

h_F = FS liquid level height in the graduated cylinder (m)

A_t = cross sectional area of the graduated cylinder (m²)

The variation of the viscosity of water with temperature influences the water flux in membrane processes. Therefore, the experimentally determined water fluxes were normalised to a standard temperature. In low pressure membrane systems, a reference temperature (T_R) of 20°C is typically implemented (Water Environment Federation, 2006). The correlation used for the temperature correction of the experimental water fluxes is given in Equation 3-2 (Kim & Park, 2011; Jacangelo, et al., 1995).

$$J_W = J_{W_T} \exp[-0.0239(T - T_R)] \tag{3-2}$$

where J_W = normalised water flux at T_R (L·m⁻²·h⁻¹)

J_{W_T} = water flux at experimental temperature T (L·m⁻²·h⁻¹)

T = experimental temperature (°C)

T_R = reference temperature (20°C)

The experimental water flux was not corrected with respect to:
   i)   the effects of CP on the osmotic pressure gradient,
   ii)   small deviations in the absolute osmotic pressure of the DS arising from its large make-up volume and
   iii)   the effect of reverse solute flux on the osmotic pressure gradient.

58

3.1.5.3 Osmotic pressure and reverse solute flux

The osmotic pressures of the FS and DS were evaluated from the conductivity of the respective solutions. This also facilitated the quantification of the reverse draw solute flux. An Eutech® PC 150 conductivity probe was used for the measurements. All measurements were automatically normalised by the conductivity meter to a standard temperature of 20°C.

The conductivity of a solution is temperature and concentration dependent (See & White, 1997). Therefore, conductivity vs. concentration data (for a NaCl draw solution, Section 3.2.2.1) at the reference temperature were regressed for conductivity measurements ranging from 2 μS·cm⁻¹ to 5200 μS·cm⁻¹ for the FS and 1.75 S·m⁻¹ to 5.97 S·m⁻¹ for the DS. The two correlations are provided in Appendix B.1. For the DS, normal seawater concentrations could be considered with the regressed data, but dilution of the DS sample was required at conductivities greater than 6 S·m⁻¹.

Once the draw solute concentration of the respective solutions could be derived from the conductivity of the solutions, Equation 3-3 was used to determine the osmotic pressure difference between the FS and DS. The osmotic coefficient is incorporated to account for the deviation of the draw solute from ideal behaviour.

$$\Delta\pi = n\varphi\Delta C R_g T \tag{3-3}$$

where $\Delta\pi$ = osmotic pressure difference between the FS and DS (bar)

n = van't Hoff factor (-)

φ = osmotic coefficient (-)

ΔC = draw solute concentration difference (mol·L⁻¹)

R_g = universal gas constant (L·bar·K⁻¹·mol⁻¹)

T = temperature (K)

The reverse solute flux (RSF) was determined from the draw solute concentration in the FS, in accordance with the methodology of Cath, et al. (2013). The specific RSF was determined by dividing the RSF by the water flux (J_W). As the initial draw solute concentration of the FS was zero, Equation 3-4 was valid, where C_F and V_F refer to the draw solute concentration and volume of the FS, respectively.

$$RSF = \frac{C_F V_F}{A_m \Delta t} \tag{3-4}$$

3.1.5.4 Modelling of the FS hydrodynamic conditions

The hydrodynamic pattern in the FS reactor was approximated as flow in a rectangular duct, where the geometry is created vertically by the walls of the FS reactor and horizontally by the distribution plate and membrane surface (Figure 3-4). The Reynolds number (Re) in such a geometry is determined from the hydraulic diameter, described by Equation 3-5 (Çengel & Cimbala, 2014).

$$d_h = \frac{2h_{mix}w_c}{h_{mix} + w_c} \tag{3-5}$$

where d_h = hydraulic diameter (m)

   h_{mix} = height of the distribution plate above the membrane surface (m)

   w_c = width of the DS channel (m)

For the purpose of evaluating the ECP modulus in the FS, the mass transfer coefficient at the submerged membrane surface was estimated from the following correlation for the Sherwood number (Sh) in stirred cells for Re<2000 (De & Bhattacharjee, 1994; Opong & Zydney, 1991; Smith, et al., 1968):

$$Sh = \frac{kd_h}{D} = 0.23Re^{0.567}Sc^{0.33} \tag{3-6}$$

where k = mass transfer coefficicient (m·s⁻¹)

   d_h = hydraulic diameter (m)

   D = diffusion coefficient (m²·s⁻¹)

   Re = Reynolds number

   Sc = Schmidt number

3.1.5.5 Cross-flow velocity of the DS

The cross-flow velocity (CFV) in the DS channel was quantified from the volumetric flowrate of the DS (Cath, et al., 2013), as measured with the in-line flowmeter. The inclusion of a diamond-patterned spacer in the cross-flow channel was accounted for in determining the CFV, as the volume of the DS channel was effectively reduced by the spacer. The porosity of the spacer-filled DS channel is described by Equation 3-7 (Siddiqui, et al., 2017).

$$\phi_c = 1 - \frac{V_{spacer}}{V_c} = 1 - \frac{V_{spacer}}{h_c \times w_c \times l_c} \tag{3-7}$$

60

where ϕ_c = porosity of the DS channel with the spacer

V_{spacer} = volume of the spacer (m3)

V_c = volume of the DS channel (m3)

h_c = height of the DS channel (m)

w_c = width of the DS channel (m)

l_c = length of the DS channel (m)

The channel porosity was not quantified in this work. An average channel porosity of 0.85 was assumed, based on the work of Siddiqui, et al. (2017), in order to determine the CFV with Equation 3-8, where Q_D is the DS volumetric flowrate and A_c the cross-sectional area of the DS channel.

$$CFV = \frac{Q_D}{A_c} = \frac{Q_D}{l_c \times w_c \times \phi_c} \tag{3-8}$$

3.1.6 Characterisation

The design of the bench-scale FO system was characterised prior to experimentation. Preliminary experiments were also performed to evaluate the robustness of the setup. This was done in accordance with the method developed in Section 3.1.5.

3.1.6.1 *Hydrodynamic conditions in the FS reactor*

The flow pattern created by the hydrodynamic agitator within the FS reactor is illustrated in Figure 3-8a. The flow pattern created by a radial impeller in a cylindrical tank is illustrated in Figure 3-8b. By comparison, it is clear that the prototype agitator delivers the desired flow pattern.

As shown by the arrows in Figure 3-8a, the submersible pump draws liquid from the bulk FS, which is then pumped to the distribution plate along the extension of the pump outlet. The liquid is then ejected downwards from the distribution plate along the short edge of the membrane (Figure 3-8a, left). The flow pattern continues horizontally over the membrane surface under the plate towards the opposite side from which it was ejected. Thereafter, the circulated liquid returns to the bulk FS above the plate after flowing through the small channel between the FS reactor wall and plate edge (Figure 3-8a, right).
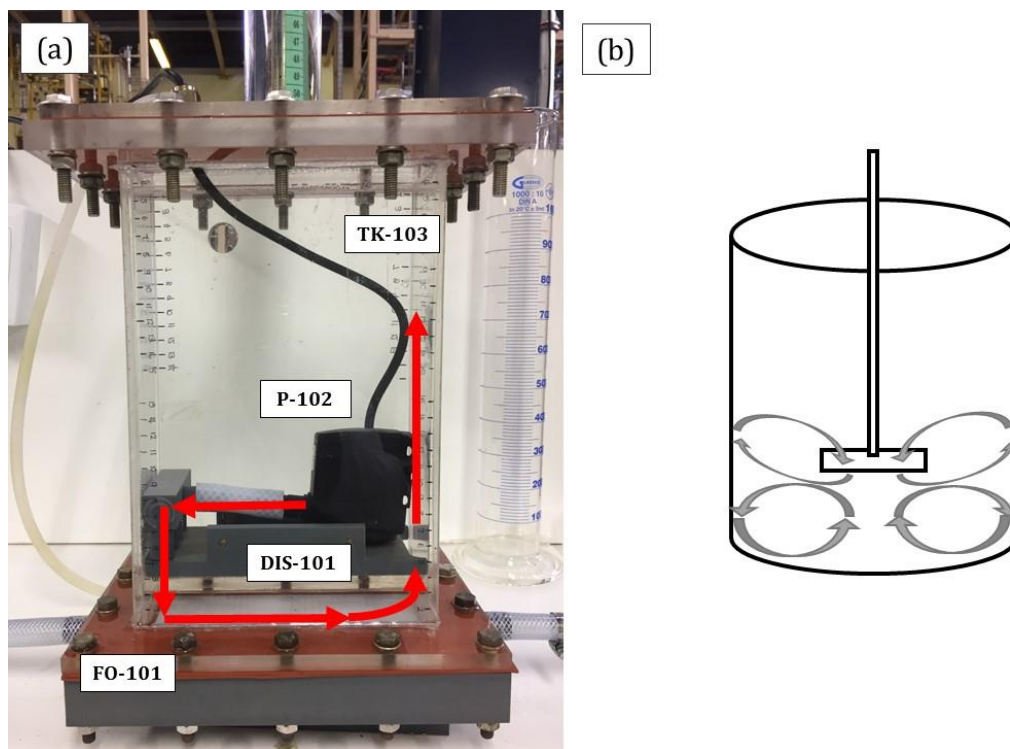
Figure 3-8: The flow pattern created by (a) the prototype agitator (submersible pump, P-102, and distribution plate, DIS-101) in the FS reactor (TK-103) and (b) a radial impeller in a cylindrical vessel.

The intensity of the agitation at the membrane surface was changed by adjusting the height of the agitation device above the submerged membrane. Three agitation intensities were considered in this work: with the device at a 1) low (32 mm), 2) medium (102 mm) and 3) maximum (212 mm) elevation above the membrane in the FS reactor. The Reynolds number and flow velocity over the membrane surface at these settings are indicated in Table 3-2.

Table 3-2: The Reynolds number and flow velocity over the submerged membrane surface (v_s) at a low, medium and high agitation intensity.

Agitation	Reynolds number (Re$_s$)	Flow velocity (v_s) / cm·s⁻¹
Low	1 100 (laminar regime)	0.8
Medium	1 700 (laminar regime)	1.7
High	2 700 (turbulent regime)	5.6

The Reynolds number of 1 700 was applied in the majority of the FO tests after evaluation of the FO performance at all three conditions. This Reynolds number correlates with that previously implemented in the submerged FO experimental apparatus of Chowdhury & McCutcheon (2018) and Chowdhury, et al. (2017), as well as that in typical cross-flow configurations (Giagnorio, et al., 2019; McCutcheon & Elimelech, 2006). The functionality of the agitation mechanism is addressed in Section 4.1.2.

3.1.6.2 Hydrodynamic conditions in the DS channel

In accordance with standard methodology for testing FO membrane performance (Cath, et al., 2013), a design CFV of 0.25 m·s⁻¹ was used for determining the geometry of the DS channel. However, severe upward protrusion of the submerged FO membrane was observed at a measured DS flowrate of 1.8 L·min⁻¹ required to achieve this CFV. In this case, the hydrostatic pressure of the FS above the submerged membrane was no longer dominant over the pressure in the DS channel at this flowrate, which resulted in the 'swelling' of the DS channel. Protrusion or 'bulging' of the membrane by the pressure in the DS channel subjects the membrane to tensile stress. Cracks in the active layer and stretching of the support layer have been observed from similar cases in FO research (Kim & Elimelech, 2012).

A CFV of 0.16 m·s⁻¹ with a DS flowrate of approximately 1.2 L·min⁻¹ (100 rpm pump speed) could be attained without protrusion of the FO membrane. With a Reynolds number of 450 at this condition, the flow in the DS channel was laminar, which is typical for cross-flow channels (Alshwairekh, et al., 2018; Lian, et al., 2018; Devia, et al., 2015; Sharif & Arayafar, 2014; McCutcheon & Elimelech, 2006).

The CFV is heavily dependent on the estimated channel height (h_c) and porosity (ϕ_c) as indicated from a sensitivity analysis shown in Figure 3-9. The inverse relationship between the CFV and channel geometry implicates that a CFV of 20 m·s⁻¹ or 14 m·s⁻¹ may be obtained if the channel height is under or overestimated by 0.3 mm, respectively. As the channel height affects both the hydraulic diameter and linear flow velocity, the Reynolds number remains constant with the variation of the channel height. However, the flow regime remains in the laminar region at a channel porosity as low as 0.5.

The measurement of the DS flowrate at the outlet of the membrane cell was considered sufficient to estimate the CFV in the membrane cell. In this system, a large fraction (>100) of the outlet DS flowrate with respect to the permeate flowrate, named the flow factor, was attained. Hence, there is small relative difference between the outlet DS flowrate measured with FM-101 (1.2 L·min⁻¹) and the inlet DS flowrate calculated from the FO permeate flowrate, as shown in Figure 3-10. At the maximum relative difference in the flowrate of ~1%, the approximation of the CFV to two decimal figures remained at 0.16 m·s⁻¹.
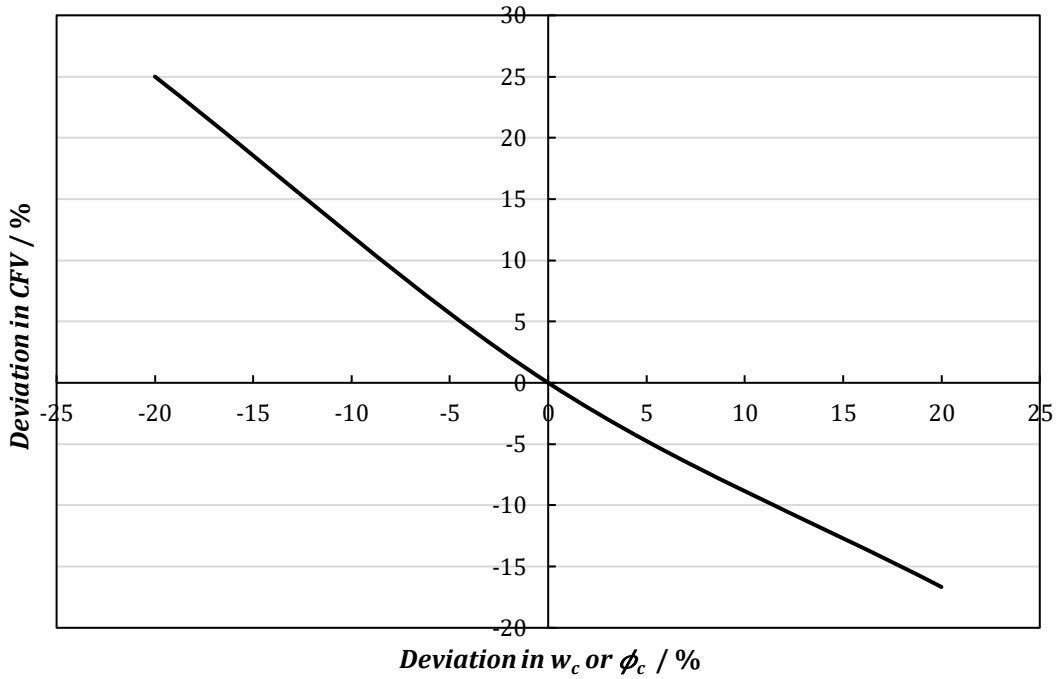
Figure 3-9: Sensitivity analysis indicating the deviation in the CFV with the deviation in the DS channel height (h_c) and porosity (ϕ_c) between -20% and +20%.
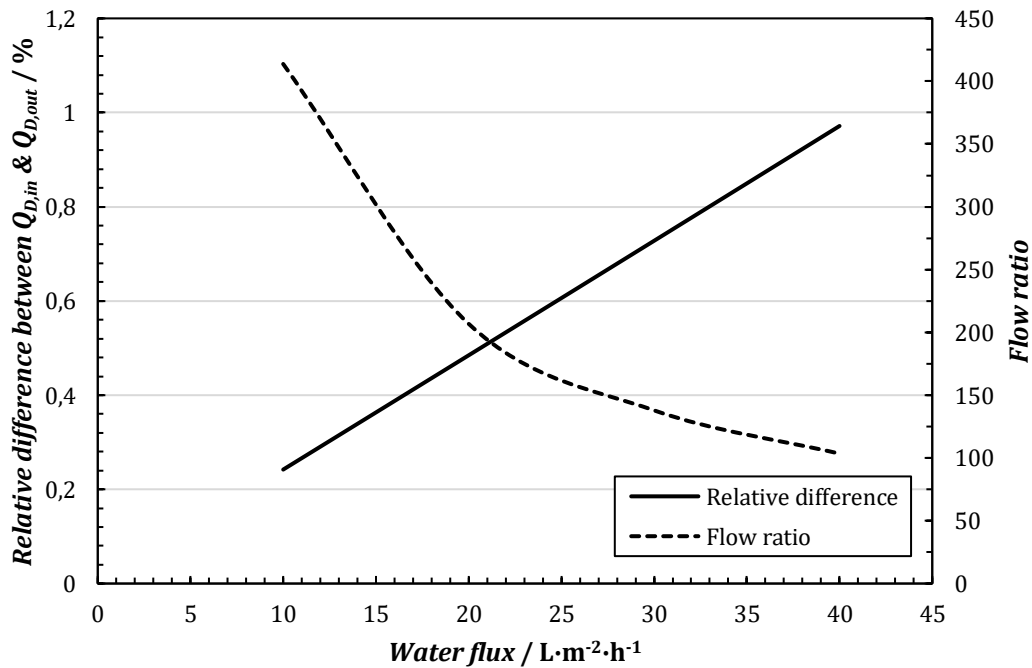
Figure 3-10: The 1) relative difference between the inlet DS flowrate and outlet DS flowrate (1.2 L·min⁻¹) and 2) flow factor as a function of the FO water flux between 10 L·m⁻²·h⁻¹ and 40 L·m⁻²·h⁻¹. The flow factor refers to magnitude of the outlet DS flowrate relative to the FO permeate flowrate.

3.1.6.3 Operating temperatures and correction factors

The FO experiments were performed with the FS and DS kept at ambient temperature. However, slight heating of the FS occurred as a result of the heat transfer from the submersible pump motor when it was in operation. In order to avoid the establishment of a significant temperature gradient between the FS and DS and its subsequent effect on the FO mass transport, heat supply from the DS tank heater (HX-101) was controlled to keep the temperature of the DS within 1°C of the FS temperature (Cath, et al., 2013). At this maximum solution temperature difference, the relative standard error in the temperature corrected water flux of 0.8% was considered acceptable.

The validity of the temperature correction factor (Equation 3-2), used for the normalisation of the experimental water flux, was evaluated from experimental measurements at solution temperatures in close proximity to the reference temperature of 20°C. Five examples of such measurements, within 0.5°C of the reference temperature, are summarised in Table 3-3. From the small relative difference (≤1%) between the uncorrected and corrected water flux of the example measurements, the temperature correction factor was considered sufficient to collate all experimental data.

Table 3-3: Comparison of the uncorrected water flux (J_{W_T}) and temperature corrected water flux (J_W) at experimental temperatures close to the reference temperature of 20°C. RDP_{J_W} refers to the percentage relative difference in J_W.

Case number	T / °C	J_{W_T} / L·m^{-2}·h^{-1}	J_W / L·m^{-2}·h^{-1}	RDP_{J_W} / %
1	19.6	9.1	9.2	1.0
2	19.7	32.8	32.9	0.2
3	19.9	26.5	26.6	0.2
4	20.0	32.0	32.0	0.1
5	20.2	34.0	33.8	0.4

3.1.6.4 Hydrostatic effects on the water flux

With the reactor loaded with feed solution, the submerged FO membrane was subjected to a hydrostatic pressure. In addition to the osmotic pressure gradient between the FS and DS, this hydrostatic pressure creates an additional driving force for water transport across the FO membrane (Equation 2-2). The hydrostatic pressure above the submerged membrane varied from 30 to 80 millibar (gauge) with the liquid level varying between a maximum and minimum height in the graduated cylinder of the reactor where flux measurements could be recorded.

The small effect of the hydrostatic pressure on the FO water flux is illustrated in Figure 3-11. The standard deviation and relative standard deviation in the water flux measured between the maximum and minimum height in the graduated cylinder were 0.27 L·m^{-2}·h^{-1} and 1.6%, respectively. Corrections in the water flux to account for the hydrostatic pressure of the FS were

not made due its insignificant effect relative to other factors influencing the FO membrane performance such as the increase in the FS osmotic pressure arising from RSD.
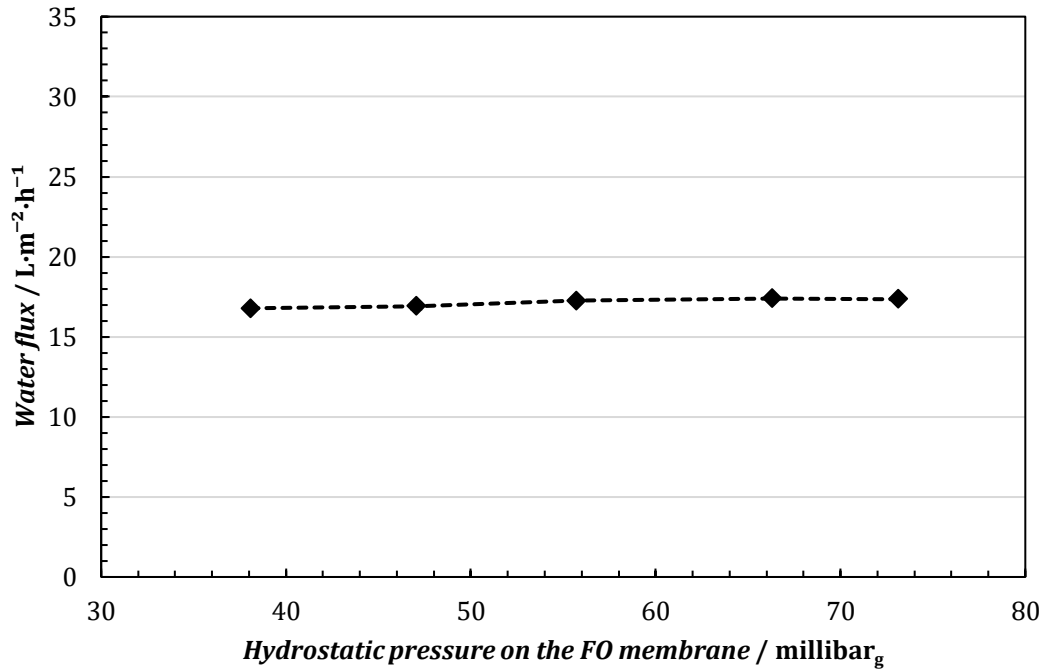
Figure 3-11: The effect of the hydrostatic pressure on the FO water flux. The data were measured in the AL-FS membrane orientation with a 35 g·L⁻¹ NaCl draw solution with $Re_s=1\,700$ in the FS. All water fluxes are normalised to 20°C.

3.1.6.5 Feed concentration factor

The volume of the graduated cylinder of the FS reactor was approximately 0.74 litres. Therefore, an experimental test, without replenishment of the FS within the reactor, could be performed up to a final concentration factor of 1.15 (Equation 3-9). Depending on the FO water flux and membrane orientation, the duration of an FO experiment without replenishment of the feed ranged between 60 and 120 minutes at this concentration factor.

$$CF = \frac{V_{F(i)}}{V_P} = \frac{V_{F(i)}}{V_{F(i)} - V_{F(f)}} \qquad (3\text{-}9)$$

where　　$V_{F(i)}$ = initial volume of the FS (L)

　　　　　V_P = volume of the permeate (L)

　　　　　$V_{F(f)}$ = initial volume of the FS (L)

The advantage of this low concentration factor is that the quality of the FS would not be significantly affected as it becomes more concentrated with permeation of pure water to the DS.

66

Thus, the water flux and initial concentration of the spiked feed solute could be maintained relatively constant over the duration of the FO tests. However, it is acknowledged that MBRs are typically run for extended periods of time before membrane replacement or cleaning (Holloway, et al., 2015a) and that the interpretation of the results of this work is subject to this condition.

3.1.7 Summary

Throughout the design process and characterisation of the submerged FO system, the seven design requirements listed in Section 3.1.2 were successfully met to facilitate the experimental investigation of the water permeability and solute rejection in the submerged FO configuration. The design parameters of the submerged FO system and its operating conditions based on the design are summarised in Table 3-4.

Table 3-4: Summary of the design parameters and operating conditions of the constructed submerged FO setup.

Design parameter	Value	Unit
Membrane active area, A_m	169.2×10^{-4}	m²
DS channel cross-sectional area, A_c	1.41×10^{-4}	m²
DS channel porosity, ϕ_D	0.85	-
Maximum FS volume	5.7	L
DS volume	200	L
Operating conditions		
DS channel CFV	0.16	m·s⁻¹
DS flowrate, Q_D	1.2	L·min⁻¹
FS Reynolds number, Re_s	1 100/1 700/2 700	-
Normalisation temperature for J_{W_T}	20	°C

3.2 Materials

3.2.1 FO membrane

A TFC FO8040 membrane from CSM products (Toray Chemical Korea), originally in a spiral wound module, was used throughout the experimental phase of this study. The characteristics of the membrane, as stated by the manufacturer, are provided in Table 3-5.

Table 3-5: Characteristics of the FO8040 TFC membrane (CSM Toray, 2015).

Characteristic	Description
Membrane thickness	100 µm
Membrane type	TFC with polyamide coating
Water flux / L·m⁻²·h⁻¹	35 ± 3
Specific reverse NaCl flux / g·L⁻¹	< 0.5
Operational lifetime	Dependent on usage and application
Shelf life	Minimum of 6 months
Operational pH range	2-11

To obtain flat-sheet membrane coupons compatible with the submerged FO module, the spiral wound module was disassembled. After its disassembly for the extraction of the flat sheets, the membrane layers were rolled up and stored in an air-tight plastic bag with a 1 wt% solution of sodium metabisulfite (SMBS), away from direct sunlight to prevent dehydration of the membrane. For the experimental runs, a 220×130 mm coupon was cut from a membrane sheet and subsequently conditioned in deionised water for at least 24 hours prior to its first usage.

Scanning Electron Microscopy (SEM) analysis was used to obtain images of both the active and support layer of the FO membrane. The morphological differences between the two layers are visible from Figure 3-12, which presents images of the cross-sections and surfaces of both layers.
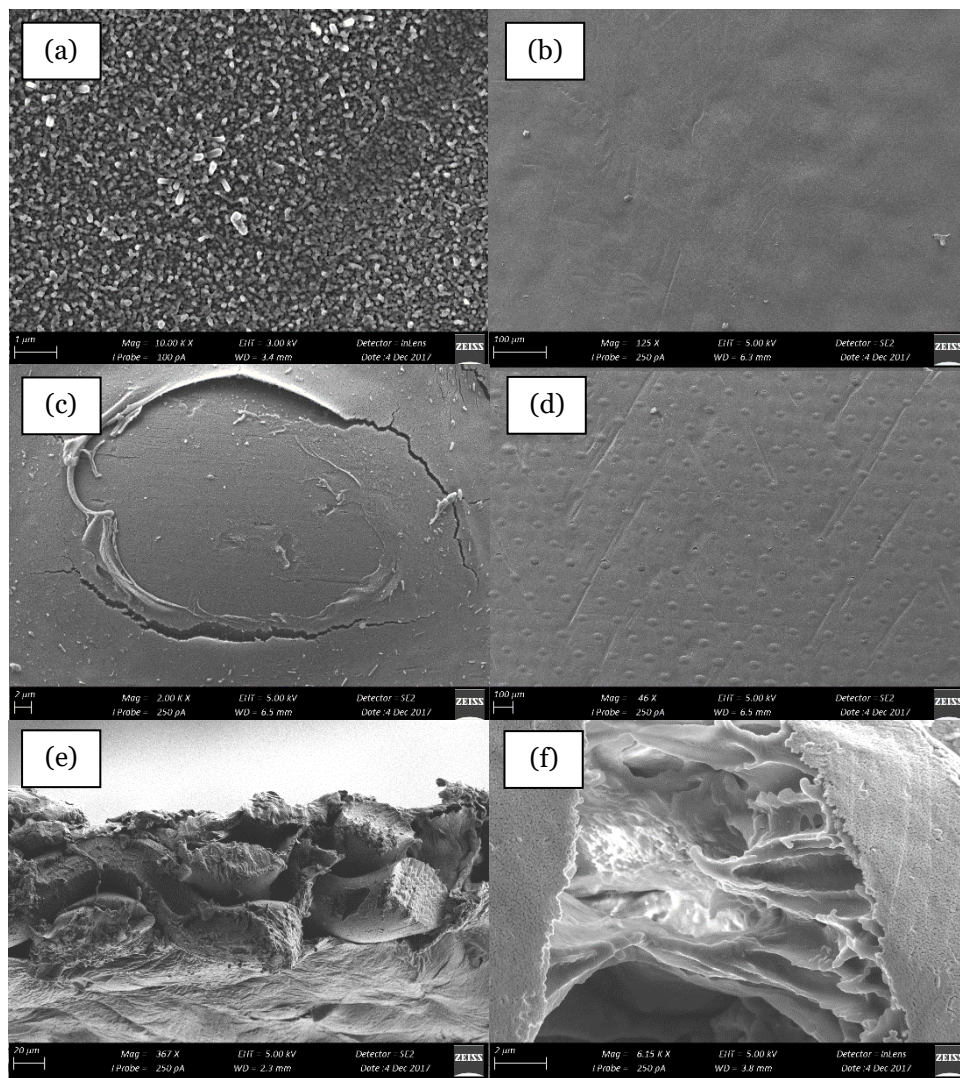

Figure 3-12: SEM images of the FO membrane. Images (a) and (b) show the surface of the membrane active layer in 10 000x and 125x magnification, respectively. Images (c) and (d) show the surface of the support layer in 2 000x and 46x magnification, respectively. Images (e) and (f) show the cross section and tortuosity of the support layer, respectively, in 367x magnification.

68

The determination of the FO membrane transport parameters (*A*, *B* and *S*) with the standard protocol suggested by Cath, et al. (2013) was not considered in this study. A structural parameter (*S*) of 466×10^{-6} m has previously been reported by Kim, et al. (2017) for this particular FO8040 membrane. This value was utilised in the estimation of the ICP moduli (Equations 2-12 and 2-13).

3.2.2 Chemicals and solution chemistry
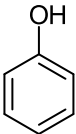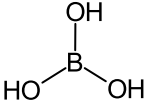
3.2.2.1 Draw solution osmotic agent

Sodium and chloride constitute approximately 90% of the total dissolved solids (TDS) in seawater. For this reason, sodium chloride (NaCl) was identified as the appropriate draw solute to simulate seawater as the draw solution in FO. Due to the large volumes of DS required in this work, food grade iodated table salt (99.5% NaCl) was acquired for the preparation of the DS.

3.2.2.2 Feed solution trace solutes

The relevance of phenol, boron and lithium as model solutes in this study has been discussed in Sections 2.3.4 and 2.3.5. Their structural and physicochemical properties have been summarised in Table 2-11. High purity (≥99%) phenol, boric acid and lithium chloride crystals were purchased from Merck® for the preparation of the feed solutions containing these solutes. Table 3-6 provides a summary of the products used. Aqueous solutions of phenol were prepared from a 200 mg·L⁻¹ stock solution. Boron and lithium were prepared in respective 1000 mg·L⁻¹ stock solutions.

Table 3-6: Chemicals used for the preparation of feed solutions containing phenol, boron and lithium.

Trace solute	Chemical	Linear formula	Assay	MW / $g \cdot mol^{-1}$	Structure
Phenol	Phenol	C_6H_5OH	≥99.0%	94.11	
Boron	Boric acid	H_3BO_3	≥99.5%	61.83	
Lithium	Lithium chloride	LiCl	≥99%	42.39	

3.2.2.3 Background solutions and their chemistry

The 200 L draw solution of the desired osmotic pressure was prepared in the DS tank by dissolving the appropriate amount of NaCl in deionised water. For pure water permeability experiments,

deionised water (<10 mg·L^{-1} TDS) was used as the feed solution. Feed solutions spiked with the model solutes were prepared in volumes of 6 litres by combination of a predetermined amount of the respective stock solution with deionised water. Phenol solutions were prepared with an additional 2 g·L^{-1} of NaCl (refer to Section 3.3.3.1). The solution pH was unadjusted and uncontrolled, but measured, in each experiment. All phenol solutions were neutral (pH 7.7 $\pm$ 0.1) as the phenol concentration was low enough to avoid the alteration of the solution pH. The pH of the boron and lithium solutions varied between 6.8 $\pm$ 0.1 and 7.9 $\pm$ 0.1 (refer to Figure 4-20).

3.3 Methods

In this section, the experimental plan, as established from the objectives numbered 3 and 4 in Chapter 1, is outlined. The experimental procedures followed in the execution of water permeability and solute transport tests are provided, as well as a discussion of the analytical methods and uncertainty analysis.

3.3.1 Experimental plan

For a systematic approach to the objectives, the experimental plan consisted of two phases. Throughout each experimental phase, a number of factors were varied among certain levels. The responses at each level were then determined from the experimental runs. The experimental plan followed throughout this study is provided in Figure 3-13.
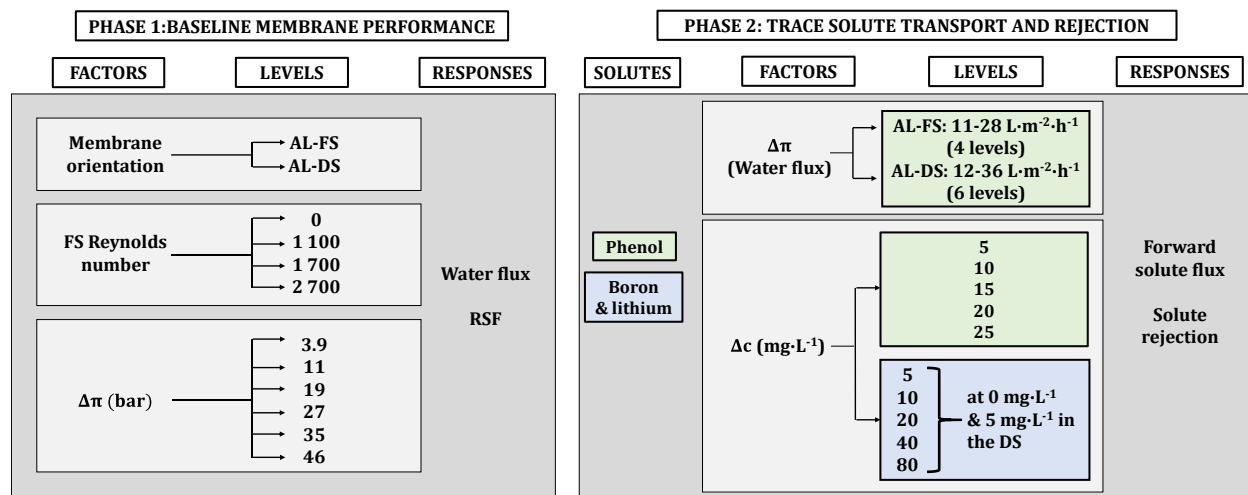
Figure 3-13: A summary of the experimental plan to 1) establish the baseline performance of the FO membrane and 2) investigate the trace solute transport in FO. The symbols $\Delta\pi$ and Δc refer to the osmotic pressure and solute concentration gradients, respectively.

3.3.1.1 Phase 1

In the first phase of this work, the baseline performance of the submerged FO membrane was evaluated in accordance with the method developed and system characterisation in Section 3.1.

Pure water permeability tests were conducted with consideration of the 1) membrane orientation, 2) hydrodynamic conditions in the FS and 3) water and draw solute transport, with the latter perceived when the osmotic pressure gradient is varied. The water flux and reverse draw solute flux were considered as the primary responses in this experimental phase.

The effect of turbulence at the submerged membrane surface was evaluated from experimental runs with and without agitation in FS reactor. The FO membrane performance was further investigated at the three characterised agitation intensities, expressed in terms of the Reynolds number. For all these experimental runs, the NaCl concentration in the DS was fixed at 35 g·L^{-1} (π=27 bar). Subsequently, the water and NaCl transport was investigated over a range of osmotic pressure gradients between the FS and DS, including that generated by seawater (27 bar) and RO brine (46 bar). Here, the agitation intensity was fixed at Re=1700. Only the osmotic pressure of the DS was altered to change the osmotic pressure gradient between the FS and DS.

3.3.1.2 *Phase 2*

The first experimental phase established the baseline operating conditions for the second experimental phase, in which the transport of the feed solutes, phenol, boron and lithium, were investigated. The effect of the osmotic pressure and trace solute concentration gradients across the FO membrane was investigated. Throughout this experimental phase, the Reynolds number at the submerged membrane surface in the FS was fixed at 1 700. The experiments were performed in both the AL-FS and AL-DS membrane orientations.

Phenol was used as the model solute to evaluate the effect of the osmotic pressure gradient on the solute transport in FO. The feed phenol concentration was fixed at 10 mg·L^{-1} while the DS osmotic pressure was varied to establish water fluxes in the ranges indicated in Figure 3-13. In addition, the phenol transport was investigated at feed concentrations ranging from 5 to 25 mg·L^{-1} in increments of 5 mg·L^{-1} with a DS of 35 g·L^{-1} and 60 g·L^{-1} NaCl. The feed solution pH was uncontrolled, but measured to be constant at 7.7 $\pm$ 0.1 among all feed concentrations of phenol.

The transport of boron and lithium as a function of their concentration gradients between the FS and DS was evaluated on two isopleths, namely experiments with 1) a blank 35 g·L^{-1} NaCl DS and 2) a 35 g·L^{-1} NaCl DS spiked with 5 mg·L^{-1} of both boron and lithium. For example, at a concentration gradient of 5 mg·L^{-1}, one experiment was performed with a FS solute concentration of 5 mg·L^{-1} and none of the solute in the DS. A second experiment was performed with 10 mg·L^{-1} of the solute in the FS and 5 mg·L^{-1} in the DS. The scenario with a spiked draw solution was related to boron and lithium being seawater constituents. Boron and lithium were spiked into the same

71

FS and DS at equal concentrations to generate concentration gradients ranging between 5 mg·L^{-1} and 80 mg·L^{-1}, at which the FS pH was measured to be 7.9 ± 0.1 and 6.8 ± 0.1, respectively.

It is emphasised that the concentration gradients of phenol, boron and lithium included in the experimental plan exceeded environmentally relevant concentrations. At very low concentrations of phenol (<1 mg·L^{-1}), its adsorption to the membrane surface and system components significantly affected its observed rejection. Also, due to the high toxicity of phenol, the increments in its concentration gradient were kept to a minimum. The accuracy in the boron and lithium determination was compromised at low solution concentrations. A DS boron concentration of 5 mg·L^{-1} was relevant to the actual boron level in seawater. However, the DS lithium concentration had to be elevated significantly relative to that found in seawater (0.17 mg·L^{-1}) for the purpose of analysis.

The forward solute flux and rejection were regarded as the primary responses for evaluating the solute transport in FO, based on the background provided in Section 2.3.1. However, consideration of the water flux was made in each experiment for the purpose of validating the experimental setup and to account for the potential increase in the FS osmotic pressure with the solute concentrations.

3.3.2 Experimental procedures

3.3.2.1 *Membrane and solution preparation*

Each experimental run was performed after prior equilibration of the complete membrane system with the ambient temperature. In order to prepare the membrane, it was allowed a flux stabilisation period, typically between one and three hours, during which the membrane was exposed to a FS and DS identical to that considered in the succeeding experiment. The membrane coupon inserted in the FO module was never allowed to run dry between experiments by ensuring that it was submerged in water at all times.

The membrane module was prepared for solute transport experiments with prior flushing of the FS reactor with a solution of the particular trace solute being investigated. This allowed the membrane and system components to be completely saturated with the solute. In a similar fashion, the DS tank and pipelines were flushed with 35 g·L^{-1} NaCl background solution containing 5 mg·L^{-1} of both boron and lithium before experiments with a spiked DS were performed.

3.3.2.2 *Raw data collection*

During all of the water permeability and solute transport experiments, raw data was collected according to the requirements listed in Section 3.1.5.1. The volume of the feed solution was

recorded at intervals of 10 minutes. The temperature and conductivity of the FS, inlet DS and outlet DS were measured with the handheld Eutech® PC 150 conductivity meter every 20 minutes. The pH of each feed solution, although this was unadjusted, was also recorded.

3.3.2.3 Water permeability tests

Pure water permeability experiments were performed in the first experimental phase (Figure 3-13). After membrane stabilisation, fresh deionised water was loaded into the FS reactor. The DS was then circulated through the cross-flow channel of the membrane cell at a CFV of 0.16 m·s⁻¹ (1.2 L·min⁻¹) for a period of two to three hours during which the data were recorded.

To be able to continuously measure the FO water flux during the water permeability tests, the liquid level of the feed had to be maintained in the graduated part of the FS reactor. This was done by replenishment of the feed volume with deionised water during the experiment. This was particularly required in cases were the water flux was high, as in the AL-DS orientation. This protocol was considered viable as it did not create a significant disturbance in the FO flux, as seen from the time-based water flux curves presented in Section 4.1.1. However, this dilution was accounted for in the determination of the reverse solute flux.

As required, the agitation intensity or Reynolds number at the submerged membrane surface was varied by changing the height of the mixer (h_{mix}) above the submerged membrane surface. For the evaluation of the membrane performance at different osmotic pressure gradients, the osmotic pressure of the DS was adjusted by the addition of NaCl or deionised water to the existing solution in the DS tank. The conductivity measurement of the DS was used to confirm that the desired NaCl concentration was achieved.

3.3.2.4 Trace solute transport tests

All trace solute transport experiments were performed with an initial FS volume of 5.7 litres and final FS concentration factor of 1.15 (permeate volume of 740 ml) in order to compare the experimental results. At this concentration factor, replenishment of the FS was not required, which further simplified the experiments and sample analysis. Test durations varied between 1 and 3 hours, depending on the membrane orientation being investigated.

When a spiked DS with 5 mg·L⁻¹ of both boron and lithium was required in the experiments, the appropriate mass of boric acid and lithium chloride was sufficiently mixed into the 35 g·L⁻¹ NaCl background draw solution. The DS was then sampled in triplicate for the exact determination of the boron and lithium concentrations.

After flushing of the submerged FO unit, the prepared and sampled FS was loaded into the reactor. The height of the initial liquid volume in the reactor was noted from the graduated cylinder to determine the final height at which the required FS concentration factor would be reached. The FS was then concentrated by circulation of the DS through the membrane cell at a CFV of 0.16 m·s⁻¹ (1.2 L·min⁻¹). At termination of the test at the concentration factor of 1.15, triplicate samples of the final FS were immediately drawn from the reactor with a 15 ml syringe.

The initial and final solute concentrations in the FS were analysed from the triplicate samples drawn prior to and after the experiments. The permeation of small amounts of the solutes to the DS were calculated by mass balance for the purpose of presenting the solute concentration gradients in the results. Equation 3-10 was used to quantify the solute flux at the experimental temperature (J_{S_T}). The subscripts i and f refer to the initial and final conditions.

$$J_{S_T} = \frac{\Delta m_{S_F}}{A_m \Delta t} = \frac{c_{F(i)} V_{F(i)} - c_{F(f)} V_{F(f)}}{A_m \Delta t} \tag{3-10}$$

where J_{S_T} = solute flux at the experimental temperature T (mg·m⁻²·h⁻¹)

Δm_{S_F} = change in the mass of solute in the FS (mg)

A_m = membrane area (m²)

Δt = permeation time (h)

c_F = FS solute concentration (mg·L⁻¹)

V_F = FS volume (L)

In order to normalise the solute flux at the experimental temperature to the reference temperature of 20°C, a correction factor was derived from the temperature- and solution viscosity-dependence of solute diffusion in liquids (Equation 2-5). The correction factor is shown in brackets in Equation 3-11, where J_S represents the temperature corrected solute flux.

$$J_S = J_{S_T} \left(\frac{T_R}{T} \frac{\mu_{W_T}}{\mu_{W_{T_R}}} \right) \tag{3-11}$$

where J_S = solute flux at the reference temperature T_R (mg·m⁻²·h⁻¹)

J_{S_T} = solute flux at experimental temperature T (mg·m⁻²·h⁻¹)

T_R = reference temperature (20°C)

T = experimental temperature (°C)

μ_{W_T} = dynamic viscosity of the solution at the experimental temperature (kg·m⁻¹·s⁻¹)

$\mu_{W_{T_R}}$ = dynamic viscosity of the solution at tthe reference temperature (kg·m⁻¹·s⁻¹)

By combination of J_S with the expression on the right hand side of Equation 3-10, the final FS solute concentration could also be corrected to determine the observed solute rejection at the reference temperature (R_S) according to Equation 3-12 (Volpin, et al., 2019), where the symbols are as defined above.

$$R_S = \frac{m_{S_{F(f)}}}{m_{S_{F(i)}}} = \frac{c_{F(f,T_R)}V_{F(f)}}{c_{F(i)}V_{F(i)}}$$ (3-12)

To validate this method of normalising the solute flux and rejection, uncorrected values measured at an experimental temperature approximately equal to the reference temperature were compared to the temperature corrected values (Table 3-7). Relative differences of ≤3.0% in the solute flux and ≤0.1% in the solute rejection were obtained. Hence, this method of normalising the solute flux and rejection was considered acceptable.

Table 3-7: Comparison of the uncorrected solute flux (J_{S_T}) and rejection (R_{S_T}) to the temperature corrected solute flux (J_S) and rejection (R_S) at experimental temperatures close to the reference temperature (T_R) of 20°C. *RDP* refers to the percentage relative difference.

T / °C	J_{S_T} / mg·m⁻²·h⁻¹	J_S / mg·m⁻²·h⁻¹	RDP_{J_S} / %	R_{S_T} / %	R_S / %	RDP_{R_S} / %
20.4	210.4	210.8	0.1	86.6	86.6	0.0
20.3	40.6	41.0	1.0	94.3	94.3	0.0
20.6	234.2	227.4	3.0	92.9	93.0	0.1

3.3.3 Analytical methods

3.3.3.1 *Phenol*

The phenol concentration in the FS was determined by ultraviolet-visible (UV-Vis) spectroscopy at its wavelength of maximum absorbance of 270 nm. A calibration curve with a coefficient of determination (R^2) of 0.999 was prepared for the quantification (Appendix B.2). The absorbance of the reverse diffused NaCl had to be accounted for at this wavelength. An investigation showed that the absorbance of NaCl is constant with its increasing concentration at the wavelength of 270 nm. However, the variability of reverse solute diffusion with factors such as solution temperature may have influenced the validity of always assigning an allowance in the absorbance for NaCl when the initial FS was deionised water. To this end, phenol was spiked in the feed with a background solution of 2 g·L⁻¹ NaCl.

3.3.3.2 *Boron and lithium*

The concentrations of boron and lithium in the FS were analysed with inductively coupled plasma-optical emission spectroscopy (ICP-OES) on a Thermo-Fischer ICAP 6000 by the analytical

laboratory at the Department of Process Engineering, Stellenbosch University. Gold or yttrium was used as the internal standard in the analyses and quality control samples were used to confirm the accuracy of the analysis. The boron and lithium concentrations in the DS were quantified with inductively coupled plasma-mass spectroscopy (ICP-MS) due to the high concentrations of NaCl.

3.3.4 Uncertainty analysis

3.3.4.1 Water flux

Errors in the FO water flux mainly originated from its temperature correction with the average temperature of the FS and DS. It has already been mentioned in Section 3.1.6.3 that the relative standard error in the normalised water flux was 0.8% at a maximum allowable temperature difference of 1°C between the FS and DS.

Uncertainties in the water flux resulted from inaccurate readings of the change in the FS volume from the graduated cylinder of the reactor, which can be attributed to the parallax error. It was estimated that the measurement of the liquid level in the FS reactor was within the interval -0.5 mm to +0.5mm of the true value. The relative uncertainty in the water flux arising from this fluctuation is presented in Figure 3-14 as a function of the water flux.
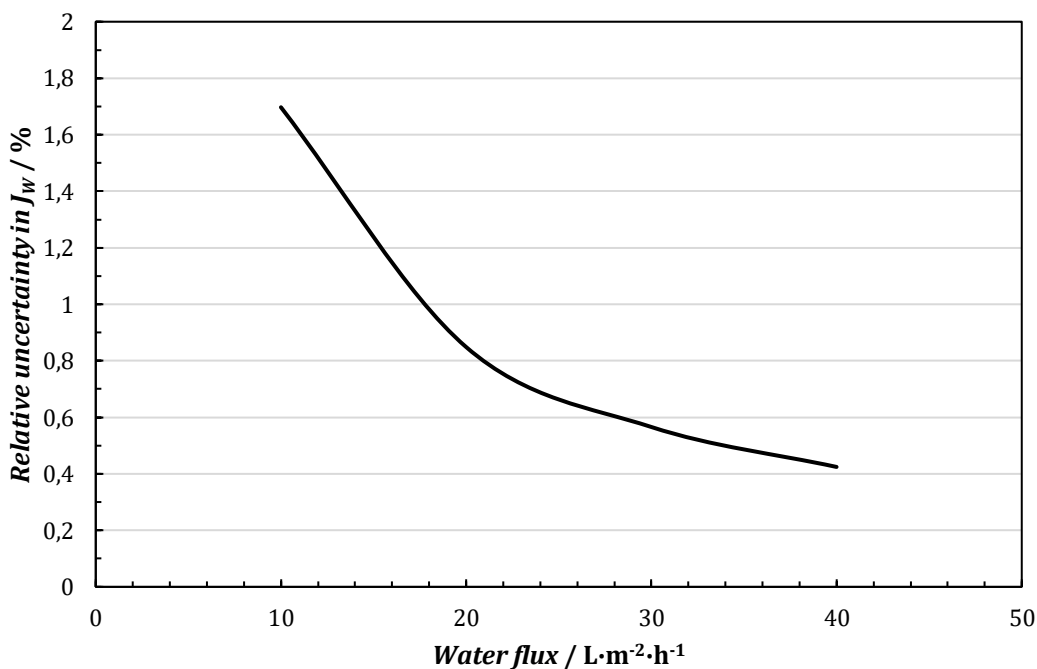
Figure 3-14: The relative uncertainty in the water flux (J_W) resulting from an absolute fluctuation of 0.5 mm in the measurement of the liquid level in the FS reactor.

It is clear from Figure 3-14 that the relative uncertainty in the water flux remained below 2% at admissible FO water fluxes ranging from 10 L·m⁻²·h⁻¹ to 40 L·m⁻²·h⁻¹. This uncertainty in the water flux was not indicated in the time-based flux curves presented in the results as the size of the data markers compensate for this. It is noted that the error bars of data points representing an average water flux in the results indicate the experimental standard deviation of the water flux evaluated from the repeated observations taken over the duration of the particular experimental run.

3.3.4.2 *Analytical uncertainty*

The uncertainty in the feed solute flux and rejection was evaluated from the analysis of triplicate samples. Firstly, the experimental variance, s^2, of the mean initial or final concentration was calculated with Equation 3-13. The term $s^2\left(c_{FS_k}\right)$ refers to the variance of the experimental observations and n refers to the number of independent observations, which in this case was equal to 3.

$$s^2\left(\bar{c}_{F_k}\right) = \frac{s^2\left(c_{F_k}\right)}{n} \tag{3-13}$$

The combined standard uncertainty (u_c) in the solute flux or rejection was derived from their respective analytical expressions (Equations 3-10 and 3-12) according to Equation 3-14. The experimental variance of the mean initial and final solute concentrations in the feed solution, or $s^2(\bar{c}_{F_k})$, were implemented as u, which is the standard uncertainty of the input, x_i. X refers to the estimate of the solute flux or rejection (Alshwairekh, et al., 2018).

$$u_c^2\left(X\right) = \sum_{i=1}^{N}\left(\frac{\partial f}{\partial x_i}\right)u^2(x_i) \tag{3-14}$$

The uncertainty in the solute flux or solute rejection evaluated with Equation 3-14 is represented by error bars throughout the presentation of the experimental results in Chapter 4.

Chapter 4

Experimental results and discussion

4.1 Baseline membrane performance

The baseline performance of the FO8040 was assessed by considering the 1) orientation of the membrane with respect to the feed solution, 2) hydrodynamic conditions at the submerged membrane surface and 3) water and NaCl transport at different osmotic pressure gradients. The normalised water flux (J_W), was considered as the primary indicator of the FO performance. The reverse solute flux (RSF) provided a further indication of the migration of the draw solute (NaCl) to the feed solution, which resulted in limited mass transfer by concentration polarisation and the increase in the osmotic pressure of the feed solution. The investigation of the baseline membrane performance ensured that:

i)   repeatable FO water fluxes could be attained among different membrane coupons,

ii) the margins of the experimental water flux were established,

iii) the effect of the membrane orientation on the FO performance was understood,

iv) the hydrodynamic conditions created by the prototype agitator were effective and

v)   the FO mass transport phenomena particular to the submerged FO configuration were evaluated.

4.1.1 Membrane orientation

Water permeability experiments were performed in triplicate or quadruplicate in the AL-FS and AL-DS membrane orientations at identical operating conditions. Besides demonstrating the effect of the membrane orientation on the water flux, this provided an indication of the repeatability of

78

the water flux among different membrane coupons. Hence, a range in which the water flux may have deviated among different membrane coupons in each membrane orientation could be determined. This would serve as a guideline for the validation of the membrane system for subsequent data collection.

The repeated water permeability experiments, each with a duration of three hours, were performed with a DS of 35 g·L⁻¹ NaCl and constant agitation of the feed solution at a Reynolds number of 1 700. As discussed in Section 3.1.5.2, the experimental water fluxes could be collated by means of the normalisation of the data to the reference temperature of 20°C. Figure 4-1 and Figure 4-2 present the normalised water fluxes as a function of time in the AL-FS and AL-DS membrane orientations, respectively.
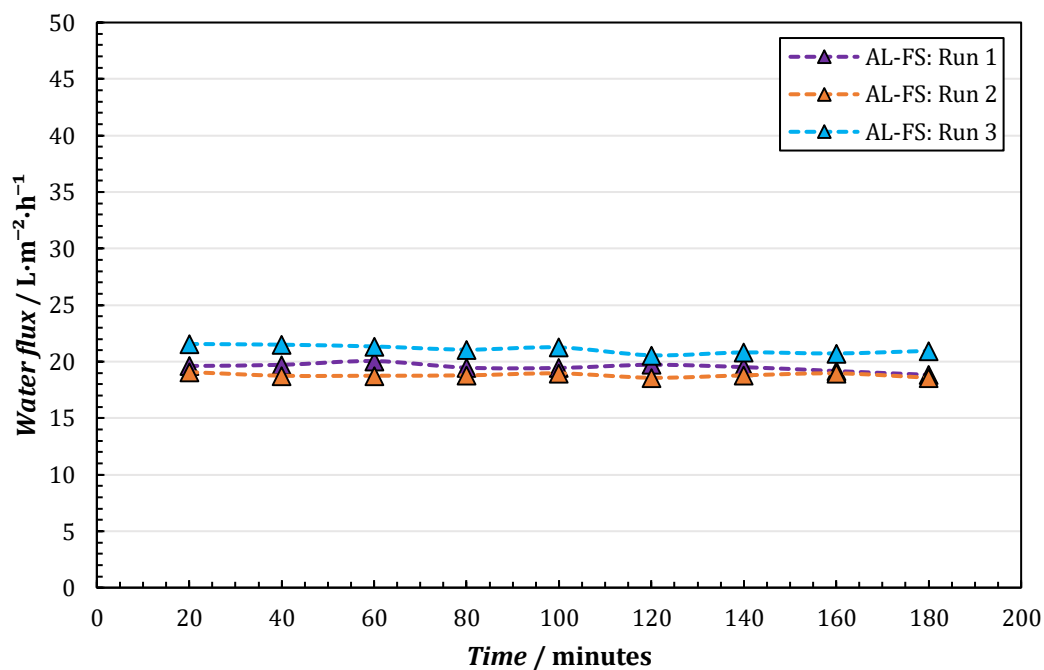
Figure 4-1: The water flux (J_W) as a function of the permeation time for triplicate experimental runs performed in the AL-FS orientation with different membrane coupons. The experimental conditions for the repeated runs were identical with a FS of deionised water, a 35 g·L⁻¹ NaCl DS ($\Delta\pi$=27 bar), FS Reynolds number of 1 700 and DS CFV=0.16 m·s⁻¹. All water fluxes are normalised to 20°C.

79
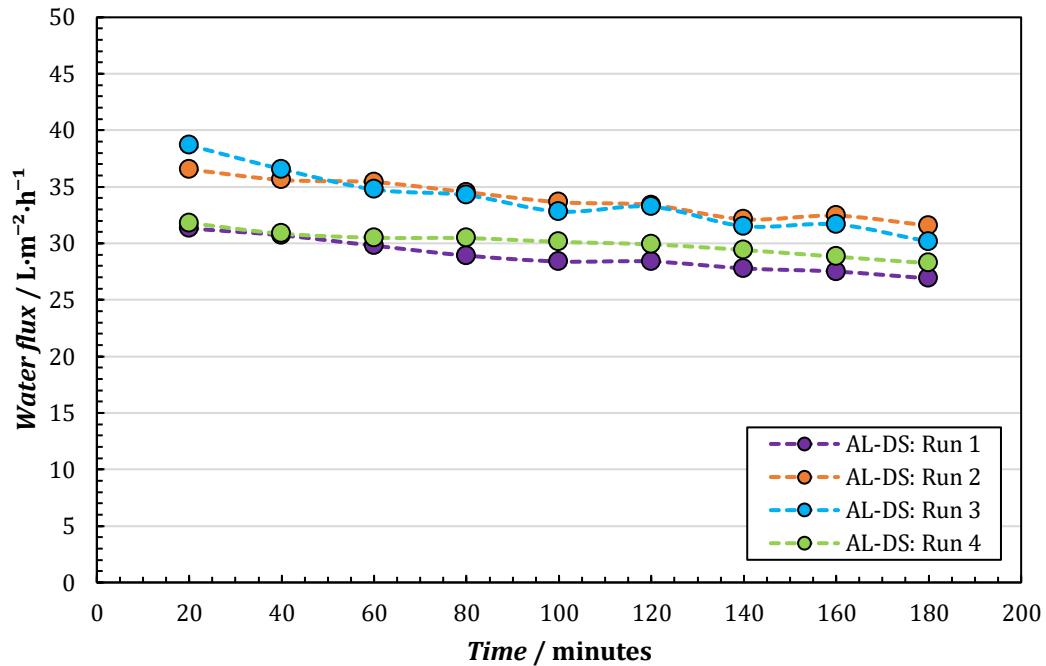
Figure 4-2: The water flux (J_W) as a function of the permeation time for triplicate experimental runs performed in the AL-DS orientation with different membrane coupons. The experimental conditions for the repeated runs were identical with a FS of deionised water, a 35 g·L^{-1} NaCl DS ($\Delta\pi$=27 bar), FS Reynolds number of 1 700 and DS CFV=0.16 m·s^{-1}. All water fluxes are normalised to 20°C.

The data in Figure 4-1 and Figure 4-2 are summarised in Table 4-1 in terms of the average water flux. Variation in the water flux among the different membrane coupons, indicated by the standard deviation, can be attributed to the morphological inconsistencies throughout the membrane area of the FO8040 module used in this work, as well as the variability in the extent of concentration polarisation (CP) and reverse solute flux (RSF). The uncertainty in the measurement of the water flux has already been discussed in Section 3.3.4.1. The results in Table 4-1 confirm that the uncertainty in the measurement of the water flux was significantly smaller than the standard deviation in the water flux among the membrane coupons.

A margin of repeatability of the water flux at each time instant among different membrane coupons was also constructed from the data sets presented in Figure 4-1 and Figure 4-2. This is shown in Figure 4-3 for the respective membrane orientations. The error bars indicate the standard deviation of the water flux among the repeated experimental runs at the same time instant. For the validation of the FO system prior to an experimental run, the normalised water flux was used as a criterion. The margin of the FO water flux for each membrane orientation indicated in Figure 4-3 was then used as the guideline.

80

Table 4-1: The average water flux in the AL-FS and AL-DS orientation determined from the repeated experimental runs in Figure 4-1 and Figure 4-2. The standard deviation represents the sample standard deviation of the average water flux among the triplicate runs in the AL-FS orientation and the quadruplicate runs in the AL-DS orientation.

Membrane orientation	Water flux		
	Average / $L \cdot m^{-2} \cdot h^{-1}$	Standard deviation / $L \cdot m^{-2} \cdot h^{-1}$	Relative standard deviation / %
AL-FS	19.8	1.2	5.9
AL-DS	31.6	2.3	8.2
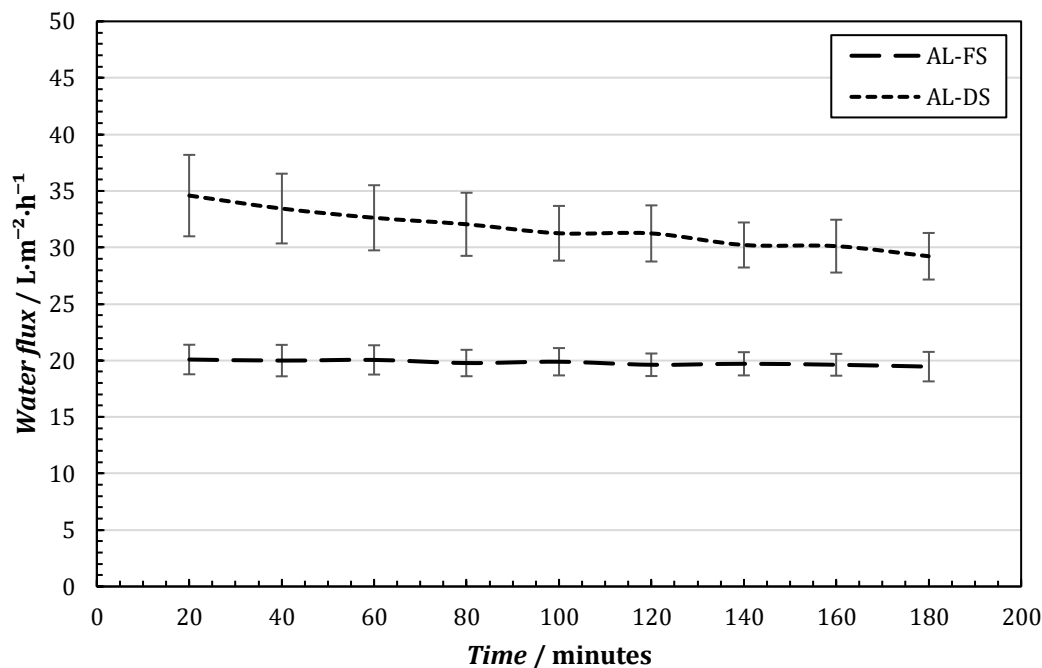
Figure 4-3: Repeatability margins of the water flux (J_w) in the AL-FS and AL-DS membrane orientations. The margins were constructed from the standard deviation of the water flux among the repeated experiments at the same time instant (Figure 4-1 and Figure 4-2). All water fluxes are normalised to 20°C.

The experimental water flux of 19.8 $L \cdot m^{-2} \cdot h^{-1}$ in the AL-FS membrane orientation was within 20% of that reported by Kim, et al. (2017) for the same membrane with a 35 $g \cdot L^{-1}$ NaCl DS. The water flux in the AL-FS membrane orientation was approximately 40% lower than that in the AL-DS orientation. This finding agrees with the membrane behaviour widely reported in the literature of FO (Tang, et al., 2010; McCutcheon & Elimelech, 2006; Gray, et al., 2006).

It is also evident from Figure 4-1 and Figure 4-2 that there is a discernible difference in the water flux stability between the AL-FS and AL-DS membrane orientations, as previously observed by Tang, et al. (2010). The water flux in the AL-DS membrane orientation shows a significant decline from approximately 35 $L \cdot m^{-2} \cdot h^{-1}$ to 29 $L \cdot m^{-2} \cdot h^{-1}$ over a period of three hours (Figure 4-2 and Figure 4-3), while the water flux in the AL-FS orientation remains within 0.6 $L \cdot m^{-2} \cdot h^{-1}$ for the same

81

permeation time. This difference in the flux stability can be related to difference in the extent of RSF and CP occurring in the respective membrane orientations. The occurrence of RSF is confirmed by the increase in the NaCl concentration of the FS, as shown in Figure 4-4.
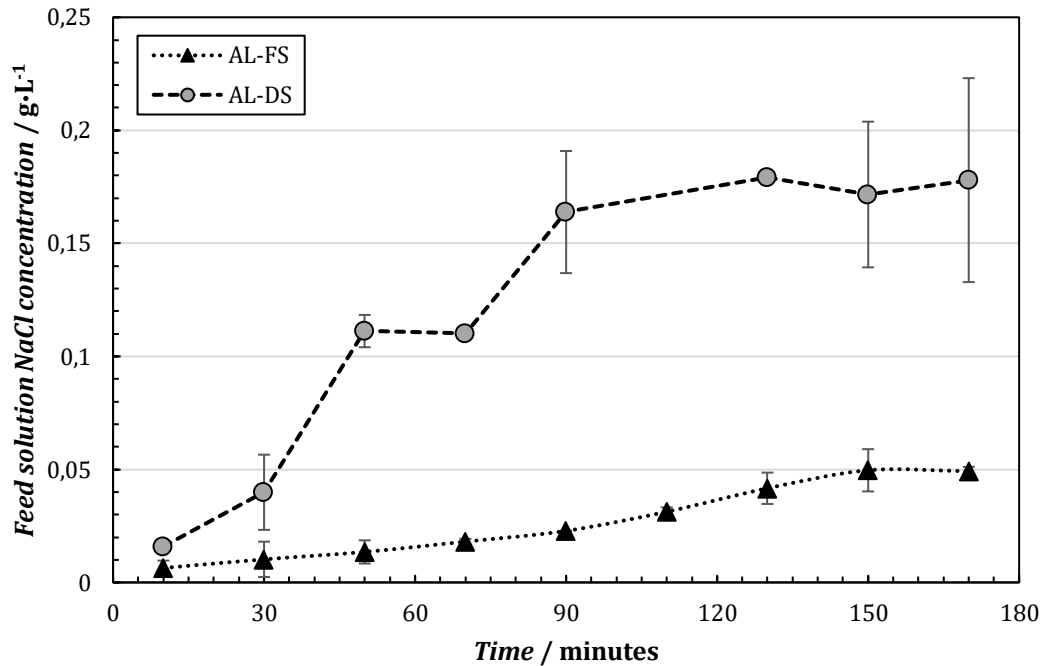
Figure 4-4: The NaCl concentration of the feed solution as a function of the water permeation time in the AL-FS and AL-DS orientation. The DS was a 35 g·L⁻¹ NaCl solution ($\Delta\pi$=27 bar) and the initial FS was deionised water. The FS was agitated at a Reynolds number of 1 700 and the DS CFV was 0.16 m·s⁻¹.

The experimental data presented in Figure 4-4 translate into specific reverse solute fluxes of 0.29 g·L⁻¹ and 0.85 g·L⁻¹ for the AL-FS and AL-DS orientation, respectively. A similar specific RSF of 0.37 g·L⁻¹ in the AL-FS orientation has previously been reported by Kim, et al. (2017) for the FO8040 membrane used in this work. It is also highlighted that the specific RSF in the AL-DS orientation was higher than the limit of 0.50 g·L⁻¹ specified by the membrane manufacturer. The specific RSF in the AL-FS orientation was sufficiently lower than this limit.

The lack of a stable water flux in the AL-DS membrane orientation (Figure 4-2) is evidence of a decreasing driving force for water permeation resulting from the gradual accumulation of the reverse diffused draw solute within the support layer of the membrane, or concentrative internal concentration polarisation (CICP), as well as the resulting increase in the total NaCl concentration of the FS over time. The specific RSF of 0.85 g·L⁻¹ is also consistently greater than the NaCl concentration of the FS indicated in Figure 4-4. This suggests that the accumulation of the draw solute in the support layer is predominantly caused by reverse solute flux rather than the forward convection of the FS contaminated with the draw solute (refer to Section 2.1.3.5.1).

An exceptionally stable water flux in the AL-FS orientation, as observed from Figure 4-3, has previously been reported in literature (Zhao, et al., 2011; Tang, et al., 2010). This stability is at the expense of a lower water flux due to the more severe dilutive internal concentration polarisation (DICP) in the AL-FS orientation relative to the CICP in the AL-DS orientation (She, et al., 2016). The stable performance of the AL-FS orientation can also be related to the self-compensation effect of DICP. Any decrease in water flux resulting from an increased FS osmotic pressure by RSF (Figure 4-4) is counteracted by reduced DICP in the support layer. In other words, the loss in the effective osmotic pressure gradient between the DS and FS is recovered by a reduced dilution of the draw solute within the support layer at a lower water flux.

4.1.2 Hydrodynamic conditions

Turbulence at the submerged membrane surface was established by the internal recirculation of the feed solution within the dead-end reactor. In this section, the effect of these hydrodynamic conditions on the submerged FO membrane performance is presented. This includes a demonstration of how the turbulence mitigates concentrative external concentration polarisation (CECP), what the effect of the agitation intensity is and evidence of DICP in FO membranes.

4.1.2.1 Mitigation of CECP

The purpose of the hydrodynamic conditions as mitigating CECP at the submerged FO membrane surface is demonstrated by a comparison of the FO water flux at non-agitated conditions to that at agitated conditions, the latter achieved with a Reynolds number of 1 700. The experimental runs were performed with a feed solution of deionised water and NaCl draw solution of 35 g·L⁻¹. The time-based water flux curves for the experimental runs with and without agitation are presented in Figure 4-5.
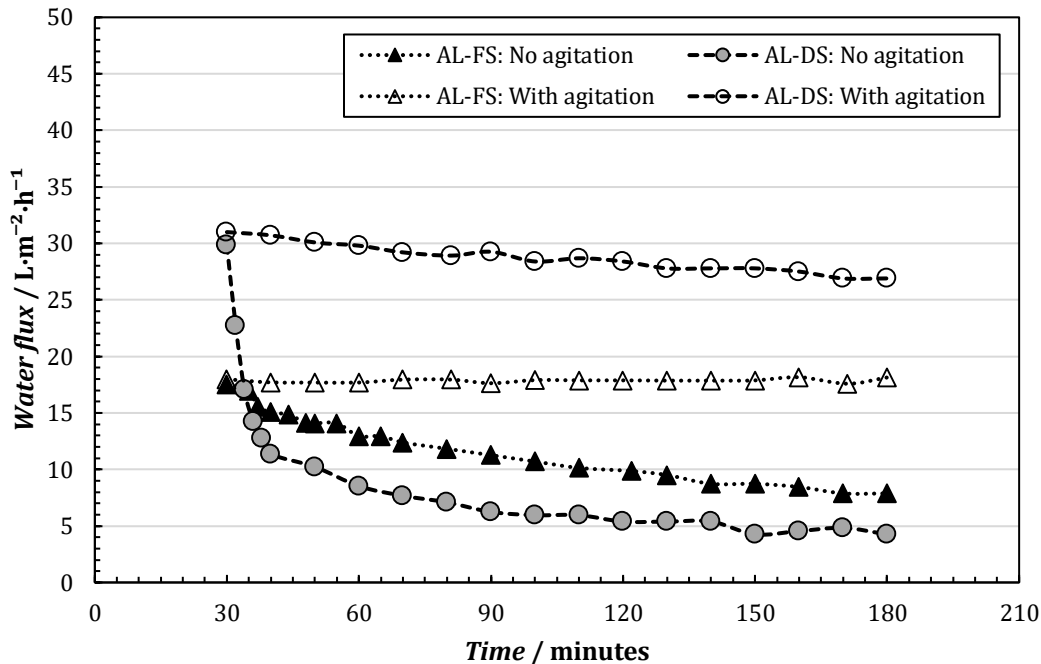
Figure 4-5: The water flux (J_W) in the AL-FS and AL-DS orientation as a function of time with and without agitation of the FS. Agitation was supplied at a Reynolds number of 1 700. The FS was deionised water and the DS a 35 g·L^{-1} NaCl solution ($\Delta\pi$=27 bar). The CFV of the DS was 0.16 m·s^{-1}. All water fluxes are normalised to 20°C.

It is clear from Figure 4-5 that there is a distinct difference in the FO water flux under agitated and non-agitated conditions in both membrane orientations. In the AL-FS membrane orientation, the water flux remained constant at approximately 18 L·m^{-2}·h^{-1} with hydrodynamic conditions. Under non-agitated conditions in this membrane orientation, there was a steady decline in the water flux to approximately 8 L·m^{-2}·h^{-1} over a permeation time of 180 minutes. As discussed in Section 4.1.1, the AL-DS membrane orientation exhibited a greater, but less stable water flux with agitation than the AL-FS orientation. The hydrodynamic conditions still proved to be effective in the AL-DS orientation as a very steep decline in the water flux occurred when the feed solution was not agitated. However, the flux decline in the AL-DS orientation with no agitation was excessive, such that there was an inversion in the membrane behaviour after approximately 35 minutes; the water flux in the AL-FS orientation became greater than that in the AL-DS orientation.

The decline in the water flux under stagnant FS conditions, observed from Figure 4-5, is indicative of the CECP arising from the RSF, as the initial feed solution was deionised water. With no agitation, the mass transfer boundary layer at the submerged membrane surface remains stagnant while becoming increasingly concentrated by the reverse diffused draw solute (Loeb, et al., 1997). This results in a decreasing osmotic pressure gradient between the FS and DS. In contrast,

agitation of the FS provides a constant and rapid dilution of the reverse diffused draw solute at the surface of the submerged membrane. This avoids the formation of a more concentrated boundary layer on the membrane surface relative to the bulk feed solution (Hancock & Cath, 2009). As a result, the effective osmotic pressure gradient, which is normally reduced by the CECP of reverse diffused draw solute, is recovered. It is highlighted that the change in the extent of CECP may affect the RSF across the membrane (Hancock & Cath, 2009); the RSF can decrease with an increase in CECP. Still, the CECP remains significant under non-agitated conditions, as depicted by the continuous flux decline in Figure 4-5.

To confirm that CECP was negligible under agitated conditions, the CECP modulus was evaluated for each membrane orientation at the experimental water flux. Values of 3.9 and 9.0 were obtained for the AL-FS and AL-DS orientation, respectively, which suggest that CECP was significant with agitation of the FS (Section 2.1.3.5.2). This contradiction could be attributed to a number of reasons. Firstly, there exists an inaccuracy in the estimation of the flow velocity over the membrane and hydraulic diameter of the module as a result of the nature of the flow pattern within the reactor. Secondly, the correlation of the Sherwood number is not customised to this particular flow geometry (Equation 3-6). Both these factors contribute to an erroneous prediction of the mass transfer coefficient. Such an inaccuracy in modelling of the fluid flow in the submerged FO configuration was also obtained in the study by Chowdhury, et al. (2017).

The distinctive effect of agitation on the water flux in the AL-DS orientation in the submerged FO system further suggests that CECP on the support layer, in addition to CICP within the support layer, cannot be neglected, as suggested by She, et al. (2016). This is an indication that the thickness of the boundary layer on the support layer under non-turbulent conditions is significant relative to the structural parameter of the support layer and contributes to the overall mass transfer resistance. Furthermore, the remaining flux decline in the AL-DS orientation, despite the hydrodynamic conditions, confirms that CICP cannot be mitigated by the alteration of the local hydrodynamic conditions at the surface of the membrane.

The less severe flux decline in the AL-FS orientation with no agitation is the result of the lower RSF relative to that in the AL-DS orientation. As mentioned in the Section 4.1.1, the specific RSF in the AL-FS orientation was approximately 3 times smaller than that in the AL-DS orientation. At a lower RSF, the boundary layer on the surface of the submerged membrane becomes concentrated at a slower rate than in the AL-DS orientation. For this reason, the water flux under stagnant feed conditions was generally greater in the AL-FS orientation than in the AL-DS orientation.

In conclusion, this evaluation confirmed that CECP limits mass transfer in the submerged FO configuration when the hydrodynamic conditions are sub-optimal. The prototype agitation device was effective in mitigating this phenomena. As significant CECP can further enhance membrane fouling (She, et al., 2016), sufficient turbulence at the surface of a submerged membrane is crucial in submerged membrane reactors for the treatment of wastewater with a high fouling potential.

4.1.2.2 *Effect of agitation intensity*

It has been demonstrated that the purpose of hydrodynamic conditions at the submerged membrane surface is to avoid the formation of a concentrated external boundary layer. Therefore, a variation in the intensity of the hydrodynamic conditions is expected to alter the thickness of the boundary layer, thereby affecting the extent of CECP. Consequently, the water flux will be affected. In this section, the effect of the agitation intensity on the FO water flux is presented.

The intensity of the agitation at the submerged membrane surface was varied among Reynolds numbers of 1 100, 1 700 and 2 700. These Reynolds numbers correspond to FS flow velocities of 0.8 cm·s⁻¹, 1.7 m·s⁻¹ and 5.6 cm·s⁻¹ over the membrane, respectively. The water flux achieved at each of the hydrodynamic conditions, in both the AL-FS and AL-DS membrane orientations, is presented in Figure 4-6. The time-based flux curves are provided in Figure 4-7 and Figure 4-8.
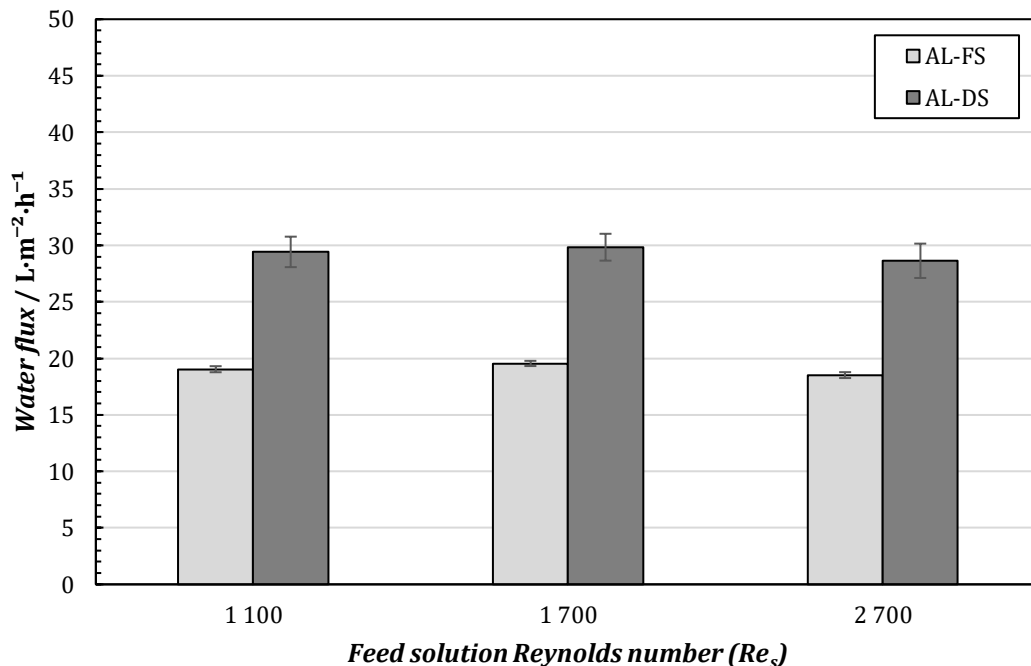
Figure 4-6: The experimental water flux (J_W) in the AL-FS and AL-DS orientation at FS Reynolds numbers of 1 100, 1 700 and 2 700. The FS was deionised water and the DS was a 35 g·L⁻¹ NaCl solution ($\Delta\pi$=27 bar) circulated at a CFV of 0.16 m·s⁻¹. All water fluxes are normalised to 20°C. The error bars represent the standard deviation of the water flux over a permeation time of 2 hours.

Figure 4-7: The water flux (J_W) in the AL-FS orientation as a function of time at FS Reynolds numbers of 1 100, 1 700 and 2 700. The experimental conditions were as indicated for the data in Figure 4-6. All water fluxes are normalised to 20°C.

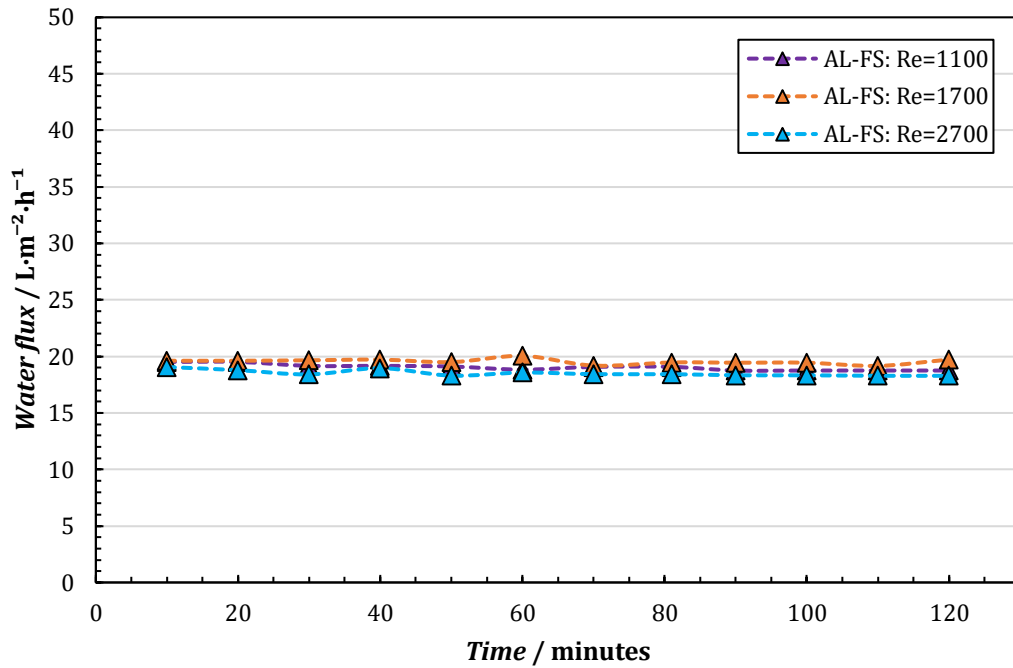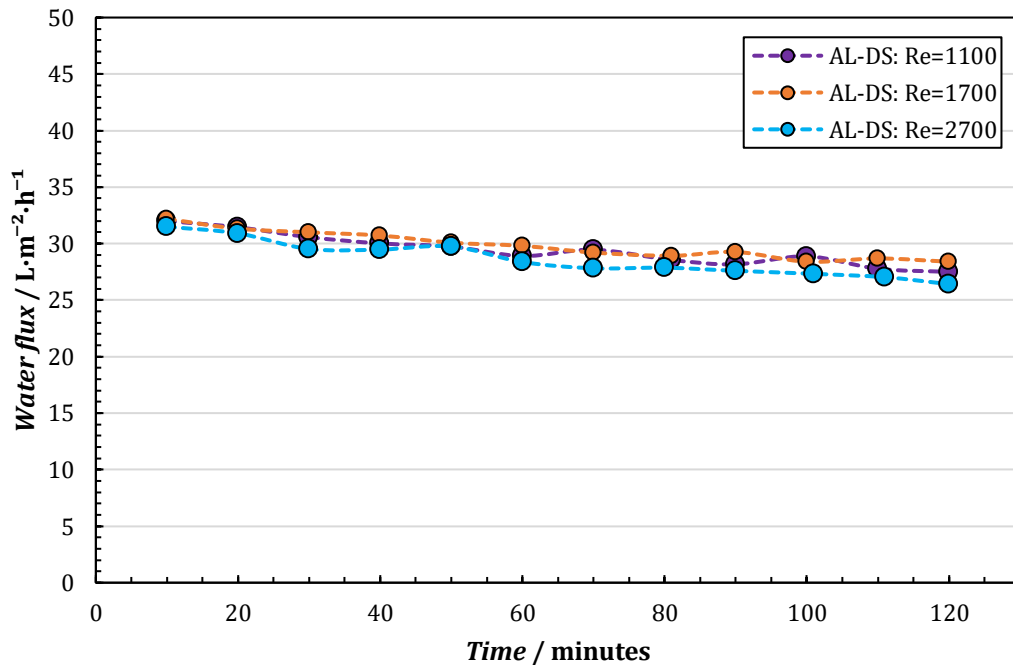
Figure 4-8: The water flux (J_W) in the AL-DS orientation as a function of time at FS Reynolds numbers of 1 100, 1 700 and 2 700. The experimental conditions were as indicated for the data in Figure 4-6. All water fluxes are normalised to 20°C.

It is evident from Figure 4-6 that the water flux in each membrane orientation was statistically similar among the agitation intensities investigated. Furthermore, no flux decline deviant from the baseline data can be observed from Figure 4-7 and Figure 4-8. With an increase in the agitation intensity, or FS Reynolds number, it was expected that the water flux would increase as a result of a reduction in the thickness of the concentrated boundary layer on the submerged membrane surface.

The above results suggest that moderate hydrodynamic conditions (Re=1 100) were adequate to maintain sufficient homogenisation of the external boundary layer on the submerged membrane surface to mitigate the limiting effect of CECP. Intense mixing up to a Reynolds number of 2 700 did not provide an improvement in the mass transfer. Thus, it can be concluded that the boundary layer remained unaltered with the variation in the hydrodynamic conditions from a Reynolds number of 1 100 to 2 700.

A similar observation to this with regards to the effect of agitation intensity on the water flux was made in the study by Zhou, et al. (2012), where agitation above 300 rpm with a magnetic stirrer in the DS chamber did not provide any improvement in the FO water flux. In the study by Blandin, et al. (2018) an increase in the recirculation velocity of the FS from approximately 1.0 cm·s⁻¹ to 5.0 cm·s⁻¹ only provided a 1.5 L·m⁻²·h⁻¹ increase in the water flux.

Contradictive to the above observation in the submerged FO configuration, an increase in the CFV in cross-flow channels generally provides an increase in the water flux (Devia, et al., 2015; Kim, et al., 2015). This difference in the water flux behaviour between the two module configurations can be related to the differences in their flow regimes and geometries. In the submerged configuration, turbulence provides bulk mixing of the FS. In cross-flow channels, the flow pattern is in closer contact to the membrane surface, as well as the porous support layer. However, the Reynolds numbers in the cross-flow configuration are typically lower (<1000) at common cross-flow velocities up to 0.25 m·s⁻¹ (Lian, et al., 2018; Devia, et al., 2015; McCutcheon & Elimelech, 2006). Therefore, the mass transfer coefficient in a cross-flow membrane module is improved to a greater extent when the velocity over the membrane is increased.

4.1.2.3 Evidence of DICP

With the evaluation of the submerged FO system, long-term water permeability tests with intermittent agitation were performed. In the AL-FS orientation, the water flux behaviour depicted in Figure 4-9 was observed when agitation was terminated for an extended period of time and subsequently switched on again. It can be observed that the steady state water flux under agitated conditions, denoted by steady state 1 and steady state 2, was not identical before and after

the period of no agitation. After a period of 150 minutes with no agitation (t=30 minutes to t=180 minutes), the water flux under agitated conditions was increased from 18 L·m^{-2}·h^{-1} (steady state 1) to 25 L·m^{-2}·h^{-1}. This was followed by a steady decline to a new steady-state flux of 21 L·m^{-2}·h^{-1} (steady state 2).
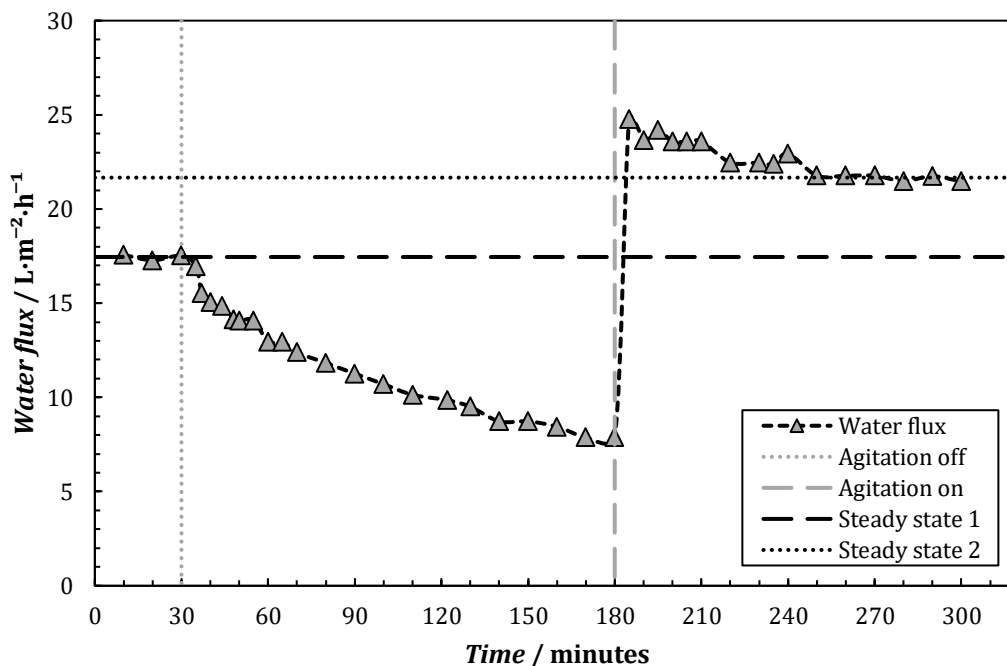
Figure 4-9: The water flux (J_W) in the AL-FS orientation as a function of time with intermittent agitation of the FS at a Reynolds number of 1 700. The FS was deionised water and the DS was a 35 g·L^{-1} NaCl solution ($\Delta\pi$=27 bar). The agitation was switched off at t=30 minutes and switched on again at t=180 minutes. The CFV of the DS was 0.16 m·s^{-1}. All water fluxes are normalised to 20°C.

This FO water flux behaviour shown in Figure 4-9 provides evidence of how the convective water flow across the membrane affects the concentration of the draw solute at the active-support layer interface and consequently the extent of DICP, according to Equation 2-13 (McCutcheon & Elimelech, 2006). Figure 4-9 illustrates that the flux decreased to approximately 8 L·m^{-2}·h^{-1} over a period of 150 minutes of no agitation. When agitation was switched on, the water flux was immediately improved to 25 L·m^{-2}·h^{-1}, as mentioned above. The DICP moduli at these conditions were approximated as 0.42 and 0.07, respectively. These values are smaller than unity, which confirms that the solute concentration within the support layer is lower than that in the bulk draw solution. Thus, DICP was indeed significant in both instances. However, the extent of the DICP is less severe at the low flux before the start of agitation as the DICP modulus is closer to unity in this case. At a lower water flux, the convective water flow dilutes the draw solute in the support layer to a lesser extent than at a higher water flux.

89

The peak in the water flux to a magnitude higher than steady state 1 when the agitation was switched on at t=185 minutes can be attributed to the lingering effect of the reduced DICP attained at conditions of no agitation, or a low water flux. The greater dilution of the draw solute in the support layer with a higher water flux did not occur instantly due to the hindered diffusion in this region of the membrane. Hence, a larger effective driving force than that in the first 30 minutes of the permeation time was established. The water flux exhibited a gradual flux decline towards a new baseline flux of 22 L·m^{-2}·h^{-1} (steady state 2) from the instant of t = 185 minutes to t = 250 minutes while the draw solute became increasingly diluted by the higher water flux under turbulent conditions. Subsequent investigation showed that the membrane was only able to achieve the water flux at steady state 1 once it was allowed to equilibrate at stagnant conditions overnight.

The FO water flux behaviour discussed here provides more insight into the hindered diffusion that occurs in the porous support layer of the FO membrane and how the convective flow of the water flux affects the concentration of the draw solute within the support layer. The effective osmotic pressure gradient is not dependent on the concentration of the draw solution per se. As widely reported in literature, cross-flow of the high salinity DS cannot mitigate the hindered diffusion in the support layer (She, et al., 2016).

4.1.3 Water and NaCl transport

Figure 4-10 shows the experimental FO water flux as a function of the osmotic pressure gradient across the membrane, as well as the theoretical water flux approximated from solution diffusion theory (Equation 2-6). The water permeability coefficient of the membrane was estimated from the values reported by Volpin, et al. (2018) and Kim, et al. (2017) for the same FO8040 membrane used in this study (ca. 6.7 L·m^{-2}·h^{-1}·bar). To evaluate the experimental water flux, the osmotic pressure of the draw solution was varied between 3.9 bar and 46 bar with a feed solution of deionised water. The draw solution NaCl concentrations corresponding to the osmotic pressure gradients indicated in Figure 4-10 are listed in Table 4-2.
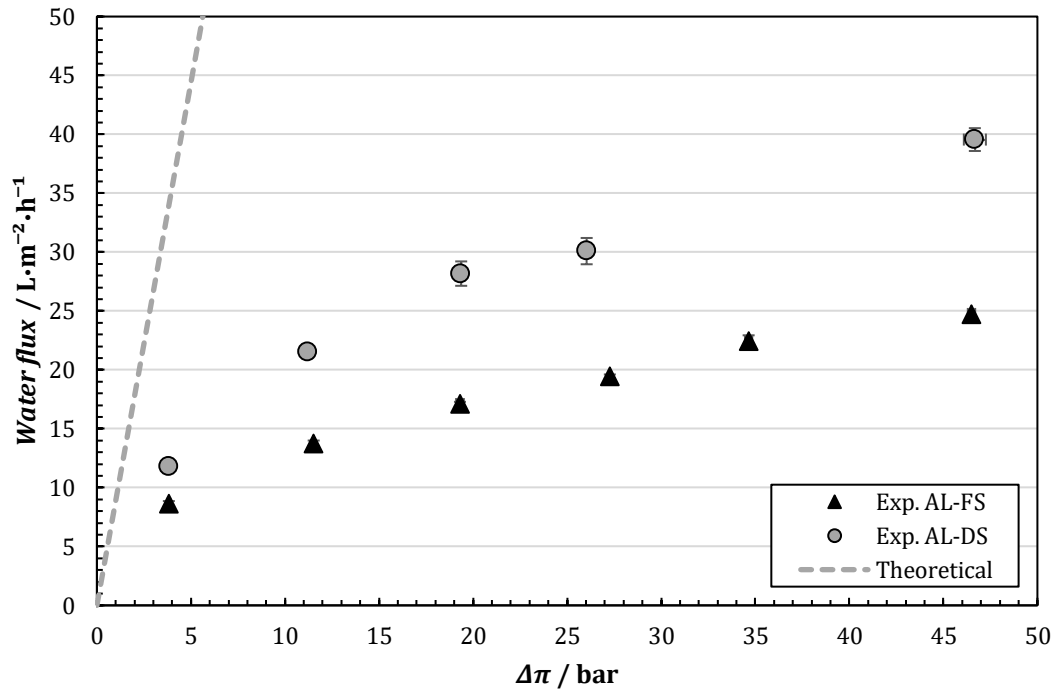
Figure 4-10: The theoretical and experimental water flux (J_W) in the AL-FS and AL-DS membrane orientation as a function of the osmotic pressure gradient ($\Delta\pi$). The FS was deionised water and the DS osmotic pressure was varied. The feed was agitated at a Reynolds number of 1 700 and the DS was circulated at a CFV of 0.16 m·s⁻¹. All water fluxes are normalised to 20°C. The horizontal and vertical error bars represent the standard deviation of the osmotic pressure gradient and water flux over a permeation time of three hours, respectively.

Table 4-2: The NaCl concentration of the draw solution corresponding to the experimental osmotic pressure gradients shown in Figure 4-10.

Osmotic pressure gradient ($\Delta\pi$) / bar	Draw solution NaCl concentration / g·L⁻¹
3.9	5
11	15
19	25
27	35 (seawater)
35	45
46	60 (seawater RO concentrate)

It is clear from Figure 4-10 that the experimental water flux deviated significantly from the theoretical prediction as a result of the mass transfer limiting phenomena inherent to the FO process. The experimental water fluxes in the AL-FS orientation were 30-40% lower than that in the AL-DS orientation and a greater proportionality exists between the osmotic pressure and the water flux in the latter orientation. The difference in the water flux behaviour between the AL-FS and AL-DS orientation is attributed to the different types of CP that occur in the respective orientations as a result of the asymmetric structure of the membrane.

The lower fluxes in the AL-FS orientation confirm that phenomenon of DICP has a more adverse effect on the FO water flux than CICP, as the former results in a greater loss of the effective driving force (She, et al., 2016). Furthermore, by the self-compensation effect of DICP, any increase in the draw solution concentration is compromised by the increased dilution of the draw solute within the support layer by the convective water flux. Hence, there is only a marginal gain in the effective driving force for water flux with an increase in the osmotic pressure gradient. For this reason, the relationship between the osmotic pressure gradient and water flux is non-linear (McCutcheon & Elimelech, 2006) and the increase in the water flux is smaller in the AL-FS orientation than in the AL-DS orientation for the same increment in the osmotic pressure gradient. The effects of CECP in the AL-FS orientation was assumed to be negligible, based on the findings discussed in Section 4.1.2.1.

The non-linearity between the osmotic pressure gradient and the water flux in the AL-DS orientation is related to the limiting effects of dilutive external concentration polarisation (DECP) and CICP. The occurrence of DECP is confirmed by the DECP moduli (<1) presented in Figure 4-11. At higher water fluxes, the external boundary layer on the membrane surface in contact with the draw solution is diluted to a greater extent (corresponding to a decrease in the DECP modulus), which results in a loss of the driving force for water permeation.
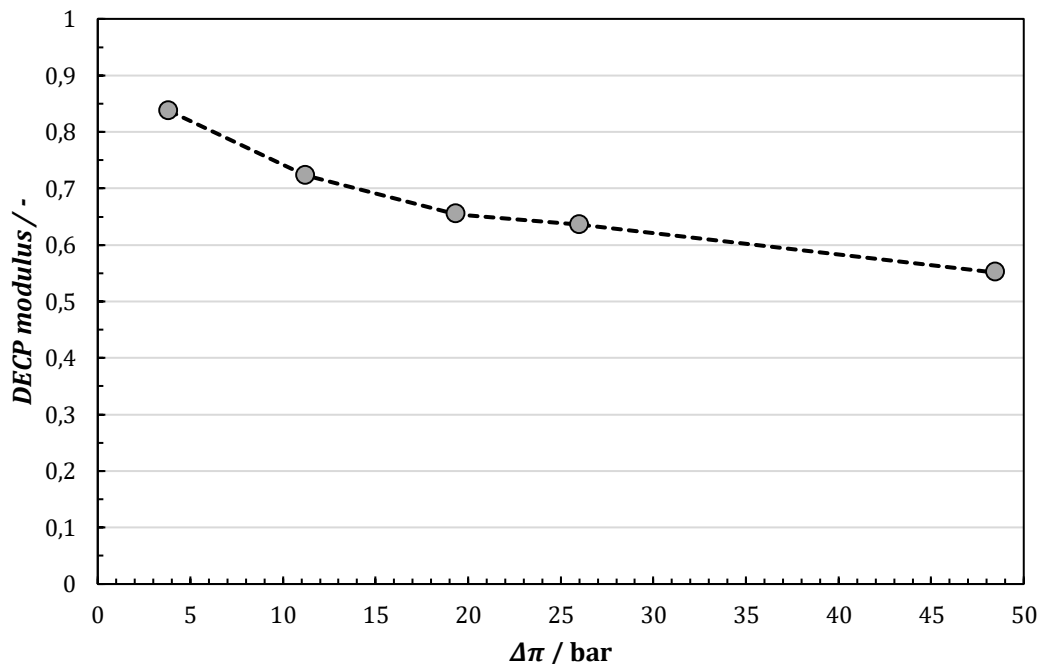
Figure 4-11: The DECP modulus as a function of the osmotic pressure gradient, with the AL-DS water fluxes as shown in Figure 4-10.

Although ICP is normally less severe when the support layer is in contact with the deionised water FS, severe RSF in the AL-DS orientation (Figure 4-12), contributed to the concentration of the boundary layer within the support layer in contact with the FS. Hence, CICP, which has an exponential dependence on the water flux, was significant in compromising the effective osmotic pressure gradient in the AL-DS orientation.
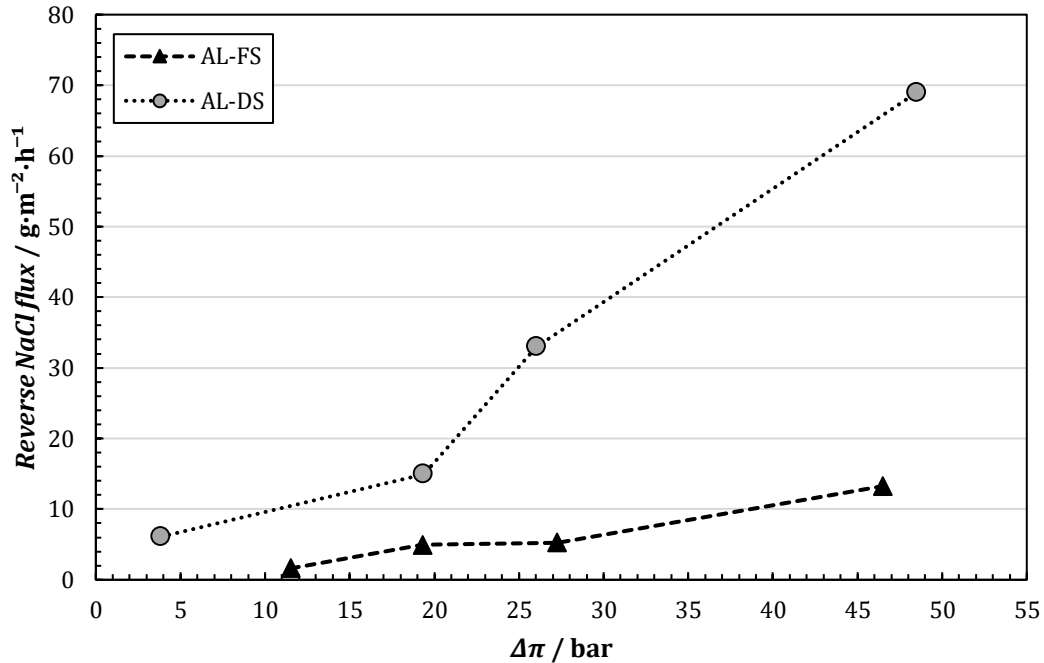
Figure 4-12: The reverse NaCl flux in the AL-FS and AL-DS orientation as a function of the osmotic pressure gradient between the FS and DS. The FS was deionised water and the DS osmotic pressure was varied. The experimental conditions were as indicated for the data presented in Figure 4-10.

It is clear from Figure 4-12 that the reverse NaCl flux increased with an increase in the osmotic pressure gradient. This is the result of the increase in the concentration of NaCl in the draw solution, which is effectively the driving force for reverse solute flux. Therefore, besides the exponential dependence of concentration polarisation on the water flux (Equations 2-10 and 2-12), the increase in reverse NaCl flux with the osmotic pressure gradient further contributed to an increase in CICP. For this reason, the increase in the water flux became diminished at higher osmotic gradients in the AL-DS orientation. This rationale is in agreement with what has previously been reported by McCutcheon & Elimelech (2006); CICP resulting from significant salt passage from the DS shows a non-linear relationship between the osmotic pressure gradient and water flux when the feed solution is deionised water.

93

In the broader context of the practical applications of the FO process, it has been reported that FO water fluxes greater than 30 L·m⁻²·h⁻¹ are required to render the FO-RO hybrid process economically viable (Wang, et al., 2018; Blandin, et al., 2016). Concluding from this investigation of the performance of a TFC FO membrane, realistic draw solution osmotic pressures, such as that of seawater, cannot generate such favourable water fluxes in the more stable AL-FS orientation. The experimental water fluxes remained below 25 L·m⁻²·h⁻¹ up to a DS osmotic pressure equivalent to that of RO concentrate in this membrane orientation. Due to the flux inefficiency of FO membranes, elevated NaCl concentrations in the draw solution would be required to establish sufficiently high water fluxes in the AL-FS orientation.

The results suggest that a water flux of 30 L·m⁻²·h⁻¹ is indeed possible in the AL-DS orientation with a seawater draw solution. However, the high reverse draw solute flux in this orientation is not desired. It has costly effects on the performance on the FO process as it compromises stable membrane performance. Reverse salt flux also alters the chemistry of the feed solution, which potentially aggravates membrane fouling (Lay, et al., 2010).

4.2 Solute transport

Phenol, boron and lithium were used as model feed solutes in the evaluation of the solute transport by the submerged FO membrane. The properties of these solutes are summarised in Table 2-11. Among them, a wide range of structural and physicochemical properties, that govern their rejection by FO membranes, are exhibited. Phenol was selected due to the occurrence of phenolic EDCs in wastewater. Boron and lithium were considered as they occur in both wastewater and seawater, with the latter being used as the draw solution in the FO-RO process.

As mentioned in Section 3.3.2.4, the forward solute flux and rejection were considered throughout the analysis of the solute transport. The forward solute flux is useful to elaborate the difference in the mechanisms by which the solutes are transported and rejected (Schutte, 2003), while the rejection only provides an indication of the removal efficiency of the membrane. Throughout this discussion, the error bars of the solute flux and rejection indicate the uncertainty evaluated from triplicate samples.

The effect of the water flux on the transport of a feed solute in FO is elucidated with phenol as the model solute. The effect of the solute concentration gradient, which is the driving force for solute diffusion, is presented in the case of all three model solutes. In addition, the transport of boron and lithium was evaluated with a draw solution containing elevated levels of these solutes, with concern to seawater as draw solution in FO.

94

4.2.1 Phenol

4.2.1.1 *Effect of the osmotic pressure gradient*

The transport of phenol across the FO membrane was evaluated at osmotic pressure gradients between 8 bar and 90 bar in the AL-FS orientation and between 8 bar and 144 bar in the AL-DS orientation. Only the draw solution NaCl concentration was varied while the NaCl concentration of the feed was fixed at 2 g·L^{-1} NaCl (refer to Section 3.3.3.1). The feed phenol concentration was 10 mg·L^{-1} with neutral pH conditions (7.7 ± 0.1). It is once again highlighted that this feed concentration is higher than typical domestic wastewater contaminant concentrations (±0.1 to 100 µg·L^{-1}). The accuracy of the solute flux and rejection was compromised by the adsorption of phenol to the FO system components at feed concentrations lower than 5 mg·L^{-1}.

The water fluxes generated in the AL-FS and AL-DS orientation at the investigated osmotic pressure gradients are presented in Figure 4-13. In accordance with the solution-diffusion model (Table 2-5), the phenol transport behaviour is presented in Figure 4-14 in terms of the solute flux normalised to the feed concentration ($J_{PhOH}/c_{f,PhOH}$), as a function of the water flux. The normalised solute flux also compensates for minor deviations in the initial feed phenol concentration from the standard concentration of 10 mg·L^{-1}.
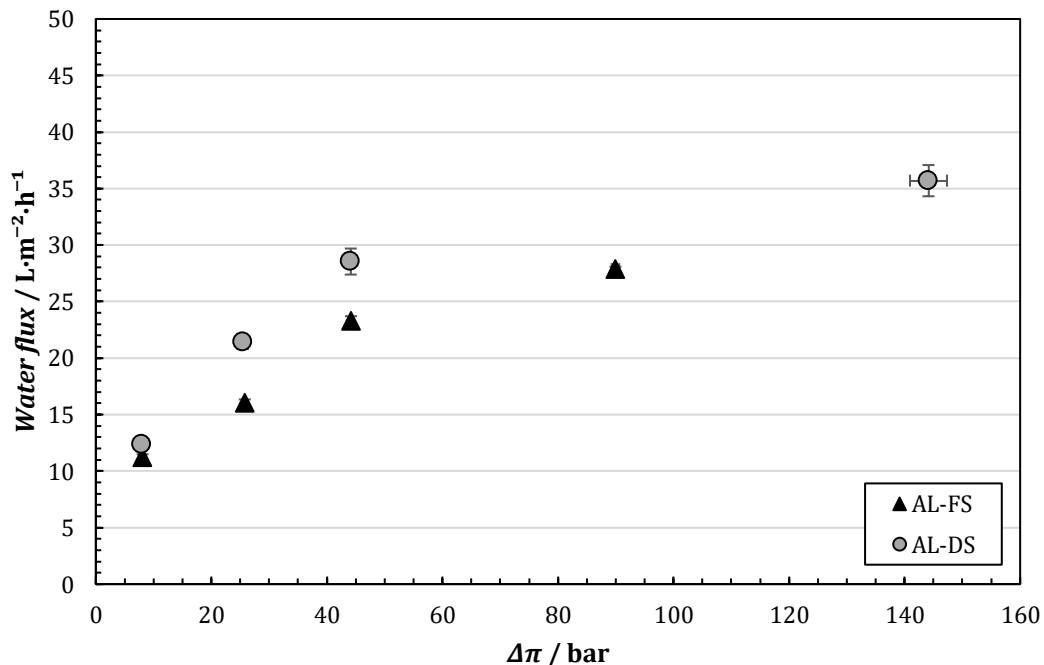
Figure 4-13: The water flux in the AL-FS and AL-DS orientation as a function of the osmotic pressure gradient (Δπ) at which the transport of phenol was investigated. The FS was a 2 g·L^{-1} NaCl solution with 10 mg·L^{-1} phenol. The NaCl concentration in the DS was varied. The feed solution was agitated at a Reynolds number of 1 700 and the DS CFV was 0.16 m·s^{-1}. All water fluxes are normalised to 20°C.
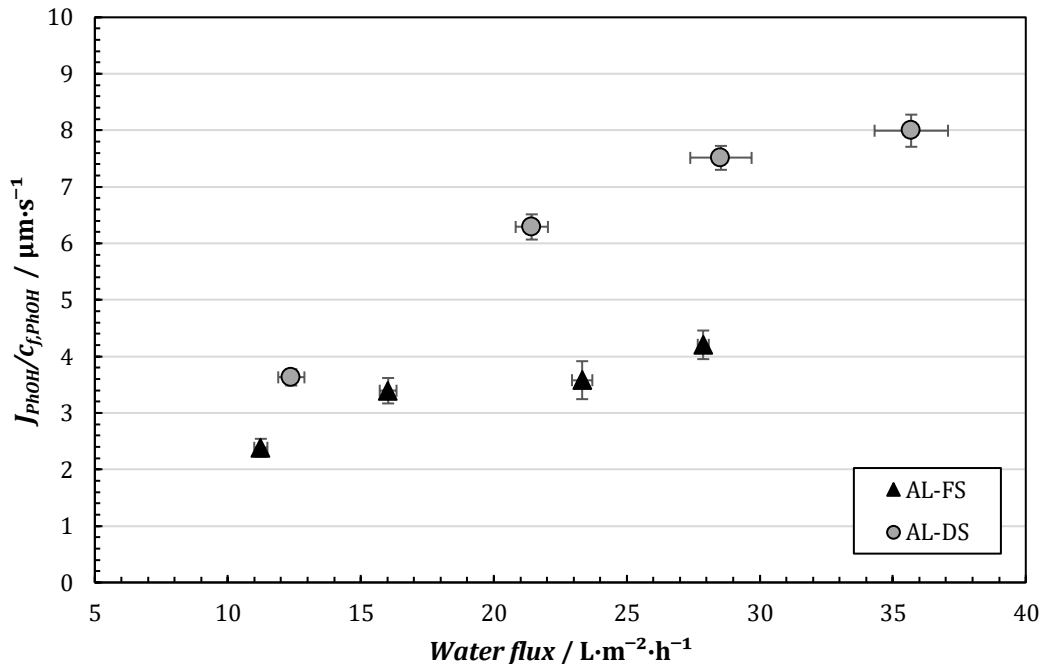
Figure 4-14: The normalised phenol solute flux ($J_{PhOH}/c_{f,PhOH}$) in the AL-FS and AL-DS orientation as a function of the water flux. The feed phenol concentration was 10 mg·L⁻¹ with a 2 g·L⁻¹ NaCl background solution (pH 7.7 ± 0.1). All solute and water fluxes are corrected to the reference temperature of 20°C.

It is evident from Figure 4-14 that the normalised phenol solute flux increased with the water flux. The same observation has previously been reported by Zhang, et al. (2017), with phenol as the particular model solute. The difference in the solute flux behaviour between the two membrane orientations depicts the difference in their solute transport mechanisms.

In the AL-FS orientation, solution-diffusion dictates the permeation of phenol across the active layer and the convective forces of the water flux carry the solute through the support layer on the draw solution side of the membrane. The trend of the experimentally determined phenol solute flux in the AL-FS orientation shown in Figure 4-14 is consistent the prediction from the solution-diffusion theory (Equation 2-19) that the phenol solute flux increases with an increasing water flux for a constant bulk feed phenol concentration.

The water flux is coupled to the concentration of the solute at the active-support layer interface according to Equation 2-16 presented in Section 2.3.1. With increasing water flux, the concentration of phenol at the active-support layer interface becomes more dilute. As a result, the phenol concentration gradient between the bulk feed solution and the active-support layer interface, which is the driving force for phenol transport, is enhanced (Jin, et al., 2011). Therefore, the rate of permeation of the solute, or solute flux, increases.

In the AL-DS orientation, convective water flow as well as diffusion results in phenol freely entering the support layer of the membrane from the bulk feed solution. Due to the retention of phenol in the porous support layer (CICP), the phenol concentration at the interface between the support and active layer becomes higher than the concentration in the bulk feed solution (Jin, et al., 2011). When the water flux increases, the extent of the ICP of phenol grows exponentially, which results in the increase in the phenol solute flux (relate Equation 2-17). It is for this reason that the difference in the phenol solute flux between the two orientations is greater at higher water fluxes (Jin, et al., 2011), as observed from Figure 4-14.

In addition to the CICP of phenol in the support layer, the higher phenol solute flux in the AL-DS orientation than in the AL-FS orientation is related to the more rapid dilution of the solute at the smooth surface of the active layer facing the draw solution. In the AL-FS orientation, the porous structure of the support layer inhibits the efficient dilution of the diffusing solute normally provided by the cross-flow of the draw solution. This retarded dilution in the AL-FS orientation establishes a lower effective phenol concentration gradient between the bulk feed solution and active-support layer interface, which results in a lower phenol solute flux than in the AL-DS orientation.

The observed phenol rejection in the AL-FS and AL-DS membrane orientations as a function of the experimental water flux is presented in Figure 4-15. In the AL-FS orientation, the phenol rejection increased from 90.6% to 93.3% when the water flux increased from 11 $L \cdot m^{-2} \cdot h^{-1}$ to 28 $L \cdot m^{-2} \cdot h^{-1}$. This trend in the phenol rejection is in agreement with previous findings reported in literature (Huang, et al., 2018; Xiao, et al., 2017; Cui, et al., 2016). In the AL-DS orientation, a pronounced increase in the phenol rejection occurred when the water flux was increased above 20 $L \cdot m^{-2} \cdot h^{-1}$. An improvement in the phenol rejection from 86.6% to 90.6% was obtained when the water flux was increased from 21 $L \cdot m^{-2} \cdot h^{-1}$ to 36 $L \cdot m^{-2} \cdot h^{-1}$.
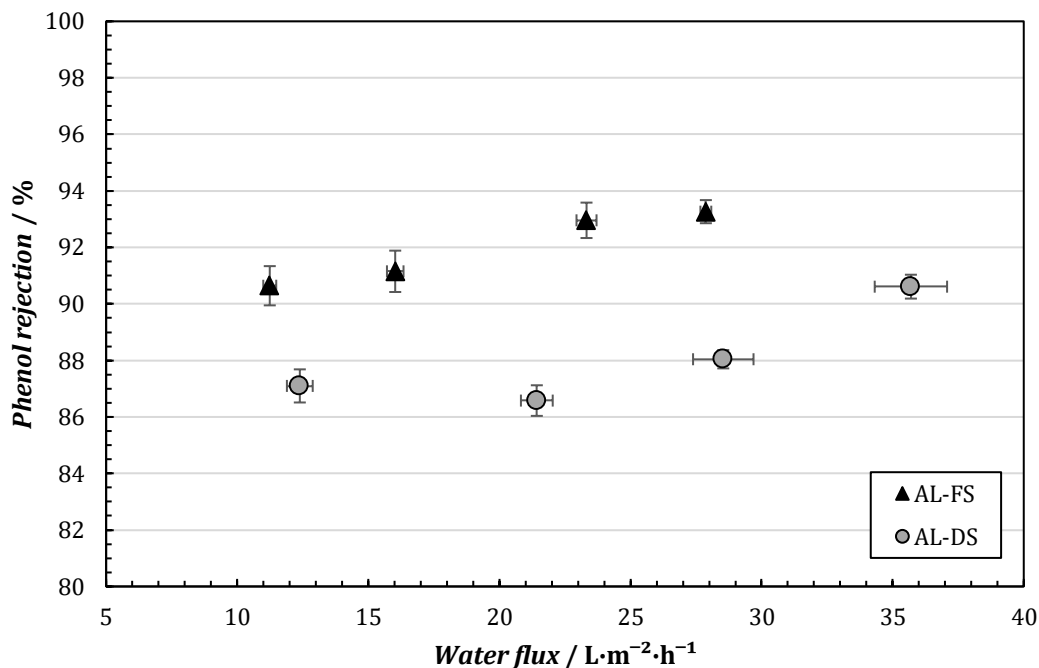
Figure 4-15: The phenol rejection in the AL-FS and AL-DS orientation as a function of the water flux. The phenol concentration in the feed solution was fixed at 10 mg·L⁻¹ with a 2 g·L⁻¹ NaCl background solution (pH 7.7 ± 0.1). All rejections and water fluxes are normalised to 20°C. All other experimental conditions are as indicated for the data in Figure 4-13.

The general increase in the phenol rejection with the water flux observed from Figure 4-15 can be attributed to the 'dilution effect' previously described by Seidel, et al. (2001). At a higher water flux, there is a higher resistance imposed on the diffusion of the solute by the steric exclusion resulting from a greater amount of water molecules passing through the membrane. Consequently, the concentration of the permeate decreases and the solute rejection increases with an increase in the water flux. It is emphasised that an increase in the water flux increases the rate at which convection transports the solute to the active-support layer interface (Figure 4-14), but the relative amount of the solute to water permeating across the membrane becomes retarded with an increase in the water flux, which results in the increased solute rejection.

It is clear from Figure 4-15 that the phenol rejection in the AL-DS orientation was lower than that in the AL-FS orientation at the same experimental water flux. This is attributed to the CICP in the AL-DS orientation that increases the effective phenol concentration gradient across the membrane. Thereby, the rate of diffusion of phenol is higher than in the AL-FS orientation, as portrayed in Figure 4-14 by the higher phenol solute flux in the AL-DS orientation.

According to the prediction of the solute rejection from solution-diffusion theory (Equation 2-20) the increase in the phenol rejection becomes less pronounced as the water flux increases in the

AL-FS orientation. This is evident from Figure 4-15 where there was no significant increase in the solute rejection as the water flux was increased from 23 $L \cdot m^{-2} \cdot h^{-1}$ to 28 $L \cdot m^{-2} \cdot h^{-1}$, compared to that observed at lower water fluxes. This plateau in the phenol rejection was also observed by Xiao, et al. (2017) at approximately the same experimental water flux generated by a TFC membrane.

In contrast, Equation 2-22 predicts that once the water flux in the AL-DS orientation becomes sufficiently large for a particular solute resistivity in the support layer (Equation 2-8), the solute rejection will start to decrease as a result of the greater convective transport and ICP of the solute in the support layer. If this is the case, the pronounced increase in the phenol rejection in the AL-DS orientation from 88% to 91% when the water flux increased from 29 $L \cdot m^{-2} \cdot h^{-1}$ to 36 $L \cdot m^{-2} \cdot h^{-1}$ may rather be attributed to the retarded forward diffusion of the solute by the reverse diffusion of the draw solute (Section 2.3.2).

The effect of RSF on the solute rejection in FO is not accounted for in the solute transport equations derived from solution-diffusion theory (Table 2-5). At a higher water flux, a greater RSF is the direct result of the higher concentration difference of the draw solute across the membrane (refer to Figure 4-12). Hence, the forward solute diffusion is more retarded at higher water fluxes. This is demonstrated in Figure 4-14 by the smaller increment in the phenol solute flux in the AL-DS orientation at water fluxes above 20 $L \cdot m^{-2} \cdot h^{-1}$. Accordingly, the increase in the solute rejection is greater at higher water fluxes in the membrane orientation.

It is further highlighted that the ionic strength of the background feed solution may have contributed to the reduction of the phenol permeability, which favours the phenol rejection. It has previously been shown that an ionic solution 'shrinks' the membrane matrix, which results in a lower permeability of the feed solutes (Bellona, et al., 2004; Braghetta, et al., 1997). According to Equations 2-20 and 2-22, a lower solute permeability favours the solute rejection. To study this point, the phenol permeability coefficient (B) at the experimental conditions considered here was regressed from the AL-FS data presented in Figure 4-15. A permeability coefficient of approximately 4.9×10^{-7} $m \cdot s^{-1}$ was obtained (R^2=0.61). Typical values of the phenol permeability coefficient, with specifically a TFC FO membrane and deionised water feed, are one order of magnitude higher (Xiao, et al., 2017; Zhang, et al., 2017). Thus, the ionic strength of the background FS (2 $g \cdot L^{-1}$ NaCl) may have reduced the permeability of phenol.

In conclusion, the experimental results presented in this section demonstrate that the solute removal by FO membranes can be improved by increasing the osmotic pressure gradient between the feed and draw solution, but the membrane orientation has a strong influence on the solute transport. The AL-FS orientation would be preferable in practical applications of the FO process

due to the higher solute rejection and lower passage of the solute to the DS relative to the AL-DS orientation at the same water flux. However, in the AL-FS orientation, the advantage in the solute rejection becomes smaller at higher water fluxes. Still, the lower solute rejection at moderate water fluxes renders the AL-DS orientation unfavourable. The solute rejection can be enhanced with higher water fluxes in this membrane orientation, but at the expense of a higher RSF.

4.2.1.2 *Effect of the phenol concentration gradient*

To evaluate the effect of the concentration gradient of phenol on its transport, the phenol concentration in the feed solution was varied between 5 mg·L^{-1} and 25 mg·L^{-1}. The background feed solution contained 2 g·L^{-1} of NaCl. Draw solutions with a NaCl concentration similar to that of seawater (35 g·L^{-1}) and RO concentrate (60 g·L^{-1}) were used in the experiments, which provided osmotic pressures of approximately 27 bar and 46 bar, respectively. The experiments were conducted in both the AL-FS and AL-DS orientations.

Figure 4-16 shows the experimental water fluxes attained as the phenol concentration gradient was varied. The water flux was unaffected as the feed phenol concentrations were sufficiently low to prevent an alteration in the osmotic pressure of the feed solution. Despite the mild acidity of phenol (pK$_a$=9.98), the pH of the feed solution remained relatively constant at 7.7 ± 0.1 with an increase in the phenol concentration up to 25 mg·L^{-1}. Based on this evaluation, the effects of the water flux and solution chemistry on the phenol transport could be considered insignificant.
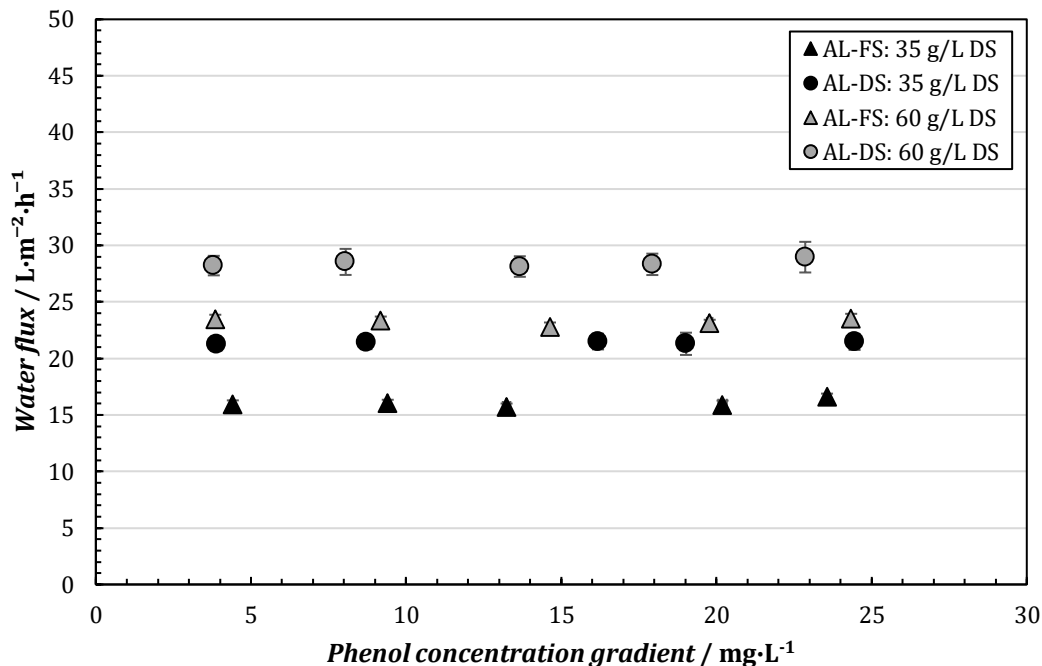
Figure 4-16: The water flux achieved in the AL-FS and AL-DS membrane orientations for the investigation of the effect of the phenol concentration gradient on its flux and rejection. The NaCl concentration of the DS was 35 g·L⁻¹ or 60 g·L⁻¹. The NaCl concentration in the feed was 2 g·L⁻¹ (pH 7.7 ± 0.1). Agitation was supplied in the feed solution at a Reynolds number of 1 700 and the DS CFV was 0.16 m·s⁻¹. All water and solute fluxes are normalised to 20°C.

Figure 4-17 and Figure 4-18 illustrate the effect of the phenol concentration gradient on its flux and rejection, respectively. As described analytically by Equations 2-19 and 2-21, the experimentally determined phenol solute flux approached a proportional relationship with its driving force for diffusion which is the phenol concentration gradient. In the AL-FS orientation with a 35 g·L⁻¹ NaCl DS, the phenol solute flux doubled from 120 mg·m⁻²·h⁻¹ to 240 mg·m⁻²·h⁻¹ when the phenol concentration was increased by approximately the same factor from 9 mg·L⁻¹ to 20 mg·L⁻¹. In the AL-DS orientation, the proportionality was roughly equal to that in the AL-FS orientation. However, the phenol solute flux was almost double that obtained in the AL-FS orientation at the same phenol concentration gradient and DS concentration, 210 mg·m⁻²·h⁻¹ and 400 mg·m⁻²·h⁻¹, respectively.
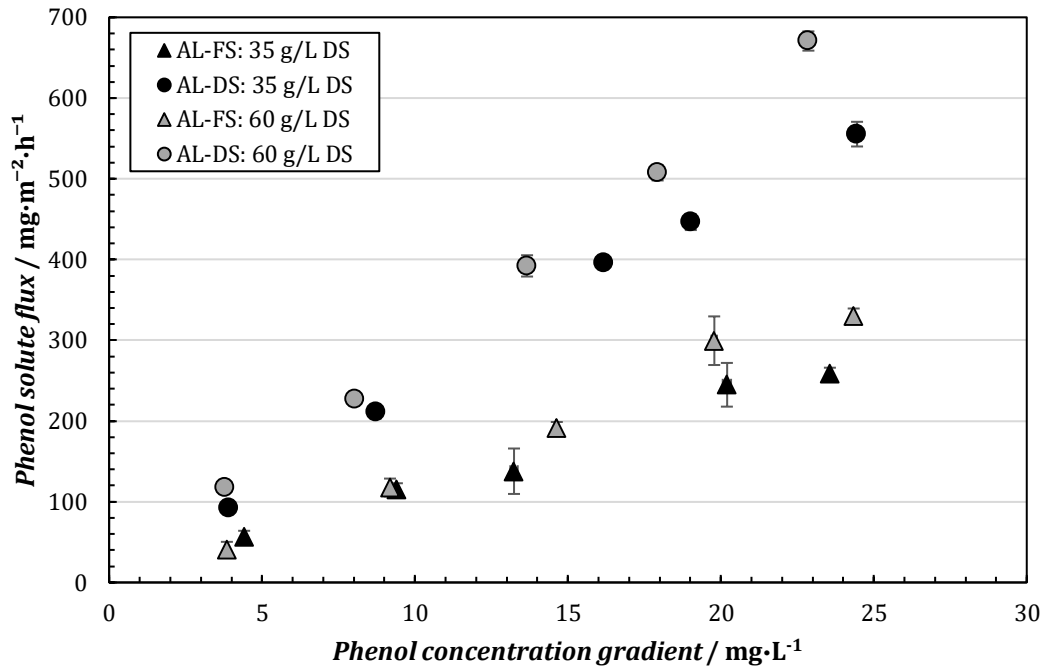
Figure 4-17: The phenol solute flux in the AL-FS and AL-DS membrane orientation as a function of the phenol concentration gradient with a 35 g·L^{-1} or 60 g·L^{-1} NaCl DS. The background feed solution contained 2 g·L^{-1} of NaCl (pH 7.7 ± 0.1). The feed was agitated at a Reynolds number of 1 700. All solute fluxes are normalised to 20°C.
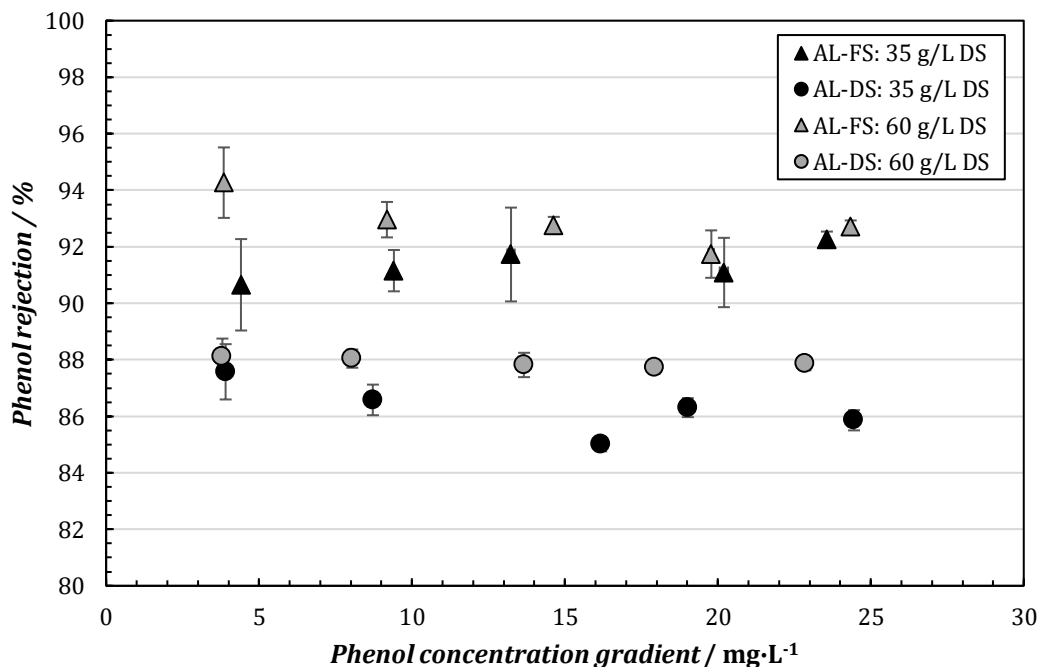
Figure 4-18: The phenol rejection in the AL-FS and AL-DS membrane orientation as a function of the phenol concentration gradient with a DS of 35 g·L^{-1} or 60 g·L^{-1} NaCl. The background FS was a 2 g·L^{-1} NaCl solution (pH 7.7 ± 0.1). The feed was agitated at a Reynolds number of 1 700. All solute rejections are normalised to 20°C.

The higher phenol solute flux in the AL-DS orientation is attributed to the combined effect of the 1) higher water flux in this orientation (Figure 4-16) and 2) CICP of phenol in the support layer of the FO membrane. The water flux in the AL-DS orientation was approximately 20-30% higher than that in the AL-FS orientation at the DS concentrations investigated. As discussed in Section 4.2.1.1, CICP of phenol within the support layer in the AL-DS orientation establishes a greater effective phenol concentration gradient across the membrane relative to that in AL-FS orientation for the same bulk feed solution concentration of phenol.

It is clear from Figure 4-18 that the phenol rejection in the AL-FS and AL-DS orientation was statistically constant with respect to the phenol concentration gradient. With a 35 g·L^{-1} NaCl draw solution, the phenol rejection was 91.1 ± 1.1% in the AL-FS orientation and 86.1 ± 0.4% in the AL-DS orientation. The lower phenol rejection in the AL-DS orientation is coupled with the higher phenol solute flux relative to that in the AL-FS orientation observed in Figure 4-17. Moderate outliers in the data can be observed from Figure 4-18, but this is attributed to the high susceptibility of the observed phenol rejection to small variations in the degree of adsorption of phenol to the FO membrane and walls of the FS reactor.

A greater phenol concentration gradient may induce a greater phenol solute flux as shown in Figure 4-17, but the mass of phenol permeating is proportional to its driving force for diffusion. For this reason, the experimentally determined rejection of phenol is independent of the solute concentration gradient. This rationale is in agreement with the predictions of the solute rejection from theory (Equations 2-20 and 2-22).

A constant rejection of phenol with an increasing concentration in the feed has also been observed in previous experimental studies with TFC membranes (Huang, et al., 2018; Cui, et al., 2016). In the work of Cui, et al. (2016), a phenol rejection of ±72-75% was observed at high FS phenol concentrations ranging between 500 mg·L^{-1} and 2000 mg·L^{-1}. Huang, et al. (2018) reported a phenol rejection of ±85-88% in the AL-FS orientation and ±83% in the AL-DS orientation at solute concentration gradients ranging between 100 mg·L^{-1} and 500 mg·L^{-1} at a feed solution pH of 7. With a similar NaCl concentration in the draw solution (~60 g/L NaCl), the TFC membrane implemented in this study showed superior phenol rejections of 92.9 ± 0.7% in the AL-FS orientation and 87.9 ± 0.4% in the AL-DS orientation. This can possibly be attributed to the higher solution pH in this experimental study (7.7 ± 0.1). Xiao, et al. (2017) previously reported the pH-dependence of the phenol rejection by TFC FO membranes.

4.2.2 Boron and lithium

The transport of boron and lithium was investigated on two isopleths at concentration gradients ranging from approximately 5 mg·L⁻¹ to 80 mg·L⁻¹. Both a 1) blank DS containing no boron and lithium and a 2) spiked DS with 5 mg·L⁻¹ of both boron and lithium were considered. The concentration of NaCl in the draw solution was 35 g·L⁻¹ to simulate seawater. Boric acid (H_3BO_3) and lithium chloride (LiCl) were spiked into the same feed solution of deionised water to establish equal concentrations of boron and lithium. The experimental water flux attained in the AL-FS and AL-DS orientation at each of the operating conditions is presented in Figure 4-19. The TDS concentration and pH of the feed solution as a function of the concentration gradient of boron and lithium, collectively, are indicated in Figure 4-20.
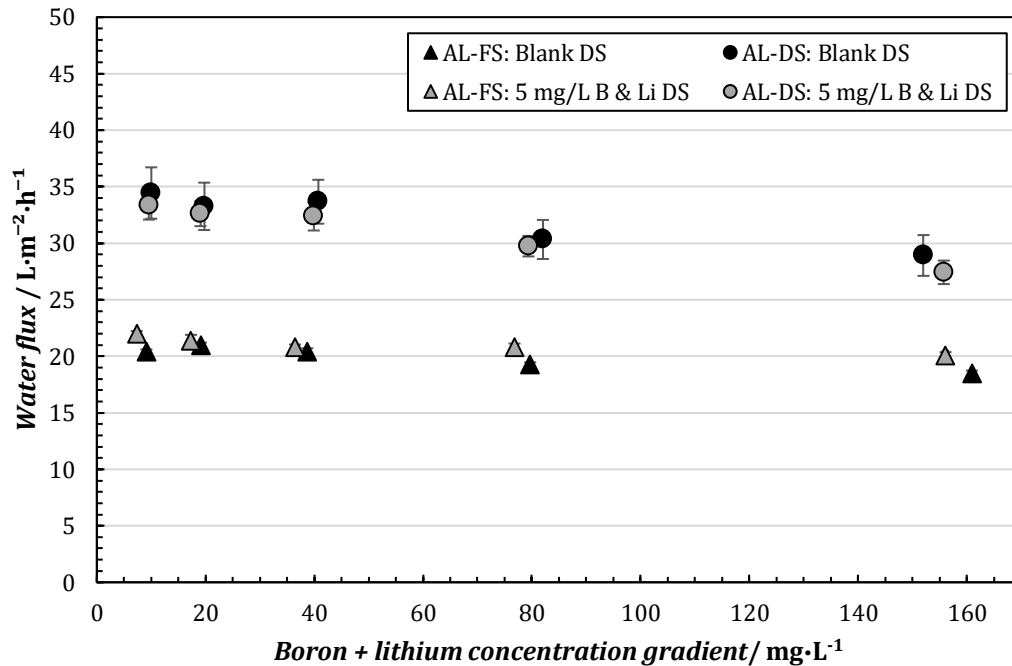
Figure 4-19: The water flux in the AL-FS and AL-DS orientation with variation in the concentration gradient of boron and lithium collectively. The boron and lithium concentrations in the feed solution were equal. The NaCl concentration of the DS was 35 g·L⁻¹ and the background feed solution was deionised water. Agitation was supplied in the feed at a Reynolds number of 1 700 and the DS CFV was 0.16 m·s⁻¹. All water fluxes are normalised to 20°C.
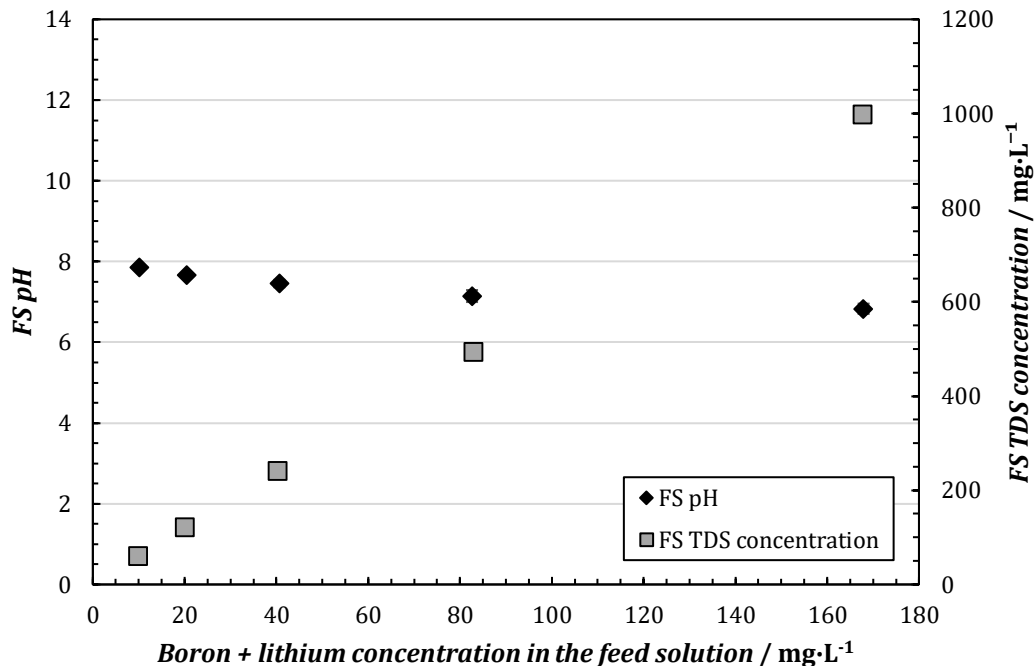
Figure 4-20: The pH and TDS concentration of the feed solution with increasing concentrations of boron (as boric acid) and lithium (as lithium chloride). The absolute boron and lithium concentrations in the feed solution were equal.

It is evident from Figure 4-19 that the water flux was affected by the increasing concentrations of boric acid and lithium chloride in the feed solution. The water flux in the AL-FS orientation was reduced by 10% while that in the AL-DS orientation was reduced by 17% as the TDS concentration (H_3BO_3 and LiCl) in the FS was increased to approximately 1000 mg·L^{-1} (Figure 4-20). This corresponded to a loss of approximately 0.8 bar in the driving force for the water flux. Although the water flux was not constant with an increase in the boron and lithium concentration gradients, the water fluxes between the two isopleths in each membrane orientation were comparable for the analysis of the results. Figure 4-20 shows that the pH of the feed solution was 7.9 ± 0.1 at the minimum concentration gradient of boron and lithium and 6.8 ± 0.1 at their maximum concentration gradient. This decrease in the pH of the feed solution is attributed to the chemistry of boric acid, whereby its partial dissociation into borate anions releases H$^+$ ions into the solution (Peryea & Lageshulte, 2000).

The flux of boron and lithium as a function of their concentration gradients with the blank and spiked draw solution is presented in Figure 4-21 and Figure 4-22, respectively. As found with phenol as the model solute, the solute flux of boron and lithium increased with their increasing concentration gradients between the feed and draw solution. This depicts the diffusive mechanism by which these solutes are transported across the membrane.
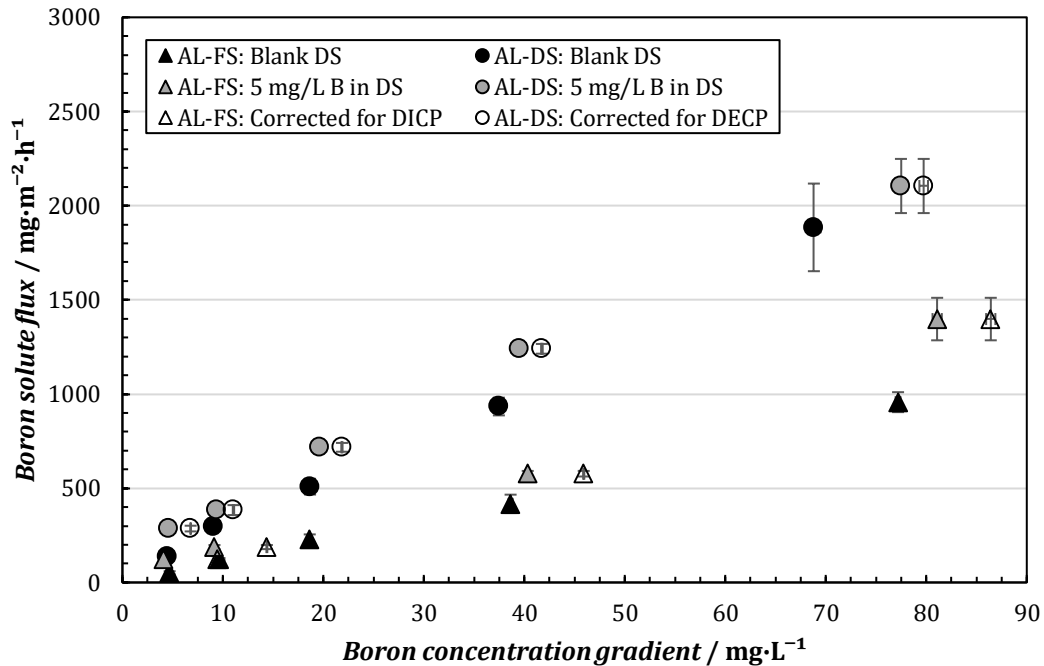
Figure 4-21: The boron solute flux as a function of the boron concentration gradient with a blank and 5 mg·L⁻¹ boron DS (35 g·L⁻¹ NaCl). The correction of DICP was made with a structural parameter (*S*) of 466 × 10⁻⁶ m (Kim, et al., 2017). The FS pH decreased from 7.9 ± 0.1 to 6.8 ± 0.1 over the concentration range investigated (Figure 4-20).
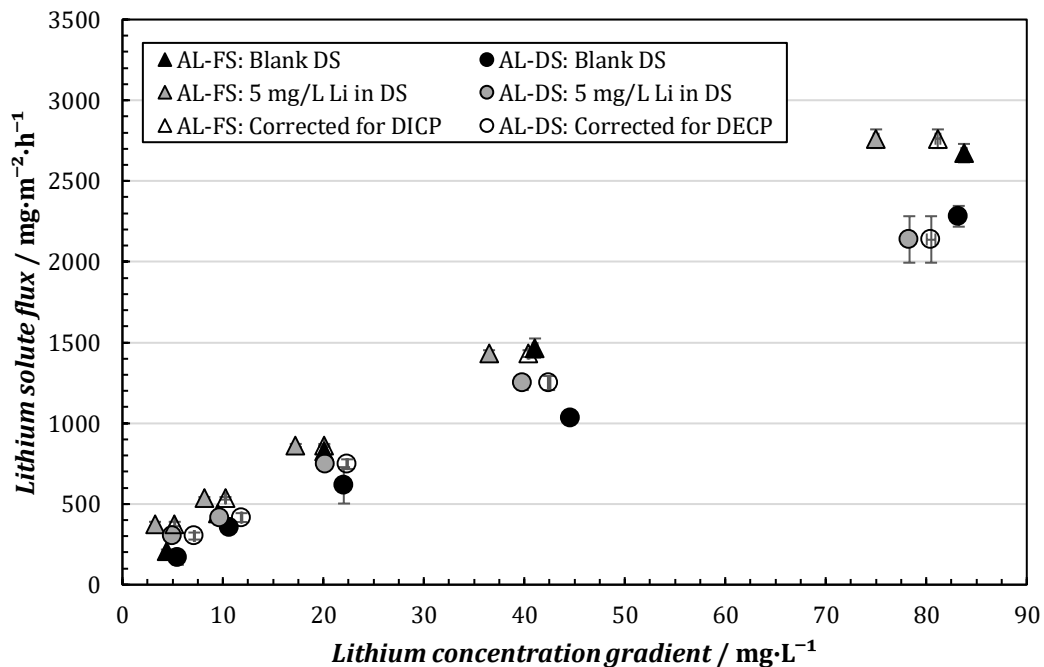
Figure 4-22: The lithium solute flux as a function of the lithium concentration gradient with a blank and 5 mg·L⁻¹ lithium DS (35 g·L⁻¹ NaCl). The correction of DICP was made with a structural parameter of 466 × 10⁻⁶ m (Kim, et al., 2017). The FS pH decreased from 7.9 ± 0.1 to 6.8 ± 0.1 over the concentration range investigated (Figure 4-20).

106

In Figure 4-21 and Figure 4-22, the boron and lithium solute fluxes (uncorrected) with a draw solution spiked with each of these solutes (grey filled markers) appear to be higher than that with a blank DS (black filled markers). This result can be attributed to the dilution of the boron and lithium on the draw solution side of the membrane by the convective flow of the water flux, or dilutive CP. Thereby, the effective concentration gradient of the solutes are greater than the perceived concentration gradients. In other words, the dilutive CP of boron and lithium in the draw solution shifts the solute flux data to the left. It is highlighted that dilutive CP has an opposite effect on the forward solute flux to what it has on the water flux. The reason for this is that the concentration gradients of the feed solute and draw solute are in conflicting directions; the concentration gradient of the draw solute is used as the driving force for water flux while the feed solute permeates in the direction of the water flux.

To illustrate the rationale above, the experimental boron and lithium fluxes were corrected with respect to DICP and DECP in the AL-FS and AL-DS orientations, respectively. This was done by application of the DICP and DECP moduli (Equations 2-13 and 2-10) to establish the actual concentration gradient. For the ICP modulus, the structural parameter reported by Kim, et al. (2015) for this particular FO8040 membrane was assumed to be sufficient (466×10^{-6} m).

The solute fluxes corrected for DICP and DECP are presented alongside the experimental data in Figure 4-21 and Figure 4-22. A significant portion of the discrepancy between the data with a blank and spiked DS could be remediated by the corrections used to determine the effective concentration gradient. Some inconsistencies may remain for several reasons including the 1) inaccuracy in the estimation of the mass transfer coefficient (k) for DECP, 2) variability between the FO membranes used to collect the data and 3) the small discrepancies in the experimental water fluxes achieved (Figure 4-19).

The experimentally determined rejection of boron as a function of its concentration gradient is presented in Figure 4-23. On average, 92.5 ± 1.0% of the boron in the FS could be rejected in the AL-FS orientation and 89.9 ±0.7% in the AL-DS orientation. The result of a higher boron rejection in the AL-FS orientation is consistent with the experimental findings and modelling predictions[11] (Table 2-5) of the boron rejection in FO by Jin, et al. (2011) and Luo, et al. (2016).

---

[11] Solution-diffusion theory
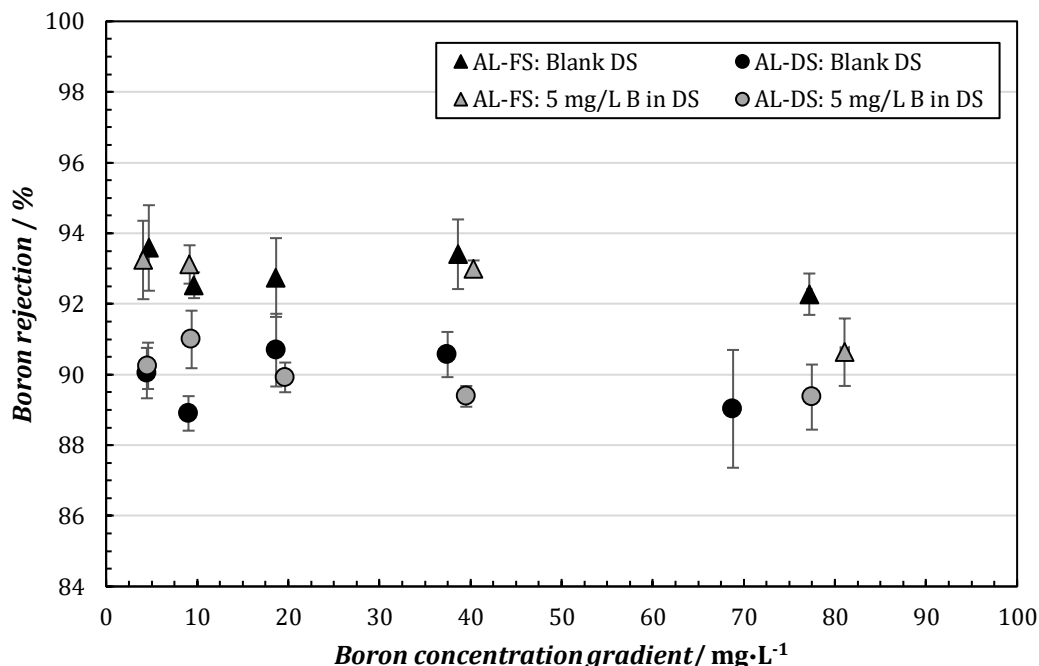
Figure 4-23: The boron rejection in the AL-FS and AL-DS orientation as a function of the boron concentration gradient with a blank and 5 mg·L⁻¹ boron DS. The DS NaCl concentration was 35 g·L⁻¹. All boron rejections are normalised to 20°C. The FS pH decreased from 7.9 ± 0.1 to 6.8 ± 0.1 over the concentration range investigated (Figure 4-20).

Up to the concentration gradient of 40 mg·L⁻¹, the boron rejection remained unaffected, as previously observed by Fam, et al. (2014) and Kim, et al. (2012). The decreased boron rejection above 40 mg·L⁻¹ in both membrane orientations can be attributed to the 1) lower water flux and 2) lower pH of the feed solution relative to that at lower concentration gradients (≤40 mg·L⁻¹) as shown in Figure 4-19 and Figure 4-20, respectively. At the solution pH considered here (6.8-7.9), which is below the pK_a of boric acid (9.24), the proportion of neutral boric acid (H_3BO_3) to the borate anion ($B(OH)_4^-$) increases with decreasing pH. The speciation of boric acid is shown in Equation 4-1 (Choi & Chen, 1979).

$$H_3BO_3 + H_2O \leftrightarrow B(OH)_4^- + H^+ \text{ (pK}_a\text{=9.24)} \tag{4-1}$$

At a lower solution pH, a greater amount of boron exists as boric acid rather than borate anions. Boric acid has a smaller hydrated radius than the charged borate anion. Hence, the lower boron rejection at the lower solution pH, or high boron concentration gradient, is related to the dominant presence of the boric acid molecules that pass through the FO membrane more readily than the borate anions. In addition, boric acid molecules encounter no electrostatic repulsion by the negatively charged membrane surface, as opposed to the negatively charged borate anions.

108

Figure 4-23 further illustrates that there is no statistically significant effect of an elevated boron concentration in the bulk DS on the boron rejection. Although DICP enhances the effective concentration gradient of the solute, its rejection remains unaffected as the latter is independent of the driving force for diffusion which is the solute concentration gradient (Equations 2-20 and 2-22).

The rejection of lithium as a function of its concentration gradient is presented in Figure 4-24. It is clear that the rejection behaviour of lithium is a complete inversion of that exhibited by the neutral solutes considered in this work, phenol and boron (dominant as boric acid). The lithium rejection was influenced by the change in the FS and DS chemistries, but in the AL-FS orientation only. In addition, the lithium rejection was higher in the AL-DS orientation than in the AL-FS orientation (compare Figure 4-18 and Figure 4-23). This behaviour implies that a different mechanism dominates the rejection of lithium in the AL-FS orientation from that of phenol and boron.

The total lithium concentration in the feed solution is dominated by its free ion Li^+ (Wen, et al., 2006). Thus, the electrostatic interaction of lithium with the negatively charged TFC membrane surface is a significant factor in its rejection mechanism (Jang, et al., 2018; Nguyen, et al., 2015; Yaroshchuk, 2000). At the solution pH under consideration here (6.8 ± 0.1 to 7.9 ± 0.1), a charge attraction between lithium and the negative surface charge of the TFC membrane enhanced the concentration of the lithium ions at the membrane surface, a phenomena which has previously been called 'charge concentration polarisation' (Verliefde, et al., 2008).

The lower lithium rejection in the AL-FS orientation can be related to the slightly higher lithium solute flux in this membrane orientation, relative to that in the AL-DS orientation, observed in Figure 4-22. The lithium solute flux in the AL-FS orientation converged with that of the AL-DS orientation to a greater extent than in the case of boron. In the case of a neutrally charged species, ICP and higher water fluxes in the AL-DS orientation would normally facilitate a higher solute flux through the membrane relative to the AL-FS orientation. However, the electrostatic interactions of lithium cations with the negatively charged active layer in the AL-FS orientation favoured the flux of lithium, such that the latter becomes greater than that in the AL-DS orientation.
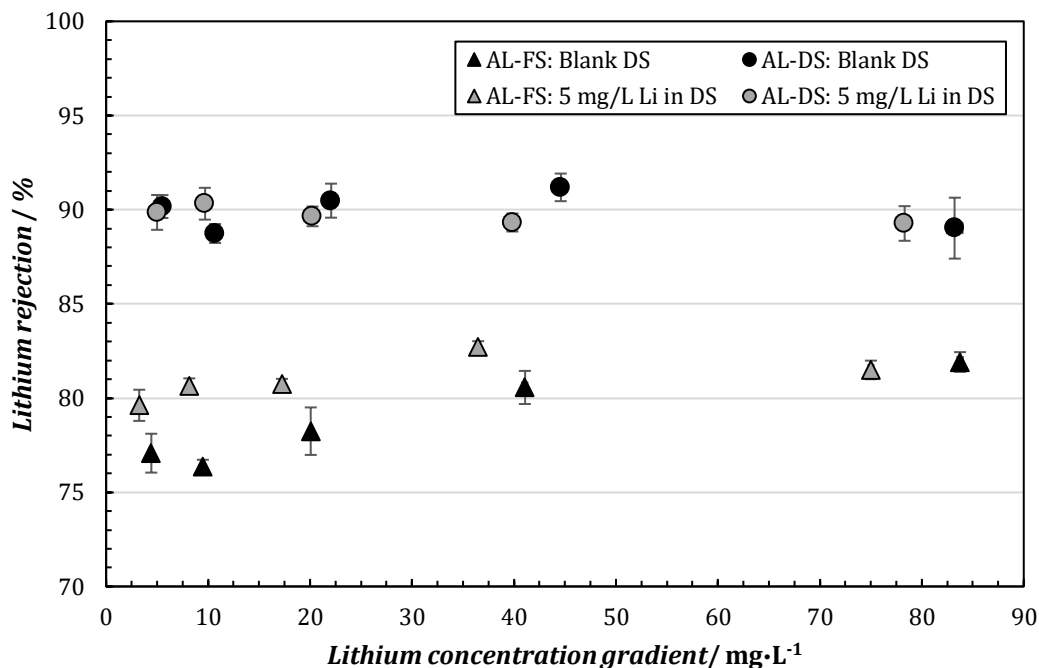
Figure 4-24: The lithium rejection in the AL-FS and AL-DS orientation as a function of the lithium concentration gradient with a blank and spiked DS. The DS NaCl concentration was 35 g·L⁻¹. All lithium rejections are normalised to 20°C. The FS pH decreased from 7.9 ± 0.1 to 6.8 ± 0.1 over the concentration range investigated (Figure 4-20).

It can be observed from Figure 4-24 that the lithium rejection increased from 77.1% to 81.9% in the AL-FS orientation with a blank DS when its concentration gradient was increased together with that of boric acid. This finding is partially consistent with that reported by Liu, et al. (2019); the rejection of caesium (Cs), an alkali metal like lithium, also increased with an increasing boric acid concentration in the FS. The caesium rejection was also lower in the AL-FS orientation relative to the AL-DS orientation, as observed for lithium in Figure 4-24.

The dependence of the membrane partitioning of ionic species, such as lithium considered here, on the chemistry of the feed solution, is somewhat complex (Wen, et al., 2006). The increase in the lithium rejection in the AL-FS orientation, presented here as a function of the lithium concentration gradient, can firstly be attributed to the reduction in the electrostatic interactions of lithium with the negatively charged membrane surface, caused by the increasing ionic strength of the feed solution (Verliefde, et al., 2008). With an increasing amount of lithium in the FS, the negative membrane surface charge becomes 'shielded' (Liu, et al., 2019; Wen, et al., 2006). The membrane would subsequently assume a small positive charge, which results in an increased repulsion of positive lithium ions and the arrangement of the solution anions, such as Cl⁻, on the 'layer' of positive charge. Consequently, the electrostatic interaction of the lithium ions with the membrane surface is weakened and their retention on the feed side of the membrane is increased.

Secondly, with the decrease in the solution pH, caused by increasing the amount of boric acid in the same FS in which the lithium was spiked (refer to Figure 4-20), the negative charge on the membrane surface may have become reduced (Pramanik, et al., 2019). This could have potentially resulted in a reduced electrostatic attraction of lithium to the membrane, relative to that at a higher FS pH (greater negative membrane charge). Thus, the lithium rejection may have increased as result of the decreasing FS pH, caused by the boric acid, over the range of lithium concentration gradients investigated.

Figure 4-24 further illustrates that the draw solution spiked with 5 mg·L^{-1} of lithium generally provided an improvement in the lithium rejection in the AL-FS orientation. However, the effect became diminished at higher concentration gradients of lithium, or higher ionic strengths and lower pH conditions in the FS. Up to a 4.3% increase in the lithium rejection was obtained at lower concentration gradients (<40 mg·L^{-1}), while there was no significant improvement in the rejection at concentration gradients approximating 80 mg·L^{-1}.

As shown in Table 2-11, the hydrated radius of lithium is larger and its diffusion coefficient smaller than that of the draw solution counter ion (Cl$^-$). Nevertheless, the reverse flux of the chloride ions to the feed solution may have facilitated the transport of lithium ions from the bulk draw solution to the negatively charged active layer, as these two ions are electrostatically coupled. At lower ionic strengths and higher pH conditions in the feed solution (lower lithium concentration gradients), both the reverse solute flux and electrostatic interactions of positively charged lithium ions with the membrane are potentially greater (Zheng, et al., 2019). As a result, more lithium ions from the draw solution may be permitted to interact with the negatively charged membrane active layer and the forward permeation of lithium ions from the feed solution becomes hindered to a greater extent. Thus, the improvement in the lithium rejection with a spiked DS appeared to be greater at lithium lower concentration gradients.

The lithium rejection in the AL-DS orientation remained constant at approximately 89.8 ± 0.8% with respect to its concentration gradient and concentration in the draw solution (Figure 4-24). This finding suggests that the electrostatic interactions of the lithium cations with the membrane were potentially insignificant when the porous support layer was in contact with the feed solution (Alturki, et al., 2013). In conjunction with the significant TDS concentration of the feed solution (Figure 4-20), the significant RSF in the AL-DS orientation may have contributed to the 'shielding' of the electronegativity of the membrane active layer. Therefore, the rejection mechanism of lithium is potentially governed by steric exclusion in the AL-DS orientation. Accordingly, the ionic strength of the FS had no effect on the lithium rejection in this membrane orientation. Identical

results were reported by Liu, et al. (2019) for the rejection of caesium in the AL-DS orientation at increasing concentrations of boric acid in the feed solution.

4.2.3 Rejection mechanisms of the model solutes

Due to the differences in the physicochemical properties of phenol, boron (dominant as boric acid) and lithium, these solutes were likely rejected by different mechanisms at the particular experimental conditions considered here. In the literature review (Section 2.3.2), three solute rejection mechanisms were highlighted: 1) steric exclusion, 2) electrostatic repulsion and 3) hydrophobic interaction. The anticipated rejection mechanisms of the model solutes are discussed here.

Phenol is a nonionic solute with a relatively low hydrophobicity (Table 2-11). Still, its potential adsorption to the membrane surface was found to significantly affect its observed rejection. Therefore, experiments were performed with prior saturation of the membrane with phenol. The reverse diffusion of the draw solute can further hinder the adsorption of this hydrophobic solute to the membrane. For these reasons, steric exclusion was expected to dominate over hydrophobic interactions in the rejection mechanism of phenol at the experimental conditions considered (Heo, et al., 2013). Phenol has a molecular weight smaller than the MWCO of typical TFC membranes, with the latter ranging from 120 g·mol^{-1} to 170 g·mol^{-1} (Cui, et al., 2016). Thus, phenol can easily diffuse through the active layer of the FO membrane.

Steric exclusion and electrostatic interaction are possible rejection mechanisms for inorganic solutes. As mentioned in Section 4.2.2, the majority of boron existed as neutral boric acid at the neutral pH conditions in the feed solution. It is therefore suggested that the boron rejection was predominantly governed by steric exclusion from the dense active layer of the FO membrane. This mechanism of boron rejection has also been suggested by Fam, et al. (2014). The small Stokes radius of boric acid (0.155 nm[12]) relative to the typical effective mean pore size of TFC membranes (≥0.390 nm[13]) permits its diffusion across membranes.

In contrast, the lithium rejection by FO membranes is presumed to be more complex as a result of the combination of electrostatic repulsion and steric exclusion. With a hydrated radius of 0.328 nm (Volkov, et al., 1997; Kielland, 1937), lithium ions may still readily diffuse through the matrix of the active layer of TFC FO membranes, but significant electrostatic interactions between the active layer and lithium ions further enhance their passage across the membrane. Thus, the

---

[12] Tu, et al. (2013)
[13] Cui, et al. (2016)

electrostatic interactions between lithium and the membrane in the AL-FS orientation are more significant at a lower ionic strength and higher pH in the FS. As concluded in Section 4.2.2, steric exclusion potentially dominates the rejection mechanism of lithium in the AL-DS orientation.

The flux and rejection of the three model feed solutes at the concentration gradient of 10 mg·L^{-1} are compared in Figure 4-25 and Figure 4-26, respectively. By their dominant rejection mechanism of steric exclusion, phenol and boron were rejected to the same degree in the AL-FS orientation due to their comparable molecular weights (Table 2-11). The slightly lower rejection of phenol compared to boron in the AL-DS orientation may have resulted from the significantly lower experimental water flux at which the phenol rejection was tested (Figure 4-25).
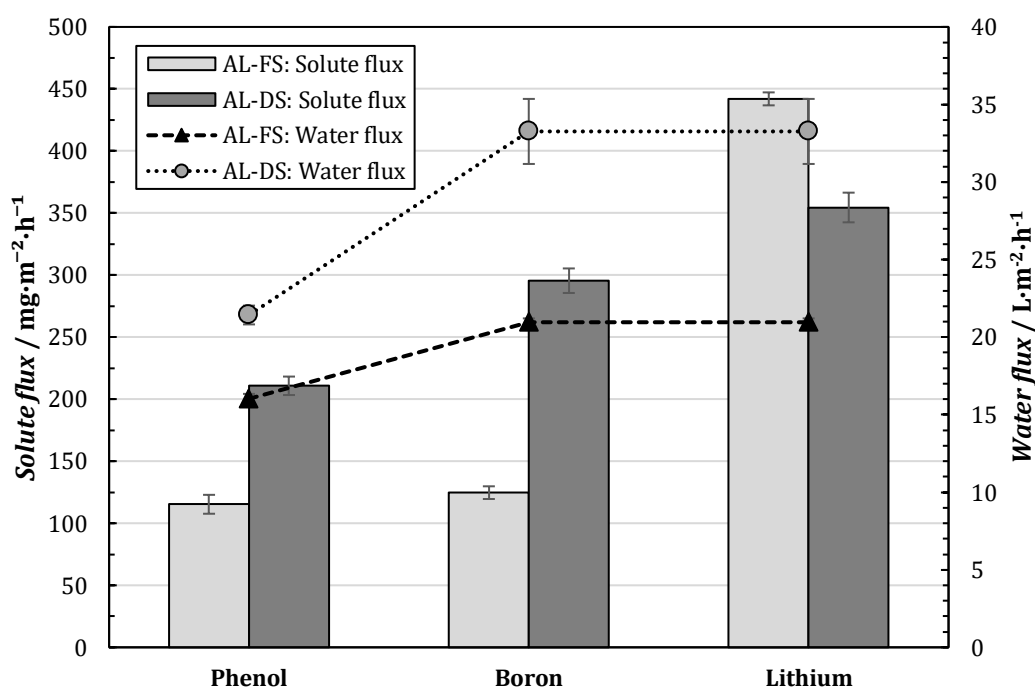
Figure 4-25: Comparison of the solute flux of phenol, boron and lithium in the AL-FS and AL-DS membrane orientation at a concentration gradient of 10 mg·L^{-1} and experimental water fluxes indicated. All solute and water fluxes are normalised to 20°C. The pH of all solutions was neutral (7.7 ± 0.1).

113
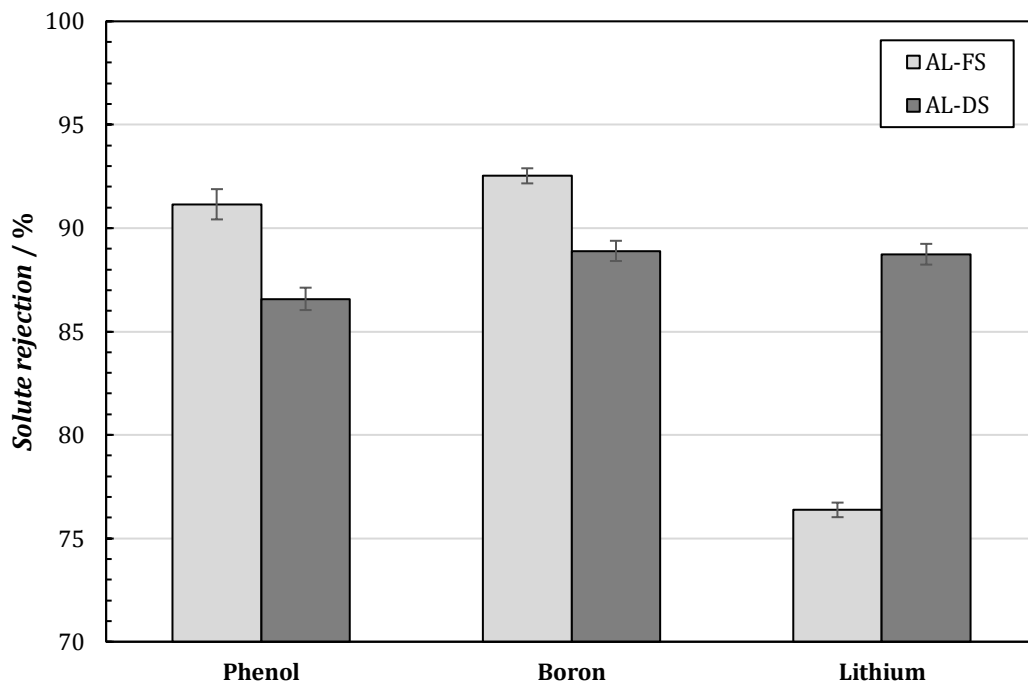
Figure 4-26: Comparison of the rejection of phenol, boron and lithium in the AL-FS and AL-DS membrane orientation at a concentration gradient of 10 mg·L^{-1} and experimental water fluxes indicated in Figure 4-25. All solute rejections are normalised to 20°C. The pH of all solutions was neutral (7.7 ± 0.1).

The significance of electrostatic interactions in the transport of inorganic solutes through charged membranes is demonstrated by the prominent difference between the boron and lithium flux and rejection in the AL-FS orientation (Figure 4-25 and Figure 4-26). As a result of the electrostatic attraction between the positively charged lithium ions and the negatively charged active layer, the lithium rejection was significantly lower than that of boron, by approximately 16%. In contrast, boron and lithium were rejected to the same extent in the AL-DS orientation. This finding is related to the comparable ionic radius of lithium and Stokes radius of boric acid, as indicated in Table 2-11. Accordingly, both solutes were rejected by the mechanism of steric exclusion in the AL-DS orientation.

Chapter 5

Simulation of the FO-RO hybrid

5.1 Introduction

The FO-RO hybrid process, used for simultaneous wastewater treatment and seawater desalination, has been introduced in Section 1.2 and reviewed in Section 2.4. This process has been considered as an energy-efficient alternative to standalone pressure-driven membrane processes. By osmotic dilution, the desalination energy in the RO stage can be reduced by the combination of the FO permeate and saline RO feed stream (Figure 2-7).

However, recent studies have shown by closer analysis that the standalone RO process cannot be completely outperformed by the FO-RO process. It has been found that the FO-RO hybrid can achieve favourable economic returns in operation, but only up to a threshold water recovery of 63% in the FO stage at a RO recovery of 50% (Cath, et al., 2010). Above this threshold FO recovery, the capital costs associated with increasing the total FO membrane area may compromise the total cost savings achieved with the reduction in the energy consumption of the desalination stage. The reason for this is that the osmotic pressure of the seawater is the limiting factor in the water flux that the FO stage can generate with wastewater effluent as the feed (Chekli, et al., 2016).

Despite the limitation in the energy savings of the FO-RO hybrid, this process configuration provides a dual-barrier rejection mechanism for the efficient removal of wastewater contaminants. The impaired water fed to the FO stage is effectively treated by two membranes, with intermediate dilution by the seawater draw solution, thereby contributing to an improved purity of the RO permeate. The quality of the product water from the FO-RO hybrid depends on the rejection capacity of both the FO and RO membranes, as well as the operating conditions of the process including the water recovery in the respective stages.

The FO-RO hybrid process in question here, used for the osmotic dilution of seawater prior to desalination, does not require closed-loop re-concentration of the draw solution. Instead, it is operated with both the feed solution and draw solution in a once-through configuration. Therefore, it offers the true benefit of FO as a low-energy process; it eliminates costs associated with the re-concentration of the draw solution and avoids operational complexities (Shaffer, et al., 2012; Park, et al., 2012; Chekli, et al., 2016). The benefits of the process related to energy consumption and product water quality are summarised below (Chekli, et al., 2016; Blandin, et al., 2016):

i) Dilution of the seawater by the FO permeate reduces the energy consumption of desalination in the RO stage.

ii) Wastewater contaminants are rejected in two membrane stages and the weakly rejected contaminants in the FO stage are further diluted in the process as a result of the combination of the FO permeate with the seawater. Both these factors contribute to an improved final permeate quality.

iii) The pre-treatment of the impaired water and lower operating pressure in the RO stage reduces the fouling propensity of the RO membrane.

iv) An opportunity for the safe and beneficial reuse of impaired water is realised.

In this chapter, the objective of determining the permeate quality of the FO-RO hybrid process is addressed for the purpose of investigating the benefit of its dual-barrier rejection mechanism over a standalone RO process. A simulation was done with a simple mathematical model incorporating the phenol, boron and lithium rejections of the commercially available FO8040 membrane (Toray), which were experimentally determined in this study. Firstly, the mass balance of the FO-RO hybrid and algorithm for evaluating the permeate quality is explained. Practical operating conditions and the relevant rejections and recoveries in the respective FO and RO stages of the FO-RO hybrid are further substantiated. Finally, the results of a preliminary simulation of the permeate quality of the FO-RO hybrid are provided, followed by the case studies for boron, phenol and lithium.

5.2 Mass balance and algorithm

Figure 5-1 illustrates the FO-RO process configuration considered in the simulation, based on that proposed in literature (Section 2.4.1), and the respective symbols used to denote the flowrate (Q) and solute concentration (C) of a particular stream. Seawater is fed to the FO stage as the draw solution (Q_{sw}), which is diluted by the FO permeate ($Q_{p,FO}$). The diluted seawater (Q_{dsw}), with a

lower osmotic pressure than the feed seawater, is the feed stream to the RO desalination stage. An example flow sheet of the mass balance is provided in Appendix D.2.
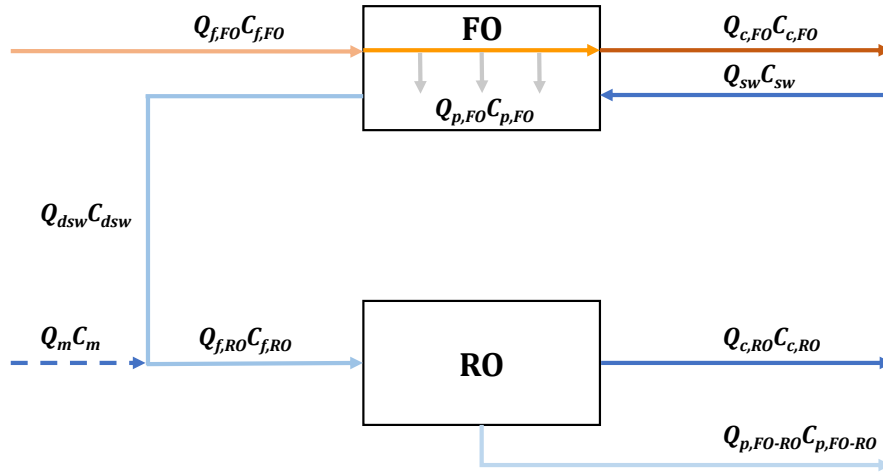
Figure 5-1: Schematic illustration of the FO-RO hybrid configuration considered in the simulation. The subscripts f, p and c refer to the feed, permeate and concentrate streams of membrane treatment stages, respectively. The subscripts sw, dsw and m denote the seawater feed (draw solution), the diluted seawater and seawater make-up streams, respectively.

The basis for solving the mass balance of the FO-RO hybrid was the RO permeate flowrate ($Q_{p,RO}$). The RO feed and permeate flowrates ($Q_{f,RO}$ and $Q_{f,RO}$) could then be calculated from the assumed water recovery in the RO stage (r_{RO}). The FO permeate flowrate ($Q_{p,FO}$) was assumed as a fraction of the RO permeate flowrate. Thus, the flowrate of the seawater feed to the FO stage was equal to the flowrate of RO concentrate discharge ($Q_{sw}=Q_{c,RO}$). In cases where the FO permeate flowrate was not equal to the RO permeate flowrate, a seawater make-up (Q_m) to the RO stage had to be provided. Finally, with an assumed recovery in the FO stage (r_{FO}), the flowrate of the wastewater feed ($Q_{f,FO}$) and concentrate ($Q_{c,FO}$) to and from the FO stage, respectively, could be obtained.

With $C_{f,FO}$ defined, the concentration of the solute in the FO concentrate was calculated from the formula defined for the observed FO rejection (R_{FO}) in Section 3.3.2.4 (Equation 3-12). Accordingly, the concentration of the solute in the FO permeate was defined by Equation 5-1.

$$C_{p,FO} = \frac{Q_{f,FO}C_{f,FO}(1 - R_{FO})}{Q_{p,FO}} \tag{5-1}$$

As the concentration of the solute in the seawater feed (C_{sw}) and make-up (C_m) was fixed, the concentration of the diluted seawater and RO feed could subsequently be solved by mass balance.

117

The permeate concentration from the RO stage in the FO-RO hybrid could then be calculated from the solute rejection of the RO membrane (R_{RO}):

$$C_{p,FO-RO} = C_{f,RO}(1 - R_{RO})$$ (5-2)

The overall rejection of the multi-barrier process (R_{FO-RO}) was defined from the ratio of the RO permeate solute concentration ($C_{p,FO-RO}$) to the FO feed solute concentration ($C_{f,FO}$), as shown by Equation 5-3.

$$R_{FO-RO} = \left(1 - \frac{C_{p,FO-RO}}{C_{f,FO}}\right) \times 100$$ (5-3)

5.3 Practical considerations

The operating conditions, solute rejections and feed water concentrations applied in this FO-RO hybrid simulation are substantiated in the following sub-sections, with the parameters summarised in Table 5-1 at the end of this section.

5.3.1 Operating conditions

The modelling of the FO-RO hybrid process required the assumption of 1) the respective water recoveries in the FO and RO stages and 2) the FO permeate flowrate. Although the optimisation of the FO-RO hybrid is not within the scope of this study, some practical considerations were made in defining the operating conditions. Herewith it is also highlighted that the trace constituents of the seawater (boron and lithium) are distinguished from the TDS concentration of the seawater (major constituents including NaCl).

As the RO permeate flowrate was fixed in the model, the RO recovery would influence the volumetric flowrate of the RO feed and RO concentrate. As a result, the TDS concentration of these streams for a particular FO permeate flowrate would also be affected. In practice, a higher RO recovery may imply a lower throughput of seawater in the FO-RO hybrid, lower energy requirements for desalination and a smaller discharge of RO concentrate for a fixed permeate flowrate. This is substantiated in Figure 5-2 by the decrease in the flowrate and TDS concentration of the RO feed with an increase in the RO recovery, as evaluated from the formulated FO-RO hybrid model.

The recovery of a standalone seawater RO system is typically limited to 40-60% (Quist-Jensen, et al., 2016; McMordie Stoughton, et al., 2013). However, in a FO-RO hybrid configuration, the RO stage is capable of operating at higher recovery rates as a result of the prior dilution of the seawater

to lower osmotic pressures (Seo, et al., 2019; Teusner, et al., 2017). In the optimisation study by Jeon, et al. (2016), the energy consumption in the RO stage was minimised at RO recoveries of 66.7% and 50%% with a FO permeate flowrate equal to and 50% of the RO permeate, respectively.
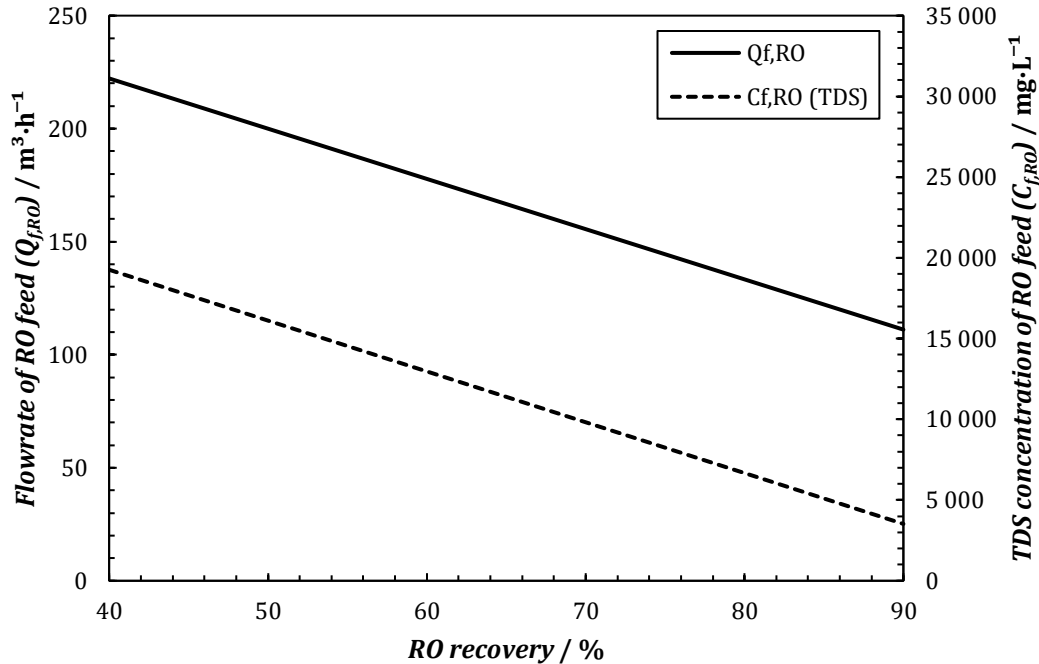
Figure 5-2: The flowrate ($Q_{f,RO}$) and TDS concentration ($C_{f,RO}$) of the RO feed stream as a function of the RO recovery as determined from the FO-RO hybrid simulation (Figure 5-1). The TDS concentrations of the seawater and wastewater feed were 35 000 mg·L⁻¹ and 850 mg·L⁻¹, respectively. The RO permeate flowrate was fixed at 100 m³·h⁻¹

Due to this variability of recovery rates in RO systems, the solute removal by the FO-RO hybrid was evaluated at both a 45% and 70% RO recovery in this study. The FO recovery was fixed at 50%, as the quality of the FO concentrate was not of importance. It is highlighted that the FO recovery would be a critical consideration in a model that takes its direct effect on the solute rejection into account.

The FO permeate flowrate is another parameter that influences the economic operability of the FO-RO hybrid. The FO permeate is responsible for decreasing the TDS concentration of the seawater prior to desalination. A greater degree of dilution requires greater FO water fluxes. However, a more rigorous method of modelling the FO-RO hybrid than that applied here is required to relate the FO water flux to the degree of dilution of the seawater draw solution. As the reduction of the energy requirement in the RO desalination stage by osmotic dilution is the purpose of implementing FO-RO hybrids, FO permeate flowrates of 50% and 100% of the RO permeate flowrate were considered in this model. The reduction in the TDS concentration of the

seawater fed to the RO stage ($C_{f,RO}$) over this range of FO permeate flowrates is presented in Figure 5-3 as a percentage of the TDS concentration in the seawater fed to the complete process (C_{sw}). Similar FO permeate flowrates, which ranged from 38% to 100% of the RO permeate flowrate, were considered in the modelling studies of Teusner, et al. (2017) and Jeon, et al. (2016).
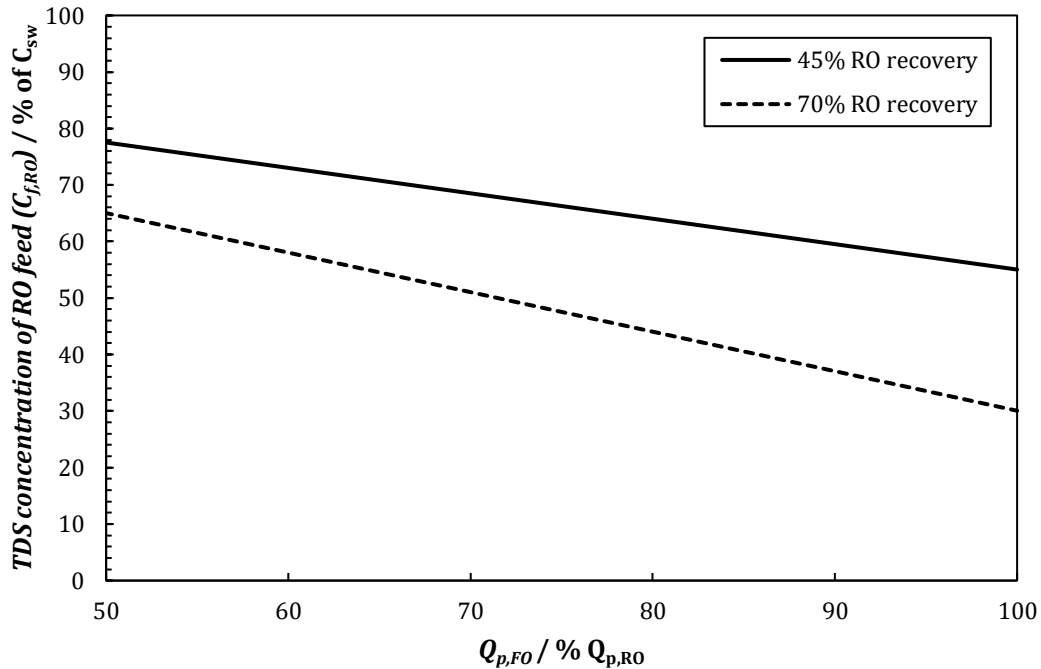
Figure 5-3: The TDS concentration of the seawater fed to the RO stage of the FO-RO hybrid ($C_{f,RO}$) as a percentage of the TDS concentration of the seawater fed to the complete process at FO permeate flowrates ranging from 50% to 100% of the RO permeate flowrate.

5.3.2 FO and RO trace solute rejections

For the FO stage of the FO-RO hybrid, the experimentally determined phenol rejection of the FO8040 membrane, obtained with a 35 g·L⁻¹ NaCl draw solution in the AL-FS orientation (Figure 4-18), was implemented in the case study. The boron and lithium rejections determined with the same DS NaCl concentration and membrane orientation were applied in the case studies of these solutes, but for the case of a spiked draw solution (Figure 4-23 and Figure 4-24) as an influent seawater already containing boron and lithium was considered. These rejections of phenol, boron and lithium are indicated in Table 5-1. As concluded in Chapter 4, the AL-DS membrane orientation would not be preferable in practice because of its flux instability and lower solute removal efficiency.

In order to apply reasonable estimates of the RO rejection in the FO-RO hybrid simulation for case studies concerning the model solutes, an assessment of the removal efficiencies of

commercially available seawater RO membranes was made from published work. With seawater RO as an established technology and boron a common constituent in seawater, the RO rejection of boron has been well defined in literature relative to than that of lithium and phenol.

For simplification, the solute rejection was assumed independent of the TDS concentration of the RO feed stream and applied pressure in the RO stage. This assumption is acceptable as it has generally been found that the solute rejection plateaus at the applied pressures typical to low-pressure RO and seawater RO (Somrani, et al., 2013; Li, et al., 2010). For this reason, the RO solute rejections were surveyed from data recorded at feed pressures relevant to low-pressure or seawater RO.

i)   The rejection of phenol by commercially available polyamide RO membranes at moderate to higher feed pressures has been reported by Schutte (2003) as 92% at a feed pressure of 28 bar and 94% at 56 bar.

ii)   The newest RO membranes with a higher water selectivity are capable of providing boron rejections between 87-93% (Farhat, et al., 2013; Dominguez-Tagle, et al., 2011; Koseoglu, et al., 2008) in single-pass configurations at a solution pH of 8.

iii) Somrani, et al. (2013) observed a plateau in the lithium rejection of a low-pressure RO XLE (DOW Filmtec) membrane at approximately 88% with an operating pressure of 25 bar.

It is clear that the surveyed RO rejections of phenol, boron and lithium differ marginally from that obtained with the FO8040 membrane used in the experimental investigation of this work. Therefore, for the purpose of this simulation of demonstrating the benefits of the FO-RO hybrid for contaminant removal, equal FO and RO membrane rejections were assumed to be sufficient. Thus, the experimentally determined FO rejections, substantiated above, were applied in the RO stage. It is stressed that the experimental FO rejections are dependent on conditions such as the particular water recovery achieved in the experiments (Equation 3-12). For this reason, preliminary simulation results showing the effect of the membrane rejection behaviour on the FO-RO permeate quality is included in Section 5.4.1.

5.3.3 Trace solute concentrations

Organic compounds such as phenol can occur over a wide range of concentrations (±0.1 to 100 $\mu g \cdot L^{-1}$) in domestic wastewater (Coday, et al., 2014). The overall rejection of the FO-RO hybrid would not be influenced by the magnitude of the concentration of phenol in the FO feed water, as an influent seawater draw solution contains no traceable phenol. The concentration of phenol in the FO feed water was assumed at a nominal value of 100 $\mu g \cdot L^{-1}$.

Central to the experimental study presented in Section 4.2.2, seawater as the draw solution in the FO stage already contains boron and lithium at respective concentrations of approximately 4.5 mg·L⁻¹ and 0.17 mg·L⁻¹ (Busch, et al., 2003; Quist-Jensen, et al., 2016). Therefore, an impaired feed solution with higher, but relevant concentrations of boron and lithium had to be considered in the simulation. The respective concentrations of boron and lithium in produced water typically range from 8.0 mg·L⁻¹ and 0.3 mg·L⁻¹ upwards (Neff, et al., 2011). However, to provide a means of comparing the overall rejection of boron and lithium (as solutes present in both the feed and draw solution) with only their FO and RO rejections taking effect, equal ratios of the seawater concentration to the FO feed water concentration ($C_{sw}/C_{f,FO}$) were implemented for boron and lithium. Thus, boron and lithium wastewater concentrations of 8.0 mg·L⁻¹ and 0.3 mg·L⁻¹ were applied in the model.

Table 5-1: Summary of the major parameters of the modelled FO-RO hybrid process.

Parameter	FO stage	RO stage	Unit	Comment
Recovery, r	50	45/70	%	
Permeate flowrate, Q_p	50/100	100	m³·h⁻¹	
Seawater intake TDS	35 000	-	mg·L⁻¹	
Wastewater intake TDS	850		mg·L⁻¹	
Seawater make-up flowrate, Q_m	-	50	m³·h⁻¹	For $Q_{p,FO}=0.5Q_{p,RO}$
Seawater make-up TDS	-	35 000	mg·L⁻¹	
TDS rejection	98.5	98.5	%	
Phenol rejection	91	91	%	
Boron rejection	93	93	%	
Lithium rejection	81	81	%	

5.4 Simulation results

5.4.1 Preliminary simulation

As discussed in Section 5.3.2, equal FO and RO rejections were assumed to be sufficient for the purpose of simulating the phenol, boron and lithium concentrations in the permeate of the FO-RO hybrid. This membrane rejection behaviour is subject to variation due to its dependence on a variety of process conditions such as the water recovery, solution pH, temperature and pressure. Here, a preliminary analysis of the removal of an unspecified solute is provided, mainly to illustrate the extent to which the permeate quality of the hybrid process is affected by the rejection behaviour in the respective FO and RO stages, varying from a weakest value of 50% to a strongest value of 95%.

Two scenarios were considered in this analysis. The first scenario addresses the case where the solute is present in the influent wastewater only, with concern to the occurrence of TrOCs, such

as phenol, in wastewater. The second scenario relates to a solute, such as boron, being present in both the influent wastewater and seawater to the FO-RO hybrid. The permeate quality of the FO-RO hybrid process at alternating membrane rejections in both scenarios are presented in Figure 5-4 and Figure 5-5, respectively, for a 45% and 70% RO recovery. Wastewater and seawater solute concentrations of 1 mg·L^{-1} and 0.6 mg·L^{-1} were regarded, based on the remarks in Section 5.3.3.
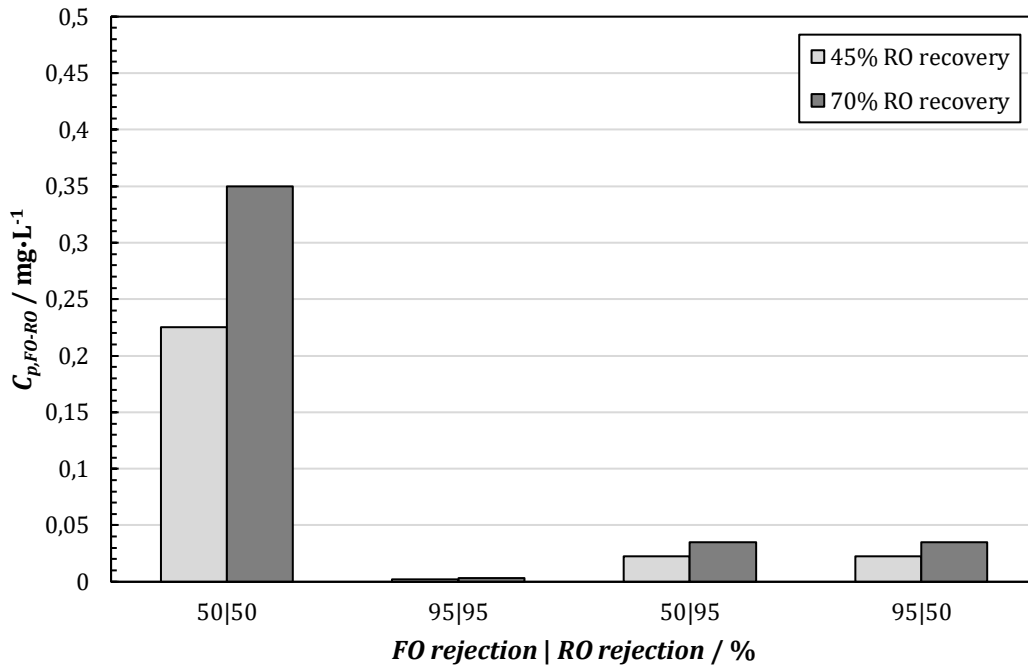
Figure 5-4: The concentration of an unspecified solute in the permeate of the FO-RO hybrid process at varying FO and RO membrane rejections, with the solute occurring in the influent wastewater to the process only at a concentration of 1 mg·L^{-1}. The FO permeate flowrate was fixed at 100% of the RO permeate flowrate and the FO recovery was 50%.
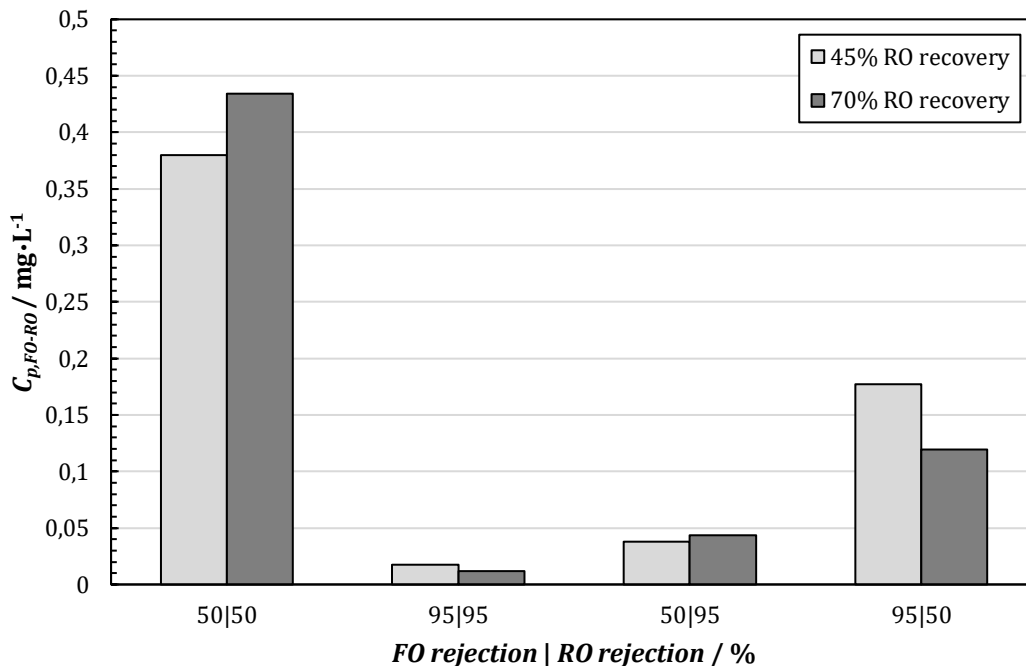
Figure 5-5: The concentration of an unspecified solute in the permeate of the FO-RO hybrid process at varying FO and RO membrane rejections, with the solute occurring in both the influent wastewater and seawater to the process, at concentrations of 1 mg·L^{-1} and ~0.6 mg·L^{-1}, respectively (refer to Section 5.3.3). The FO permeate flowrate was fixed at 100% of the RO permeate flowrate and the FO recovery was 50%.

It is evident from Figure 5-4 that, when the FO and RO rejections are equal, the quality of the permeate is improved hundredfold with an increase in the membrane rejection from 50% to 95% and the solute present in the wastewater only. In the same scenario, unequal FO and RO membrane rejections, in any order, provide the same permeate quality. However, when the solute occurs in the influent seawater to the process at a concentration of ~0.6 mg·L^{-1} (Figure 5-5), it is noteworthy that the permeate concentration is lower when the RO rejection is higher than the FO rejection, compared to when the FO rejection is higher than the RO rejection.

It is once again emphasised that the rejection in the RO stage is uncoupled from the RO recovery in this simulation, with the latter only used to evaluate the mass balance. Figure 5-4 shows that when the solute is present in the feed wastewater only, a lower RO recovery favours the quality of the FO permeate for a fixed FO permeate flowrate. With a decrease in the RO recovery and fixed RO permeate flowrate, the volumetric capacity of the seawater draw solution is increased, which reduces the concentration of the solute in the RO feed stream.

When the solute is present in both the influent wastewater and seawater to the process (Figure 5-5), the permeate quality is favoured by a decrease in the RO recovery only when the FO rejection is at the weaker value of 50%. Further investigation showed that this trend is dependent on the

124

magnitude of the particular FO and RO rejections. In the alternative cases in Figure 5-5 where the FO rejection is at 95%, an increase in the RO recovery facilitates smaller seawater feed and make-up requirements. Thereby, the dilution of the solute in the seawater is greater for a fixed FO permeate flowrate. As a result, the concentration of the solute in the permeate is reduced.

5.4.2 Case studies

The concentrations of phenol, boron and lithium in the permeate of the FO-RO hybrid are provided in Table 5-2, as simulated with the rejections of the FO8040 membrane, operating conditions and feed concentrations substantiated in Section 5.3. The overall FO-RO hybrid rejection, determined with Equation 5-3, is also provided for each case. The complete simulation results are provided in Appendix D.

Table 5-2 shows that the FO-RO hybrid process improves the phenol removal from 91%, which is obtained with a single membrane stage, to >98%. This FO-RO hybrid rejection correlates well with that experimentally determined by Cath, et al. (2010) and Hancock, et al. (2011) for a wide range of organic compounds with a seawater draw solution. The removal of boron and lithium can be improved by the FO-RO hybrid from 93% and 81% in the standalone units to >96% and >90%, respectively.

Table 5-2: The simulated FO-RO permeate concentrations and overall rejections of phenol, boron and lithium. $C_{p,FO-RO}$ is the concentration of the solute in the permeate, $Q_{p,FO}$ is the FO permeate flowrate, $Q_{p,RO}$ is the RO permeate flowrate, $C_{f,FO}$ is the concentration of the solute in the influent wastewater and C_{sw} is the concentration of the solute in the influent seawater (Figure 5-1).

Solute	$Q_{p,FO}$ / % of $Q_{p,RO}$	45% RO recovery		70% RO recovery	
		$C_{p,FO-RO}$ / µg·L^{-1}	R_{FO-RO} / %	$C_{p,FO-RO}$ / µg·L^{-1}	R_{FO-RO} / %
Phenol ($C_{f,FO}$=100 µg·L^{-1}, C_{sw}= 0 µg·L^{-1})	50	0.365	99.6	0.567	99.4
	100	0.729	99.3	1.134	98.9
Boron ($C_{f,FO}$=1.8C_{sw}= 8 000 µg·L^{-1}, C_{sw}= 4 500 µg·L^{-1})	50	262	96.7	232	97.1
	100	209	97.4	149	98.1
Lithium ($C_{f,FO}$=1.8C_{sw}= 300 µg·L^{-1}, C_{sw}= 170 µg·L^{-1})	50	29.9	90.1	28.6	90.5
	100	27.6	90.9	25.0	91.7

In conjunction with the preliminary simulation results provided in the previous sub-section, Table 5-2 shows that a decrease in the FO permeate flowrate favours the phenol removal for a fixed RO permeate flowrate. At a lower FO permeate flowrate, the mass of phenol permeating to the seawater draw solution is lower. Conversely, an increase in the FO permeate flowrate improves

the boron and lithium removal. This follows the same trend for TDS transport within the FO-RO hybrid as shown in Figure 5-3 and once again illustrates the dilution effect of the FO permeate for solutes entering the FO-RO hybrid through the influent seawater.

The phenol concentration in the FO-RO permeate for the outermost scenarios in Table 5-2, named Case 1 (45% RO recovery, 50% FO permeate flowrate) and Case 2 (70% RO recovery, 100% FO permeate flowrate), are compared to the permeate concentration of a standalone wastewater RO process in Figure 5-6. The standard for the maximum phenol concentration in drinking water of $0.5\ \mu g \cdot L^{-1}$ (Busca, et al., 2008) is also included for comparison to these permeate qualities.

It is highlighted that a 70% RO recovery is potentially feasible for the FO-RO hybrid process, as the osmotic dilution of seawater in the FO stage favours a higher RO recovery. However, as shown in both Table 5-2 and Figure 5-6, the concentration of phenol in the permeate of the FO-RO hybrid at this RO recovery would not adhere to the drinking water standard of phenol. This standard for phenol can only be achieved when the RO recovery is 45% and the FO permeate flowrate is 50% (Case 1, Figure 5-6), where the resulting concentration is $0.3\ \mu g \cdot L^{-1}$. Nevertheless, in all other cases shown in Table 5-2, the phenol concentration in the permeate of the FO-RO hybrid would be sufficient for surface water and wastewater discharge (Busca, et al., 2008).
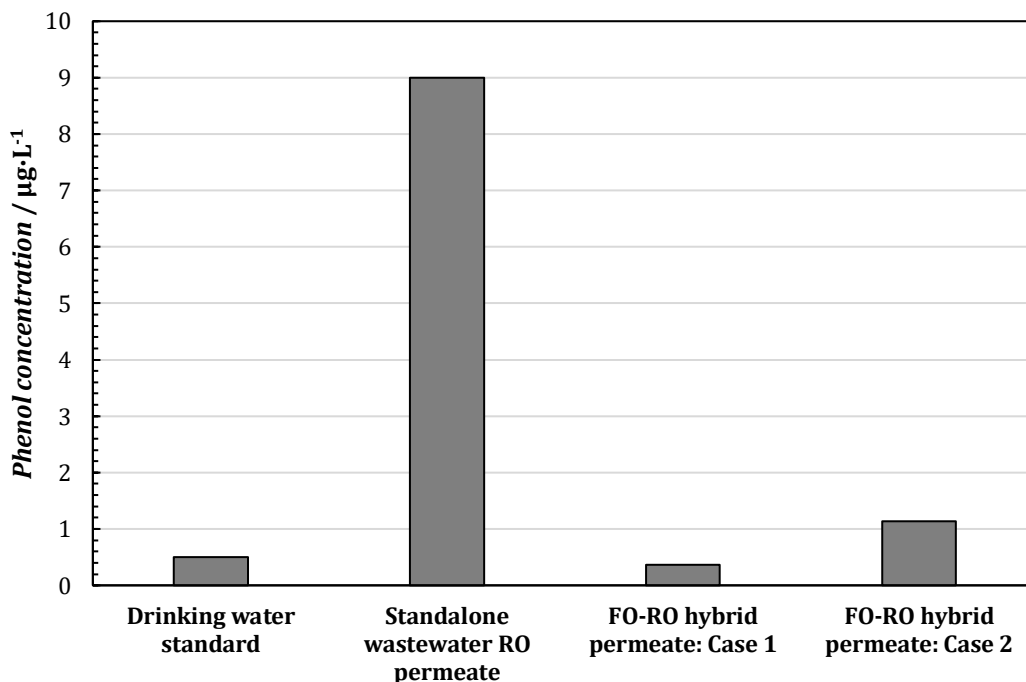
Figure 5-6: The phenol concentrations pertaining to the guideline for drinking water standards (Busca, et al., 2008) and the permeate from a standalone RO process and the FO-RO hybrid process treating a wastewater with a phenol concentration of $100\ \mu g \cdot L^{-1}$. The phenol rejection in all cases is 91%. Case 1 (FO-RO hybrid): 45% RO recovery, 50% FO permeate flowrate. Case 2 (FO-RO hybrid): 70% RO recovery, 100% FO permeate flowrate.

Figure 5-7 shows a comparison of the boron and lithium permeate concentrations in Case 1 and Case 2 of the FO-RO hybrid to that of standalone wastewater and seawater RO processes, treating the same wastewater and seawater, respectively. The drinking water standard for boron of 500 µg·L⁻¹ (World Health Organization, 2003) is also included in the comparison[14]. Despite the significant boron concentration in the influent seawater of 4 500 µg·L⁻¹, the boron concentration of the permeate in both Case 1 and 2 of the FO-RO hybrid (149 µg·L⁻¹ and 262 µg·L⁻¹, respectively) is sufficient for drinking water standards. Further investigation showed that a wastewater containing up to 120 µg·L⁻¹ boron can be treated while still producing a permeate boron concentration within this standard.
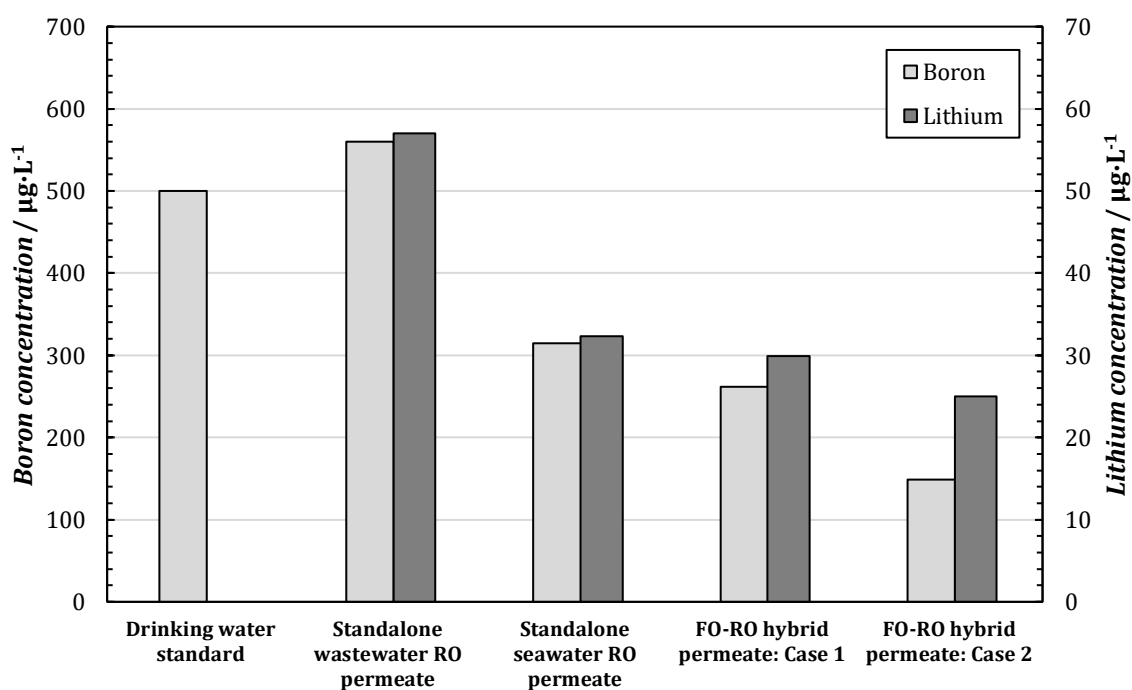
Figure 5-7: The boron and lithium concentrations pertaining to drinking water guidelines and the permeate of standalone RO processes and the FO-RO hybrid. All FO and RO boron and lithium rejections were 93% and 81%, respectively. For the FO-RO hybrid and standalone wastewater RO process, a wastewater of 8 000 µg·L⁻¹ boron and 300 µg·L⁻¹ lithium was considered. For the FO-RO hybrid and standalone seawater RO process a seawater of 4 500 µg·L⁻¹ boron and 170 µg·L⁻¹ lithium was considered. Case 1 (FO-RO hybrid): 45% RO recovery, 50% FO permeate flowrate. Case 2 (FO-RO hybrid): 70% RO recovery, 100% FO permeate flowrate.

It is shown in Figure 5-7 that the FO-RO hybrid is capable of providing a permeate containing a lithium concentration of approximately 8% and 15% of that in the influent wastewater and seawater to the process, respectively. As a result of the weaker lithium rejection in both membrane stages (81%) compared to boron (93%), the permeate lithium concentration of the FO-RO hybrid converges with that of the standalone processes to a greater extent. For example, with a 70% RO

---

[14] No standard has been established for lithium

recovery and 100% FO permeate flowrate (Case 2), the lithium concentration in the FO-RO hybrid permeate is approximately 44% and 77% of that in the standalone wastewater and seawater RO permeates, respectively. For the identical case of the FO-RO hybrid, the permeate boron concentration is 27% and 47% of that of the same respective standalone processes. This demonstrates that the value in adding the FO stage to the RO stage for solute removal increases with an increase in the FO membrane rejection.

Of great importance to this study, Figure 5-6 and Figure 5-7 confirm that the dual-barrier rejection and intermediate dilution effects of the FO-RO hybrid process contribute to an improved permeate quality relative to that of a standalone RO process. Thereby, potable water standards can potentially be achieved. One shortcoming of this simulation approach is that the FO permeate flowrate, which is effectively the FO water flux, is not coupled to the solute rejection. A more rigorous model is required to relate these two quantities. Nevertheless, representative solute rejections and operating conditions were considered.

Chapter 6

Conclusions and future directions

6.1 Conclusions

The primary aim of this study was to investigate the solute transport and rejection behaviour in a submerged FO system with a commercially available CSM FO8040 membrane (Toray). As application and closure of this study, the benefit of the dual-barrier rejection mechanism of the FO-RO hybrid process over a standalone RO process was investigated by implementing the experimentally determined solute rejections. The conclusions drawn from this study are therefore discussed with consideration of the research objectives stipulated in Section 1.4.

i.   Performance of the FO8040 membrane

Pure water permeability tests were performed with a draw solution of typical seawater osmotic pressure. In the AL-FS orientation, the FO8040 membrane achieved a water flux and specific reverse NaCl flux of 19.6 ± 1.2 L·m^{-2}·h^{-1} and 0.29 g·L^{-1}, respectively, with an exceptional stability in the water flux arising from dilutive internal concentration polarisation (DICP). This water flux and specific reverse NaCl flux correlated well with that reported in literature for this FO membrane. In the AL-DS orientation, a higher water flux of 31.6 ± 2.3 L·m^{-2}·h^{-1} was established at the expense of a higher specific reverse NaCl flux of 0.85 g·L^{-1}, which resulted in a distinctive water flux instability.

Turbulence at the submerged membrane surface was necessary to prevent concentrative external concentration polarisation (CECP) of the reverse diffused NaCl. In the absence of turbulence, this CECP resulted in a water flux decline to 8 L·m^{-2}·h^{-1} and 4 L·m^{-2}·h^{-1} in the AL-FS and AL-DS membrane orientations, respectively. A Reynolds number of $1\,100$ at the submerged membrane surface was sufficient to mitigate CECP and the subsequent decline in the water flux.

129

The water flux was highly non-linear with respect to the osmotic pressure gradient in both membrane orientations. In the AL-FS orientation, DICP limited the water flux to 25 $L \cdot m^{-2} \cdot h^{-1}$ up to a draw solution NaCl concentration of 60 $g \cdot L^{-1}$. A significant increase in the reverse NaCl flux with the osmotic pressure gradient, as well as dilutive internal concentration polarisation (DICP), limited the water flux to 40 $L \cdot m^{-2} \cdot h^{-1}$ in the AL-DS orientation up to this draw solution NaCl concentration.

ii. Solute transport and rejection in FO

The transport and rejection of phenol, boron and lithium, as organic and inorganic water contaminants with different structural and physicochemical properties and potentially weak membrane rejections, were investigated at different operating conditions. The following conclusions were drawn from the experimental study:

1. The solute rejection was improved by increasing the osmotic pressure gradient due to the increased hindrance to solute diffusion by a higher water flux. In the AL-DS orientation, retarded forward diffusion of the feed solute by the significant reverse NaCl flux enhanced the increment in the solute rejection at higher water fluxes.

2. The rejection of the neutrally charged solutes, boron (dominant as boric acid) and phenol, was independent of their concentration gradients in both the AL-FS and AL-DS membrane orientations. The pH-dependence of the boron rejection by membranes was observed at a higher concentration gradient of 80 $mg \cdot L^{-1}$, where a reduction in the feed solution pH resulted in a decrease in the boron rejection.

3. In the AL-FS orientation, the rejection of lithium improved as the feed solution lithium chloride and boric acid concentrations were increased simultaneously. The increase in the ionic strength and decrease in the pH of the feed solution reduced the electrostatic interactions of lithium with the membrane.

4. Consistent with point 2 above, the rejection of boron and lithium was unaffected when they were spiked in the draw solution at 5 $mg \cdot L^{-1}$ at a constant concentration gradient, with the exception of lithium in the AL-FS orientation, where electrostatic interactions may have been significant.

5. For the neutrally charged phenol and boron species, the solute rejection in the AL-FS orientation was higher than in the AL-DS orientation. The rejection of lithium was lower in

the AL-FS orientation, likely as a result of its electrostatic attraction to the negatively charged membrane active layer that enhanced its concentration gradient across the membrane.

By the governing rejection mechanism of size exclusion, the FO8040 membrane achieved respective boron and phenol rejections of 91% and 93% at neutral pH conditions (7.6 ± 0.1) in the AL-FS orientation. It is presumed that electrostatic interactions significantly compromised the lithium rejection, such that it was approximately 16% lower than that of phenol and boron at the same solution conditions.

iii. Solute removal by the FO-RO hybrid process

By the dual-barrier rejection and intermediate dilution effects of the FO-RO process, the phenol, boron and lithium rejections of 91%, 93% and 81% in the standalone units could be improved to >98%, >96% and >90% overall FO-RO rejections, respectively. At a higher RO recovery of 70%, which is facilitated by the osmotic dilution of the seawater, the FO-RO hybrid could achieve an improved phenol permeate concentration of 1.1 μg·L^{-1}, relative to 9 μg·L^{-1} provided by a standalone wastewater RO unit. Despite boron and lithium being present in both the influent wastewater and seawater to the process, standalone seawater RO permeate concentrations of 315 μg·L^{-1} boron and 32 μg·L^{-1} lithium could be improved to 149 μg·L^{-1} and 25 μg·L^{-1}, respectively. It was found that the value of adding the FO stage to the RO stage increases with an increase in the FO membrane rejection.

6.2 Future directions

Based on the findings from this research, the following recommendations are made for future studies:

- The AL-DS membrane orientation is not favourable for stable membrane performance and solute removal in wastewater treatment due to the high reverse NaCl flux and forward solute flux in this membrane orientation. Salinity build-up in the submerged FO configuration and low solute rejections are a direct consequent of this. If the high water flux of this membrane orientation is desired, further membrane development is required to decrease the solute permeability and structural parameter of FO membranes.

- This study was limited as it only considered a background feed solution of deionised water. It would be useful to expand the experimental study on organic solute transport to the context of wastewater treatment by considering a feed solution of typical wastewater composition. Thereby, the effect of fouling on the removal of organic compounds can be

studied. Further work is also required to study the mitigation of ECP in the submerged FO configuration with the combined and synergistic effect of fouling.

- The FO-RO hybrid process is promising for the efficient removal of feed water contaminants. However, the application of this process on a larger scale is still limited by the low water fluxes delivered by commercially available FO membranes, which increases the membrane capital cost to achieve favourable water recoveries. Optimisation of the water permeability of FO membranes is required to enable the FO-RO hybrid to compete with existing NF-RO hybrid processes.

References

Achilli, A., Cath, T. Y. & Childress, A. E., 2010. Selection of inorganic-based draw solutions for forward osmosis applications. *Journal of Membrane Science,* Volume 364, pp. 233-241.

Achilli, A., Cath, T. Y., Marchand, E. A. & Childress, A. E., 2009. The forward osmosis membrane bioreactor: A low fouling alternative to MBR processes. *Desalination,* Volume 239, pp. 10-21.

Adams Kszos, L. & Stewart, A. J., 2003. Review of Lithium in the Aquatic Environment: Distribution in the United States, Toxicity and Case Example of Groundwater Contamination. *Ecotoxicology,* Volume 12, pp. 439-447.

Alshwairekh, A., Alghafis, A. A., Usta, M. & Alwatban, A., 2018. *The Effect of Porous Support Layer in Forward Osmosis Membranes-A Computational Fluid Dynamics Simulation.* Pittsburgh, Pennsylvania, USA, s.n.

Altaee, A., Sharif, A., Zaragoza, G. & Ismail, A. F., 2015. Evaluation of FO-RO and PRO-RO designs for power generation and seawater desalination using impaired water feeds. *Desalination,* Volume 368, pp. 27-35.

Alturki, A. A. et al., 2013. Removal of trace organic contaminants by the forward osmosis process. *Separation and Purification Technology,* Volume 103, pp. 258-266.

Alturki, A. et al., 2012. Performance of a novel osmotic membrane bioreactor (OMBR) system: Flux stability and removal of trace organics. *Bioresource Technology,* Volume 113, pp. 201-206.

Anku, W. W., Mamo, M. A. & Govender, P. P., 2017. Phenolic Compounds in Water: Sources, Reactivity, Toxicity and Treatment Methods. In: M. Soto-Hernandez, M. Palma-Tenago & M. del Rosario Garcia-Mateos, eds. *Phenolic Compounds - Natural Sources, Importance and Applications.* London: IntechOpen, pp. 419-443.

Awad, A. M. et al., 2019. The status of forward osmosis technology implementation. *Desaliantion,* Volume 461, pp. 10-21.

Baker, R. W., 2012. *Membrane Technology and Applications.* 3rd ed. California: John Wiley & Sons.

Bell, E. A. et al., 2017. Produced water treatment using forward osmosis membranes: Evaluation of extended-time performance and fouling. *Journal of Membrane Science,* Volume 525, pp. 77-88.

Bellona, C., Drewes, J. E., Xu, P. & Amy, G., 2004. Factors affecting the rejection of organic solutes during NF/RO treatment-a literature review. *Water Research,* 38(12), pp. 2795-2809.

Benavides, S., Oloriz, A. S. & Phillip, W. A., 2015. Forward Osmosis Processes in the Limit of Osmotic Equilibrium. *Industrial & Engineering Chemistry Research,* Volume 54, pp. 480-490.

Bi, Q., Zhang, Z., Zhao, C. & Tao, Z., 2014. Study on the recovery of lithium from high Mg2+/Li+ ratio brine by nanofiltration. *Water Science & Technology,* 70(10), pp. 1690-1694.

Blandin, G., Rodriguez-Roda, I. & Comas, J., 2018. Submerged Osmotic Processes: Design and Operation to Mitigate Mass Transfer Limitations. *Membranes,* Volume 8, p. 72.

Blandin, G. et al., 2016. Efficiently Combining Water Reuse and Desalination through Forward Osmosis-Reverse Osmosis (FO-RO) Hybrids: A Critical Review. *Membranes,* 6(37).

Blandin, G., Verliefde, A. R., Tang, C. Y. & Le-Clech, P., 2015. Opportunities to reach economic sustainability in forward osmosis-reverse osmosis hybrids for seawater desalination. *Desalination,* Volume 363, pp. 26-36.

Bowen, W. R. & Mukhtar, H., 1996. Characterisation and prediction of separation performance of nanofiltration membranes. *Journal of Membrane Science,* Volume 112, pp. 263-274.

Braghetta, A., DiGiano, F. A. & Ball, W. P., 1997. Nanofiltration of Natural Organic Matter: pH and Ionic Strength Effects. *Journal of Environmental Engineering,* 123(7), pp. 628-641.

Bui, N.-N., Arena, J. T. & McCutcheon, J. R., 2015. Proper accounting of mass transfer resistances in forward osmosis: improving the accuracy of model predictions of structural parameter. *Journal of Membrane Science,* Volume 492, pp. 289-302.

Busca, G., Berardinelli, S., Resini, C. & Arrighi, L., 2008. Technologies for the removal of phenol from fluid streams: A short review of recent developments. *Journal of Hazardous Materials,* Volume 160, pp. 265-288.

Busch, M. et al., 2003. *Boron Removal in Sea Water Desalination.* s.l., International Desalination Association.

Cath, T. Y., Childress, A. E. & Elimelech, M., 2006. Forward osmosis: Principles, applications, and recent developments. *Journal of Membrane Science,* Volume 281, pp. 70-87.

Cath, T. Y. et al., 2013. Standard Methodology for Evaluating Membrane Performance in Osmotically Driven Membrane Processes. *Desalination,* Volume 312, pp. 31-38.

Cath, T. Y. et al., 2010. A multi-barrier osmotic dilution process for simultaneous desalination and purification of impaired water. *Journal of Membrane Science,* Volume 362, pp. 417-426.

Çengel, Y. A. & Cimbala, J. M., 2014. *Fluid Mechanics: Fundamentals and Applications.* 3rd ed. Asia: McGraw-Hill.

Chekli, L. et al., 2016. A comprehensive review of hybrid forward osmosis systems: Performance, applications and future prospects. *Journal of Membrane Science,* Volume 497, pp. 430-449.

Chen, M. et al., 2006. Pharmaceuticals and Endocrine Disruptors in Wastewater Treatment Effluents and in the Water Supply System of Calgary, Alberta, Canada. *Water Quality Research Journal,* 41(4), pp. 351-364.

Choi, B. G. et al., 2017. Pilot-scale evaluation of FO-RO osmotic dilution process for treating wastewater from coal-fired power plant integrated with seawater desalination. *Journal of Membrane Science,* Volume 540, pp. 78-87.

Choi, W.-W. & Chen, K. Y., 1979. Evaluation of Boron Removal by Adsorption on Solids. *Environmental Science & Technology,* 13(2), pp. 189-196.

Choi, Y. et al., 2015. Economic Evaluation of a Hybrid Desalination System Combining Forward and Reverse Osmosis. *Membranes,* 6(3).

Choi, Y. J., Lee, S., Koo, J. & Hwang, T. M., 2016. Theoretical and experimental investigation of boron rejection by forward osmosis membrane. *Desalination and Water Treatment,* pp. 1-11.

Chowdhury, M. R. & McCutcheon, J. R., 2018. Elucidating the impact of temperature gradients across membranes during forward osmosis: Coupling heat and mass transfer models for better prediction of real osmotic systems. *Journal of Membrane Science,* Volume 553, pp. 189-199.

Chowdhury, M. R., Ren, J., Reimund, K. & McCutcheon, J. R., 2017. A hybrid dead-end/cross-flow forward osmosis system for evaluating osmotic flux performance at high recovery of produced water. *Desalination,* Volume 421, pp. 127-134.

Chun, Y., Mulcahy, D., Zou, L. & Kim, I. S., 2017. A Short Review of Membrane Fouling in Forward Osmosis Process. *Membranes,* 7(30).

Coday, B. D., Heil, D. M., Xu, P. & Cath, T. Y., 2013. Effects of transmembrane hydraulic pressure on performance of forward osmosis membranes. *Environmental Science and Technology,* 247(1-3), pp. 239-246.

Coday, B. D., Yaffe, B. G., Xu, P. & Cath, T. Y., 2014. Rejection of Trace Compounds by Forward Osmosis Membranes: A Literature Review. *Environmental Science and Technology,* Volume 48, pp. 3612-3624.

Cornelissen, E. R. et al., 2008. Membrane fouling and process performance of forward osmosis membranes on activated sludge. *Journal of Membrane Science,* Volume 319, pp. 158-168.

Corzo, B. et al., 2017. Evaluation of draw solutions and commercially available forward osmosis membrane modules for wastewater reclamation at pilot scale. *Chemical Engineering Journal,* Volume 326, pp. 1-8.

CSM Toray, 2015. *Technical Specifications CSM module FO8040,* Seoul, South Korea: s.n.

Cui, Y. et al., 2016. Removal of organic micro-pollutants (phenol, aniline and nitrobenzene) via forward osmosis (FO) process: Evaluation of FO as an alternative method to reverse osmosis. *Water Research,* Volume 91, pp. 104-114.

Cui, Z. F., Chang, S. & Fane, A. G., 2003. The use of gas bubbling to enhance membrane processes. *Journal of Membrane Science,* Volume 221, pp. 1-35.

Cussler, E. L., 2007. *Diffusion: Mass Transfer in Fluid Systems.* 3rd ed. New York: Cambridge University Press.

David, F., Vokhmin, V. & Ionova, G., 2001. Water characteristics depend on the ionic environment. *Journal of Molecular Liquids,* Volume 90, pp. 45-62.

De, S. & Bhattacharjee, S., 1994. Development of correlations for mass transfer coefficient in ultrafiltration systems. *Development in Chemical Engineering and Mineral Processing,* Volume 3, pp. 187-206.

Devia, Y. P. et al., 2015. Effect of Operating Conditions on Forward Osmosis for Nutrient Rejection Using Magnesium Chloride as a Draw Solution. *International Journal of Environmental and Ecological Engineering,* 9(6), pp. 691-696.

D'Haese, A. et al., 2013. Trace organic solutes in closed-loop forward osmosis applications: Influence of membrane fouling and modeling of solute build-up. *Water Research,* Volume 47, pp. 5232-5244.

Dominguez-Tagle, C., Romero-Ternero, V. J. & Delgado-Torres, A. M., 2011. Boron removal efficiency in small seawater reverse osmosis systems. *Desalination,* Volume 265, pp. 43-48.

Edward, J. T., 1970. Molecular Volumes and the Stokes–Einstein Equation. *Journal of Chemical Education,* Volume 47, p. 261.

Elimelech, M. & Bhattacharjee, S., 1998. A novel approach for modeling concentration polarization in crossflow membrane filtration based on the equivalence of osmotic pressure model and filtration theory. *Journal of Membrane Science,* Volume 145, pp. 223-241.

Elimelech, M. & Phillip, W. A., 2011. The Future of Seawater Desalination: Energy, Technology, and the Environment. *Science,* Volume 333, pp. 712-717.

Eyvaz, M. et al., 2018. Forward Osmosis Membranes – A Review: Part I. In: H. Du, A. Thompson & X. Wang, eds. *Osmotically Driven Membrane Processes - Approach, Development and Current Status.* London: IntechOpen, pp. 11-40.

Fam, W. et al., 2014. Boron transport through polyamide-based thin film composite forward osmosis membranes. *Desalination,* Volume 340, pp. 11-17.

Fam, W., Phuntsho, S., Lee, J. H. & Shon, H. K., 2013. Performance comparison of thin-film composite forward osmosis membranes. *Desalination and Water Treatment,* Volume 51, pp. 6274-6280.

Fang, Y. et al., 2014. Evaluation of the pore size distribution of a forward osmosis membrane in three different ways. *Journal of Membrane Science,* Volume 454, pp. 390-397.

Farhat, A., Ahmad, F., Hilal , N. & Arafat, H. A., 2013. Boron removal in new generation reverse osmosis (RO) membranes using two-pass RO without pH adjustment. *Desalination,* Volume 310, pp. 50-59.

Foxboro, 1999. *Conductivity Ordering Guide.* [Online] Available at: http://ips-dc33-sql/PriceBook/PriceSheet.asp?mscssid=&PS=6%2D3P [Accessed 2017].

Fritzmann, C., Löwenberg, J., Wintgens, T. & Melin, T., 2007. State-of-the-art of reverse osmosis desalination. *Desalination,* Volume 216, pp. 1-76.

Geise, G. M., Paul, D. R. & Freeman, B. D., 2014. Fundamental water and salt transport properties of polymeric materials. *Progress in Polymer Science,* Volume 39, pp. 1-42.

Giagnorio, M. et al., 2019. Hybrid Forward Osmosis–Nanofiltration for Wastewater Reuse: System Design. *Membranes,* 9(61).

Gray, G. T., McCutcheon, J. R. & Elimelech, M., 2006. Internal concentration polarization in forward osmosis-role of membrane orientation. *Desalination,* Volume 197, pp. 1-8.

Gross, K. C. & Seybold, P. G., 2001. Substituent Effects on the Physical Properties and pKa of Phenol. *International Journal of Quantum Chemistry,* Volume 85, pp. 569-579.

Gu, Y., Wang, Y.-N., Wei, J. & Tang, C. Y., 2013. Organic fouling of thin-film composite polyamide and cellulose triacetate forward osmosis membranes by oppositely charged macromolecules. *Water Research,* Volume 47, pp. 1867-1874.

Hai, F. I., Yamamoto, K. & Lee, C. H., 2014. *Membrane Biological Reactors: Theory, Modeling, Design, Management and Applications to Wastewater Reuse.* London: IWA Publishing.

Hancock, N. T., Black, N. D. & Cath, T. Y., 2012. A comparative life cycle assessment of hybrid osmotic dilution desalination and established seawater desalination and wastewater reclamation processes. *Water Research,* Volume 46, pp. 1145-1154.

Hancock, N. T. & Cath, T. Y., 2009. Solute coupled diffusion in osmotically driven membrane processes. *Environmental Science and Technology,* 43(17), pp. 6769-6775.

Hancock, N. T. et al., 2011. Comprehensive Bench- and Pilot-Scale Investigation of Trace Organic Compounds Rejection by Forward Osmosis. *Environmental Science and Technology,* Volume 45, pp. 8483-8490.

Heo, J. et al., 2013. Comparison of flux behaviour and synthetic organic compound removal by forward osmosis and reverse osmosis membranes. *Journal of Membrane Science,* Volume 443, pp. 69-82.

Hidalgo, A. M. et al., 2011. Behaviour of RO98pHt polyamide membrane in reverse osmosis and low pressure reverse osmosis. *Environmental Technology,* 32(13), pp. 1497-1502.

Hill, G. A. & Robinson, C. W., 2004. Substrate inhibition kinetics: phenol degradation by Pseudomonas putida. *Biotechnology & Bioengineering,* Volume 17, pp. 1599-1615.

Holloway, R. W., Achilli, A. & Cath, T. Y., 2015a. The osmotic membrane bioreactor: a critical review. *Environmental Science: Water Research & Technology,* Volume 1, pp. 581-605.

Holloway, R. W., Childress, A. E., Dennett, K. E. & Cath, T. Y., 2007. Forward osmosis for concentration of anaerobic digester centrate. *Water Research,* 41(17), pp. 4005-4014.

Holloway, R. W., Maltos, R., Vanneste, J. & Cath, T. Y., 2015. Mixed draw solutions for improved forward osmosis performance. *Journal of Membrane Science,* Volume 491, pp. 121-131.

Holloway, R. W. et al., 2015b. Long-term pilot scale investigation of novel hybrid ultrafiltration-osmotic membrane bioreactors. *Desalination,* Volume 363, pp. 64-74.

Huang, Y. et al., 2018. Phenol Removal from Water by Polyamide and AgCl Mineralized Thin-Film Composite Forward Osmosis Membranes. *Industrial & Engineering Chemistry Research,* Volume 57, pp. 7021-7029.

Hurter, M., 2019. *A critical evaluation of the mass transfer and fouling behaviour in forward osmosis with integrated flow-reversal,* Stellenbosch University: Faculty of Engineering.

Jacangelo, J. G., Adham, S. S. & Laine, J. M., 1995. Mechanism of cryptosporidium, giardia, and MS2 virus removal by MF and UF. *Journal - American Water Works Association,* Volume 87, pp. 107-121.

Jang, D., Jeong, S., Jang, A. & Kang, S., 2018. Relating solute properties of contaminants of emerging concern and their rejection by forward osmosis membrane. *Science of the Total Environment,* Volume 639, pp. 673-678.

Jeon, J., Park, B., Yoon, Y. & Kim, S., 2016. An optimal design approach of forward osmosis and reverse osmosis and reverse osmosis hybrid process for seawater desalination. *Desalination and Water Treatment,* 57(55), pp. 26612-26620.

Jianfeng, S., Nghiem, L., Li, X.-M. & He, T., 2017. Lithium extraction from Chinese salt-lake brines: Opportunities, challenges, and future outlook. *Environmental Science: Water Research & Technology,* Volume 3, pp. 593-597.

Jin, X. et al., 2012a. Rejection of pharmaceuticals by forward osmosis membranes. *Journal of Hazardous Materials,* Volume 227-228, pp. 55-61.

Jin, X., She, Q., Ang, X. & Tang, C. Y., 2012b. Removal of boron and arsenic by forward osmosis membrane: influence of membrane orientation and organic fouling. *Journal of Membrane Science,* 389(0), pp. 182-187.

Jin, X. et al., 2011. Boric Acid Permeation in Forward Osmosis Membrane Processes: Modeling, Experiments and Implications. *Environmental Science and Technology,* Volume 45, pp. 2323-2330.

Judd, S., 2008. *The MBR book: Principles and applications of membrane bioreactors for water and wastewater treatment*. Oxford: Elsevier.

Kaye, G. W. & Laby, T. H., 1971. *Tables of Physical and Chemical Constants*. London: Longman.

Kielland, J., 1937. Individual activity coefficients of ions in aqueous solutions. *Journal of the American Chemical Society,* Volume 59, pp. 1675-1678.

Kim, B., Gwak, G. & Hong, S., 2017. Review on methodology for determining forward osmosis (FO) membrane characteristics: Water permeability (A), solute permeability (B), and structural parameter (S). *Desalination,* Volume 422, pp. 5-16.

Kim, C. et al., 2012. Boron transport in forward osmosis: Measurements, mechanisms, and comparison with reverse osmosis. *Journal of Membrane Science,* Volume 419-420, pp. 42-48.

Kim, J. et al., 2017. Practical considerations for operability of an 8" spiral wound forward osmosis module: Hydrodynamics, fouling behaviour and cleaning strategy. *Desalination,* Volume 404, pp. 249-258.

Kim, J. E., Phuntsho, S., Lotfi, F. & Shon, H. K., 2015. Investigation of pilot-scale 8040 FO membrane module under different operating conditions for brackish water desalination. *Desalination and Water Treatment,* Volume 53, pp. 2782-2791.

Kim, Kim, J. H., Park, M. & Lee, J., 2015. Impacts of Spacers on Forward Osmosis Processes. In: H. K. Shon, S. Phunthsho, T. C. Zhang & R. Y. Surampalli, eds. *Forward Osmosis: Fundamentals and Applications*. s.l.:American Society of Civil Engineers.

Kim, S. et al., 2018. Removal of contaminants of emerging concern by membranes in water and wastewater: A review. *Chemical Engineering Journal,* Volume 335, pp. 896-914.

Kim, T. U., Drewes, J. E., Xu, P. & Amy, G., 2007. Solute transport model for trace organic neutral and charged organic compounds through nanofiltration and reverse osmosis membranes. *Water Research,* 41(17), pp. 3977-3988.

Kim, Y. C. & Elimelech, M., 2012. Adverse impact of feed channel spacers on the performance of pressure retarded osmosis. *Environmental Science and Technology,* 46(8), pp. 4673-4681.

Kim, Y. C. & Park, S.-J., 2011. Experimental Study of a 4040 Spiral-Wound Forward-Osmosis Membrane Module. *Environmental Science and Technology,* Volume 45, pp. 7737-7745.

Klaysom, C., Cath, T. Y., Depuydt, T. & Vankelecom, I. F., 2013. Forward and pressure retarded osmosis: potential solutions for global challenges in energy and water supply. *Chemical Society Reviews,* 42(16), pp. 6959-6989.

Kochkodan, V., Darwish, N. B. & Hilal, N., 2015. The Chemistry of Boron in Water. In: N. Kabay, N. Hilal & M. Bryak, eds. *Boron Separation Processes.* Swansea: Elsevier, pp. 35-62.

Koseoglu, H. et al., 2008. Boron removal from seawater using high rejection SWRO membranes - impact of pH, feed concentration, pressure, and cross-flow velocity. *Desalination,* Volume 227, pp. 253-263.

Kucera, J., 2010. *Reverse Osmosis: Design, Processes and Applications for Engineers.* 2nd ed. Massachusetts: Wiley.

Lachish, U., 2007. Osmosis and thermodynamics. *American Journal of Physics,* 75(11), pp. 997-998.

Lay, W. C., Liu, Y. & Fane, A. G., 2010. Impacts of salinity on the performance of high retention membrane bioreactors for water reclamation: a review. *Water Research,* 44(1), pp. 21-40.

Lay, W. C. et al., 2011. Study of integration of forward osmosis and biological process: Membrane performance under elevated salt environment. *Desalination,* Volume 283, pp. 123-130.

Lee, J. M., 1980. *Recovery of lithium from brines.* United States, Patent No. 4221767.

Lee, K. L., Baker, R. W. & Lonsdale, H. K., 1981. Membranes for power generation by pressure-retarded osmosis. *Journal of Membrane Science,* Volume 8, pp. 141-171.

Lee, S., Boo, C., Elimelech, M. & Hong, S., 2010. Comparison of fouling behaviour in forward osmosis (FO) and reverse osmosis (RO). *Journal of Membrane Science,* Volume 365, pp. 34-39.

Lee, S., Le-Clech, P. & Blandin, G., 2015. Pressure-Assisted Osmosis (PAO) for Water Purification. In: H. Kyong Shon, S. Phuntsho, T. C. Zhang & R. Y. Surampalli, eds. *Forward Osmosis: Fundementals and Applications.* United States of America: American Society of Civil Engineers, pp. 445-463.

Lew, C., Hu, J., Song, L. & Lee, L. Y., 2005. Development of an integrated membrane process for water reclamation. *Water Science & Technology,* 51(6-7), pp. 455-463.

Lian, B., Blandin, G., Leslie, G. & Le-Clech, P., 2018. Impact of module design in forward osmosis and pressure assisted osmosis: An experimental and numerical study. *Desalination,* Volume 426, pp. 108-117.

Liang, Q. et al., 2009. The synthesis of the crown ether PU foam and the application in separating lithium and magnesium.. *Journal of Chengdu University of Technology,* 36(3), pp. 326-332.

Li, J., Liu, Q., Liu, Y. & Xie, J., 2017. Development of electro-active forward osmosis membranes to remove phenolic compounds and reject salts. *Environmental Science: Water Research and Technology,* Volume 3, pp. 139-146.

Li, J. et al., 2018. Enrichment of lithium from salt lake brine by forward osmosis. *Royal Society Open Science,* Volume 5:180965.

Liu, X., Wu, J. & Wang, J., 2019. Removal of nuclides and boric acid from simulated wastewater by forward osmosis. *Progress in Nuclear Technology,* Volume 114, pp. 155-163.

Li, Y., Wei, J., Wang, C. & Wang, W., 2010. Comparison of phenol removal in synthetic wastewater by NF and RO membranes. *Desalination and Water treatment,* Volume 22, pp. 211-219.

Loeb, S., 1976. Production of energy from concentrated brines by pressure-retarded osmosis: I. Preliminary technical and economic correlations. *Journal o Membrane Science,* Volume 1, pp. 49-63.

Loeb, S., Titelman, L., Korngold, E. & Freiman, J., 1997. Effect of porous support fabric on osmosis through a Loeb-Sourirajan-type asymmetric membrane. *Journal of Membrane Science,* Volume 129, pp. 243-249.

Lonsdale, H. K., Merten, U. & Riley, R. L., 1965. Transport properties of cellulose acetate osmotic membranes. *Journal of Applied Polymer Science,* Volume 9, p. 1341.

Luo, L. et al., 2016. Experiments and Modeling of Boric Acid Permeation through Double-Skinned Forward Osmosis Membranes. *Environmental Science and Technology,* Volume 50, pp. 7696-7705.

Luo, W., Hai, F. I., Price, W. E. & Nghiem, L. D., 2015. Water extraction from mixed liquor of an aerobic bioreactor by forward osmosis: membrane fouling and biomass characteristics assessment. *Separation and Purification Technology,* Volume 145, pp. 56-62.

Luo, W. et al., 2017. Osmotic versus conventional membrane bioreactors integrated with reverse osmosis for water reuse: Biological stability, membrane fouling, and contaminant removal. *Water Research,* Volume 109, pp. 122-134.

Lutchmiah, K. et al., 2011. Water recovery from sewage using forward osmosis. *Water Science and Technology,* 64(7), pp. 1443-1449.

Lutchmiah, K. et al., 2014. Forward osmosis for application in wastewater treatment: A review. *Water Research,* Volume 58, pp. 179-197.

Maltos, R. A. et al., 2018. Produced water impact on membrane integrity during extended pilot testing of forward osmosis – reverse osmosis treatment. *Desalination,* Volume 440, pp. 99-110.

Manickam, S. S. & McCutcheon, J. R., 2017. Understanding mass transfer through asymmetric membranes during forward osmosis: A historical perspective and critical review on measuring structural parameter with semi-empirical models and characterization approaches. *Desalination,* Volume 421, pp. 110-126.

Mazlan, N. M., 2016. *Forward Osmosis for Desalination and Water Recovery,* s.l.: Imperial College London.

McCutcheon, J. R. & Elimelech, M., 2006. Influence of concentrative and dilutive internal concentration polarization on flux behavior in forward osmosis. *Journal of Membrane Science,* Volume 284, pp. 237-247.

McCutcheon, J. R., McGinnis, R. L. & Elimelech, M., 2006. Desalination by ammonia-carbon dioxide forward osmosis process: influence of draw and feed solution concentrations on process performance. *Journal of Membrane Science,* Volume 278, pp. 114-123.

McGinnis, R. L. & Elimelech, M., 2007. Energy requirements of ammonia-carbon dioxide forward osmosis desalination. *Desalination,* Volume 207, pp. 370-382.

McGovern, R. K. & Lienhard, J. H., 2014. On the potential of forward osmosis to energetically outperform reverse osmosis desalination. *Journal of Membrane Science,* Volume 469, pp. 245-250.

McMordie Stoughton, K. L., Duan, X. & Wendel, E. M., 2013. *Reverse Osmosis Optimization,* Richland: Federal Energy Management Program.

Mehta, G. D. & Loeb, S., 1978. Internal polarization in the porous substructure of a semipermeable membrane under pressure-retarded osmosis. *Journal of Membrane Science,* 4(2), pp. 261-265.

Mehta, G. D. & Loeb, S., 1979. Performance of Permasep B-9 and B-10 membranes in various osmotic regions and at high osmotic pressures. *Journal of Membrane Science,* Volume 4, pp. 335-349.

Mi, B. & Elimelech, M., 2008. Chemical and physical aspects of organic fouling of forward osmosis membranes. *Journal of Membrane Science,* Volume 320, pp. 292-302.

Mi, B. & Elimelech, M., 2010a. Organic fouling of forward osmosis membranes: fouling reversibility and cleaning without chemical reagents. *Journal of Membrane Science,* Volume 348, pp. 337-345.

Mi, B. & Elimelech, M., 2010b. Gypsum scaling and cleaning in forward osmosis: measurements and mechansims. *Environmental Science & Technology,* Volume 44, pp. 2022-2028.

Mulder, M., 1996. *Basic Principles of Membrane Technology.* 2nd ed. Dordrecht, The Netherlands: Kluwer Academic Publishers.

Nagy, E., 2012. Nanofiltration. In: E. Nagy, ed. *Basic Equations of the Mass Transport Through a Membrane Layer.* London: Elsevier, pp. 249-266.

Neff, J. M., Lee, K. & Deblois, E., 2011. Produced water: Overview of Composition, Fates, and Effects. In: K. Lee & J. Neff, eds. *Produced Water: Environmental Risks and Advances in Mitigation Technologies.* New York: Springer, pp. 3-54.

Nghiem, L. D., Schäfer, A. I. & Elimelech, M., 2006. Role of electrostatic interactions in the retention of pharmaceutically active contaminants by a loose nanofiltration membrane. *Journal of Membrane Science,* Volume 286, pp. 52-59.

Nghiem, L. D., Schafer, A. I. & Elimelech, M., 2010. Pharmaceutical retention mechanisms by nanofiltration membranes. *Environmental Science and Technology,* 39(19), pp. 7698-7705.

Nguyen, T. P. N., Jun, B.-M., Lee, J. H. & Kwon, Y.-N., 2015. Comparison of integrally asymmetric and thin film composite structures for a desirable fashion of forward osmosis. *Journal of Membrane Science,* Volume 495, pp. 457-470.

Opong, W. S. & Zydney, A. L., 1991. Diffusive and convective protein transport through asymmetric membranes. *AIChe Journal,* Volume 37, pp. 1499-1510.

Oram, B., 2014. *Lithium In Drinking Water.* [Online] Available at: https://water-research.net/index.php/lithium

Oren, Y. S. & Biesheuvel, P. M., 2018. Theory of ion and water transport in reverse osmosis membranes. *Physical Review Applied,* Volume 02034, p. 9.

Park, S.-M.et al., 2012. Optimization of hybrid system consisting of forward osmosis and reverse osmosis: a Monte Carlo simulation approach. *Desalination and Water Treatment,* 43(1-3), pp. 274-280.

Paul, D. R., 1974. Diffusive Transport in Swollen Polymer Membranes. In: H. B. Hopfenberg, ed. *Permeability of Plastic Films and Coatings.* New York: Plenum Press, pp. 35-48.

Pereira, D. M., Valentão, P., Pereira, J. A. & Andrade, P. B., 2009. Phenolics: From Chemistry to Biology. *Molecules,* Volume 14, pp. 2202-2211.

Perry, M., 2013. *Forward osmosis (FO) membranes and membrane processes.* [Online] Available at: http://www.forwardosmosistech.com/forward-osmosis-membranes-and-membrane-processes/
[Accessed 27 July 2019].

Perry, M., 2013. *The principles of forward osmosis (FO).* [Online] Available at: http://www.forwardosmosistech.com/the-principles-of-forward-osmosis/
[Accessed 28 March 2018].

Peryea, F. J. & Lageshulte, J. M., 2000. Boron Fertilizer Product and Concentration Influence Spray Water pH. *HortTechnology,* 10(2), pp. 350-353.

Phillip, W. A., Yong, J. S. & Elimelech, M., 2010. Reverse draw solute permeation in forward osmosis: modeling and experiments. *Environmental Science and Technology,* Volume 44, pp. 5170-5176.

Phunthso, S. et al., 2013. Assessing the major factors affecting the performances of forward osmosis and its implications on the desalination process. *Chemical Engineering Journal,* Volume 231, pp. 484-496.

Pramanik, B. K. et al., 2019. Lithium enrichment from a simulated salt lake brine using an integrated nanofiltration-membrane distillation process. *Journal of Environmental Chemical Engineering.*

Qin, J. J. et al., 2009. Optimization of operating conditions in forward osmosis for osmotic membrane bioreactor. *Open Chemical Engineering Journal,* Volume 3, pp. 27-32.

Qiu, G. & Ting, Y.-P., 2014. Short-term fouling propensity and flux behaviour in an osmotic membrane bioeactor for wastewater treatment. *Desalination,* Volume 332, pp. 91-99.

Qiu, G. et al., 2016. The potential of hybrid forward osmosis membrane bioreactor (FOMBR) processes in achieving high throughput treatment of municipal wastewater with enhanced phosphorous recovery. *Water Research,* Volume 105, pp. 370-382.

Quist-Jensen, C. A., Macedonio, F. & Drioli, E., 2016. Integrated Membrane Desalination Systems with Membrane Crystallization Units for Resource Recovery: A New Approach for Mining from the Sea. *Crystals,* 6(36).

Saren, Q., Qiu, C. Q. & Tang, C. Y., 2011. Synthesis and characterization of novel forward osmosis membranes based on layer-by-layer assembly. *Environmental Science and Technology,* Volume 45, pp. 5201-5208.

Sauchelli, M. et al., 2018. Transport of trace organic compounds through novel forward osmosis membranes: Role of membrane properties and the draw solution. *Water Research,* Volume 141, pp. 65-73.

Schutte, C. F., 2003. The rejection of specific organic compounds by reverse osmosis membranes. *Desalination,* Volume 158, pp. 285-294.

Schwarzenbach, R. P. et al., 2006. The challenge of micropollutants in aquatic systems. *Science,* Volume 313, pp. 1072-1077.

See, D. M. & White, R. E., 1997. Temperature and Concentration Dependence of the Specific Conductivity of Concentrated Solutions of Potassium Hydroxide. *Journal of Chemical & Engineering Data,* 42(6), pp. 1266-1268.

Seidel, A., Waypa, J. J. & Elimelech, M., 2001. Role of Charge (Donnan) Exclusion in Removal of Arsenic from Water by Negatively Charged Porous Nanofiltration Membrane. *Environmental Engineering Science,* 18(2), pp. 105-113.

Seo, J. et al., 2019. An optimization strategy for a forward osmosis-reverse osmosis hybrid process for wastewater reuse and seawater desalination: A modeling study. *Desalination,* Volume 463, pp. 40-49.

Shaffer, D. L. et al., 2015. Forward osmosis: Where are we now?. *Desalination,* Volume 356, pp. 271-284.

Shaffer, D. L., Yip, N. Y., Gilron, J. & Elimelech, M., 2012. Seawater desalination for agriculture by integrated forward and reverse osmosis: Improved product water quality for potentially less energy. *Journal of Membrane Science,* Volume 415-416, pp. 1-8.

Sharif, A. & Arayafar, M., 2014. *Forward osmosis.* Surrey, Great Britain, Patent No. WO2015087063A1.

She, Q. et al., 2013. Effect of feed spacer induced membrane deformation on the performance of pressure retarded osmosis (PRO): implications for PRO operation. *Journal of Membrane Science,* Volume 445, pp. 170-182.

She, Q., Jin, X., Li, Q. & Tang, C. Y., 2012. Relating reverse and forward solute diffusion to membrane fouling in osmotically driven membrane processes. *Water Research,* Volume 46, pp. 2478-2486.

She, Q., Wang, R., Fane, A. G. & Tang, C. Y., 2016. Membrane fouling in osmotically driven membrane processes: A review. *Journal of Membrane Science,* Volume 499, pp. 201-233.

Siddiqui, A. et al., 2017. Porosity of spacer-filled channels in spiral-wound membrane systems: quantification methods and impact on hydraulic characterization. *Water Research,* Volume 119, pp. 304-311.

Smith, K. A., Colton, C. K. & Merril, E. W., 1968. Convective transport in a batch dialyzer: determination of the true membrane permeability from a single measurement. *Chemical Engineering Progress Symposium Series,* 64(84), pp. 45-58.

Snyder, S. A. et al., 2007. Role of membranes and activated carbon in the removal of endocrine disruptors and pharmaceuticals. *Desalination,* Volume 202, pp. 156-181.

Somrani, A., Hamzaoui, A. H. & Pontie, M., 2013. Study on lithium separation from salt lake brines by nanofiltration (NF) and low pressure reverse osmosis (LPRO). *Desalination,* Volume 317, pp. 184-192.

Straub, A. P. & Elimelech, M., 2016. Pressure-retarded osmosis for power generation from salinity gradients: Is it viable?. *Energy & Environmental Science,* Volume 9, pp. 31-48.

Suh, C. & Lee, S., 2012. Modeling reverse draw solute flux in forward osmosis with external concentration polarization in both sides of the draw and feed solution. *Journal of Membrane Science,* Volume 427, pp. 365-374.

Sunbul, Y. A., 2018. *Boron Removal from Seawater by Thin-Film Composite Reverse Osmosis Membranes,* Thuwal: King Abdullah University of Science and Technology.

Tan, C. H. & Ng, H. Y., 2008. Modified models to predict flux behavior in forward osmosis in consideration of external and internal concentration polarizations. *Journal of Membrane Science,* Volume 324, pp. 209-219.

Tan, C. H. & Ng, H. Y., 2010. A novel hybrid forward osmosis–nanofiltration (FO–NF) process for seawater desalination: Draw solution selection and system configuration. *Desalination and Water Treatment,* Volume 13, pp. 356-361.

Tang, C. Y. et al., 2011. Modeling double-skinned FO membranes. *Desalination,* Volume 283, pp. 178-186.

Tang, C. Y. et al., 2010. Coupled effects of internal concentration polarization and fouling on flux behavior of forward osmosis membranes during humic acid filtration. *Journal of Membrane Science,* Volume 354, pp. 123-133.

Tansel, B., 2012. Significance of thermodynamic and physical characteristics on permeation of ions during membrane separation: Hydrated radius, hydration free energy and viscous effects. *Separation and Purification Technology,* Volume 86, pp. 119-126.

Ternes, T. A., Joss, A. & Siegrist, H., 2004. Scrutinizing pharmaceuticals and personal care products in wastewater treatment. *Environmental Science and Technology,* 38(20), pp. 392A-399A.

Teusner, A., Blandin, G. & Le-Clech, P., 2017. Augmenting water supply by combined desalination/water recycling methods: An economic assessment. *Environmental Technology,* Volume 38, pp. 257-265.

Tu, K. L., Chivas, A. R. & Nghiem, L. D., 2013. Enhanced boron rejection by NF/RO membranes by complexation with polyols: Measurements and mechanisms. *Desalination,* Volume 310, pp. 115-121.

Turek, M., Dydo, P., Trojanowska, J. & Bandura, B., 2007. Electrodialytic treatment of boron-containing wastewater. *Desalination,* 205(1-3), pp. 185-191.

USEPA, 1979. *Toxic Substances Control Act (TSCA),* Washington, DC: United States Environmental Protection Authority.

Valladares Linares, R. et al., 2013. Water harvesting from municipal wastewater via osmotic gradient: An evaluation of process performance. *Journal of Membrane Science,* Volume 447, pp. 50-56.

Valladares Linares, R. et al., 2016. Hybrid SBR-FO system for wastewater treatment and reuse: Operation, fouling and cleaning. *Desalination,* Volume 393, pp. 31-38.

Valladares Linares, R. et al., 2014. Higher boron rejection with a new TFC forward osmosis membrane. *Desalination and Water Treatment,* 55(10), pp. 2734-2740.

Valladares Linares, R., Yangali-Quintanilla, V., Li, Z. & Amy, G., 2011. Rejection of micropollutants by cleaned and fouled forward osmosis membrane. *Water Research,* Volume 45, pp. 6737-6744.

van't Hoff, J., 1888. The function of osmotic pressure in the analogy between solutions and gases. *Philosophical Magazine,* Volume 26, pp. 81-105.

Verliefde, A. R., 2008. *Rejection of organic micropollutants with high pressure membranes (NF/RO),* TU Delft: Civil Engineering and Geosciences.

Verliefde, A. R. et al., 2008. The role of electrostatic interactions on the rejection of organic solutes in aqueous solutions with nanofiltration. *Journal of Membrane Science,* Volume 322, pp. 52-66.

Vital, B., Bartacek, J., Ortega-Bravo, J. C. & Jeison, D., 2018. Treatment of acid mine drainage by forward osmosis: Heavy metal rejection and reverse flux of draw solution constituents. *Chemical Engineering Journal,* Volume 332, pp. 85-91.

Volkov, A. G., Paula, S. & Deamer, D. W., 1997. Two mechanisms of permeation of small neutral molecules and hydrated ions across phospholipid bilayers. *Bioelectrochemistry and Bioenergetics,* Volume 42, pp. 153-160.

Volpin, F. et al., 2019. Optimisation of a forward osmosis and membrane distillation hybrid system for the treatment of source-separated urine. *Separation and Purification Technology,* Volume 212, pp. 368-375.

Volpin, F. et al., 2018. Hybrid forward osmosis-reverse osmosis for wastewater reuse and seawater desalination: Understanding the optimal feed solution to minimise fouling. *Process Safety and Environmental Protection,* Volume 117, pp. 523-532.

Wang, J. et al., 2014. A critical review of transport through osmotic membranes. *Journal of Membrane Science,* Volume 454, pp. 516-537.

Wang, Y.-N.et al., 2018. Membranes and processes for forward osmosis-based desalination: Recent advances and future prospects. *Desalination,* Volume 434, pp. 81-99.

Wang, Y.-N., Li, W., Wang, R. & Tang, C. Y., 2017. Enhancing boron rejection in FO using alkaline draw solutions. *Water Research,* Volume 118, pp. 20-25.

Wang, Y. et al., 2016. Quantitative evaluation of concentration polarization under different operating conditions for forward osmosis process. *Desalination,* Volume 398, pp. 106-113.

Water Environment Federation, 2006. *Membrane Systems for Wastewater Treatment.* Access Engineering: McGraw-Hill Professional.

Wei, J. et al., 2013. Comparison of NF-like and RO-like thin film composite osmotically-driven membranes-implications for membrane selection and process optimization. *Journal of Membrane Science,* Volume 427, pp. 460-471.

Wen, X. et al., 2006. Preliminary study on recovering lithium chloride from lithium-containing water by nanofiltration. *Separation & Purification Technology,* Volume 49, pp. 230-236.

Widjojo, N. et al., 2011. The role of sulphonated polymer and macrovoid-free structure in the support layer for thin-film composite (TFC) forward osmosis (FO) membranes. *Journal of Membrane Science,* Volume 383, pp. 214-223.

Wijmans, J. G. & Baker, R. W., 1995. The solution-diffusion model: a review. *Journal of Membrane Science,* 107(1-2), pp. 1-21.

Winkelmann, J., 2017. Diffusion coefficient of phenol in water. In: M. D. Lechner, ed. *Diffusion in Gases, Liquids and Electrolytes.* Berlin, Heidelberg: Springer, p. 755.

World Health Organization, 2003. *Boron in drinking-water: background document for development of WHO guidelines for drinking-water quality,* Geneva: WHO.

Xiao, T. et al., 2017. Phenol rejection by cellulose triacetate and thin film composite composite forward osmosis membranes. *Separation and Purification Technology,* Volume 186, pp. 45-54.

Xie, M., Nghiem, L. D., He, T. & Price, W. E., 2015. Removal of Emerging Trace Organic Chemicals by Forward Osmosis. In: H. K. Shon, S. Phunthso, T. C. Zhang & R. Y. Surampilli, eds. *Forward Osmosis: Fundamentals and Applications.* Virginia: American Society of Civil Engineers, pp. 363-394.

Xie, M., Nghiem, L. D., Price, W. E. & Elimelech, M., 2012a. Comparison of the removal of hydrophobic trace organic contaminants by forward osmosis and reverse osmosis. *Water Research,* Volume 46, pp. 2683-2692.

Xie, M., Price, W. E., Nghiem, L. D. & Elimelech, M., 2013b. Effects of feed and draw solution temperature and transmembrane temperature difference on the rejection of trace organic contaminants by forward osmosis. *Journal of Membrane Science,* Volume 438, pp. 57-64.

Xu, R. et al., 2010. Investigations on boron levels in drinking water sources in China. *Environmental Monitoring and Assessment,* 165(1-4), pp. 15-25.

Yaroshchuk, A. E., 2000. Dielectric exclusion of ions from membranes. *Advances in Colloid and Interface Science,* Volume 85, pp. 193-230.

Yip, N. Y. et al., 2011. Thin-film composite pressure retarded osmosis membranes for sustainable power generation from salinity gradients. *Environmental Science & Technology,* Volume 45, pp. 4360-4369.

Yong, J. S., Phillip, W. A. & Elimelech, M., 2012. Coupled reverse draw solute permeation and water flux in forward osmosis with neutral draw solutes. *Journal of Membrane Science,* Volume 392-393, pp. 9-17.

Yoon, Y., Westerhoff, P., Snyder, S. A. & Wert, E. C., 2006. Nanofiltration and ultrafiltration of endocrine disrupting compounds, pharmaceuticals and personal care products. *Journal of Membrane Science,* 270(1-2), pp. 88-100.

Zhang, J. et al., 2012. Membrane biofouling and scaling in forward osmosis membrane bioreactor. *Journal of Membrane Science,* Volume 403-404, pp. 8-14.

Zhang, X. et al., 2017. Effects of feed solution pH and draw solution concentration on the performance of phenolic compound removal in forward osmosis process. *Journal of Environmental Chemical Engineering,* Volume 5, pp. 2508-2514.

Zhao, S. F., Zou, L., Tang, C. Y. & Mulcahy, D., 2012. Recent developments in forward osmosis: Opportunities and challenges. *Journal of Membrane Science,* Volume 396, pp. 1-21.

Zhao, S., Zou, L. & Mulcahy, D., 2011. Effects of membrane orientation on process performance in forward osmosis applications. *Journal of Membrane Science,* Volume 382, pp. 308-315.

Zheng, L. et al., 2019. New insights into the relationship between draw solution chemistry and trace organic rejection by forward osmosis. *Journal of Membrane Science,* Volume 587, p. 117184.

Zhou, A., Zhang, T. C. & Yuan, Y., 2012. *Performance of Forward Osmosis Processes under Different Operating Conditions and Draw Solutes.* s.l., World Environmental and Water Resources Congress: Crossing Boundaries.

Appendix A

Experimental setup

Supplementary to the illustrations and information provided in Chapter 3, images and detailed drawings of the components of the experimental setup are provided here.

A.1   Photographs
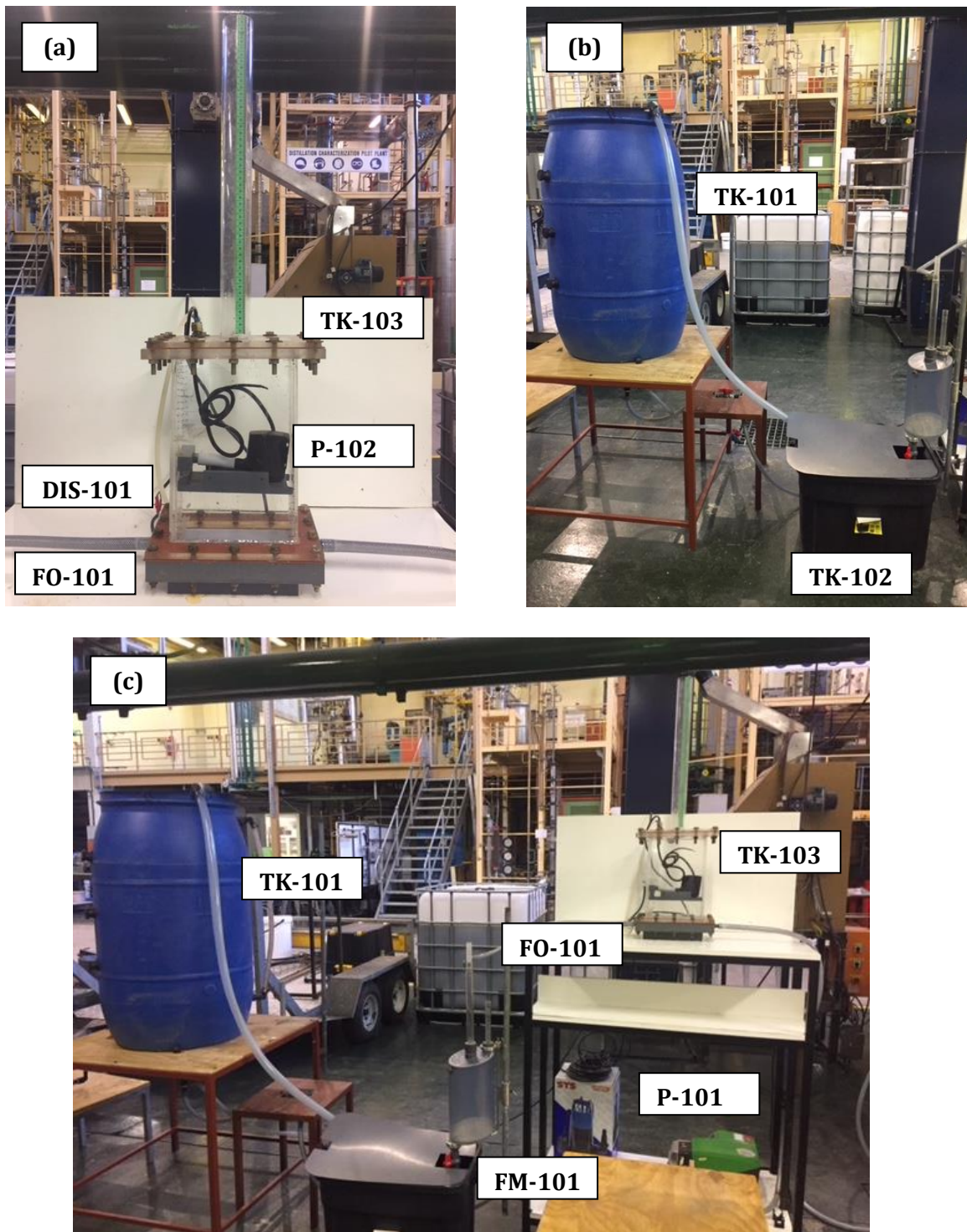
Figure A-1: Photographs of the designed and constructed experimental setup, illustrating the FS reactor (TK-103) with the agitator (P-102 and DIS-101) and membrane cell (FO-101) in (a), the DS tank (TK-101) and DS reservoir (TK-102) containing the submersible recycle pump (P-102 not pictured) in (b) and the DS peristatic pump (P-101) and in-line flowmeter (FM-101) in (c).

154

A.2   Design drawings

A.2.1 Membrane cell (FO-101)

UNLESS OTHERWISE STATED
TOLERANCES ± 0,1
ANGLES 1˚

UNIVERSITEIT VAN STELLENBOSCH

STUDENTE No. 17614252 TEKENAAR L.A. van Wyk NAGESIEN

ITEM	BESKRYWING	AANTAL	MATERIAAL / SPESIFIKASIES

SKAAL OP A 1:2
MATE IN mm

TITEL: FO membrane cell (FO-101)

DATUM JULY 2017 VEL No. VAN VELLE No.

156

A.2.2 FS reactor (TK-103)

10 60 60 60 60 10

87
87

10
51
52
51
10

Ø46

14 x Ø8

A-A (0.2 : 1)

A

A

504

10

130 130

	UNLESS OTHERWISE STATED
	TOLERANCES ± 0,1
	ANGLES 1˙

ITEM	BESKRYWING	AANTAL	MATERIAAL / SPESIFIKASIES

| SKAAL OP A | 0.2:1 | TITEL: | Graduated cylinder of FS reactor (TK-103) |
| MATE IN | mm | | |

UNIVERSITEIT VAN STELLENBOSCH

| STUDENTE No. | 17614252 | TEKENAAR | L.A. VAN WYK | NAGESIEN | DATUM JULY 2017 | VEL No. | VAN | VELLE | No. |

158

A.2.3 Distribution plate (DIS-101)

UNLESS OTHERWISE STATED
TOLERANCES ± 0,1
ANGLES 1˙

UNIVERSITEIT VAN STELLENBOSCH

STUDENTE No. 17614252	TEKENAAR L.A. VAN WYK	NAGESIEN

ITEM	BESKRYWING	AANTAL	MATERIAAL / SPESIFIKASIES

SKAAL OP A 1:2
MATE IN mm
DATUM JULY 2017

TITEL: Distribution plate (DIS-101)

VEL No.   VAN   VELLE   No.

A-A (1:2)

A.2.4 In-line flowmeter (FM-101)

ITEM	BESKRYWING	AANTAL	MATERIAAL / SPESIFIKASIES

UNLESS OTHERWISE STATED
TOLERANCES ± 0,1
ANGLES 1°

UNIVERSITEIT VAN STELLENBOSCH

SKAAL OP A		TITEL: In-line flow measuring cylinder (FM-101)
MATE IN mm		

STUDENTE No. 17614252   TEKENAAR L.A. VAN WYK   NAGESIEN   DATUM JULY 2017   VEL No.   VAN   VELLE   No.

160

Appendix B

Analytical methods

B.1   Estimation of solution salinity

Two different correlations, appropriate for two respective conductivity ranges, were regressed for the estimation of the solution NaCl concentration from the experimentally measured conductivity. For a conductivity range from 2 to 5200 μS·cm^{-1} for the feed solution, the data from Foxboro (1999) were regressed, as shown in Figure B-1.
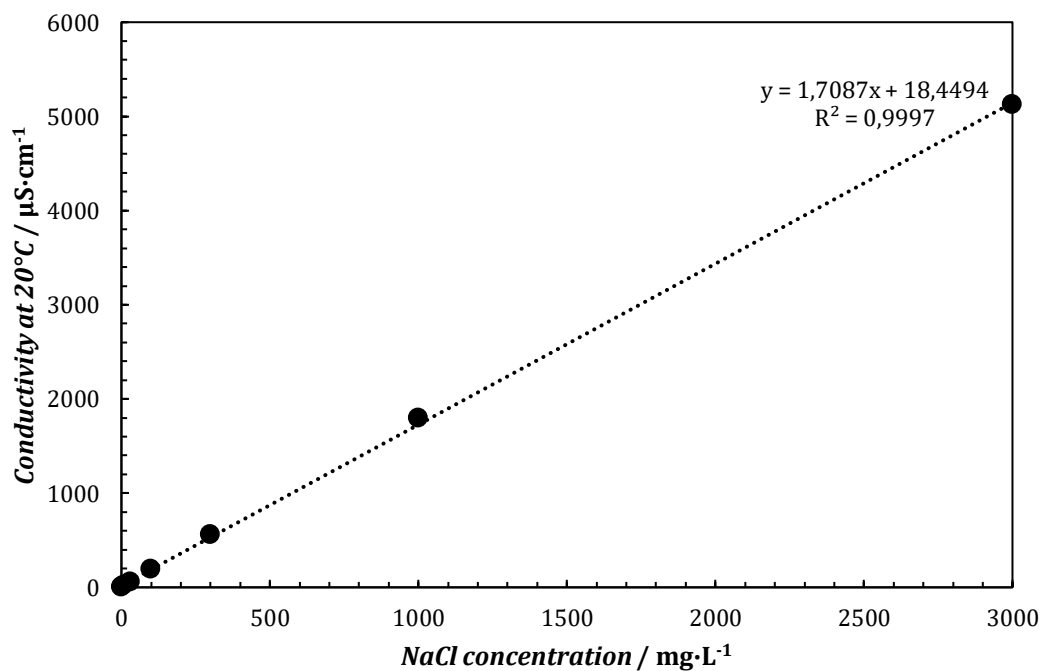
Figure B-1: Conductivity of the solution as a function of the NaCl concentration at 20°C (Foxboro, 1999).

161

For a conductivity range of 1.75 to 5.97 S·m⁻¹ for the draw solution, the NaCl concentration data from Kaye & Laby (1971), with a temperature and conductivity dependence, were regressed. The correlation is expressed by Equation B-1. The temperature and conductivity coefficients in Equation B-1 are listed in Table B-1.

$$C = (a + bT + cT^2 + dT^3 + eT^4) \times (f + g\kappa + h\kappa^2 + i\kappa^3 + j\kappa^4 + k\kappa^5) \qquad \text{(B-1)}$$

where C = NaCl concentration (mg·L⁻¹)

         $a - e$ = Temperature coefficients

         $f - k$ = Conductivity coefficients

Table B-1: The regressed temperature and conductivity coefficients according to Equation B-1.

Temperature coefficient	Value	Conductivity coefficient	Value
a	1.20×10^3	f	-1.10
b	-3.98×10^1	g	9.95
c	9.56×10^{-1}	h	1.17×10^{-1}
d	1.63×10^{-2}	i	8.06×10^{-2}
e	1.41×10^{-4}	j	1.30×10^{-2}
		k	6.68×10^{-14}

B.2 UV-Vis calibration

A calibration curve was generated for the UV-Vis analysis of phenol in the feed solution between concentrations of 1 mg·L^{-1} and 30 mg·L^{-1}. The calibration data, as shown in Figure B-2, were obtained from independently prepared phenol solutions.
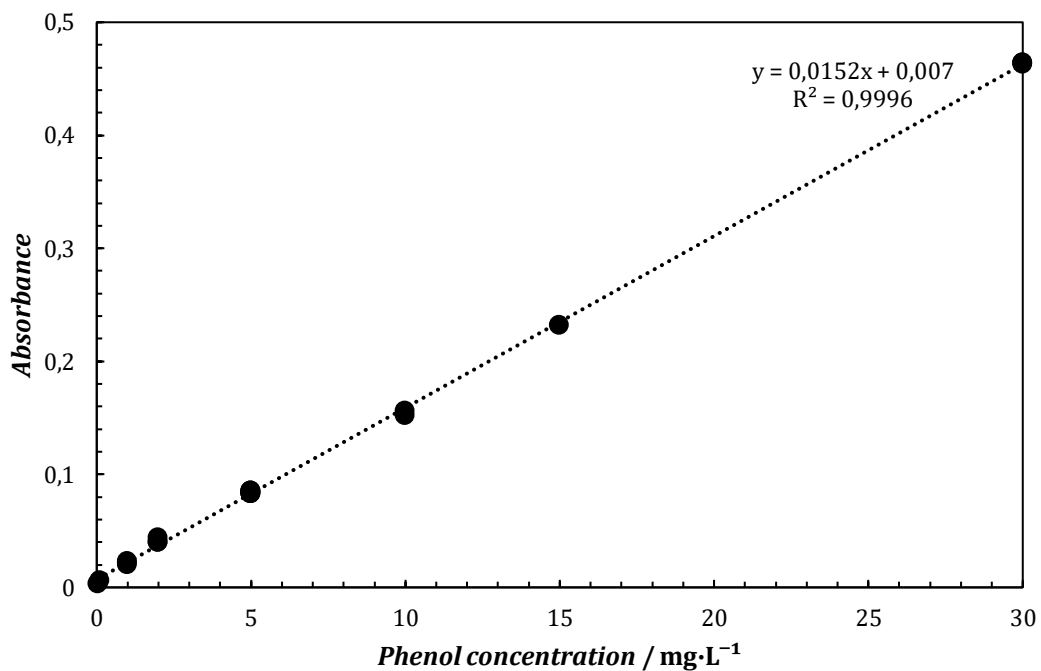
Figure B-2: Calibration curve for the UV-Vis analysis of phenol at concentrations between 1 mg·L^{-1} and 30 mg·L^{-1}.

Appendix C

Validation of experimental data

The data of the solute transport and rejection experiments, presented in Section 4.2, were validated with the replication of experiments. The data points at the lowest and highest solute concentration gradients of phenol, boron and lithium were considered. The observed rejection of the three model solutes was used for the validation and an ANOVA analysis was performed for each data point. As shown in Table C-1, the p-values of all the replicates were greater than the significance level of α=0.05. Hence, the experimental data could be considered valid.

Table C-1: The p-values, with α=0.05, of the solute rejection for the replicated experiments at the endpoints of the respective ranges of the solute concentration gradients (Δc_S) in the AL-FS and AL-DS membrane orientation.

Δc_S	Membrane orientation	
	AL-FS	AL-DS
Phenol		
Low	0.51	0.49
High	0.46	-
Boron		
Low	0.42	0.46
High	1.10	2.04
Lithium		
Low	0.06	0.71
High	-	0.80

Appendix D

FO-RO hybrid simulation

D.1   Simulation results

In support of the simulation results presented in Section 5.4.2, a summary of the stream flowrates and solute concentrations for each case study is provided here.

D.1.1 50% FO permeate flowrate

Table D-1: Stream summary for the FO-RO hybrid simulation with a FO permeate flowrate of 50% of the RO permeate flowrate and 45% RO recovery. Q refers to the stream flowrate and C to the stream concentration.

Stream	Symbol subscript	Q / m³·h⁻¹	C / mg·L⁻¹			
			TDS	Phenol	Boron	Lithium
FO feed	f,FO	100.0	850	1.000×10^{-1}	8.00	0.302
FO concentrate	c,FO	50.0	1 675	1.820×10^{-1}	14.88	0.490
FO permeate	p,FO	50.0	26	1.800×10^{-2}	1.12	0.115
Feed seawater	sw	122.2	35 000	-	4.50	0.170
Diluted DS	dsw	172.2	24 846	5.226×10^{-3}	3.52	0.154
Seawater make-up	m	50.0	35 000	-	4.50	0.170
RO feed	f,RO	222.2	27 131	4.050×10^{-3}	3.74	0.158
RO concentrate	c,RO	122.2	48 996	7.065×10^{-3}	6.58	0.262
RO permeate	p,RO	100.0	407	3.645×10^{-4}	0.26	0.030
Total seawater intake	-	172.2	35 000	-	4.50	0.170
Combined discharge	-	172.2	35 257	5.785×10^{-2}	8.99	0.328

165

Table D-2: Stream summary for the FO-RO hybrid simulation with a FO permeate flowrate of 50% of the RO permeate flowrate and 70% RO recovery. Q refers to the stream flowrate and C to the stream concentration.

Stream	Symbol subscript	Q / m³·h⁻¹	C / mg·L⁻¹			
			TDS	Phenol	Boron	Lithium
FO feed	f,FO	100.0	850	1.000×10^{-1}	8.00	0.302
FO concentrate	c,FO	50.0	1 675	1.820×10^{-1}	14.88	0.490
FO permeate	p,FO	50.0	26	1.800×10^{-1}	1.12	0.115
Feed seawater	sw	42.9	35 000	-	4.50	0.170
Diluted DS	dsw	92.9	16 168	9.692×10^{-3}	2.68	0.140
Seawater make-up	m	50.0	35 000	-	4.50	0.170
RO feed	f,RO	142.9	22 759	6.300×10^{-3}	3.32	0.151
RO concentrate	c,RO	42.9	75 067	1.968×10^{-2}	10.51	0.436
RO permeate	p,RO	100	341	5.670×10^{-4}	0.23	0.029
Total seawater intake	-	92.9	35 000	-	4.50	0.170
Combined discharge	-	92.9	35 548	1.071×10^{-1}	12.87	0.465

D.1.2 100% FO permeate flowrate

Table D-3: Stream summary for the FO-RO hybrid simulation with a FO permeate flowrate of 100% of the RO permeate flowrate and 45% RO recovery. Q refers to the stream flowrate and C to the stream concentration.

Stream	Symbol subscript	Q / m³·h⁻¹	C / mg·L⁻¹			
			TDS	Phenol	Boron	Lithium
FO feed	f,FO	200.0	850	1.000×10^{-1}	8.00	0.302
FO concentrate	c,FO	100.0	1 675	1.820×10^{-1}	14.88	0.490
FO permeate	p,FO	100.0	26	1.800×10^{-1}	1.12	0.115
Feed seawater	sw	122.2	35 000	-	4.50	0.170
Diluted DS	dsw	222.2	19 261	8.100×10^{-3}	2.98	0.145
Seawater make-up	m	0.0	-	-	4.50	0.170
RO feed	f,RO	222.2	19 261	8.100×10^{-3}	2.98	0.145
RO concentrate	c,RO	122.2	34 784	1.413×10^{-1}	5.25	0.241
RO permeate	p,RO	100.0	289	7.290×10^{-4}	0.21	0.028
Total seawater intake	-	122.2	35 000	-	4.50	0.170
Combined discharge	-	222.2	19 885	8.967×10^{-1}	9.58	0.353

Table D-4: Stream summary for the FO-RO hybrid simulation with a FO permeate flowrate of 100% of the RO permeate flowrate and 70% RO recovery. Q refers to the stream flowrate and C to the stream concentration.

Stream	Symbol subscript	Q / m³·h⁻¹	C / mg·L⁻¹			
			TDS	Phenol	Boron	Lithium
FO feed	f,FO	200.0	850	1.000×10^{-1}	8.00	0.302
FO concentrate	c,FO	100.0	1 675	1.820×10^{-1}	14.88	0.490
FO permeate	p,FO	100.0	26	1.800×10^{-2}	1.12	0.115
Feed seawater	sw	42.9	35 000	-	4.50	0.170
Diluted DS	dsw	142.9	10 518	1.260×10^{-2}	2.13	0.131
Seawater make-up	m	0.0	-	-	-	-
RO feed	f,RO	142.9	10 518	1.260×10^{-2}	2.13	0.131
RO concentrate	c,RO	42.9	34 691	3.935×10^{-2}	6.67	0.380
RO permeate	p,RO	100.0	158	1.134×10^{-2}	0.15	0.025
Total seawater intake	-	42.9	35 000	-	4.50	0.170
Combined discharge	-	142.9	11 580	1.392×10^{-1}	12.45	0.457

D.2 Example flow sheet

FO feed

Q	200.0	m³/h
	200000	litres/h
C_TDS	**850**	mg/litre
C_PhOH	**0.100**	mg/litre
C_B	**8.000**	mg/litre
C_Li	**0.300**	mg/litre

Forward osmosis unit

Recovery of water	**0.5**
Salt rejection	**0.985**
PhOH rejection	**0.91**
B rejection	**0.93**
Li rejection	**0.81**

FO concentrate

Q	100.0	m³/h
	100000	litres/h
C_TDS	1675	mg/litre
C_PhOH	0.182	mg/litre
C_B	14.880	mg/litre
C_Li	0.486	mg/litre

FO permeate

Q	100.0	m³/h
	100000	litres/h
C_TDS	26	mg/litre
C_PhOH	0.018	mg/litre
C_B	1.120	mg/litre
C_Li	0.114	mg/litre

Pre-treated seawater

Q	42.9	m³/h
	42857	litres/h
C_TDS	**35000**	mg/litre
C_PhOH	**0.000**	mg/litre
C_B	**4.500**	mg/litre
C_Li	**0.170**	mg/litre

Diluted draw solution

Q	142.9	m³/h
	142857	litres/h
C_TDS	10518	mg/litre
C_PhOH	0.01	mg/litre
C_B	2.13	mg/litre
C_Li	0.13	mg/litre

Reverse osmosis unit

Recovery of water	**0.7**
Salt rejection	**0.985**
PhOH rejection	**0.93**
B rejection	**0.90**
Li rejection	**0.88**

Pre-treated seawater

Q	0	m³/h
	0	litres/h
C_TDS	**35000**	mg/litre
C_PhOH	**0.000**	mg/litre
C_B	**4.500**	mg/litre
C_Li	**0.170**	mg/litre

RO feed

Q	142.9	m³/h
	142857	litres/h
C_TDS	10518	mg/litre
C_PhOH	0.013	mg/litre
C_B	2.134	mg/litre
C_Li	0.131	mg/litre

RO permeate

Q	**100**	m³/h
	100000	litres/h
C_TDS	157.7678	mg/litre
C_PhOH	0.001	mg/litre
C_B	0.213	mg/litre
C_Li	0.016	mg/litre

RO concentrate

Q	42.9	m³/h
	42857	litres/h
C_TDS	34691	mg/litre
C_PhOH	0.040	mg/litre
C_B	6.615	mg/litre
C_Li	0.399	mg/litre

Figure D-1: Example flow diagram for the mass balance of the FO-RO hybrid. The fixed values are indicated in red text.

Appendix E

Operating procedures

The operation of the bench-scale experimental setup is discussed here. Firstly, the safety precautions and measures for equipment protection are outlined. The procedures for solution preparation, process start-up and shut-down and measurement and sampling are further discussed.

E.1 Safety precautions

1) Personal protective equipment

A laboratory coat, closed-shoes and safety-glasses should be worn by the operator. For the handling of the phenol, boron or lithium containing solutions, a respirator and protective gloves are required.

2) Process safety

The following should be taken into consideration for safe operation of the setup:

i) Water is contained and transport throughout this system. Periodical inspection should be performed to ensure that the insulation of electrical wiring and equipment is sufficient.

ii) Spillages must be contained and cleaned to avoid slipping.

iii) The work-bench must be secured in place by locking the swivel castors of the trolley.

E.2 Equipment protection

1) Feed solution reactor (TK-103)

The feed solution reactor and cover is fabricated from highly brittle Perspex®. Care should be taken to fasten bolts to the predetermined torque. The distribution plate should be secured with the Grubbs screws in the FS reactor with caution, to avoid the formation of cracks at the joints.

2) DS submersible pump (P-103)

The flow switch of the submersible pump located in TK-102 should be free of obstructions in the upward or downward direction to avoid the loss of draw solution by overflow and the pump from running dry.

3) DS tank heater (HX-101)

During the preparation of a new draw solution, the tank heater must be disconnected and removed from TK-101 to avoid thermal shock to the element by colder water.

E.3   Solution preparation

1) Sodium chloride draw solution

Product information: Iodated table salt (500g)
Solution preparation: The predetermined mass of table salt is added into the draw solution tank (TK-101) with deionised water to prepare a 200 litre draw solution. Compressed air can be utilised to mix the contents of the tank and accelerate the dissolution of the salt.

2) Feed solution of trace phenol concentrations (5-25 mg·L^{-1})

Product information: Phenol crystals
Solution preparation: Phenol solutions must be prepared under a fume hood with the appropriate protective equipment. The predetermined volume of the 200 mg·L^{-1} phenol stock solution is combined with deionised water to prepare 6 litres of feed solution. A predetermined mass of NaCl is added to establish a 2 g·L^{-1} background solution. Each solution is stored in a 10 litre container.

3) Feed solution of trace boron and lithium concentrations (5-80 mg·L^{-1})

Product information: Lithium chloride and boric acid crystals
Solution preparation: The predetermined volumes of the respective 1000 mg·L^{-1} lithium and boron stock solutions are combined with deionised water to prepare a feed solution of 6 litres. Each solution is stored in a 10 litre container.

E.4   Start-up

E.4.1 Pre-start-up checklist

1) FS reactor, membrane and pumps

i)   Ensure that the bolts of the feed solution reactor and membrane cell are fastened such that there are no leakages at the contact surfaces.

ii)   Secure the distribution plate in the desired position in the feed solution reactor.

iii)   Detach the cover of the FS reactor and discard all the flushing solution appropriately.

iv)   Ensure that the membrane is in the desired orientation and that there is no visible damage to the membrane surface.

v)   Ensure that the draw solution pump (P-101) is set at 100 rpm for a cross-flow velocity of 0.16 m·s⁻¹.

   2) Valves and tubing

i)   VA-101 and VA-104 must be open.

ii)   VA-102 and VA-103 must be closed.

iii)   Follow the process train and ensure that all tubing is connected.

   3) Draw solution and feed solution

i)   Ensure that all solution in the reservoir tank (TK-102) has been recycled to the feed tank (TK-101).

ii)   Measure the conductivity of the draw solution. The NaCl concentration can be adjusted by adding water or table salt.

iii)   Ensure that the temperatures of the draw solution and feed solution are within 1°C. The tank heater (HX-101) can be switched on to adjust the temperature of the draw solution.

iv)   If a solute rejection experiment is performed, sample the prepared feed solution in triplicate.

E.4.2 Start-up procedure

1) Switch off the electrical supply to the pumps.

2) Load an initial amount of feed solution into the base of the reactor.

3) Submerse the agitator pump (P-102), that is attached to the reactor cover, into the feed solution. Secure the rubber gasket in place and attach the cover to the reactor base with the bolts. Torque the bolts to 1.5 N·m

4) Load the remaining volume of the feed solution into the reactor and graduated cylinder of the cover. Release trapped air in the reactor by carefully tipping the reactor to the sides.

5) Note the height of the liquid level from the graduated cylinder as soon as possible.

6) Open valve VA-103 and connect the electrical supply. Switch the agitator pump (P-102) and draw solution pump (P-101) on with the respective switches.

E.5   Obtaining measurements and samples

1) Water flux

The water flux is quantified from the change in the feed solution volume, measured from the graduated cylinder of the reactor. The time elapsed between measurements of the level height must be recorded.

2) Conductivity and temperature of the draw and feed solution

The conductivity and temperature of the respective solutions are measured simultaneously. The inlet draw solution is sampled through VA-102 and the outlet draw solution through VA-104. The measurement probe is submerged into the feed solution in the reactor through the graduated cylinder to obtain a measurement. If the temperature of the feed solution increases significantly above that of the draw solution, heat from HX-101 can be supplied to the contents of the draw solution feed tank (TK-101).

3) Draw solution flow rate and cross-flow velocity

The draw solution flowrate is measured with the in-line flowmeter, FM-101. To start the measurement, the ball valve (VA-104) is closed and the stopwatch is started. The time elapsed to fill the cylinder to the calibrated volume is recorded. The ball valve can be opened to terminate the measurement and allow the draw solution to pass into the reservoir (TK-102).

4) Sampling of the feed solution

Triplicate samples of the feed solution are drawn for analysis of the trace solutes. At the end of each FO test, a 15 ml syringe with a lengthened suction tube is used to draw the samples from the feed solution reactor through the graduated cylinder.

E.6   Shut-down

1) Switch pump P-101 off at by pressing the green button. Switch pump P-102 off on the switch located on the work bench.
2) Close valve VA-103 to avoid any draw solution flooding the system.
3) If no heating of the draw solution is further required, switch the tank heater (HX-101) off.
4) Disconnect the electrical supply from the equipment.
5) If required, the feed solution can be discarded. The reactor must be disassembled to load the flushing solution for the subsequent experiment.
6) The membrane must not be allowed to run dry overnight.